VOLUME 109 NUMBER 1

THE ASTROPHYSICAL JOURNAL

AN INTERNATIONAL REVIEW OF SPECTROSCOPY AND ASTRONOMICAL PHYSICS

JANUARY 1949

ANALYSIS OF THE FIRST ROCKET ULTRAVIOLET SOLAR SPECTRA
E. Durand, J. J. Oberly, and R. Tousey 1

TELLURIC BANDS OF CH_4 IN THE SOLAR SPECTRUM
Robert R. McMath, Orren C. Mohler, and Lee Goldberg 17

NEW SOLAR LINES IN THE SPECTRAL REGION 1.52–1.75 μ
Lee Goldberg, Orren C. Mohler, and Robert R. McMath 28

MULTIPLET INTENSITIES FOR THE NEBULAR LINES ^4S–^2D of O II
L. H. Aller, C. W. Ufford, and J. H. Van Vleck 42

THEORETICAL CONTOURS OF ABSORPTION LINES *Daniel L. Harris III* 53

EXACT CURVES OF GROWTH FOR THE FORMATION OF ABSORPTION LINES ACCORDING TO THE MILNE-EDDINGTON MODEL. I. TOTAL FLUX
Marshal H. Wrubel 66

THE WOLF-RAYET SPECTROSCOPIC BINARY HD 190918 *O. C. Wilson* 76

HIGH-DISPERSION SPECTROGRAMS OF T CORONAE BOREALIS *Reeve F. Sanford* 81

STELLAR SPECTRA WITH EMISSION LINES IN THE OBSCURING CLOUDS OF OPHIUCHUS AND SCORPIUS *Otto Struve and Margaret Rudkjobing* 92

SPECTROGRAPHIC OBSERVATIONS OF TW ANDROMEDAE
W. A. Hiltner, Burke Smith, and O. Struve 95

RADIAL-VELOCITY OBSERVATIONS WITH THE BRUCE SPECTROGRAPH
Daniel M. Popper 100

IDENTIFICATION OF A MOLECULAR BAND AT λ 3682 IN THE SPECTRA OF LATE-TYPE STARS *George H. Herbig* 109

SPECTROGRAPHIC OBSERVATIONS OF THE ECLIPSING VARIABLE RS SAGITTARII *Jorge Sahade* 116

ANALYSIS OF THE METALLIC-LINE STARS. II *Jesse L. Greenstein* 121

VARIATIONS IN THE STELLAR LUMINOSITY FUNCTION. II. A REGION IN ORION *S. W. McCuskey* 139

THE OSCILLATIONS OF A ROTATING STAR *T. G. Cowling and R. A. Newing* 149

DYNAMICAL FRICTION *Marvin Lee White* 159

A NONHOMOGENEOUS COSMOLOGICAL MODEL *Guy C. Omer, Jr.* 164

NOTES

PHOTOELECTRIC OBSERVATIONS OF W VIRGINIS *Katherine C. Gordon and Gerald E. Kron* 177

NOTE ON THE PAPER, "THE ABSORPTION-LINE SPECTRA OF THE CENTRAL STARS OF THE PLANETARY NEBULAE" *Lawrence H. Aller* 179

EDITOR'S NOTE 179

REVIEWS 180

THE UNIVERSITY OF CHICAGO PRESS
CHICAGO, ILLINOIS, U.S.A.

January 1949 Vol. 109, No. 1

THE ASTROPHYSICAL JOURNAL

AN INTERNATIONAL REVIEW OF SPECTROSCOPY AND ASTRONOMICAL PHYSICS

Edited by

W. W. MORGAN
Managing Editor
Yerkes Observatory of the University of Chicago

S. CHANDRASEKHAR

PAUL W. MERRILL
Mount Wilson Observatory of the Carnegie Institution of Washington

HARLOW SHAPLEY
Harvard College Observatory
Cambridge, Massachusetts

N. U. MAYALL
Lick Observatory
University of California

With the Collaboration of the American Astronomical Society

Collaborating Editors:

1947-49
LYMAN SPITZER, JR.
Princeton University Observatory

A. N. VYSSOTSKY
Leander McCormick Observatory

ALBERT E. WHITFORD
Washburn Observatory

1948-50
CECILIA H. PAYNE-GAPOSCHKIN
Harvard College Observatory

H. N. RUSSELL
Princeton University

ANDREW McKELLAR
Dominion Astrophysical Observatory, Victoria

1949-51
W. BAADE
Mount Wilson Observatory

LEO GOLDBERG
Observatory of the University of Michigan

G. HERZBERG
National Research Council, Ottawa

The Astrophysical Journal is published bimonthly by the University of Chicago at the University of Chicago Press, 5750 Ellis Avenue, Chicago, Illinois, during July, September, November, January, March, and May. ¶The subscription price is $12.00 a year; the price of single copies is $3.00. Orders for service of less than a full year will be charged at the single-copy rate. ¶Postage is prepaid by the publishers on all orders from the United States and its possessions, Argentina, Bolivia, Brazil, Chile, Colombia, Costa Rica, Cuba, Dominican Republic, Ecuador, Guatemala, Haiti, Republic of Honduras, Mexico, Morocco (Spanish Zone), Nicaragua, Panama, Paraguay, Peru, Rio de Oro, El Salvador, Spain (including Balearic Islands, Canary Islands, and the Spanish Offices in Northern Africa; Andorra), Spanish Guinea, Uruguay, and Venezuela. ¶Postage is charged extra as follows: for Canada and Newfoundland, 42 cents on annual subscriptions (total $12.42); on single copies, 7 cents (total $3.07); for all other countries in the Postal Union, 96 cents on annual subscriptions (total $12.96), on single copies 16 cents (total $3.16). ¶Patrons are requested to make all remittances payable to The University of Chicago Press, in United States currency or its equivalent by postal or express money orders or bank drafts.

The following is an authorized agent:

For the British Empire, except North America and Australasia: The Cambridge University Press, Bentley House, 200 Euston Road, London, N.W. 1, England. Prices of yearly subscriptions and of single copies may be had on application.

Claims for missing numbers should be made within the month following the regular month of publication. The publishers expect to supply missing numbers free only when losses have been sustained in transit, and when the reserve stock will permit.

Business correspondence should be addressed to The University of Chicago Press, Chicago 37, Illinois.

Communications for the editors and manuscripts should be addressed to: W. W. Morgan, Editor of THE ASTROPHYSICAL JOURNAL, Yerkes Observatory, Williams Bay, Wisconsin.

Line drawings and photographs should be made by the author, and all marginal notes such as co-ordinates, wave lengths, etc., should be included in the cuts. It will not be possible to set up such material in type.

One copy of the corrected galley proof should be returned as soon as possible to the editor, Yerkes Observatory, Williams Bay, Wisconsin. Authors should take notice that the manuscript will not be sent to them with the proof.

The cable address is "Observatory, Williamsbay, Wisconsin."

The articles in this journal are indexed in the *International Index to Periodicals*, New York, N.Y.

Applications for permission to quote from this journal should be addressed to The University of Chicago Press, and will be freely granted.

Entered as second-class matter, July 31, 1940, at the Post-Office at Chicago, Ill., under the Act of March 3, 1879.
Acceptance for mailing at special rate of postage provided for in United States Postal Act of October 3, 1917, Section 1103, amended February 28, 1925.

[PRINTED IN U.S.A.]

THE ASTROPHYSICAL JOURNAL

AN INTERNATIONAL REVIEW OF SPECTROSCOPY AND ASTRONOMICAL PHYSICS

VOLUME 109 JANUARY 1949 NUMBER 1

ANALYSIS OF THE FIRST ROCKET ULTRAVIOLET SOLAR SPECTRA

E. DURAND, J. J. OBERLY, AND R. TOUSEY

United States Naval Research Laboratory, Washington, D.C.

Received April 28, 1948

ABSTRACT

Solar spectra obtained from V-2 flights on October 10, 1946, and March 7, 1947, were analyzed. The spectrum in the hitherto unobserved region from 2900 to 2200 A was found to be intensely complex and filled with unresolved blends. The low resolution (1.5 A) made positive identification difficult in many instances. Tables showing the wave length, visual estimated intensities, character, and identification of the lines observed are given. Reproductions of densitometer traces are given, and part of the spectrum is shown replotted on an intensity scale.

Certain multiplets of *Fe* I, *Fe* II, *Si* I, and *Mn* II appeared in great strength. Four lines—*Si* I, 2882 A; *Mg* I, 2852 A; *Mg* II, 2803 A; and *Mg* II, 2796 A—were very broad, similar to H and K of *Ca* II. The *Mg* II pair showed a central core of emission of great strength. The structure between 2200 and 2300 A could not be interpreted in terms of atomic lines and may be caused by atmospheric bands of *NO*.

I. INTRODUCTION

The first successful attempt to photograph the sun's spectrum from above the ozone layer was made at White Sands, New Mexico, on October 10, 1946,[1, 2] using a vacuum-grating spectrograph designed at the Naval Research Laboratory and installed in the tail fin of a German V-2 rocket. Radiation was observed down to wave lengths as short as 2100 A. A second flight on March 7, 1947,[3, 4, 5] gave spectra of considerably improved resolution. During April of that year the Applied Physics Laboratory of the Johns Hopkins University launched a rocket carrying a spectrograph equipped with a servo-controlled mirror designed to track the sun in one axis. An analysis of the excellent spectra which they obtained will be published shortly.[6] A third successful flight with a Naval Research Laboratory instrument was made on October 9, 1947. This report is an extension of the analysis already published[3] of the spectra obtained on the flights sponsored by this laboratory.

[1] W. A. Baum, F. S. Johnson, J. J. Oberly, C. C. Rockwood, C. V. Strain, and R. Tousey, *Phys. Rev.*, **70**, 781, 1946.

[2] *Naval Research Laboratory Report No. R-3030*, chap. iv, Sec. A.

[3] E. Durand, J. J. Oberly, and R. Tousey, *Phys. Rev.*, **71**, 827, 1947.

[4] *Naval Research Laboratory Report No. R-3120*, chap. ii, Sec. A.

[5] *Naval Research Laboratory Report No. R- 171*, chap. v.

[6] J. J. Hopfield and H. E. Clearman, Jr., *Phys. Rev.*, **73**, 877, 1948.

II. THE SPECTROGRAPH

The spectrograph was designed at the Naval Research Laboratory and was built by Baird Associates in Cambridge, Massachusetts. It is shown in Figures 1 and 2. It has previously been described in detail,[2,7] but, since these reports are not generally available,[8] a brief description will be given here.

The rocket is vertical when launched and remains so during the accelerating period of about 1 minute. For the balance of the flight it is uncontrolled, and its orientation with respect to the sun may vary greatly, depending on its chance residual angular momentum at fuel burnout. For midday flights the spectrograph is mounted with its cone axis vertical in either the east or the west tail fin. It is provided with two optical entrance axes, one aimed north, the other south, pointing to the sun. Both axes are 45° down from the zenith. Either axis may be used to obtain spectra, the former serving if by chance the rocket rolls 180° about its axis.

To increase further the acceptance angle of the spectrograph, 2-mm spheres of lithium fluoride are used to collect radiation in place of the usual condenser and slit or the ground-quartz diffusion plate and slit that have been used on other rocket spectrographs.[6] A solar image—about 0.03 mm in diameter—is formed behind the spheres and acts effectively as a narrow slit.

This arrangement permits usable spectra to be obtained with the sun as much as 70° in any direction away from either axis. It suffers from the drawback, however, that there is some defocusing for large angles and that changes in solar position during an exposure produce a displacement of the solar image and a blurring of the spectrum, especially for displacements parallel to the dispersion. The advantage in speed over the diffusing system, however, is tremendous.

After leaving the bead, the radiation falls on a small mirror and is reflected back to a concave grating at the apex of the cone. The grating, whose radius of curvature is 40 cm, is ruled with 15,000 lines per inch on aluminized glass. It focuses the spectrum on the 35-mm film, which lies on the Rowland circle at the base of the instrument.

The spectra from the two beads are displaced to either side of the median plane by a slight tilting of the small mirrors. If plane mirrors are used, the spectrum lines will be about 1 mm high because of the astigmatism characteristic of this mounting. If cylindrical mirrors are used, the astigmatism may be entirely eliminated at one wave length and greatly reduced at other wave lengths. The resulting reduction in height of the spectrum increases the photographic density obtained for a given exposure and usually reduces the blurring action referred to above. On the other hand, densitometry of the spectra becomes most difficult because of the changing height of the spectral lines at different wave lengths. There is also some loss of effective resolution because of the graininess of the photographic film.

In spectrum No. 43, taken at 75 km on March 7, 1947, the roll of the rocket during the exposure was such that the spectrum moved perpendicular to the plane of dispersion. This fortunate chance gave a resolution nearly as good as the best obtained in the laboratory, and most of the analysis presented in this report was based on this particular spectrum. It is reproduced in Figure 3.

The instrument was equipped with a motor-driven shutter and film-transport mechanism which automatically provided exposures of 0.1, 0.6, and 3.0 seconds. This exposure cycle was repeated over and over until the rocket was well past the top of the flight, after which the remaining film, if any, was wound up into an armor-steel cassette. Eastman ultraviolet sensitized type 103-O film was used.

[7] *Naval Research Laboratory Report No. 2955*, chap. iii, Sec. H.

[8] A limited number of copies of these reports is available at the Technical Information Office, Naval Research Laboratory, Washington 20, D.C.

FIG. 1.—This spectrograph was used in the flight of October 10, 1946. It was recovered in perfect operating condition after falling 108 miles from the top of the rocket flight. This photograph was taken after the flight. The only damage was the small dent in the case, which may be seen in the photograph.

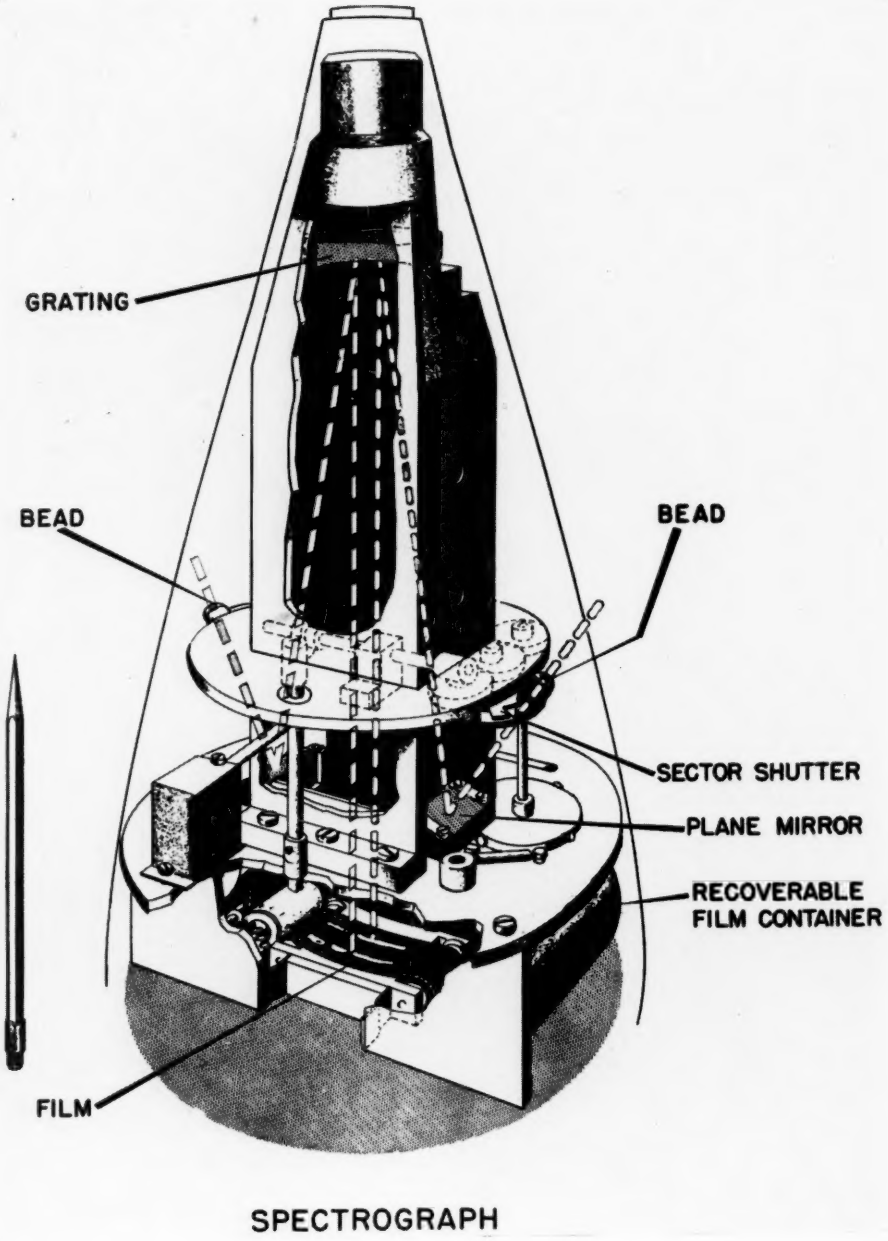

FIG. 2.—Schematic diagram of rocket spectrograph

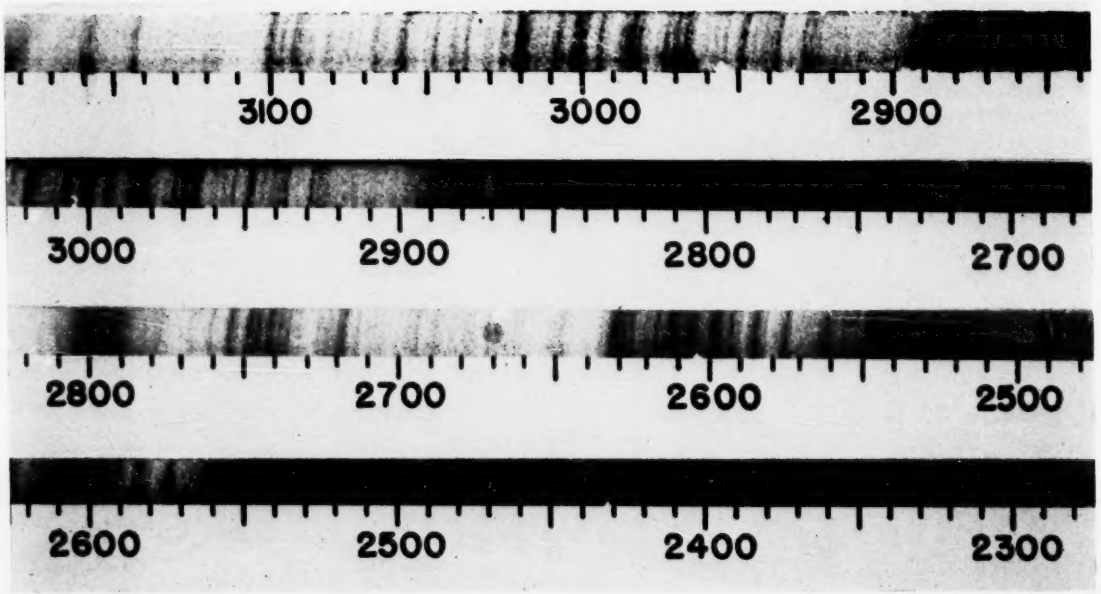

FIG. 3.—Solar ultraviolet spectrum from 3180 A to 2350 A. Note the *Mg* II emission lines at 2796 A and 2803 A (line *3* of the spectrum).

III. THE SPECTRA

Because of the changes in rocket orientation referred to above, many of the spectra were either blurred or of low density. Densitometer traces of three of the best spectra are reproduced in Figure 4. Figure 4, *A*, is the trace of the high-resolution spectrum of Figure 3. Figure 4, *B*, is the trace of a spectrum taken at 35 km on October 10. It was not used in the analysis but is of interest because it shows the shortest solar wave lengths observed—2100 A or less—and also shows the often predicted "window" in this region between the absorption bands of O_2 and those of O_3. The radiation between 2300 and 2630 A is absorbed by the residual ozone above the spectrograph.[9]

Figure 4, *C*, is the trace of another October 10 spectrum, taken at 55 km. At this altitude, less than 1 per cent of the total ozone remained between the instrument and the sun, so that the entire spectral region obscured at 35 km may be seen.

IV. WAVE LENGTHS

Most of the wave-length determinations are based on visual comparator observations. A few unresolved and weak lines showing up on the tracings in the long-wave-length regions and many of the low-density lines in the short-wave-length regions were taken from the densitometer traces. These are denoted by a "D" following the observed wave lengths in Table 1.

Several determinations were made by independent observers. The constants for the wave-length equation were chosen to give the best over-all fit for fourteen strong lines of *Fe* I and *Fe* II distributed through the spectrum. The probable wave-length error for other lines varies from 0.2 to 1.0 A, depending on sharpness and freedom from blending.

V. INTENSITIES

Most of the intensity estimates are visual. The scale is similar to that used in the revised Rowland table,[10] which means that it is an approximate measure of the central core intensity and width of the lines. A comparative study of the rocket spectra, the Rowland table, and a table of solar lines prepared by Babcock, Moore, and Coffeen from Mount Wilson plates[11] showed that the weakest observable lines in the rocket spectra corresponded roughly to a Rowland intensity of 3, while the strongest line had a Rowland intensity of about 1000. Between 2650 and 2388 A the numerical estimates were dropped because of low density. For this region the notations in Section VII are used. Below 2388 A it was considered that the resolution of the spectrum of Figure 4, *C*, was superior to that of Figure 4, *A*, since the high density gave a greater freedom from graininess. For this region the former spectrum was used, and the numerical estimates were resumed.

The spectrum in the rocket ultraviolet region is more complex than that in the previously known region. There are several regions (e.g., 2500–2550 A, Fig. 4, *A*) in which the overlapping of many strong lines produces a large general depression of the spectrum, such that the location of the background continuous spectrum can only be surmised. Certain anomalies in the visual estimates in such regions resulted. Typical examples of this effect are cited in Section VIII.

VI. IDENTIFICATIONS

The features to be identified are listed in Table 1. A finding list containing about twelve hundred entries, arranged according to wave length, was prepared. These entries

[9] This film, together with others taken at different altitudes on the same flight, was used to determine the vertical distribution of ozone in the earth's atmosphere (*Naval Research Laboratory Report No. R-3171*, chap. v).

[10] *Revision of Rowland's Preliminary Table of Solar Spectrum Wave-Lengths* (Washington, D.C.: Carnegie Institution of Washington, 1928).

[11] *Ap. J.*, **107**, 287, 1948.

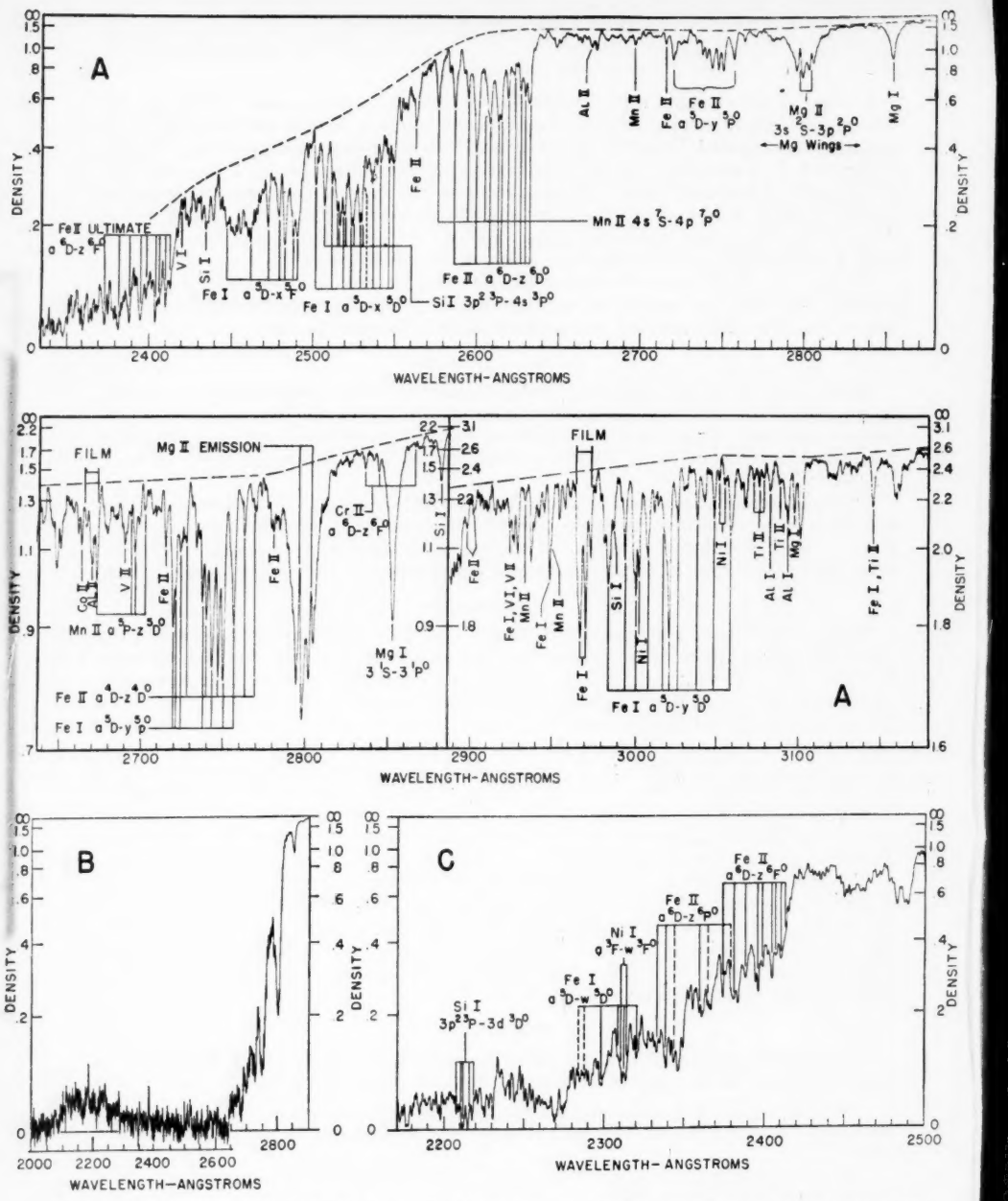

FIG. 4.—Densitometer tracings of solar spectrum. (*a*) Spectrum No. 43 taken at 75 km on March 7, 1947. The blisters which may be seen on Fig. 3 at 2670 A and 2970 A are shown by the word FILM and a limited bracket. (*b*) Spectrum No. 23 taken at 35 km on October 10, 1946. Compressed wave-length scale used to emphasize the "hump" near 2200 A. (*c*) Spectrum No. 29 taken at 55 km on October 10, 1946. Below 2415 A the resolution of No. 43 is inferior to that of No. 29 because of its very low density.

represented the classified lines that might be expected to show up at the available resolution. Most of them were taken from unpublished multiplet lists which Dr. C. E. M. Sitterly, of the National Bureau of Standards, is using for the preparation of her new violet multiplet table.

The finding list was compared with the list of observed features and the likely contributors to each observed line noted. In some cases the major contributor or contributors were easily identified, but more often there were found to be several possible contributors.

A careful study of multiplet relations and laboratory intensities was made, to determine the relative importance of the various contributors. In the third column of Table 1, probable major contributors are indicated by the symbol # preceding the element abbreviation. Absence of this symbol means either that the line is minor (less than 20 per cent) or that evidence of its importance is lacking. In cases of several possible contributors with little evidence as to relative importance, the laboratory wave lengths and intensities are omitted.

VII. SYMBOLS USED IN TABLE 1

FIRST COLUMN—OBSERVED WAVE LENGTHS

1. Lines seen by four or more observers are considered certain. Doubtful lines are indicated by "?" following the wave length. Doubtful lines showing clearly on densitometer traces are indicated by "D" following the wave length.

2. A bracket links two wave lengths which form the extremes of a broad absorption line or depressed feature. Wave lengths listed between the extremes indicate internal structure.

SECOND COLUMN—OBSERVED INTENSITIES

1. Numerical values range from 3 for the weakest observable line up to 1000 for the strongest.

2. In certain low-density regions the numerical scale was dropped. The notations used and their approximate numerical equivalents are as follows:

St (strong)	= Greater than 40
Md (medium)	= 20–40
Wk (weak)	= Less than 20

3. The following letters appearing after the intensity estimates indicate special characteristics:

n—wide line, probably a blend of contributing lines separated by 2 A or less.
N—wide line, more than 2 A. Usually used in conjunction with the bracket symbol in the wave-length column.
d?—may be double.
v—the line an imperfectly resolved violet component in the wing of a stronger line.
r—the line an imperfectly resolved red component in the wing of a stronger line.
Em—emission line.
no line—intensity minimum at the base of an emission line.

THIRD COLUMN—SPECTRUM

1. The symbol # denotes a major contributor.

FOURTH COLUMN—LABORATORY WAVE LENGTH

1. An asterisk before the entry indicates the existence of another line of the same spectrum having the same laboratory wave length.

TABLE 1

SOLAR SPECTRUM FROM 3000A to 2200A

3000A to 2488 from March 7, 1947; 2488 to 2200 from October 10, 1947. For explanation of symbols see page

OBSERVED		IDENTIFICATIONS				OBSERVED		IDENTIFICATIONS			
Solar λ	Est. I	Spectr.	Lab. λ	Lab. I	Mult.	Solar λ	Est. I	Spectr.	Lab. λ	Lab. I	Mult.
2999.4	10	#Fe I	99.512	30R	45			Fe II	47.658	13	94
94.2	20	#Fe I	94.507	100R*	3	2944.4	8n	V II	44.568	250	13
		#Fe I	94.427	100R*	1			#Fe II	44.399	13	94
91.8	4	Cr I 9; Cr II 14				41.2	8n	V II	41.485	100	13
		Fe I Uncl; Ni I 27						V II	41.372	200	13
87.7	7	#Si I	87.65	25	10			#Fe I	41.343	15r	2
		Fe I	87.292	10	45	38.8?	5	Fe II	39.506	5	71
85.1D	5r	#Fe II	85.545	13	94			Mn II	39.309	150	1
		#Fe II	84.831	15	94	36.8	18	#Fe I	36.904	60R	2
84.0	20	#Fe I	83.574	125R	1			Mg II	36.496	(35)	2
81.5	9	Ni I	81.65	20R	28	33.0	5	Mn II	33.057	100	1
		#Fe I	81.446	20r	3	28.8	20	Fe I	29.008	25r	2
78.5	5	#Fe II	79.349	8	71			#Co I	28.812	50	2
75.9	4	#V II 120 - 3 lines						Mg II	28.625	(35)	2
		Fe I	76.126	5	139	26.4	8	#Fe II	26.584	12	71
		Fe II	75.938	5	71	23.7	6	# V II	24.017	300R	13
73.1	15	#Fe I	73.237	60R	2			#Fe I	23.851	7	177
		#Fe I	73.134	60R	2			V I	23.627	70R	2
69.6	25	Fe II	70.510	10	71	17.9	4n	Fe I	18.023	10	194
		#Fe I	*70.106	40R	2			Fe II	17.465	4	72
		#Fe I	*70.106	40R	3	14.8	10n	V I	14.924	50R	2
		#Fe I	69.474	10	45			Mn I	14.62	50	1
66.0	20	#Fe I	66.901	125R	2	10.8?	N	Fe II 387; V II 13			
64.6?	10v	#Fe I	*65.255	20	2	07.8?		V II 14; V II 15			
		#Fe I	*65.255	20	174	05.6?					
		Fe II	64.629	9	94	02.2	8n	V II	03.068	100	14
		Fe II	64.131	7	357			Fe II	02.459	5	387
60.1	10n	#Fe II	61.272	5	71	2898.1	10nd?	Cr II	98.539	12	20
		#Fe II	59.601	7	359			Fe II	97.264	8	359
57.0	7	V II	57.520	100	13	93.8	8n	Fe II	94.776	7	333
		#Fe I	57.365	30R	2			V II 15 - 5 lines			
53.7	12	#Fe I	53.940	50R	2	81.1	80	#Si I	81.595	200r	11
		Fe II	53.774	11	71	78.5	8	Fe II	79.241	4	387
		Fe I	53.486	5	177			V II	79.158	40	15
51.7D	3	V II	52.07	150	13	75.8	7	Cr II	75.998	20	9
		Cr II	51.40	10	25			Fe I	75.302	5	94
49.1?	15r	Mn II	49.209	200	1	73.2	9n	Fe I 4; Fe I 48			
		Fe II	49.178	10	386			Fe II 333; Fe II 388			
47.8	30	#Fe I	47.877	60R	2	69.3	8	Fe I	69.308	10	4

TABLE 1 (Cont.)

OBSERVED		IDENTIFICATIONS				OBSERVED		IDENTIFICATIONS			
Solar λ	Est. I	Spectr.	Lab. λ	Lab. I	Mult.	Solar λ	Est. I	Spectr.	Lab. λ	Lab. I	Mult.
		V II	69.131	150	244	2781.5D		V II	81.48	100N	332
		Fe II	68.874	5	72			Mg I	*81.418	10	18
2867.4	10d?	Cr II	67.655	12	4	79.7?	6	Mg I	79.832	12	18
		Cr II	66.711	15	4			#Fe II	79.302	11	337
65.2?	6	#Cr II	65.112	25	4	78.4?	6	Co I	78.813	75	188
61.2?	5n	Cr II 4; Fe II 72; Ti II 13						Mg I	*78.277	10	18
58.8?	7	Cr II	58.92	25	4			Fe I	78.221	20	49
		#Fe II	*58.340	11	285	76.0?	4	Mg I	*76.695	10	18
		#Fe II	*58.340	11	388			Fe II	76.180	4	290
51.6	200	#Mg I	52.120	300R	1			Mn II	75.654	50	8
48.1?	5v	Fe II	48.046	8	286	72.0	10	#Fe I	72.083	20	50
43.4	15	#Fe I	43.977	20r	49	70.2D	3	Fe II	*70.507	5	288
		Fe I	43.631	10	48			Cr I	69.915	50r	11
		#Cr II	43.254	75	4	68.5	15n	#Fe II	68.940	8	74
40.5	7	Fe II	40.756	8	389			#Fe I	67.523	20	51
		Fe II	40.644	9	315			#Fe II	*67.500	13	338
		Fe II	40.342	7	285	66.7	8	#Cr II	66.542	30	5
		Cr II	40.022	30	15			Co I	66.382	50	65
35.5	15	Fe II	35.716	9	314	64.1D	3	Cr I	64.364	25r	11
		#Cr II	35.640	100	4			Co I	64.188	100r	65
34.1?	4	Co I	34.428	50	65			Fe II	63.913	3	290
		Co I	33.922	40	5	62.0	20	Fe I	62.027	15	51
31.9?	3	#Fe I	32.436	25r	49			#Fe II	61.813	9	74
		Fe II	31.562	11	315			Fe I	61.780	18	51
30.8D	3	Cr II	30.473	50	15	59.9?	8nd?	V II	60.710	60	224
26.7D		Co I	26.797	50w	186			V II	60.122	40	121
25.7	5	#Fe I	25.557	20	50			Fe I	59.814	4	52
		Co I	25.151	75w	188	55.7	60	Fe I	56.329	20	7
21.7	3	Cr II	22.020	20	27			#Fe II	55.733	15	73
		Ni I	21.30	15	30	53.6?	10	Fe I	53.687	3	51
18.2	15N	Co I	18.592	30	5			#Fe II	53.289	12	338
15.3		Co I	15.555	50r	65	49.6	60	#Fe I	50.140	25r	7
12.7	12	Fe I	13.288	30R	49			#Fe II	49.482	12	74
		Cr II	12.006	40	31			Fe II	49.324	14	73
03.7	no line	See Section IX						#Fe II	49.178	13	74
02.3	700 Em	#Mg II	02.698	40	1	46.5	50	Fe I	*46.982	20	50
01.1	no line	See Section IX						#Fe II	46.978	14	74
2796.8	no line	See Section IX						Fe II	46.487	14	73
95.4	1000 Em	#Mg II	95.523	60	1	42.6	60n	Fe I	44.068	10	7
94.1	no line	See Section IX						#Fe II	43.196	14	73
83.6?	5	#Fe II	83.690	12	337			#Fe I	42.406	30r	7
		Mg I	82.974	10	18			Fe I	42.256	20	51

TABLE 1 (Cont.)

OBSERVED		IDENTIFICATIONS				OBSERVED		IDENTIFICATIONS			
Solar λ	Est. I	Spectr.	Lab. λ	Lab. I	Mult.	Solar λ	Est. I	Spectr.	Lab. λ	Lab. I	Mult.
2739.5	40	#Fe II	39.545	15	74			#Mn II	72.588	20	14
37.1	40	#Fe I	37.310	20r	7			# V II	72.005	150r	3
		#Fe II	36.968	12	74			Cr II	71.818	25	7
35.4	4	#Fe I	35.475	8	51	2669.4	25	#Al II	69.116	10	1
33.5	15	#Fe I	33.581	15	51			Cr II	68.722	25	7
		Ti I	33.265	30	43	66.5	15	Mn II	67.033	12	15
30.7	8n	Cr I	31.914	40r	4			#Fe I	66.811	8	53
		#Fe II	30.735	11	73			#Cr II	66.026	35	7
27.3	20n	#Fe II	27.538	13	74	63.6	18	Co II	63.530	60	4
		Cr I	26.524	35r	4			Cr II	63.430	20	7
23.7	20n	Fe II	24.879	9	73			V II	63.25	250N	326
		#Fe I	23.577	15	7	61.5	10	# V I	61.424	(70R)	4
20.8	30	#Fe I	20.902	40r	7	58.4?	6	#Cr II	58.603	30	7
19.2	45	#Fe I	*19.027	60R	7	56.2?	4	# V I	56.224	(60R)	4
14.5	30	#Fe II	14.414	13	74			Mn II	55.925	10	15
11.7	N	# V II	06.17	200r	1			# V II	55.68	200N	326
		#Mn II	05.561	10	14	53.6?	3	#Cr II	53.594	25	7
		Cr II 32; Fe I 52				50.7	12	V I	51.896	(50R)	4
		Fe I 53; Fe II 292						Co I	50.266	50w	68
05.9		Fe II 316; Mn II 11				48.4	35n	V II	49.37	150N	326
01.4	20	Mn II	01.696	30	11			V I	47.710	(40R)	4
		#Mn II	01.171	12	13			Fe I	47.558	3	8
		#Mn II	01.035	10	14	46.5	45N	Fe I 57; Ti I 8			
		V II	00.944	300r	1			Ti II 26; V II 138			
2698.5	35nd?	Fe II	99.107	6	53	44.1		V II 326			
		Mn II	98.989	8	13	41.8?	55N	Mn II 15; Ti I 8			
95.5	40nd?	Co I	95.846	50w	68	39.4?		V II 138			
		Mn II	95.366	8	14	35.6?	15	#Fe I	35.808	8	57
		Co II	94.679	25	4	31.3	60d?	#Fe II	31.321	13	1
92.9	8	Mn II	93.191	15	14			#Fe II	*31.045	13	1
		Fe II	92.826	5	73			#Fe II 248 - 4 lines			
		Fe II	92.601	10	392	28.3	12	#Fe II	28.291	13	1
89.4	30nd?	#Fe I	89.212	8	53	25.4	30	#Fe II	25.664	13	1
		#V II 3 - 5 lines				23.5?	6	#Fe I	23.532	5	57
85.9	20N	# V II	83.09	100	3	21.8	8	#Fe II	21.669	10	1
		# V II	82.875	100	3	20.3?	4v	#Fe II	20.408	6	1
82.8		Co I 68; Fe II 392				17.7	45	#Fe II	17.618	12	1
79.2	10	#V II 3 - 3 lines				13.6	50	#Fe II	13.820	13	1
		Fe I	79.062	10	52	11.4	50	#Fe II	11.873	13	1
77.3D	8v	#Cr II	77.20	35	7			Fe II	11.075	6	75
		#Cr II	77.12	25	7	07.2	40	#Fe II	07.086	13	1
72.4	35	Cr II	72.838	20	7	05.2?	25v	#Mn II	05.696	75	17

TABLE 1 (Cont.)

OBSERVED		IDENTIFICATIONS				OBSERVED		IDENTIFICATIONS			
Solar λ	Est. I	Spectr.	Lab. λ	Lab. I	Mult.	Solar λ	Est. I	Spectr.	Lab. λ	Lab. I	Mult.
2598.9	80	#Fe II	99.395	14	1			#Fe I	35.604	8r	9
		Mn II	98.910	15	18			#Fe II	35.480	7	254
		#Fe II	98.369	14	1			Fe II	34.413	9	228
93.6	35	#Mn II	93.731	90	17	2532.4?	Wk	Fe II	33.626	10	228
		Fe II	93.722	7	75			Si I	32.38	20	14
91.1	30n	Cr I	91.861	50r	17	28.2	St n	#Fe II	*29.545	10	254
		#Fe II	91.542	10	75			Fe I	29.134	10r	9
88.3	20	Fe II	87.945	7	443			#Si I	28.513	175r	1
85.8	50	#Fe II	85.876	13	1			#Fe I	27.433	15r	9
		Fe I	84.536	8	57	26.2?	Wk	Fe II	25.386	10	228
82.6	30	#Fe II	82.582	10	75	23.0	St n	#Si I	24.112	125r	1
75.7	60	Fe II	76.859	7	443			#Fe I	22.848	40R	9
		#Mn II	76.113	100	17	18.7	Md	#Si I	19.206	100r	1
		V II	74.520	60	64			Fe I	18.100	12r	9
70.8?	6	Fe II	70.843	7	393	16.2?	Wk	#Si I	16.111	250r	1
62.6	50d?	#Fe II	63.472	12	75	14.5	Wk	#Si I	14.320	100r	1
		#Fe II	*62.535	13	75	10.9	20	Ni II	10.87	30	5
		Fe II	62.094	6	320			#Fe I	10.833	15R	9
60.2?	10nv	Cr I	60.69	30	17	06.7	50	#Si I	06.896	150r	1
		Fe II	60.278	7	320	03.0?	8	Fe II 297; Fe II 298			
57.1	12	Cr I	*57.14	25	17			Fe II 394; V II 35			
		Co I	56.762	50w	73	01.3	35	#Fe I	01.130	20R	9
55.1D		Fe II	55.447	5	254	2498.5?	6	Fe II	98.897	10	230
		Fe II	55.066	5	254			Fe I	98.895	10	11
		P I	54.93	30	4			Fe II	97.817	7	298
53.1	20	V II	53.668	40	64	96.4	8	Cr I	96.30	35r	20
		P I	53.28	40	4	90.4	St	#Fe I	91.155	20R	10
		Co I	53.004	40r	74			#Fe I	90.642	30R	10
49.4	Md	#Fe I	49.612	10r	9			Fe I	89.751	15r	10
		Fe II	49.453	8	254	87.8	Md	#Fe I	88.143	40R	10
		Fe II	49.399	8	254	83.0	St	#Fe I	83.270	60	10
		Fe II	48.590	6	227	79.4	Md	#Fe I	79.775	20R	10
45.9?	Wk	Fe II	46.667	8	254			V II	79.518	180	107
		#Fe I	45.977	10r	9			V II	79.043	200	107
		Fe II	45.215	7	228			C I	78.525	10	1
41.0	Wk	Fe II	41.831	7	227	73.0	Md	#Fe I	72.910	12R	10
		Fe II	41.096	7	254	63.0	Md N	#Fe I	62.645	10r	10
		#Fe I	40.971	10R	9			Fe II	61.855	8	300
		Fe II	*40.669	6	254			Fe II	61.282	8	300
38.6?	Wk	#Fe II 227 - 4 lines				60.4		Co I	60.800	20	9
35.5	Md	Fe II	*36.822	9d	228			Fe II	58.782	8	300
		P I	35.65	50	4	56.1?	Wk	See notes			

TABLE 1 (Cont.)

OBSERVED		IDENTIFICATIONS				OBSERVED		IDENTIFICATIONS			
Solar λ	Est. I	Spectr.	Lab. λ	Lab. I	Mult.	Solar λ	Est. I	Spectr.	Lab. λ	Lab. I	Mult.
2453.7?	Md N	V II	53.346	80	143	61.8	25N	#Fe II	60.287	8	43
		Mn II	52.488	25	27	2358.3		#Fe II	*59.111	8	3
50.5?		Fe II 410 - 2 lines				55.6	15n	Ni II	56.41	25	9
47.4?	Wk	Fe I	47.708	4	10	50 D	N	#Fe II	48.300	8	3
		Fe II 410 - 3 lines						#Fe II	48.118	8	43
43.4	Wk							#Fe II	44.278	8	3
39.2	Md	Fe II	39.301	8	300	44 D		#Fe II	43.495	8	3
		Co I	39.038	20R	9	39 D	20n	#Fe II	38.005	8	3
36.7	Wk	#Co I	36.657	50R	9			Ni I	37.49	50	9
		Mn II 27 - 3 lines				35 D	30N	#Fe II	32.798	8	3
35.3	Md	#Si I	35.160	100r	4	33 D					
32.3	Wk	#Co I	32.213	40R	9	31 D					
28.7	Wk	Fe II 410; Fe II 411;				29 D	n	Ni I	29.97	50	9
		V I 10				28 D	35N	#Fe II	27.391	7	3
26.0	St Nd?	#Co I	24.932	250R	9	25 D		Ni I	25.80	50	10
23.1		Fe II 411 - 3 lines				23 D	60N	#Ni I	21.39	60	10
13.6	St Nd?	#Fe II	13.308	9	2			#Fe I	20.356	(40)	16
		#Fe II	11.062	9	2			#Ni I	20.03	100	10
		#Fe II	10.521	9	2			Ni I	17.16	50	9
10.1		Co I 10; Co I 14				18 D		#Ni I	13.98	100	11
07.3?	Md	Co I	07.249	100	10	15	150N	#Fe I	13.102	(40)	16
		#Fe II	06.660	9	2			#Ni I	12.34	50	11
04.7	Md	#Fe II	04.882	9	2			#Ni I	10.96	100	11
		#Fe II	04.430	7	2			#Fe I	08.997	(30)	16
2398.8?	Md	#Fe II	*99.237	9	2	08		#Fe I 16 - 5 lines			
		Fe II	*99.237	9	43	04	N	#Fe I 17 - 3 lines			
		Ca I	98.58	(2)	4	2297		Fe I	92.523	(30)	17
95.5	St	#Fe II	95.627	9	2	92 ?D	n				
		#Fe II	95.416	7	2	80 D	N				
						36 D					
88.9	St	Fe I	89.971	(25)	13	32 D	N	Si I 2 - 6 lines			
		Co II	88.90	100	1	07 D					
		#Fe II	88.629	9	2						
85 D	100N	Fe II	83.060	4	2						
		#Fe II	82.034	9	2						
		#Fe II	80.757	7	3						
79 D		Fe II 43 - 3 lines									
73.9	30N	Fe II	75.180	10	43						
		#Fe II	73.733	8	2						
69.6	N	Fe II	68.593	7	43						
		#Fe II	64.825	8	3						
65.5		Cr I 8 - 3 lines									

NOTES FOR TABLE 1

Most of the following notes serve to call attention to features on the densitometer traces of Figure 4 that are not apparent in Table 1. All references to structure apply to Figure 4.

2966.0	Wave-length discrepancy possibly due to blister on film.
2923.7–2917.7	Depressed region. Probably contains *V* II 13 and 14 and others.
2893.8–2886.5	Depressed region.
2878.5	Probable error in visual wave length caused by neighboring *Si* I line.
2865.0–2840.0	Wings of *Mg* I 1, 2852.12 A. Several small inflections show in either wing. These are probably due to *Na* I 1, *Cr* II 4, and several multiplets of *Fe* II.
2825.8	Unresolved line in violet wing, possibly *Cu* I, 2824.7 A.
2825.0–2775.0	Wings of *Mg* II 1, 2802.698 and 2795.523. Most of the numerous inflections which may be seen in the traces were excluded from the table. Between 2812.7 and 2810.3 A the depression below the wing contour is pronounced. This is attributed to *Co* I 186 and 188, and *V* II 59, in addition to the lines tabulated.
2821.7	Four partially resolved lines fill the region between 2423.1 and 2421.0. These are identified as *Fe* I 49, 23.28; *Cr* II 15, 22.37; *Co* I 198, 21.74, plus the lines in the table.
2711.7–2705.9	Broad uniform absorption apparently caused by numerous closely spaced lines. Six individual peaks are resolved on the trace.
2689.4–2687.0	Moderate absorption between 2691 and 2687 A, on which is superimposed the listed line.
2669.4	Unresolved line in violet wing, probably *Cr* II 7.
2661.5	Unresolved line in violet wing, probably *Al* I 1, 2660.39 A.
2650.7	Unresolved line in red wing, probably *Al* I 1, 2652.48.
2562.6	*Ca* I 14, 2564.07 and 2565.17, probably present in red wing.
2516.2	See Sec. VIII for discussion of true intensity of the lines in this region.
2498.5–2496.4	Weak general depression, probably caused by *Fe* I, *Fe* II, and *Cr* I; but the ultimate lines of *B* I 1, 2497.73 and 2496.78 A may be present.
2498.0–2475.0	Large general depressed region, apparently caused by many lines of *Fe* I and *Fe* II.
2475.0–2442.0	Large general depressed region. The many lines of *Fe* I and *Fe* II present here are apparently unable to account for this feature. May be caused by unidentified band.
2456.1	The *As* I 2456.53 line was considered at the suggestion of Dr. H. N. Russell. The high excitation potential, 6.37 volts, and inconclusive evidence for *As* in the sun make this identification doubtful without further evidence. Other lines of *As* I in the region photographed are badly masked.
2395.5	Possible unidentified strong line at 2394 A.
2292.0–2200.0	See Sec. X.

FIFTH COLUMN—LABORATORY INTENSITIES

1. Intensities were taken from Mrs. Sitterly's multiplet lists (see Sec. VI). A discussion of her general notation and the types of scale used may be found on page xv of her *Revised Multiplet Table*.[12]

SIXTH COLUMN—MULTIPLET NUMBERS

1. These are arbitrary numbers assigned to the multiplets for reference purposes (see Table 2). These numbers are also used to identify certain multiplets in the text, e.g., *Fe* I 9 stands for multiplet No. 9 of the *Fe* I spectrum.

VIII. MULTIPLETS OF INTEREST

A number of important multiplets are shown in Figure 4, *A*. Many others may be picked out from Table 1 by reference to the multiplet numbers. Among the more important multiplets are *Fe* I 9 and *Si* I 1, which combine to produce the large depression in the spectrum between 2500 and 2550 A. A careful examination of these two strong multiplets reveals some of the difficulties of visual observations of the original spectra. For example, the two weak lines listed at 2514.5 A and 2516.2 A are attributed to 2514.32 and 2516.11 of *Si* I 1. They should be very strong. Reference to the densitometer record of Figure 4, *A*, shows that these lines combine with a broad line at 2518.7 A to produce a large depression in the spectrum. The apparent weakness then comes from the close

[12] Charlotte E. Moore, *A Revised Multiplet Table of Astrophysical Interest* (*Contr. Princeton U. Obs.*, No. 20).

TABLE 2

MULTIPLETS AND EXCITATION POTENTIALS

Mult. No.	E. P. Low	Multiplet
Al I		
1	0.00	$3p^2P^o$-$5s^2S$
Al II		
1	0.00	3^1S-3^3P^o
3	7.39	3^1P^o-4^1S
B I		
1	0.00	$2p^2P^o$-$3s^2S$
C I		
1	2.67	$2p^2\,^1S$-$3s^1P^o$
Ca I		
4	0.00	4^1S-5^1P^o
14	1.87	4^3P^o-$3d^4d^3P$
Co I		
2	0.00	a^4F-y^2G^o
5	0.00	a^4F-y^2D^o
9	0.00	a^4F-x^4F^o
10	0.00	a^4F-x^4G^o
14	0.00	a^4F-w^4D^o
65	0.43	b^4F-x^4D^o
68	0.43	b^4F-x^4F^o
73	0.43	b^4F-w^4D^o
186	1.87	b^4P-s^4D^o
188	1.87	b^4P-w^4P^o
198	2.13	a^2G-t^2F^o
Co II		
1	0.41	$4s^5F$-$4p^5F^o$
4	1.21	$4s^3F$-$4p^3G^o$
13	5.99	$4p^3G^o$-$5s^3F$
14	5.81	$4p^5G^o$-$5s^3F$
Cr I		
4	0.94	a^5S-w^5P^o
8	0.00	a^7S-x^7P^o
9	0.96	a^5D-y^5D^o
11	0.96	a^5D-w^5P^o
17	0.96	a^5D-u^5P^o
20	0.96	a^5D-u^5F^o
Cr II		
4	1.48	a^6D-z^6F^o
Cr II (Continued)		
5	1.48	a^6D-z^6P^o
7	1.48	a^6D-z^6D^o
9	2.41	a^6D-z^4D^o
14	3.72	a^4H-z^4H^o
15	3.72	a^4H-z^4I^o
20	3.84	a^4F-z^4G^o
25	4.13	b^4G-y^4F^o
27	4.13	b^4G-y^4H^o
31	4.90	c^2G-x^2F^o
32	4.13	b^4G-x^4G^o
Fe I		
1	0.00	a^5D-y^5D^o
2	0.00	a^5D-y^5F^o
3	0.00	a^5D-z^3P^o
4	0.00	a^5D-z^5G^o
7	0.00	a^5D-y^5P^o
8	0.00	a^5D-y^3D^o
9	0.00	a^5D-x^3D^o
10	0.00	a^5D-x^5F^o
11	0.00	a^5D-y^7P^o
13	0.00	a^5D-x^5P^o
16	0.00	a^5D-w^5D^o
17	0.00	a^5D-w^5F^o
45	0.86	a^5F-x^5F^o
48	0.86	a^5F-x^5P^o
49	0.86	a^5F-y^5G^o
50	0.86	a^5F-z^3H^o
51	0.86	a^5F-w^5D^o
52	0.86	a^5F-w^5F^o
53	0.86	a^5F-v^5D^o
57	0.86	a^5F-x^5G^o
94	1.48	a^3F-u^5D^o
126	2.17	a^5P-t^5D^o
139	2.27	a^3P-u^3D^o
174	2.68	a^3G-v^3H^o
175	2.68	a^3G-x^1H^o
177	2.68	a^3G-s^3G^o
194	3.22	b^3H-t^3H^o
Fe II		
1	0.00	a^6D-z^6D^o
2	0.00	a^6D-z^6F^o
3	0.00	a^6D-z^6P^o
43	0.23	a^4F-z^4D^o
71	0.98	a^4D-z^6F^o
72	0.98	a^4D-z^6P^o
73	0.98	a^4D-z^4F^o
74	0.98	a^4D-z^4D^o
75	0.98	a^4D-z^4P^o
94	1.66	a^4P-z^4P^o
227	2.62	a^4H-z^4G^o
228	2.62	a^4H-z^4H^o
230	2.62	a^4H-z^4I^o
248	2.79	b^4F-z^4G^o
254	2.79	b^4F-y^4F^o
285	3.14	a^4G-z^4G^o
286	3.14	a^4G-z^4H^o
288	3.14	a^4G-z^4I^o
290	3.14	a^4G-y^4F^o
292	3.14	a^4G-z^2I^o
297	3.14	a^4G-z^2I
298	3.14	a^4G-x^4
300	3.14	a^4G-y^4
314	3.18	b^2P-z^4
315	3.18	b^2P-z^2_
316	3.18	b^2P-y^4D^o
320	3.18	b^2P-z^2P^o
333	3.23	b^2H-z^4H^o
337	3.23	b^2H-z^2G^o
338	3.23	b^2H-z^2I^o
357	3.37	a^2F-z^4G^o
359	3.37	a^2F-z^2D^o
386	3.75	b^2G-z^2F^o
387	3.75	b^2G-y^2G^o
388	3.75	b^2G-z^2H^o
389	3.75	b^2G-x^4G^o
392	3.75	b^2G-y^2H^o
393	3.75	b^2G-y^2F^o
394	3.75	b^2G-x^2G^o
410	3.87	b^4D-w^4F^o

TABLE 2 (Cont.)

Mult. No.	E. P. Low	Multiplet
Fe II (Continued)		
411	3.87	$b^4D\text{-}w^4D^o$
443	4.13	$c^2G\text{-}x^2H^o$
Mg I		
1	0.00	$3^1S\text{-}3^1P^o$
18	2.70	$3^3P^o\text{-}3p^{2\,3}P^o$
Mg II		
1	0.00	$3s^2S\text{-}3p^2P^o$
2	4.40	$3p^2P^o\text{-}4s^2S$
Mn I		
1	2.27	$z^8P^o\text{-}s^8D$
Mn II		
1	1.17	$a^5S\text{-}Z^5P^o$
11	3.40	$a^3G\text{-}z^5G^o$
13	3.69	$a^3P\text{-}z^5S^o$
14	3.69	$a^5P\text{-}z^5D^o$
15	4.05	$b^5D\text{-}y^5F^o$
17	0.00	$a^7S\text{-}z^7P^o$
18	3.69	$a^3P\text{-}y^5P^o$
27	4.74	$z^7P^o\text{-}e^7D$
Na I		
1	0.00	$3^2S\text{-}5^2P^o$

Mult. No.	E. P. Low	Multiplet
Ni I		
9	0.00	$a^3F\text{-}w^3D^o$
10	0.00	$a^3F\text{-}y^3G^o$
11	0.00	$a^3F\text{-}w^3F^o$
27	0.03	$a^3D\text{-}y^3F^o$
28	0.03	$a^3D\text{-}y^3D^o$
30	0.03	$a^3D\text{-}y^1F^o$
Ni II		
5	1.85	$a^2F\text{-}z^4G^o$
9	1.85	$a^2F\text{-}z^2D^o$
P I		
4	2.31	$3p^{3\,2}P^o\text{-}4s^2P$
Si I		
1	0.00	$3p^{2\,3}P\text{-}4s^3P^o$
2	0.00	$3p^{2\,3}P\text{-}3d^3D^o$
4	0.78	$3p^{2\,1}D\text{-}3d^1D^o$
10	0.78	$3p^{2\,1}D\text{-}4s^3P^o$
11	0.78	$3p^{2\,1}D\text{-}4s^1P^o$
14	1.90	$3p^{2\,1}S\text{-}5s^1P^o$
Ti I		
8	0.00	$a^3F\text{-}u^3D^o$
43	1.04	$a^3P\text{-}t^3P^o$

Mult. No.	E. P. Low	Multiplet
Ti II		
13	1.22	$a^2P\text{-}x^2D^o$
16	1.22	$b^4P\text{-}y^4P^o$
V I		
2	0.00	$a^4F\text{-}v^4D^o$
4	0.00	$a^4F\text{-}t^4D^o$
10	0.00	$a^4F\text{-}t^4F^o$
V II		
1	0.00	$a^3D\text{-}z^5F^o$
3	0.00	$a^3D\text{-}z^5D^o$
13	0.32	$a^5F\text{-}z^5F^o$
14	0.32	$a^5F\text{-}z^3D^o$
15	0.32	$a^5F\text{-}z^5D^o$
35	1.07	$a^3F\text{-}y^3G^o$
59	1.39	$a^3P\text{-}y^5D^o$
64	1.39	$a^3P\text{-}y^3P^o$
107	1.67	$b^3F\text{-}w^3D^o$
120	1.67	$a^5P\text{-}y^5D^o$
121	1.67	$a^5P\text{-}z^5S^o$
138	1.79	$a^3G\text{-}x^3F^o$
143	1.79	$a^3G\text{-}x^3G^o$
224	2.37	$a^1I\text{-}z^1I^o$
244	2.50	$b^3H\text{-}x^3G^o$
326	4.27	$z^5G^o\text{-}e^5H$
332	4.59	$z^5F^o\text{-}e^5F$

proximity of these lines to each other and to other strong lines. Also note that 2518.7 and 2523.0 are broad and flat-bottomed. In contrast, other lines in this vicinity are quite sharp. This is clearly due to the fact that each of these lines is double, each receiving strong contributions from both *Si* I 1 and *Fe* I 9.

A second interesting pair of multiplets is *Fe* II 1 and *Mn* II 17, near 2600 A. Each of the thirteen lines of the *Fe* II multiplet is resolved, as well as two of the three *Mn* II lines. The third *Mn* line was seen by some observers as a shoulder to the violet side of the *Fe* line at 2607 A, while other observers saw the two as a single line. The densitometer trace shows that the shoulder is well defined and that both lines are definitely present.

IX. ENERGY DISTRIBUTION

Intensity calibration marks were put on each film prior to the flight, with a carbon arc as a source of radiation of known energy distribution. A curve of the solar energy distribution as a function of wave length, deduced from the October 10 spectra, has already been published.[4] Figure 5 is a similar curve, based on the March 7, 1947, spectra, except that the absorption-line structure is reproduced in more detail. Intensities are plotted as percentages of the intensity values for a 6000° K black body. The black-body curve was adjusted so that its maximum coincided with the maximum of the solar intensity-curve at about 4800 A, and the intensity at this point was taken to be 100 per cent.

The March 7 spectrograph used a cylindrical mirror, so that the calibration spectra exhibited the change in width referred to in Section II. Densitometry of these spectra was so difficult that it was finally abandoned, and the H and D characteristic curves of the October 10 film were used instead.

Developing conditions were carefully controlled, and the two films were from the same emulsion lot. The uncertainty in film contrast (γ) value is therefore probably less than 10 per cent. For the density range of 1.9 represented in Figure 5, the maximum uncertainty would be 0.19 in density, 0.125 in log intensity, or 0.10 in intensity.

Of particular interest in Figure 5 is the region surrounding the great *Mg* II pair at 2803 and 2796 A. The wings of these two lines clearly extend out 25 A or more to either side and may extend much farther still. Presumably, this magnesium absorption occurs deep in the reversing layer, where pressure-broadening effects are large.

In the "bottom" of the absorption valley three maxima may be noted. Two of these coincide within a fraction of an angstrom with the known wave lengths of the magnesium lines and are undoubtedly due to the emission of these lines in a high-temperature, low-pressure region high in the sun's atmosphere. The third peak in the center is the result of the intersection of the rising slopes of the two broad absorption lines. It is interesting to note that in Figure 4, *A*, the emission peaks are pointed, corresponding to the characteristic response of the spectrograph for isolated lines, while the third peak is of a rounded nature. The intensity minima to either side of the emission lines are obviously not central cores of true absorption lines. They are listed in Table 1 with the notation "no line."

Dr. D. H. Menzel, of Harvard, predicted that these emission lines would be found in great strength. He also was the first to point them out in the rocket spectra. In the previously known regions of the solar spectrum, only H and K of *Ca* II show emission in the total sun, and they are weak in comparison with the *Mg* II pair.

The shape of the *Mg* emission lines is undoubtedly determined primarily by the response characteristic of the spectrograph. The line 2803 A shows up as would a very sharp line. There is some suggestion, however, that 2796 A may be slightly broadened, indicating a true line width of the order of 1 A. The true intensities of these lines must be somewhat greater than is shown in Figure 5, and they might be several times greater.

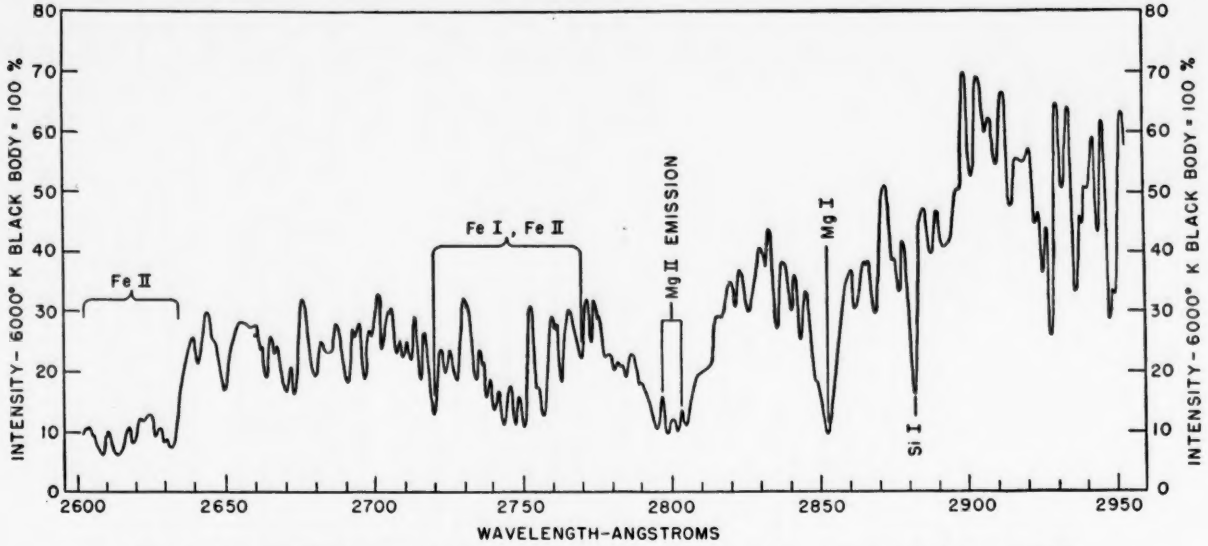

FIG. 5.—Spectrum No. 43 replotted on a linear intensity scale relative to the intensity of a black body at 6000° K

X. BANDS

The concept of the band interpretation came about from the failure of an attempt to explain the structure between 2200 A and 2280 A in terms of atomic lines. A large number of lines of *Fe* I and *Fe* II exist in this region, but no assumed values of multiplet strengths were able to account for the observed structure. For instance, although the region between 2255 and 2279 A is clearly depressed below the regions to either side, one can find no corresponding increase in either the number or the strength of the *Fe* lines in this region. Other regions that may be caused by bands lie from 2440 to 2470 A and from 2205 to 2221 A, although part of the structure in the latter region may be caused by the multiplet *Si* I 2.

It is not the purpose of this paper to analyze the possible band spectra involved, but it might be noted that there does exist a strong band of nitric oxide centered at 2264 A. Leifson[13] has shown that a layer of *NO* only 0.5 mm thick (N.T.P.) produces appreciable absorption in this band. The spectrum of Figure 4, *C*, was taken at 55 km, at which altitude the residual atmosphere above the spectrograph was equivalent to about 5 meters of air at N.T.P. Consequently, an average concentration of only 0.01 per cent of *NO* in the outer atmosphere would be detectable.

The authors are grateful to the many persons who have assisted both in the experimental work of obtaining the spectra and in the analysis which is reported here. Particular thanks are due Mr. F. S. Johnson, of the Micron Wave Section, Optics Division, for his work in preparing spectrographs for flight and supervising their installation and launching. Thanks are also due Mr. J. D. Purcell for his work with Mr. Johnson and also for his assistance in the densitometry of the film and the preparation of Figure 5; to Mrs. Sitterly, who generously supplied a veritable gold mine of material and who gave much needed help and advice based on her long experience in spectral analysis; and to Dr. E. H. Krause and the other members of the Rocket Sonde Research Section of Radio Division I for assistance in the experimental phases of the work.

[13] *Ap. J.*, **63**, 73, 1926.

TELLURIC BANDS OF CH_4 IN THE SOLAR SPECTRUM

ROBERT R. MCMATH, ORREN C. MOHLER, AND LEO GOLDBERG
McMath-Hulbert Observatory, University of Michigan
Received July 24, 1948

ABSTRACT

An all-reflecting telescope and spectrometer have been employed in conjunction with a Cashman *PbS* cell to secure a direct-intensity map of the solar spectrum in the region of 0.8–2.5 μ with a resolution of about 50,000. Four molecular-band systems at 1.66, 2.20, 2.32, and 2.37 μ have been identified as the $2\nu_3$, $\nu_1 + \nu_4$, $\nu_3 + \nu_4$ and $\nu_2 + \nu_3$ transitions of CH_4 in the earth's atmosphere.

A preliminary analysis of the wave numbers of the $2\nu_3$ rotational components indicates second-order deviations from theory. The average half-spacing B_0 is found to be 5.163, as compared with the value $B_0 = 5.252$ obtained by Childs.

A comparison of the $2\nu_3$ telluric line intensities with those produced by a measured quantity of methane at room temperature leads to a calculated methane abundance in the earth's atmosphere of 1.2 parts in a million by mass, and a temperature of $-37°$ C.

INTRODUCTION

Since June, 1947, the writers have been engaged in mapping the solar spectrum beyond the infrared limit of the photographic plate, employing a lead sulphide photoconductive cell as an energy detector. The first observations[1] were made on an experimental basis, the *PbS* cell being driven on a lead screw along the focal plane of the McGregor spectrograph. The original optical system was inefficient because of absorption by the lenses in the McGregor tower and spectrograph. Nevertheless, preliminary experiments resulted in the extension of the solar spectrum with high resolution to about 2μ.

THE ALL-REFLECTING SPECTROMETER

Late in 1947 an all-reflecting spectrometer of the Pfund type, especially designed and constructed for the infrared application, was installed inside the existing McGregor spectrograph. The new spectrometer employs a 15,000-line, plane-reflection grating, together with two parabolic and two plane mirrors. The focal length of each of the parabolic mirrors is approximately $23\frac{1}{2}$ feet. The grating, which was ruled at the Mount Wilson Observatory, produces a high concentration of energy in the first order at λ 20,000. We are indebted to Dr. I. S. Bowen for the loan of this grating. The imaging lens in the tower will soon be replaced by a 12-inch by 50-foot off-axis parabola. In the interim we have been utilizing a $10\frac{1}{2}$-inch Cassegrain reflector, which was originally employed at Lake Angelus in conjunction with the so-called "spectroheliokinematograph" for motion-picture photography of the solar disk and prominences.

The observations were carried out in the first order of the grating spectrum. A predispersing unit, consisting of a low-dispersion spectroscope, eliminates interference from overlapping orders of the grating. The entrance slit of the monochromator is located in the focal plane of the solar imaging telescope, the exit slit being also the entrance slit of the spectrometer. The optical components of the monochromator are a calcium fluoride prism and four mirrors, two plane and two parabolic. Rotation of one of the parabolic mirrors makes possible the selection of any portion of the spectrum. The construction of all mechanical parts of the spectrometer and accessories was carried out in the McMath-Hulbert Observatory shop. The optical components, with the exception of the grating, were figured by Mr. Lloyd Sprinkle, of Detroit. The *PbS* cell and amplifier were furnished

[1] McMath and Mohler, *Pub. A.S.P.*, **59**, 267, 1947.

through the kindness, respectively, of Dr. R. J. Cashman and Mr. Wallace Wilson, of the Northwestern Technological Institute.[2]

THE INFRARED SOLAR MAP

During the past fall and winter, several maps of the solar spectrum have been obtained throughout the entire region 0.80–2.5 μ. The records are in the form of pen-and-ink tracings on a direct-intensity scale. Various dispersions have been employed, ranging from 2.50 to 4.85 mm/A. It is well known from low-resolution observations that the near infrared solar spectrum is masked by heavy telluric absorption bands of H_2O between 1.35 and 1.50 μ and also between 1.75 and 1.95 μ. The intervening regions are clear of molecular absorption, however, except for systems of lines and bands, which, though numerous, are sufficiently weak and isolated to be admirably suited for identification and study.

The clear regions of the spectrum are also rich in solar atomic lines, of which approximately two hundred and fifty have been discovered from a comparison between tracings made with high and low sun. A systematic program of measurement, identification, and analysis of the solar and telluric lines in the infrared is in progress and will be reported in this *Journal* from time to time. The present contribution deals with the identification of telluric bands of methane, centered at 1.66, 2.20, 2.32, and 2.37 μ, and with the preliminary analysis of the 1.66 μ band.

THE DETERMINATION OF WAVE LENGTHS

The problem of the determination of wave lengths and the identifications of both atomic and molecular lines is a difficult one, inasmuch as no high-resolution observations in the lead sulphide region have been made in the laboratory. Two independent methods have been employed to establish the infrared wave-length scale. The first makes use of the well-known property of diffraction gratings that gives a precise superposition[3] in the spectrum of lines in different grating orders with wave lengths λ/n, where n is the order of the spectrum. The wave lengths of infrared Fraunhofer lines may thus be derived from those tabulated with high precision in the *Revised Rowland Tables*.[4] The probable errors of wave lengths determined in this way are of the order of ± 0.1 A, which should be entirely adequate for line identifications in the infrared.

A second and complementary procedure for establishing a wave-length calibration is based on the identifications of solar lines for which wave lengths have been computed from the known term values of atomic-energy levels. This procedure can be applied with certainty only when complete or nearly complete multiplets occur in the spectrum, the identifications being guided by the theoretical intensity relationships for lines in multiplets. Thus the initial wave-length calibration in the 1.6 μ region was achieved via the identification of the triad of *Fe* I multiplets that result from transitions between the term e^5D and the three higher-lying terms u^5F°, t^5D°, and u^5P°.[5] The computed wave lengths for these multiplet lines extend from λ 14,255 to λ 16,590. Since most of the term values on which they are based are known to within 0.05 cm^{-1}, they provide a firm basis for calibration over a wide region of the spectrum. Additional multiplets of *Si* I, *Al* I, *Mg* I, and *C* I permit an extension of the calibration to about λ 17,500.

It should be emphasized that the first method described above yields wave lengths in air, the second *in vacuo*. The results obtained by the two methods are in satisfactory agreement, considering the uncertainties in the infrared refractivity of air and in the

[2] For a more complete description of the instrumentation, see McMath and Mohler, *Sky and Telescope*, **7**, 143, 1948.

[3] Except for a small correction due to the variation with wave length of the refractivity of air.

[4] *Pub. Carnegie Inst. Washington*, No. 396, 1928.

[5] McMath, Adel, Mohler, and Goldberg, *Phys. Rev.*, **72**, 644, 1947.

atomic term values. For example, the computed air wave length of the $4p^3D_2 - 4d^3D_2^0$ line of *Si* I is 16,681.4 A, as compared with the measured value of 16,681.2 A.

THE CH_4 BAND AT 1.666 μ

One of the outstanding features of the infrared solar map is a molecular-band system centered at 1.666 μ, consisting of positive, negative, and zero branches, as shown in Figure 1. The *R* branch contains eleven regularly spaced components, and the *P* branch eight, while the almost completely resolved *Q* branch shows ten members. This band and three others at 2.20, 2.32, and 2.37 μ have recently been identified by the writers[6] as arising from the CH_4 molecule, on the basis of comparisons with published laboratory observations of the methane spectrum. We have now established the identification beyond any doubt by inserting in the solar beam a 25-cm-long absorption cell filled with methane at atmospheric pressure. All the bands identified as CH_4 are enormously enhanced, as may be seen in Figure 2.

The observational and other data relating to the 1.666 μ band of CH_4 are contained in Table 1. The first column gives the rotational quantum numbers associated with each transition, the second column the measured wave length in I.A., and the third column the equivalent widths in A, measured for a solar altitude of 14°34′. The fourth column gives the line frequencies in wave numbers, calculated for an index of refraction of air equal to 1.000274. The colons signify uncertainties in wave length, occasioned by apparent blending with other solar or telluric lines or by possible multiple structure of the high members of the positive and negative branches. It is interesting to note that W. H. J. Childs,[7] in a study of the 9047 cm^{-1} band, found a multiple splitting in the *R* branch that "increases in magnitude and complexity with the rotational quantum number."[8] This band is the second overtone, $3\nu_3$, and the 1.666 μ band the first overtone, $2\nu_3$, of the fundamental band at 3020 cm^{-1}. Fourteen lines of the ν_3 band have been found by Migeotte[9] in the solar spectrum.

The line spacings are given in the fifth column of Table 1. The spacings in the *P* and *R* branches increase regularly toward the long wave lengths, from 8.96 to 11.73 cm^{-1}, the average being 10.56 cm^{-1}. The 1–0 component of the *P* branch, which is absent or very weak in the solar spectrum, was likewise not found in the laboratory studies of Moorhead[10] and of Norris and Unger.[11] The wave numbers determined by the latter authors, after correction to vacuum, are given in the sixth column of Table 1. The laboratory values are systematically higher, on the average, by nearly 4 cm^{-1} than are those of the present investigation. In view of the high order of agreement between the solar wave lengths measured from overlapping grating orders and those computed from atomic-energy-level differences, we are inclined to favor the solar values.

ANALYSIS OF THE $2\nu_3$ BAND

Dennison[12] has given the following expressions for the excited rotational energy levels of the CH_4 molecule:

$$\frac{W}{hc} = \nu_0 + B_i J(J+1) - 2J\zeta B_i , \tag{1a}$$

$$\frac{W}{hc} = \nu_0 + B_i J(J+1) , \tag{1b}$$

$$\frac{W}{hc} = \nu_0 + B_i J(J+1) + 2(J+1)\zeta B_i . \tag{1c}$$

[6] *Phys. Rev.*, **73**, 1203, 1948. Spectroscopic evidence for the presence of CH_4 in the earth's atmosphere was first reported by M. Migeotte (see n. 9).

[7] *Proc. R. Soc., London, A*, **153**, 555, 1936.

[8] *Ibid.*, p. 565.

[9] *Phys. Rev.*, **73**, 519, 1948; *Ap. J.* **107**, 400, 1948.

[10] *Phys. Rev.*, **39**, 83, 1932.

[11] *Phys. Rev.*, **43**, 467, 1933.

[12] *Rev. Mod. Phys.*, **12**, 175, 1940.

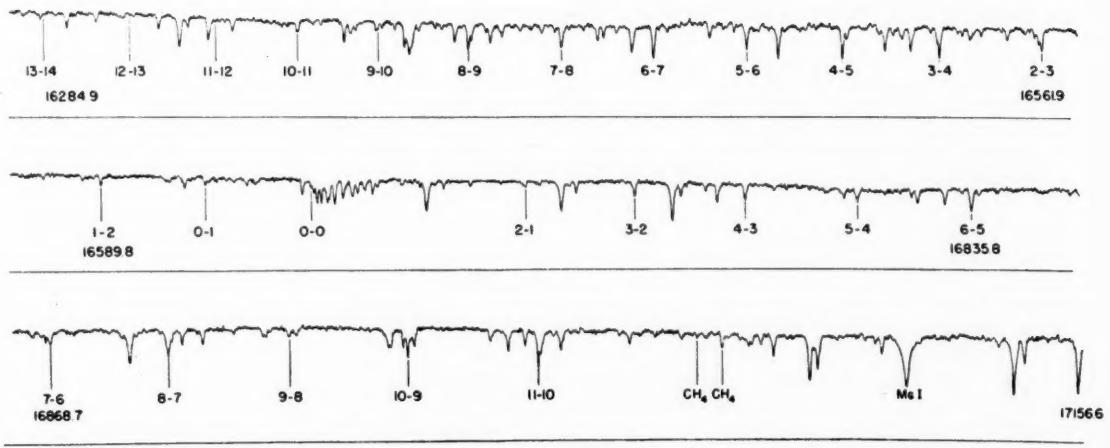

FIG. 1.—The $2\nu_3$ overtone band of CH_4 at 1.665 μ in the solar spectrum. Zero intensity is represented by the horizontal line at the bottom of the tracing.

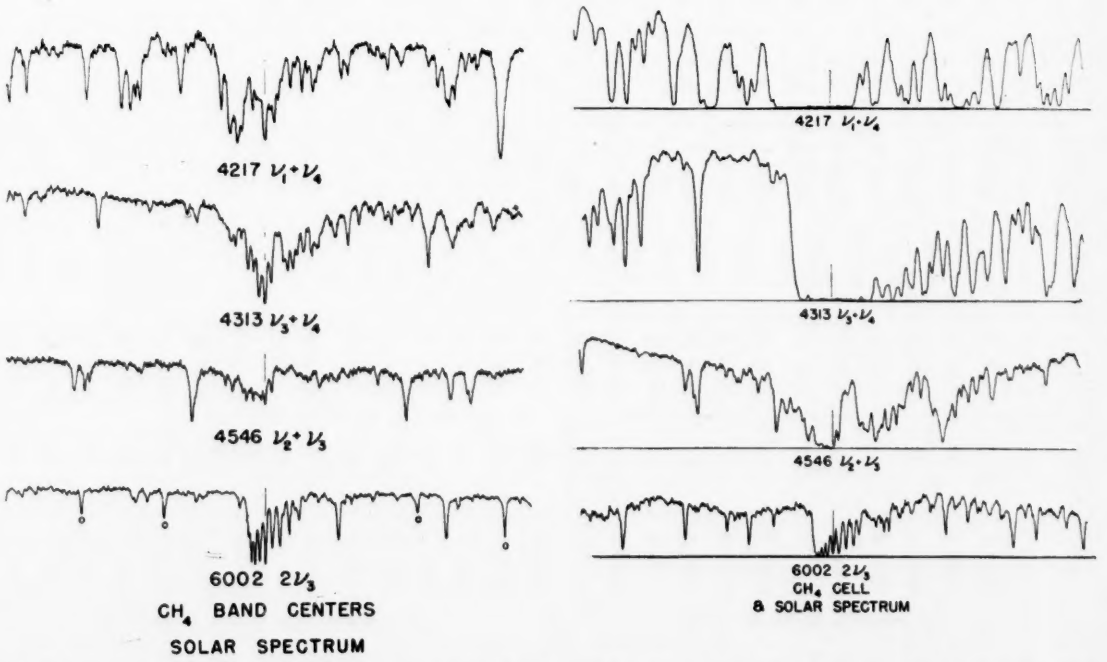

FIG. 2.—Four Q branches of CH_4 are shown to the left as they appear in the solar spectrum, and to the right as they are enhanced by a methane absorption cell. The horizontal line at the bottom of each tracing to the right represents zero intensity.

TABLE 1

1.666 μ BAND OF CH_4 IN THE SOLAR SPECTRUM

Designation	λ (Obs.)	W	ν (Obs.)	$\Delta\nu$	ν (Lab.)	Lab.−Sun	ν (Calc.)
0–1	16619.2	0.18	6015.49		6018.3	2.8	6015.57
				10.66			
1–2	16589.8	.13	6026.15		6029.7	3.5	6026.16
				10.37			
2–3	16561.3	.43	6036.52		6040.5	3.9	6036.60
				10.37			
3–4	16532.9	.49	6046.89		6051.7	4.8	6046.92
				10.18			
4–5	16505.1	.51	6057.07		6059.5	2.4	6057.09
				10.00			
5–6	16477.9	.42	6067.07		6070.1	3.0	6067.10
				10.00			
6–7	16450.8	.54	6077.07		6080.5	3.5	6076.98
				9.62			
7–8	16424.8	.46	6086.69		6090.5	3.8	6086.69
				9.61			
8–9	16398.9:	.57	6096.30		6100.3	4.1	6096.24
				9.42			
9–10	16373.6:	.45	6105.72		6109.9	4.3	6105.62
				8.96			
10–11	16349.6	.19	6114.68		6117.3	3.5	6114.83
2–1	16709.2	.15	5983.09		5989.0	5.9	5983.07
				11.01			
3–2	16740.0	.29	5972.08		5975.8	3.8	5972.00
				11.25			
4–3	16771.6	.34	5960.83		5964.8	4.0	5960.82
				11.28			
5–4	16803.4	.28	5949.55		5952.3	2.8	5949.54
				11.38			
6–5	16835.6	.48	5938.17		5942.8	4.6	5938.15
				11.55			
7–6	16868.4:	.40	5926.62		5930.8	4.1	5926.67
				11.47			
8–7	16901.1:	.58	5915.15		5920.2	5.1	5915.10
				11.73			
9–8	16934.7	.....	5903.42		5706.0	2.5	5903.45
0–0	.....	.....	.....	.....	.....	.....	6004.86
1–1	16648.8	.18:	6004.79		.....	.....	.....
				0.21			
2–2	16649.4	.27:	6004.58		.....	.....	.....
				0.33			
3–3	16650.3	.50:	6004.25		.....	.....	.....
				0.43			
4–4	16651.5	.52	6003.82		.....	.....	.....
				0.61			
5–5	16653.2	.50	6003.21		.....	.....	.....
				0.72			
6–6	16655.2	.52	6002.49		.....	.....	.....
				0.87			
7–7	16657.6	.39	6001.62		.....	.....	.....
				1.01			
8–8	16660.4	.36	6000.61		.....	.....	.....
				1.22			
9–9	16663.8	.26	5999.39		.....	.....	.....
				1.24			
10–10	16671.5	.16	5998.15		.....	.....	.....

In equations (1), $B_i = h/8\pi^2 cI_i$, where I_i is the effective moment of inertia for vibrational state i, and ν_0 is the wave number of the 0–0 rotational component. An additive constant equal to $(\zeta^2 - 2\zeta)B_i$ has been omitted from all three terms.

The parameter ζ was introduced by Teller[13] to explain the anomalous fine structure of the infrared bands of symmetrical molecules. Under certain conditions the vibratory motion of the atoms may introduce a small component of angular momentum of magnitude $\zeta(h/2\pi)$. This momentum may orient itself parallel, perpendicular, or antiparallel to the ordinary rotational angular momentum, to produce the splitting given by equations (1). The quantity ζ has the order of magnitude -0.05 for the $2\nu_3$ overtone band.[14]

For the ground state, $\zeta = 0$, and $W/hc = B_0 J(J+1)$. The selection rules permit only transitions from the ground state to state (1*a*) above for $J \rightarrow J+1$ (positive branch), to state (1*b*) for $J \rightarrow J$, and to state (1*c*) for $J \rightarrow J-1$. Accordingly, the wave numbers of the rotational components of the P, Q, and R branches are given by the following expressions:

$$\nu_P(J) = \nu_0 + B_i(J^2 - J + 2J\zeta) - B_0(J^2 + J), \tag{2}$$

$$\nu_Q(J) = \nu_0 + B_i(J^2 + J) - B_0(J^2 + J), \tag{3}$$

$$\nu_R(J) = \nu_0 + B_i[(J+1)(J+2) - 2(J+1)\zeta] - B_0(J^2 + J), \tag{4}$$

where ν_0 is the wave number of the 0–0 line, $\nu_P(J)$ is the wave number of a line of the negative branch arising from ground level J, and similarly for $\nu_Q(J)$ and $\nu_R(J)$.

We then obtain the following combination relationships:

$$\nu_R(J) - \nu_Q(J) = B_i(1-\zeta)(2J+2), \tag{5}$$

$$\nu_R(J) - \nu_P(J) = B_i(1-\zeta)(4J+2), \tag{6}$$

$$\nu_Q(J) - \nu_P(J) = B_i(1-\zeta)2J, \tag{7}$$

$$\nu_R(J-1) - \nu_P(J+1) = (B_0 - B_i\zeta)(4J+2), \tag{8}$$

$$\nu_R(J) + \nu_P(J+1) - \nu_Q(J) - \nu_Q(J+1) = 0. \tag{9}$$

By taking appropriate wave-number differences as indicated above, we should be able to determine the constants $B_i(1-\zeta)$, $B_0 - B_i\zeta$, and hence $B_0 - B_i$. The first three columns of Table 2 list the values of $B_i(1-\zeta)$ as determined from equations (5), (6), and (7), respectively; the fourth column gives $B_0 - B_i\zeta$; and the last column the quantity on the left-hand side of equation (9). The values of $B_i(1-\zeta)$ calculated from equations (5), (6), and (7) are in reasonably good agreement with one another but, nevertheless, show a systematic increase from one column to the next. This effect, which is also shown by the residuals from equation (9) in the last column of Table 2, suggests that the Q-branch frequencies predicted from theory by equation (3) are too low relative to those of the P and R branches.

All the quantities in the first four columns of Table 2 decrease systematically with increasing J, which suggests that the frequency formulae (2), (3), and (4) should contain additional terms, probably in J^3. The expressions (2) and (4) for the wave numbers of the lines in the P and R branches may be represented by a single formula, of the well-known form,

$$\nu = \nu_0 + (B_i - 2\zeta B_i + B_0)m + (B_i - B_0)m^2, \tag{10}$$

[13] *Hand- und Jahrbuch der chemischen Physik*, **9**, 125, 1934.

[14] Johnston and Dennison, *Phys. Rev.*, **48**, 868, 1935.

where $m = J + 1$ for the R branch and $m = -J$ for the P branch. Equation (10) suggests an attempt to fit the observed wave numbers to a formula of the form,

$$\nu = \nu_0 + a\,m + b\,m^2 + c\,m^3 . \tag{11}$$

The constants were determined by least squares, with the results shown in the first column of the accompanying tabulation, the second column containing the values ob-

	Lake Angelus	Norris and Unger
ν_0	6004.86	6008.0
a	10.775	11.131
b	−0.06194	−0.0449
c	−0.000794	−0.00341

tained by Norris and Unger from a similar calculation. The constant c is small but appreciable. The wave numbers calculated from equation (11) are given in the eighth

TABLE 2

CH_4 CONSTANTS CALCULATED FROM EQUATIONS (5), (6), (7), (8), AND (9)

J	$B_i(1-\zeta)$			$B_0 - B_i\zeta$	
	Eq. (5)	Eq. (6)	Eq. (7)	Eq. (8)	Eq. (9)
1	5.340	.....	.....	5.400	−0.13
2	5.323	5.343	5.372	5.407	− .23
3	5.330	5.344	5.362	5.406	− .35
4	5.325	5.347	5.374	5.408	− .41
5	5.322	5.342	5.366	5.404	− .46
6	5.327	5.342	5.360	5.402	− .42
7	5.317	5.336	5.357	5.397	− .39
8	5.316	5.328	5.341	5.390	−0.28
9	5.316	5.324	5.332	.....	.....
10	5.297	.....	.....	.....	.....

column of Table 1, under the heading "ν (Calc.)." The residuals, ν (Obs.) − ν (Calc.), are within the error of measurement, the average value being ± 0.05 cm^{-1}. The calculated value of ν_0 accords well with the assignment of quantum numbers given for the Q branch in Table 1. From a comparison of equations (10) and (11) we identify the constants a and b with $B_i - 2\zeta B_i + B_0$ and $B_i - B_0$, respectively. We have

$$\begin{aligned} a + b &= 2B_i(1 - \zeta) \\ &= 10.713 . \end{aligned} \tag{12}$$

According to Johnston and Dennison,[14] the correct value of ζ to be employed for the $2\nu_3$ band is $-\zeta_f$, where ζ_f is the appropriate value for the fundamental ν_3 band. Childs[15] finds $\zeta_f = 0.050$, from which we obtain $B_i = 5.101$ and $B_0 = 5.163$, since $B_i - B_0 = -0.0619$. Childs obtained $B_0 = 5.252$ from an analysis of Cooley's[16] measures of the ν_3 and ν_4 bands at 3020 and 1306 cm^{-1}.

[15] *Op. cit.*

[16] *Ap. J.*, **62**, 73, 1925.

TEMPERATURE AND ABUNDANCE OF CH_4

The equivalent widths of individual lines in the P, Q, and R branches of the $2\nu_3$ band are given in the third column of Table 1. The intensities were measured on a tracing obtained on March 28, 1948, between 22^h05^m and 22^h53^m U.T. The tabulated equivalent widths have been corrected to correspond with a solar altitude of 14°34′ at the midpoint of the tracing. The equivalent widths of the P and R lines were determined directly from areas measured on the tracing. Those of the overlapping Q lines were estimated from the central intensities with the aid of a calibration between central intensity and equivalent width established from measurements of the P and R lines.

We have employed the equivalent widths in the positive and negative branches in an attempt to determine both the abundance of methane and the average temperature of the absorbing column. For either an absorbing or a scattering atmosphere, the equivalent width of an absorption line is given by[17]

$$\frac{W}{\lambda} = C \cdot N \cdot S_{JJ'} e^{-E_J/kT}, \tag{13}$$

where S_{JJ}' is the strength (square of the matrix element) for a transition from lower level J to upper level J'; E_J is the energy of the lower level; T is the absolute temperature; N is the total number of atoms or molecules per square centimeter along the absorbing column; and C is a known constant. If E_J is given in wave numbers, the Boltzmann constant, k, has the value 0.695. The expression (13) is valid only if the line is unsaturated, an assumption which we adopt on the basis of the actual appearance of the CH_4 lines on the tracings. For the CH_4 molecule, the energies (in cm^{-1}) of the rotational levels in the lowest vibrational state are given by

$$E_J = B_0 J(J+1), \tag{14}$$

where B_0 has been found above to have the value 5.16 cm^{-1}.

If the theoretical line strengths, S_{JJ}', were accurately known, equation (13) would permit the calculation from the observed equivalent widths of both T and N. Since the strengths have not been calculated with sufficient accuracy, we adopted the following procedure. An auxiliary tracing of the 1.666 μ band was obtained, utilizing an incandescent lamp, together with a methane absorption cell 25 cm long, which was furnished through the kindness of Professor E. F. Barker, of the University of Michigan Physics Department. The cell was first evacuated and then filled with methane at 25-cm pressure. Since both the temperature and the abundance of the laboratory methane could be determined with precision, a comparison between the laboratory and the solar intensities leads to the evaluation of these parameters for the earth's atmosphere.

From equation (13), the ratio of equivalent widths between sun and laboratory is

$$\frac{W_s}{W_l} = \frac{N_a}{N_l} e^{-(B_0/k)J(J+1)(1/T_a - 1/T_l)}, \tag{15}$$

where N_a is the number of molecules per square centimeter along the line of sight in the earth's atmosphere, N_l is the number per square centimeter in the absorption cell, and T_a and T_l are the atmospheric and laboratory temperatures, respectively. Taking logarithms, and inserting numerical values for B_0 and k, we obtain

$$\log \frac{W_s}{W_l} = \log \frac{N_a}{N_l} - 3.224 J(J+1)\left(\frac{1}{T_a} - \frac{1}{T_l}\right). \tag{16}$$

In Figure 3, we have plotted $\log (W_s/W_l)$ against $J(J+1)$. The points are well represented by a straight line, fitted by least squares, with slope -0.00267 and intercept

[17] Menzel, *Ap. J.*, **84**, 462, 1936.

-0.0492. By comparison with equation (16) and with $T_l = 293°$ K, we find $T_a = 236°$ K and $N_l/N_a = 1.120$. At a temperature of 293° and pressure equal to 25 cm *Hg*, the number of CH_4 molecules per square centimeter along a 25-cm path is 2.05×10^{20}. Hence the number N_a along a square-centimeter column of the earth's atmosphere toward altitude 14°34′ is 1.83×10^{20} molecules, or 4.87×10^{-3} gm. The total mass of a square-centimeter column of the earth's atmosphere in this same direction is 4.09×10^{3} gm. Hence the relative mass abundance of methane is 1.18×10^{-6}, or about one part in a million.

The calculated temperature of $-37°$ C. is a reasonable value, being that normally found at a height of about 8 km.[18] Pending further study, nothing definite can be stated as to the lateral and vertical distribution of the methane in the earth's atmosphere. The indicated average height of 8 km is reasonable for the relatively light CH_4 molecule.

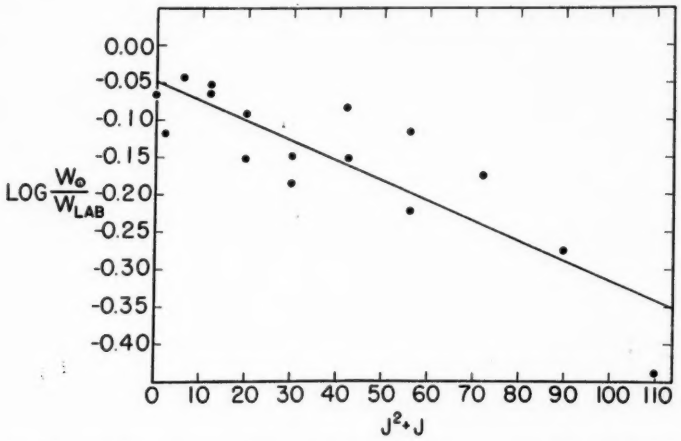

FIG. 3.—The determination of temperature and abundance of CH_4 in the earth's atmosphere

Analysis of tracings made with the sun at various altitudes may provide further information on the vertical distribution.

THE CH_4 BANDS AT 2.3 μ

Cooley,[19] Moorhead,[20] Vedder and Mecke,[21] and Nielsen and Nielsen[22] have observed the methane spectrum in the 2.3 μ region with varying degrees of resolution. The most prominent bands, with well-defined Q branches, are three combination bands—$\nu_1 + \nu_4$ at 4216.3 cm^{-1}; $\nu_3 + \nu_4$ at 4313.2 cm^{-1}; and $\nu_2 + \nu_3$ at 4546 cm^{-1}. The quoted wave numbers, *in vacuo*, are from Herzberg's[23] compilation. The appearance of the three Q branches on the Lake Angelus tracings is shown in Figure 2, which also shows the enhancement of the bands by a methane absorption cell. The vertical lines near the band centers represent the positions measured in the laboratory.

[18] *Smithsonian Physical Tables* (1934), p. 559.

[19] *Op. cit.*

[20] *Op. cit.*

[21] *Zs. f. Phys.*, **86**, 137, 1933.

[22] *Phys. Rev.*, **48**, 864, 1935.

[23] *Infra-red and Raman Spectra* (New York: D. Van Nostrand Co., 1945), p. 308.

Unlike the zero branch of the $2\nu_3$ bands, for which the intensities and spacings vary regularly with serial number, the 2.3 μ Q branches appear highly complex. It is possible that their mutilated appearance may be due to intensity anomalies rather than to irregularities in the spacing of the components.

Since the above investigation was carried out, we have secured a new set of tracings of the methane spectrum in the 1.6 and 2.3 μ regions, employing an incandescent lamp as a source in place of the sun. In view of the blended nature of the solar spectrum, the laboratory tracings are much more suitable for the measurement and analysis of molecular bands. A more precise study of the CH_4 spectrum is therefore being carried out and will be reported in the near future.

We are indebted to Professors E. F. Barker and D. M. Dennison, of the University of Michigan, for helpful advice and discussion and to Mr. Robert M. Page for computational assistance. This investigation would not have been possible without the continuing grants-in-aid by McGregor Fund.

NEW SOLAR LINES IN THE SPECTRAL REGION 1.52–1.75 μ

LEO GOLDBERG, ORREN C. MOHLER, AND ROBERT R. MCMATH
McMath-Hulbert Observatory, University of Michigan
Received July 24, 1948

ABSTRACT

Accurate wave lengths and measurements of percentage central absorption are given for nearly three hundred new solar lines discovered in the region 1.52–1.75 μ of the infrared solar spectrum. The lines were found on high-resolution, direct-intensity tracings of the spectrum obtained at the McMath-Hulbert Observatory with the McGregor spectrometer and a Cashman cell.

Ninety-three of the lines have been identified as belonging to neutral atoms of *C*, *Mg*, *Al*, *Si*, *Fe*, *Mn*, and *Ni*, mainly on the basis of wave lengths computed from term values. In addition, the third, seventh, and eighth members of the Brackett series of hydrogen have been identified, together with the *Na* I 4s–4p doublet at λλ 22,054 and 22,081.

INTRODUCTION

In a previous communication,[1] we have described a new infrared map of the solar spectrum obtained with the McGregor spectrometer of the McMath-Hulbert Observatory. The spectrometer employs a Cashman *PbS* cell of sufficient sensitivity that the solar spectrum between 0.8 and 2.5 μ may be recorded with a resolution of about 50,000, which compares favorably with the best resolution obtainable in the photographic region.

Beyond the infrared limit of the photographic plate at about λ 13,500, two fairly well-defined atmospheric windows permit the identification and study of solar lines in the regions 1.52–1.75 μ and 2.1–2.4 μ. A detailed study of the infrared tracings is now in progress, as a result of which we plan ultimately to publish a complete list of the wave lengths and intensities of all solar and atmospheric lines in the new spectral regions. We also expect in the near future to issue an atlas of the infrared solar spectrum, which will consist of reproductions of the direct-intensity tracings throughout the region from λ 8000 to λ 25,000. The new atlas will therefore partially overlap with and extend the important map by Minnaert, Mulders, and Houtgast[2] in the photographic region. The purpose of the present paper is to present a preliminary list of solar lines and identifications in the region of the atmospheric window between 1.52 and 1.75 μ.

NEW SOLAR LINES

Although we refer to the 1.6 μ region as an "atmospheric window," it must be borne in mind that more than half the lines in this region are telluric in character. The telluric spectrum consists mainly of lines of H_2O but includes also well-defined band systems of CO_2 and CH_4. The solar lines are usually readily distinguishable, however, from a comparison of tracings made with the sun at high and at low altitudes. Comparisons of this type form the basis for the selection of the nearly three hundred solar lines given in Table 1.

The wave lengths, which are given in the first column of Table 1 in I.A., were determined in the following way. The solar map is divided into 150 A segments, each tracing overlapping adjacent ones by about 7 A. On each tracing, the wave lengths of three or more lines were measured directly by the method of overlapping grating orders.[3] A wave-length scale was then drawn on each tracing at intervals of 10 A, the dispersion

[1] McMath, Mohler, and Goldberg, *Ap. J.*, **109**, 17, 1949.

[2] *A Photometric Atlas of the Solar Spectrum* (Utrecht, 1940).

[3] McMath and Mohler, *Sky and Telescope*, **7**, 143, 1948.

TABLE 1

PRELIMINARY LIST OF SOLAR LINES IN SPECTRAL REGION 1.52–1.75 μ

λ (sun)	Int.	Ident.	λ (Calc.)	λ (K and R)
15,178.3	10	⊙		
15,192.7	11	⊙		
15,207.6	26	*Ni*?	08.5	
15,217.8	12	*Mn*?		18.
15,219.7	21	*Fe*	19.5	
15,224.8	9	⊙		
15,245.2	21	*Fe*	44.8	
15,294.6	34	*Fe*?		96.
15,335.5	28	⊙		
15,343.8	12	*Fe*?	44.5	
15,377.1	19	*Si*	76.8	
15,382.2	7	⊙		
15,394.8	20	*Fe*	94.7	96.
		Fe	95.3	
15,422.3	14	⊙		
15,459.4	11	⊙		
15,461.9	6	⊙		
15,469.8	10	⊙		
15,475.3	9	*Fe*	75.1	
15,478.4	12	⊙		
15,490.4 / 15,490.8	7	*Fe* / ⊙	90.4	
15,496.6	8	*Si* atm?	96.5	
15,499.2	7	*Si*	99.4	
15,500.8 / 15,501.2	16	⊙ atm		
15,514.1	8	Atm?		
15,519.4	5	⊙ atm		
15,531.8	11	*Fe*	31.8	
		Fe	33.1	
15,534.4	13	⊙		
15,538.0	9	*Fe*	37.6	
15,540.8	4	⊙ atm		
15,542.2	12	*Fe* atm	41.6	
15,550.5	7	⊙		
15,551.5	8	⊙		
15,555.4	12	⊙		
15,557.9	20	*Si*	58.8	
15,560.9	5	⊙?		
15,566.8	5	⊙		
15,588.2	12	⊙		
15,590.1	7	⊙?		
15,591.5	21	*Si*	91.4	
15,604.2	17	⊙		
15,605.7	6	⊙ atm		
15,611.1	6	*Fe*	11.1	
15,613.6 / 15,613.9	9	⊙ atm		
15,621.5	24	*Fe*	21.6	25.
15,631.9 / 15,632.4	21	⊙ / ⊙		
15,645.0	5	⊙		
15,648.4	10	⊙		
15,652.7	8	*Fe*	53.0	
15,662.0	18	⊙		
15,665.1	8	⊙ atm		
15,673.0	4	⊙ atm		
15,674.7	5	⊙		
15,677.7	13	⊙		
15,680.2	4	*Si*	80.0	
15,682.6	6	*Fe*	83.0	
15,683.6	4	⊙		
15,686.4 / 15,686.6	16	Atm?		
15,687.7	7	Atm?		
15,691.8	17	⊙ atm		
15,692.0	18	⊙ atm		
15,693.0	?	*Mg* atm CO_2	93.1	
15,723.6	18	*Fe*	23.7	
15,740.7	30?	*Mg*? atm CO_2		
15,741.9	16	*Fe*	41.8	
15,749.1	44	*Mg*?	57.5	59.1
15,761.0	?	⊙ atm CO_2		
15,765.9	50??	*Mg* atm CO_2	67.7	68.3
15,769.3	?	*Fe* atm CO_2	69.3	71.4
15,770.7	17	⊙		
15,784.7	5	⊙ atm		
15,789.1	14	⊙		
15,798.7	16	*Fe*	99.2	
15,816.5	7	⊙?		
15,818.2	24	*Fe*	18.1	15.
15,819.1	12	⊙ atm		
15,821.7	8	⊙		
15,823.0	17	*Fe*	22.4	21.
15,825.5	6	Atm?		
15,833.8	21	⊙		
15,835.3	20	*Si*	34.6	
15,837.7	12	*Fe*	37.2	
15,840.1	5	⊙		
15,852.7	9	Atm?		
15,863.7	12	⊙ atm		
15,866.3	4	⊙ atm		
15,868.5	19	*Fe*	68.4	
15,878.3	15	*Fe*	78.3	
15,879.4	17	*Mg*	79.8	
15,884.3	19	*Si*	84.1	
15,886.1	15	⊙		
15,888.6	42	*Si*	87.7	
15,891.1	10	⊙		
15,892.3 / 15,892.7	23	⊙		
15,895.1	19	⊙		
15,899.1	11	⊙		
15,901.5	9	⊙		
15,904.1	16	*Fe*	04.5	
15,905.8	17	*Fe*	05.9	
15,909.0	4	⊙		
15,911.3	15	*Fe*	11.3	
15,920.6	21	*Fe*	21.1	
15,928.3	5	⊙		
15,929.5	4	Atm?		
15,933.8	5	⊙ atm		
15,941.9	9	Atm?		
15,945.4	5	Atm?		
15,952.6	4	⊙ atm		
15,954.1	13	*Mg*	54.7	
15,959.9	33	*Si*	60.0	
15,964.6	12	*Mn*? atm		65.
15,972.8	6	Atm?		
15,980.9	25	*Fe*	80.8	
15,982.2	7	⊙ atm		
15,992.3	3	⊙ atm		
15,998.0	7	⊙		
16,007.0	22	⊙ atm		
16,009.7	13	Atm?		
16,016.6	10	*Fe*	16.6	
16,021.7	?	⊙ atm CO_2		
16,029.6	3	⊙?		
16,038.0	14	⊙ atm		
16,040.8	18			
16,060.2	?	*Si* atm CO_2	60.9	
16,071.5	11	⊙		
16,076.0	12	⊙ atm		
16,088.9	10	⊙ atm		
16,095.0	?	*Si* atm CO_2	94.7	
16,102.6	20	⊙?		
16,115.3	?	⊙ atm CO_2		
16,119.2	5	⊙?		
16,126.2	?	⊙ atm CO_2		
16,150.9	9	⊙		
16,155.2	5	Atm?		
16,156.6	10	⊙		
16,157.4	10	*Fe*	57.5	
16,163.8	18	*Si*	63.4	
16,165.2	22	*Fe*? atm		166.
16,175.1	10	⊙		
16,178.1	5	⊙ atm		
16,179.6	10	*C*	80.0	
16,180.9	11	⊙		
16,186.0	10	⊙		
16,195.1	13	*C*	95:	
16,197.0	14	⊙		
16,198.5	13	⊙		
16,203.6	5	⊙ atm		
16,204.3	12	⊙		
16,207.8	15	⊙ atm		
16,213.7	13	⊙		
16,215.8	21	*Si*	14.9, 16.3	
16,225.8	9	*Fe*	26.0	
16,231.8	16	⊙		
16,236.2	9	⊙		
16,242.1	18	*Si*	42.1	

TABLE 1—*Continued*

λ (sun)	Int.	Ident.	λ (Calc.)	λ (K and R)	λ (sun)	Int.	Ident.	λ (Calc.)	λ (K and R)
16,246.6	9	⊙ atm			16,661.7	13	⊙		
16,252.9	5	⊙			16,665.9	16	⊙		
16,277.3	5	⊙			16,673.9	4	⊙		
16,284.9	10	⊙			16,674.4	4	⊙		
16,292.9	8	⊙			16,681.2	35	*Si*	81.4	
16,310.4	9	*Ni Fe?*	10.6, 11.0	*Ni* 13.0	16,685.9	10	⊙		
16,316.4	23	*Fe?*		17.	16,693.4	4	⊙		
16,318.7	8	⊙ atm			16,719.1	34	*Al*	19.0	19.0
16,324.3	14	⊙ atm			16,721.5	4	⊙		
16,331.6	6	⊙			16,723.3	14	⊙		
16,333.5	5	*Fe*	33.5		16,750.6	44	*Al* atm	50.6	50.6
16,364.7	8	*Ni*	63.7	63.0	16,753.2	16	⊙		
16,365.0		*Mg*	64.4		16,760.3	9	⊙		
16,366.4	6	⊙			16,763.4	21	*Al* atm	63.4	63.4
16,373.9	6	Atm?			16,779.6	6	⊙ atm		
16,377.7	5	Atm?			16,799.7	13	⊙		
16,380.3	18	⊙			16,818.9	10	⊙		
16,381.8	26	*Si*	81.1		16,828.3	21	*Si* atm	28.2	
16,382.3		*Si*	81.7		16,863.1	5	⊙		
16,384.3	4	*Fe*	83.5		16,863.6	5			
16,394.5	15	⊙			16,868.3	12	*Ni? C?* atm	68.2, 67.	*Ni* 68.5
16,396.5	4	Atm?			16,890.2	30	*C*	88.	
16,403.5	7	Atm?			16,927.5	7	⊙		
16,404.7	13	⊙			16,928.4	8	*Fe*	28.5	
16,407.5	9	*Ni?* atm		09.4	16,929.5	5	⊙		
16,418.9	7	Atm?			16,967.0	18	⊙ atm		
16,419.2	7	*C?* atm	20.7		16,996.3	16	*Ni*	96.4	99.6
16,423.0	6	Atm?			17,001.2	16	⊙		
16,427.0	4	Atm?			17,007.6	4	⊙		
16,431.2	3	Atm?			17,009.3	5	⊙		
16,435.1	10	⊙ atm			17,013.6	5	⊙ atm		
16,436.9	7	*Si*	36.0		17,015.7	5	*Fe*	15.9	
16,440.6	6	⊙ atm			17,027.5	6	⊙		
16,445.0	21	⊙			17,045.5	7	*Fe*	45.3	
16,455.2	8	Atm			17,067.7	10	⊙		
16,467.1	12	⊙ atm			17,075.0	4	⊙		
16,468.8	4	⊙ atm			17,089.0	5	⊙		
16,470.9	7	*C?*	70.0		17,090.7	4	⊙		
16,474.1	8	⊙ atm			17,097.1	5	⊙		
16,481.2	8	*Ni* atm	80.6		17,108.5	48	*Mg*	08.0	08.1
16,484.1	7	Atm?			17,161.2	15	⊙		
16,486.9	26	⊙			17,200.3	4	⊙		
16,494.5	5	*C*	94.7		17,204.3	15	⊙		
16,497.6	3	Atm?			17,205.9	14	*Si*	05.7	
16,506.4	13	⊙ atm CH_4			17,225.8	25	⊙		
16,517.4	17	*Fe?*	16.8		17,234.5	12	⊙		
16,521.8	5	⊙			17,272.0	4	⊙		
16,522.4	8	⊙			17,275.3	15	⊙		
16,524.8	17	⊙			17,293.8	5	*Fe*	93.6	
16,530.5	6	⊙ atm			17,302.2	19	⊙		
16,538.2	5	⊙			17,310.0	4	⊙		
16,539.5	7	⊙			17,323.3	12	⊙		
16,541.7	8	⊙			17,327.3	32	*Fe?*	27.3	
16,542.2	5	⊙			17,338.5	22	*Fe*	38.3	
16,543.0	4	⊙			17,433.7	5	⊙		
16,544.9	9	⊙			17,448.9	19	⊙		
16,552.3	13	⊙			17,451.4	4	⊙		
16,558.8	4	⊙			17,456.2	14	*C*	56.	
16,562.0	23	⊙ atm CH_4			17,506.2	15	⊙		
16,584.8	5	⊙			17,524.7	6	⊙ atm		
16,586.3	4	*Fe*	85.9		17,527.0	9	⊙		
16,588.0	4	⊙			17,555.1	12	⊙?		
16,622.0	5	⊙?			17,559.0	5	⊙?		
16,626.9	4	⊙			17,560.5	5	⊙?		
16,632.8	5	⊙			17,581.2	16	⊙		
16,646.0	17	*Fe*	45.9		17,593.5	6	*Si*	93.5	

being assumed linear over any one tracing. The actual dispersion on the paper varies from 4.67 mm/A at λ 15,300 to 4.85 mm/A at λ 17,500. At these dispersions the wave lengths of individual lines can easily be read to about 0.1 A by means of an auxiliary scale graduated in units of 1 A. We believe that the preliminary wave lengths given in Table 1 are in error by no more than about 0.2 A, or 0.08 cm^{-1}, which should be adequate for purposes of identification.

The intensity unit in the second column of Table 1 is the percentage central absorp-

tion, which can easily be measured with a millimeter scale. The tabulated intensities should be treated only as rough estimates of the true line strengths and are intended primarily to aid in the identifications of the lines. The equivalent widths of all solar lines are now in the process of measurement and will be published in the forthcoming complete table described above. The identifications listed in the third column of Table 1 will be discussed in the following section. The solar assignments are based, as mentioned previously, on high-low sun comparisons. In a large number of cases, solar lines blend more or less exactly with atmospheric lines. Such blends may be distinguished by measurement of the percentage increase in intensity from high to low sun. Each line has been assigned one of the following symbols: atm?, ⊙atm, ⊙?, or ⊙, the order being that of increasing freedom from blends with atmospheric lines.

IDENTIFICATIONS OF NEW SOLAR LINES

Laboratory observations of atomic lines in the lead sulphide region are exceedingly meager. The compilation by Kayser and Ritschl[4] lists ninety lines of various elements in the 1.6 μ region. A majority of these lines are due to *Sn*, *Pb*, *Hg*, *Cd*, etc.—elements that are not likely to appear in the infrared solar spectrum. The laboratory wave lengths are usually not known to better than about 2 A, which makes comparisons with solar data highly uncertain. On the other hand, the term values for the more abundant elements are known with a precision that is usually of the order of 0.1 cm^{-1}. For a well-analyzed spectrum like *Fe* I the accuracy of the wave numbers is often as high as 0.01 cm^{-1}. Infrared wave lengths computed from term values should not be in error, in most cases, by more than about 0.5 A.

As a basis for the systematic identification of infrared solar lines, we have accordingly compiled tables of predicted multiplets similar to those published by C. E. Moore[5] for the photographic region of the spectrum. The compilation is now complete for the neutral atoms of *H* through *S* and also for *Ti* I, *Fe* I, and *Ni* I. In view of the increasing importance of the infrared spectrum, the tables have been extended from 1.3 μ to about 10 μ. The *Fe* I multiplet table is based on the extensive list of term values by Russell, Moore, and Weeks;[6] up-to-date term values for all other atoms were generously furnished by Dr. Moore in advance of their appearance in her publication *Atomic Energy Levels*.[7] No definite decision has as yet been made concerning the publication of the infrared multiplet tables in their entirety. Pending publication, however, they will be made available to interested workers in infrared spectroscopy.

A total of ninety-three solar lines has been assigned identifications in the third column of Table 1, chiefly on the basis of comparison with the infrared multiplet tables. For a few lines, including all those of *Mn* I, the identifications are based entirely on the laboratory data given in Kayser and Ritschl. The fourth column of Table 1 gives the calculated wave length, also in I.A. Whenever available, the laboratory wave length taken from Kayser and Ritschl is included in the fifth column of Table 1. In Table 2 we have listed the multiplets that were employed in assigning the identifications. In general, the multiplet tables follow the form given by C. E. Moore in the *Revised Multiplet Table*.[5] The intensities contained in the second column, however, are solar values taken from Table 1. All the predicted lines of each multiplet are included in Table 2, even when coincidences are listed for but one or two members. A blank space in the intensity column indicates that the line, if present, is weaker than intensity 4. A dash signifies that the line is either outside the present region of investigation or in a region of strong atmospheric obscuration. A question mark means that the line is probably present but

[4] *Tabelle der Hauptlinien der Linienspektren aller Elemente* (Berlin: Julius Springer, 1939).

[5] *A Multiplet Table of Astrophysical Interest* (*Contr. Princeton U. Obs.*, No. 20, 1945).

[6] *Trans. Amer. Phil. Soc.*, Vol. **34**, Part II, 1944.

[7] *Atomic Energy Levels*, Vol. 1, 1948 (National Bureau of Standards Circ. 467).

TABLE 2

MULTIPLETS IN THE INFRARED SOLAR SPECTRUM

λ PRED.	INT.	E.P.		J	MULTIPLET	REMARKS
		LOW	HIGH			
				H		
21,655.4	.....	12.69	13.26	—	$4^2F^0-7^2G$, etc.	
16,806.6	.....	12.69	13.26	—	$4^2F^0-11^2G$, etc.	
16,407.2	.....	12.69	13.26	—	$4^2F^0-12^2G$, etc.	
				C I		
17,456:	14	8.96	9.67	2–1	$3p^1D-4s^1P^0$	
16,888:	30	8.96	9.69	2–3	$3p^1D-3d^1F^0$	
16,420.7	7	9.29	10.04	1, 2–2	$2p^3\,{}^3P^0-4p^3P$	
16,470.0	7	9.29	10.04	0, 1, 2–1		
16,510.2	<6	9.29	10.04	1–0		1
16,195:	13	9.90	10.67	3–3	$4p^3D-5d^3D^0$	
16,180.0	10	9.90	10.66	2–2		
16,159.4	.....	9.90	10.66	3–2		
16,113.6	.....	9.90	10.67	2–3		
16,129.8	.....	9.90	10.66	1–2		
16,867:	12	9.95	10.68	1–1	$4p^1P-5d^1P^0$	1
16,494.7	5	10.09	10.84	2–1	$4p^1D-6d^1P^0$	
				Na I		
22,054.4	28	3.18	3.74	$\frac{1}{2}-\frac{3}{2}$	$4s^2S-4p^2P^0$	
22,081.2	22	3.18	3.74	$\frac{1}{2}-\frac{1}{2}$		
				Mg I		
17,108.0	48	5.37	6.09	0–1	$4s^1S-4p^1P^0$	
15,767.7	50??	5.91	6.69	2–3, 2, 1	$4p^3P^0-4d^3D$	2
15,757.5	44	5.91	6.69	0, 1–2, 1		
15,879.8	17	5.92	6.70	3, 2, 1–2	$3d^3D-5p^3P^0$	
15,954.7	13	6.56	7.33	2–3	$4d^1D-7f^1F^0$	
16,364.4	8	6.69	7.44	3, 2, 1–4, 3, 2	$4d^3D-9f^3F^0$	
15,693.1	?	6.69	7.48	3, 2, 1–4, 3, 2	$4d^3D-10f^3F^0$	
				Al I		
16,750.6	44?	4.07	4.81	$\frac{3}{2}-\frac{5}{2}$	$4p^2P^0-4d^2D$	1
16,719.0	34	4.07	4.81	$\frac{1}{2}-\frac{3}{2}$		
16,763.4	21?	4.07	4.81	$\frac{1}{2}-\frac{1}{2}$		1

TABLE 2—*Continued*

λ Pred.	Int.	E.P.		J	Multiplet	Remarks
		Low	High			
				Si I		
15,888.7	42	5.06	5.84	1–1	$4s^1P^0-4p^1P$	
16,381.1	26	5.84	6.59	1–1	$4p^1P-3d^1P^0$	3
16,681.4	35	5.96	6.70	3–3	$4p^3D-4d^3D^0$	
16,381.7	26	5.94	6.69	2–2		3
16,216.3	21	5.93	6.69	1–1		
16,828.2	21?	5.96	6.69	3–2		1
16,436.0	7	5.94	6.69	2–1		
16,242.4	18	5.94	6.70	2–3		
16,163.4	18	5.93	6.69	1–2		
15,961.0	33	5.96	6.73	3–2	$4p^3D-5s^3P^0$	
16,094.7	29	5.94	6.70	2–1		2
16,060.9	?	5.93	6.70	1–0		2
15,558.8	20	5.94	6.73	2–2		
15,884.1	19	5.93	6.70	1–1		
15,361.8	?	5.93	6.73	1–2		1
17,593.5	6	6.07	6.77	2–1	$4p^3P-5s^1P^0$	
17,205.7	14	6.06	6.77	1–1		
17,110.4	?	6.05	6.77	0–1		4
15,834.6	20	6.20	6.97	2–2	$4p^1D-4d^1D^0$	
15,376.8	19	6.20	7.00	2–2	$4p^1D-4d^3P^0$	
15,353.5	.....	6.20	7.00	2–1		
14,924.6	—	6.23	7.06	2–3	$3d^3P^0-5p^3D$	
15,496.5	8	6.24	7.04	1–2		
15,680.0	4	6.25	7.03	0–1		
15,338.3	.....	6.23	7.04	2–2		
15,591.4	21	6.24	7.03	1–1		
15,431.3	.....	6.23	7.03	2–1		
15,499.4	7	6.97	7.76	1–2	$5p^1P-7d^3D^0$	
15,502.6	.....	6.97	7.76	1–1		
16,214.9	21	6.97	7.74	2–2	$4d^1D^0-6f^3F$	
				Fe I		
16,226.0	9	2.17	2.93	3–4	$a^5P-z^7P^0$	
15,490.4	5	2.19	2.99	2–3		
15,194.6	—	2.21	3.03	1–2		
15,077.3	—	2.17	2.99	3–3		
14,745.4	—	2.19	3.03	2–2		
14,370.6	—	2.17	3.03	3–2		
15,005.1	—	2.41	3.24	4–3	$z^7D^0-a^3D$	
14,559.1	—	2.44	3.29	3–2		
15,394.7	20	2.46	3.26	2–1		
15,454.6	.....	2.44	3.24	3–3		
14,896.3	—	2.46	3.29	2–2		

TABLE 2—*Continued*

λ Pred.	Int.	E.P. Low	E.P. High	J	Multiplet	Remarks
			Fe I—Continued			
15,653.0	8	2.47	3.26	1–1	$z^7D^0-a^3D$	
15,837.2	12	2.46	3.24	2–3		
15,138.1	—	2.47	3.29	1–2		
15,611.1	6	3.40	4.19	1–2	$a^1P-z^3P^0$	
14,659.0	—	3.40	4.24	1–1		
14,256.2	—	3.40	4.27	1–0		
14,805.9	—	5.36	6.20	3–2	$e^7D-w^3P^0$	
15,597.1	.....	5.39	6.18	2–1		
16,157.5	10	5.40	6.17	1–0		
15,255.2	.....	5.39	6.20	2–2		
15,921.1	21	5.40	6.18	1–1		5
15,565.1	.....	5.40	6.20	1–2		
15,921.1	21	5.46	6.24	5–6	$w^5F^0-e^5G$	5
14,962.9	—	5.43	6.26	4–5		
14,673.0	—	5.45	6.29	3–4		
14,418.7	—	5.47	6.32	2–3		
14,298.7	—	5.48	6.34	1–2		
15,475.1	9	5.46	6.26	5–5		
14,369.9	—	5.43	6.29	4–4		
14,174.9	—	5.45	6.32	3–3		
14,110.1	—	5.47	6.34	2–2		
14,841.6	—	5.46	6.29	5–4		
13,891.8	—	5.43	6.32	4–3		
13,878.5	—	5.45	6.34	3–2		
15,769.3	?	5.52	6.30	4–5	$e^5D-u^5F^0$	2
15,818.1	24	5.56	6.34	3–4		
15,905.9	17	5.60	6.37	2–3		
15,822.4	16	5.62	6.40	1–2		
15,741.8	16	5.63	6.41	0–1		
14,911.3	—	5.52	6.34	4–4		
15,244.8	21	5.56	6.37	3–3		
15,395.3	20	5.60	6.40	2–2		
15,531.7	11	5.62	6.41	1–1		
14,400.9	—	5.56	6.37	4–3		
14,775.2	—	5.60	6.40	3–2		
15,120.0	—	5.62	6.41	2–1		
15,621.6	24	5.52	6.31	4–4	$e^5D-t^5D^0$	
15,868.4	19	5.56	6.34	3–3		
15,878.3	15	5.60	6.37	2–2		
15,799.2	16	5.62	6.40	1–1		
14,956.0	—	5.52	6.34	4–3		
15,219.5	21	5.56	6.37	3–2		
15,373.3	?	5.60	6.40	2–1		1
15,541.6	12	5.62	6.41	1–0		1
16,619.6	?	5.56	6.31	3–4		6
16,585.9	4	5.60	6.34	2–3		
16,333.0	5	5.62	6.37	1–2		
16,016.6	10	5.63	6.40	0–1		2
14,791.3	—	5.52	6.35	4–3	$e^5D-5^0_2$	

TABLE 2—*Continued*

λ Pred.	Int.	E.P.		J	Multiplet	Remarks
		Low	High			
		Fe I—Continued				
15,683.0	6	5.56	6.35	3–3		
16,383.5	4	5.60	6.35	2–3		
14,251.5	—	5.52	6.38	4–3	$e^5D-u^5P^0$	
14,522.6	—	5.56	6.41	3–2		
14,751:	—	5.60	6.43	2–1		
15,077.4	—	5.56	6.38	3–3		
15,121.2	—	5.60	6.41	2–2		
15,145:	—	5.62	6.43	1–1		
15,723.7	18	5.60	6.38	2–3		
15,533.1	?	5.62	6.41	1–2		5
15,344.5	12	5.63	6.43	0–1		
15,537.6	9	5.77	6.56	4–4	$u^5D^0-h^5D$	
14,700.0	—	5.77	6.61	3–3		
14,124.2	—	5.79	6.66	2–2		
14,373.8	—	5.82	6.68	1–1		
14,648.0	—	5.77	6.61	4–3		
14,843.4	—	5.77	6.66	3–2		
13,800.9	—	5.79	6.68	2–1		
15,596.2	.....	5.77	6.56	3–4		
15,017.0	—	5.79	6.61	2–3		
14,724.7	—	5.82	6.66	1–2		
14,361.9	—	5.82	6.68	0–1		
15,911.3	15	5.85	6.62	4–3	$e^5F-y^1F^0$	
16,928.5	8	5.90	6.62	3–3		
17,774.7	—	5.93	6.62	2–3		
16,516.8	17	5.92	6.67	4–5	e^5F-12^0	
15,767.6	?	5.92	6.70	4–4	e^5F-13^0	4
17,327.9	32	5.99	6.70	3–4		
17,293.6	5	5.92	6.64	3–3	$v^5P^0-f^5D$	
16,935.0	7	5.95	6.67	2–2		1
16,230.8	?	5.96	6.72	1–1		7
16,388.5	.....	5.92	6.67	3–2		1
15,904.5	16	5.95	6.72	2–1		
17,903.2	—	5.95	6.64	2–3		
17,305.5	.....	5.96	6.67	1–2		
19,519.5	—	5.95	6.59	5–6	$w^3G^0-e^5H$	
18,136.1	—	5.97	6.65	4–5		
17,352.0	—	5.98	6.70	3–4		
17,716.4	—	5.95	6.65	5–5		
17,015.9	5	5.97	6.70	4–4		
16,619.7	4	5.98	6.73	3–3		6
16,645.9	17	5.95	6.70	5–4		
16,311.0	9	5.97	6.73	4–3		
17,045.3	7	6.24	6.97	3–4	z^1F^0-2	
15,980.8	25	6.24	7.02	3–4	z^1F^0-3	
17,338.3	22	6.31	7.02	4–4	t^5D^0-3	
18,239.1	—	6.34	7.02	3–4		

TABLE 2—*Continued*

λ Pred.	Int.	E.P.		J	Multiplet	Remarks
		Low	High			
	Ni I					
15,208.5	26	5.26	6.07	4–5	$x^3F^0-e^3G$	
18,112.2	—	5.39	6.07	3–4		
15,171.1	—	5.26	6.07	4–4		
14,234.8	—	5.39	6.26	3–3		
12,353.8	—	5.26	6.26	4–3		
16,363.7	8?	5.26	6.01	3–4	$e^3D-v^3F^0$	4
16,996.4	16	5.28	6.01	2–3		
16,868.2	12?	5.45	6.18	1–2		8
16,480.6	8	5.26	6.01	3–3		
13,791.5	—	5.28	6.18	2–2		
13,449.8	—	5.26	6.18	3–2		
16,310.6	9	5.26	6.02	3–2	$e^3D-w^3P^0$	
15,116.8	—	5.28	6.10	2–1		
16,589.6	?	5.45	6.19	1–0		6
16,815.6	7	5.28	6.02	2–2		
18,894.2	—	5.45	6.10	1–1		
21,624.8	—	5.45	6.02	1–2		

NOTES FOR TABLE 2

1. Blend with atm.
2. Blend with atm CO_2.
3. Blend with *Si*.
4. Blend with *Mg*.
5. Blend with *Fe*.
6. Blend with atm CH_4.
7. Blend with ⊙.
8. Blend with *C*? atm.

that an atmospheric line or another strong solar line occurs at or near the predicted position.

There are several reasons why the number of identifications is small compared with a relatively large number of predicted multiplets. First, there are many local regions of strong atmospheric absorption in the 1.6 μ window. Strong individual lines of water vapor mask many solar lines in the regions λλ 15,200–15,500 and λλ 17,000–17,500. A similar masking effect takes place in the region of the CO_2 band systems at 1.57 and 1.60 μ. Second, all but a very few of the predicted infrared lines have lower excitation potentials in excess of 4 volts, and the majority lie above 5 volts. For an excitation temperature of about 5000° K, the Boltzmann equation requires that the numbers of atoms in excited states diminish approximately as $10^{-\chi}$, where χ is the excitation potential in volts. The Boltzmann equation thus operates as a law of diminishing returns in the infrared. Third, in the absence of laboratory data, the theoretical intensity relationships for multiplets must serve as a guide for conclusive identification. In a great many important cases, particularly in *Fe* and *Si*, where departures from *LS* coupling are widespread, the intensity rules are not valid for transitions that violate the rules of *LS* coupling. Further, important members of multiplets frequently occur in regions of strong water-vapor obscuration at 1.4 and 1.8 μ. For these reasons, we have possibly been overconservative in assigning identifications, pending laboratory studies in the lead sulphide region. For example, in addition to those *Fe* identifications given in Table 1, we have found at least fifty additional coincidences with predicted lines but have tem-

porarily withheld such identifications until laboratory intensities can be secured. We understand that laboratory studies in the lead sulphide region are being carried out for *Fe* I by Dr. Russell A. Fisher, of Northwestern University, and for the alkaline earths by Dr. W. J. Humphreys, of the National Bureau of Standards.

The elements thus far identified with reasonable certainty in the infrared solar spectrum include the neutral atoms of *H*, *C*, *Na*, *Mg*, *Al*, *Si*, *Fe*, *Mn*, and *Ni*. No ionized atoms have as yet been identified, although a preliminary search has been made on the basis of published term lists. Faint lines of *Ca*, *Ti*, and *V* are suspected, but their confirmation and also those of other low-ionization-potential atoms must await observation of the sunspot spectrum. The following remarks are of interest in connection with the new identifications.

Hydrogen.—The appearance of the third, seventh, and eighth members of the Brackett series in the infrared solar spectrum is shown in the upper half of Figure 1. The lines are extremely broad and shallow. The depth of Brackett *3* is about 20 per cent, and its total width is about 40 A. The two strong lines on either side of Brackett *3* are telluric. Lines *7* and *8*, although distinctly present, can barely be distinguished from the continuous background and are overlaid with other much narrower solar and telluric lines. An analysis based on the theory of Stark broadening is being made of the profile of Brackett *3*.

Carbon.—Eight strong lines of *C* I have been found between λ 16,180 and λ 17,456. The great strength and width of the $3p^1D-3d^1F^0$ line at λ 16,888 are noteworthy. The excitation potential of this line is 8.96 volts. The behavior of this and other high-excitation lines at the extreme solar limb is being investigated by A. K. Pierce and R. M. Page.

Sodium.—No lines of *Na* I have been identified in the 1.6 μ region. We have, however, included in Table 2 the doublet at λ 22,081.2 and λ 22,054.4, which arises from the transition 4s–4p (see Fig. 1).

Magnesium.—The *Mg* I lines are extremely wide and intense in the infrared solar spectrum. The $4s^1S-4p^1P^0$ line at λ 17,108.5 is the strongest solar line in the entire 1.6 μ region. It follows, therefore, that the $4p^3P^0-4d^3D$ multiplet should also appear prominently. In the compilation by C. E. Moore,[7] the term value of the $4^3P_2^0$ level is 47,851.8 cm^{-1}, whereas the 0 and 1 levels are unresolved at 47,847.7 cm^{-1}. The three levels of 4^3D are likewise unresolved at 54,192.16 cm^{-1}. The computed wave lengths for the $4^3P^0-4^3D$ transition are, therefore, as given in Table 2, λ 15,767.7 and λ 15,757.5. The laboratory wave lengths of these lines, according to Kayser and Ritschl, are λ 15,768.3 and λ 15,759.1. The first transition is undoubtedly responsible for a strong solar line at λ 15,765.9. Although closely blended with a line of CO_2, the *Mg* line is sufficiently resolved to permit an accurate wave-length measurement and to exhibit unusual width (see Fig. 2).

On the other hand, no line of sufficient intensity can be found at or near λ 15,757.5. A CO_2 line at approximately this position is of normal intensity. At λλ 15,749.1 and 15,740.7, however, there appear two strong solar lines, whose unusually large widths are characteristic of *Mg*. Furthermore, the separation in wave numbers between the 15,766 and 15,749 lines is exactly twice the separation between λ 15,749 and λ 15,741. This result implies, in accordance with the Landé interval rule, that the three lines may originate from levels with $J = 2$, 1, and 0, respectively. On the basis of the solar evidence, we suggest tentatively that the three lines in question are to be attributed to the $4^3P^0-4^3D$ multiplet of *Mg* I. The correctness of this assignment cannot be established definitely, of course, until high-resolution observations of the infrared *Mg* spectrum are made in the laboratory.

On the assumption that the foregoing identifications are correct, we find that the term values for 4^3P^0 are 47,851.09, 47,844.32, and 47,840.94 cm^{-1}, for the 2, 1, and 0 levels, respectively. It is interesting to employ the new term values to calculate wave lengths for the multiplets $4^3S-4^3P^0$, $4^3P^0-5^3D$, $4^3P^0-6^3S$, and $4^3P^0-7^3S$. All four multiplets should appear in the solar spectrum, the first two with considerable strength. The

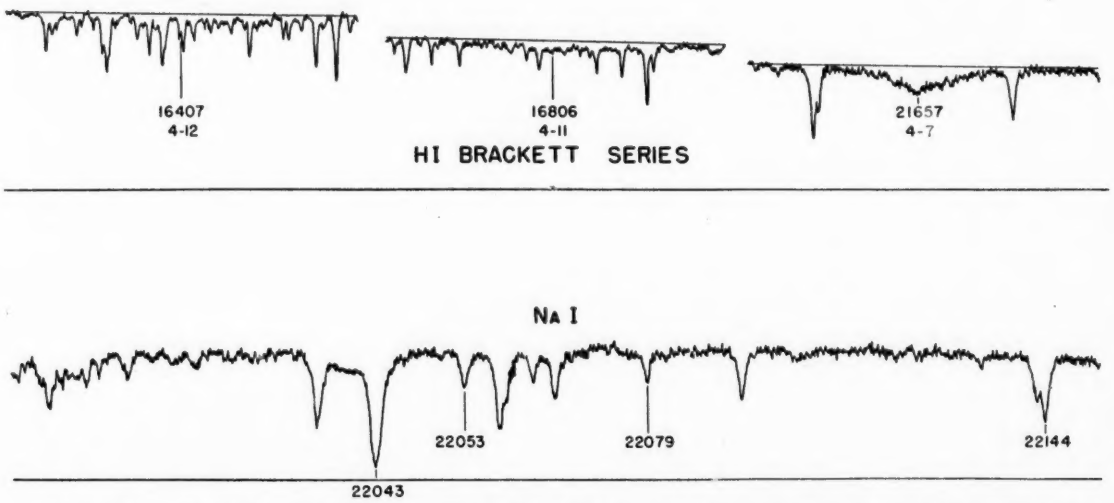

FIG. 1.—*Upper:* The third, seventh, and eighth members of the Brackett series of hydrogen, as they appear in the solar spectrum

Lower: The $4^2S-4^2P^0$ doublet of *Na* I at λ 22053 and λ 22079. The horizontal line at the bottom of each tracing represents zero intensity.

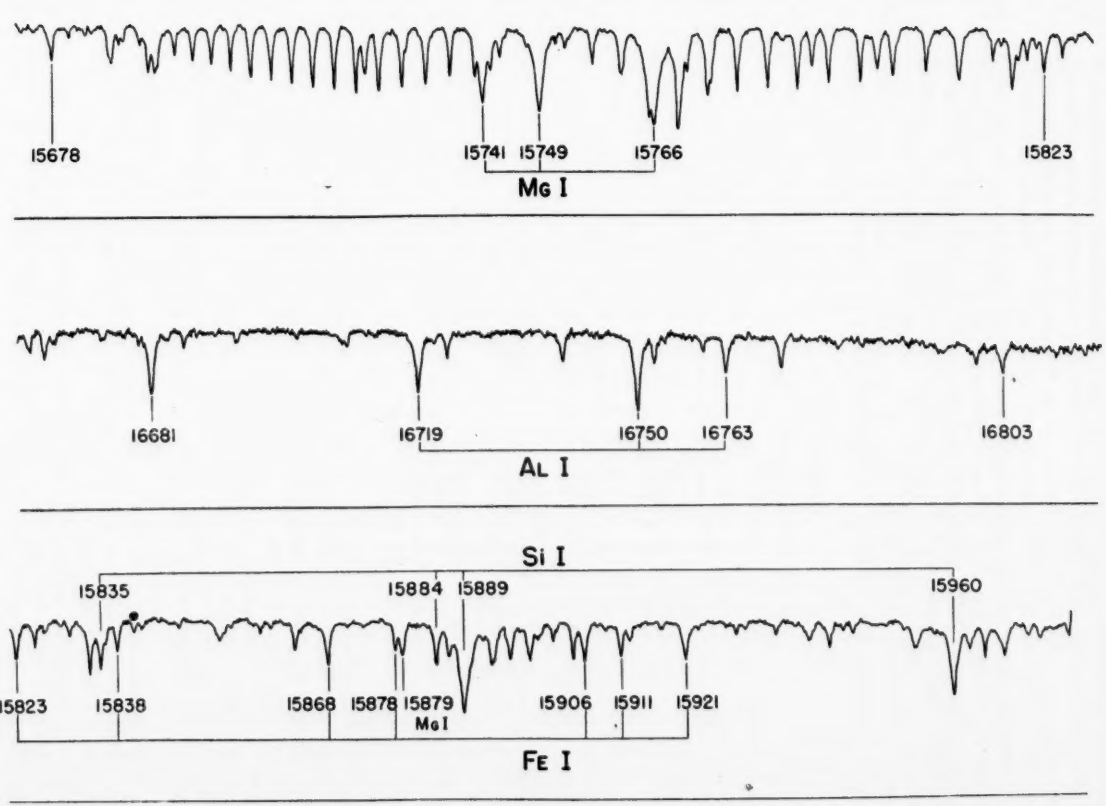

FIG. 2.—*Upper:* Magnesium lines in the solar spectrum. Note the great widths of the lines as compared with the neighboring lines of CO_2.

Middle: The $4^2P^0-4^2D$ multiplet of *Al* I. The strong line at λ 16681 is the leading member of the $4p^3D-4d^3D^0$ multiplet of *Si* I.

Lower: Strong lines of *Si* I and *Fe* I in the λ 15900 region of the solar spectrum. The horizontal line at the bottom of each tracing represents zero intensity.

results of the calculation and of a comparison with solar lines are given in Table 3. The infrared tracings show three strong lines at the calculated positions of the $4^3S-4^3P^0$ multiplet, the 15,040.4 line being closely blended with a line of water vapor. Although the spectral region at λ 15,000 consists mainly of water-vapor lines, high-low sun observations indicate that the three lines in question are of solar origin. The solar data for the remaining three multiplets were taken from the new compilation by Babcock and Moore.[8] For two of the three lines of the $4^3P^0-5^3D$ multiplet, the coincidences of computed with observed solar lines are excellent, although the relatively high excitation potential of 4^3P^0 leaves some doubt as to whether the line intensities would be expected to increase in the spot spectrum. The third line at λ 10,957.12 is masked by an intense atmospheric line. The lines of the $4^3P^0-6^3S$ multiplet also lead to good coincidences, but unfortunately with telluric lines. For the $4^3P^0-7^3S$ multiplet the coincidence of the 2–1 transi-

TABLE 3

PREDICTED MULTIPLETS OF *Mg* I

Multiplet	*J*	λ (Calc.)	λ⊙	Int.	Ident.
$4^3S-4^3P^0$	1–2	15025.1	5.0	?	⊙?
	1–1	15040.4	0.:	?	?
	1–0	15048.0	8.1	?	⊙?
$4^3P^0-5^3D$	2–3, 2, 1	10965.26	5.47	5, 8n	*Mg*?
	1–2, 1	10957.12	7.15	12nl, 12Nl	Atm
	0–1	10953.06	3.36	1, 3	⊙
$4^3P^0-6^3S$	2–1	12433.26	3.43	3	Atm
	1–1	12422.79	3.00	2	Atm
	0–1	12417.68	7.97	−1	Atm
$4^3P^0-7^3S$	2–1	9994.85	4.94	2N, 3N	⊙
	1–1	9988.09	8.29	−3	.....
	0–1	9984.76	4.18	1	Atm

tion with a diffuse solar line is convincing, particularly in view of the intensity increase in the spot spectrum. The line ascribed here to the 2–1 transition differs from that by Babcock and Moore,[9] who had tentatively assigned this transition to a line at λ 9993.17, for which the intensity decreases from 5 N in the disk spectrum to 2 N in the spot.

Aluminum.—All three members of the multiplet $4p^2P^0-4d^2D$ of *Al* I occur with considerable strength in the infrared solar spectrum (see Fig. 2). Although only the line at λ 16,719.0 is free from blending with atmospheric lines, the relative intensities indicate that the atmospheric components are weak at high solar altitudes.

Silicon.—With the single exception of *Fe* I, *Si* I is the most prolific source of solar lines in the 1.6 μ region. The line at λ 15,888.7 is one of the strongest in the entire spectrum (see Fig. 2). The occurrence of strong intersystem combinations is to be expected, since *Si* I departs widely from *LS* coupling.

Iron.—With the exception of the multiplets $e^5D-u^5F^0$, $e^5D-t^5D^0$, and $e^5D-u^5P^0$, the *Fe* I identifications are to be regarded as highly tentative. From the term values of Russell and Moore, we have predicted over fifty multiplets that obey the parity rule and give rise to lines in the 1.6 μ region. Of these, however, only the three multiplets arising from e^5D are entirely normal, in the sense that they are not either intersystem

[8] *The Solar Spectrum*, λ 6600 to λ 13,945 (*Pub. Carnegie Inst. Washington*, No. 579 [1947]).

[9] *Ibid.*

or interlimit combinations, nor do they result from double electron jumps. The identification of the remaining multiplets is uncertain because the theoretical intensity rules do not apply and no laboratory intensities are available. A number of strong infrared lines of *Fe* I are shown in Figure 2.

In conclusion, we acknowledge with thanks the invaluable contribution to the foregoing investigation by Dr. Charlotte E. Moore, of the National Bureau of Standards, who has given generously of her advice and has furnished lists of term values in advance of publication. We should also like to express our appreciation to McGregor Fund, for continuing grants-in-aid.

MULTIPLET INTENSITIES FOR THE NEBULAR LINES $^4S-^2D$ OF *O* II

L. H. ALLER,* C. W. UFFORD, AND J. H. VAN VLECK
Kirkwood Observatory, Indiana University, Bloomington, Indiana; University of Pennsylvania Philadelphia, Pennsylvania; and Harvard University, Cambridge, Massachusetts
Received July 3, 1948

ABSTRACT

The transitions $1s^22s^22p^3\ ^4S_{3/2}-^2D_{5/2}$ and $1s^22s^22p^3\ ^4S_{3/2}-^2D_{3/2}$ in *O* II are "allowed" only for electric quadrupole and magnetic dipole radiation and only if, in addition, there are deviations from Russell-Saunders coupling. The disagreement between previous theoretical computations of the relative strengths of these transitions and astrophysical observations is shown to be caused by the omission of spin-spin interaction, which is now included. The interesting feature of the calculation is that it is essential to consider not only concomitantly magnetic dipole and electric quadrupole radiation but also simultaneously the first-order effect of spin-spin coupling and the second order of spin-orbit interaction. The radial integral, η, which determines the influence of the spin-spin coupling on the transition probability was calculated by numerical integration with wave functions derived from the self-consistent field of Hartree and Black. The coupling of one spin with the orbit of another does not significantly alter the intensity ratio but does contribute to the multiplet splittings $^2D_{5/2}-^2D_{3/2}$ and $^2P_{3/2}-^2P_{1/2}$, which vanish in the conventional first approximations, since the shell is half-complete. This contribution involves the integral η as a proportionality factor and is hence examined as a control on our estimates of η.

For comparison with the theoretical calculations, the ratio of the intensities for $^4S_{3/2}-^2D_{5/2}$ and $^4S_{3/2}-^2D_{3/2}$ was measured photometrically in a number of representative planetary nebulae. The average measured value of the ratio was 0.49, to be compared with a theoretical value 0.58. The agreement is within the error of calculation.

I. INTRODUCTION

Among the strongest and most frequently observed of the forbidden lines found in the gaseous nebulae are the λ 3726.16 and λ 3728.91 lines of *O* II corresponding to the $^4S_{3/2}-^2D_{3/2}$ and $^4S_{3/2}-^2D_{5/2}$ transitions in the ground p^3 configuration. These lines are prominent in low-excitation planetary nebulae, e.g., IC 418 or NGC 40; in the diffuse nebulae, e.g., Orion or Messier 8; and in the faintly luminous patches of the Milky Way, which have been studied by Struve and his colleagues. Mayall[1] found this [*O* II] radiation which appears upon low-dispersion plates as a single unresolved line at λ 3727, in many external galaxies; and Humason[2] has studied the frequency of its appearance as a function of nebular type. The spiral nebulae show it most frequently. The bright fuzzy patches in Messier 33, the Spiral in Triangulum, show it to be stronger[3] than the well-known green "nebulium" lines of [*O* III], which are the lines usually dominant in planetary nebulae. The widespread appearance of this radiation would suggest that a knowledge of the physical parameters characterizing its production (e.g., transition probabilities) might be useful in deciphering the character of the nebulous regions in which it appears in our own and other galaxies.

Like other forbidden lines, the λ 3727 pair is produced by the collisional excitation of atoms to the upper level of the transition involved, followed by a cascade to the ground term with the emission of electric quadrupole and magnetic dipole radiation. In regions where the electron density is so high that the collisional de-excitations of the upper level are much more frequent than are radiative de-excitations, the population of the upper level follows Boltzmann's formula. Under these conditions, which may be approached in some gaseous nebulae, measures of the intensity of the lines, together with a knowledge of the electron temperature and the transition probabilities, would give us the number

* Research Associate of the W. J. McDonald Observatory of the University of Texas.

[1] *Lick Obs. Bull.*, **19**, 33, 1939.

[2] *Pub. A.S.P.*, **59**, 180, 1947.

[3] L. H. Aller, *Ap. J.*, **95**, 54, 1942.

of ionized oxygen atoms. In regions of lower density we must know the target areas for collisional excitation as well. We shall be concerned here with the calculation of the transition probabilities for the λ 3727 pair, with a view to their subsequent astrophysical applications.

The lowest configuration of *O* II is $1s^2 2s^2 2p^3$ with terms $^4S_{3/2}$, $^2D_{5/2,\,3/2}$, $^2P_{1/2,\,3/2}$ in this order from the ground state up. The spread of the configuration from ^4S to ^2P is roughly 40,000 cm^{-1}, and the multiplet separations of the ^2D and ^2P levels are, respectively, -21.0 and -1.5 cm^{-1}. Therefore, the configuration is very close to pure Russell-Saunders. The strengths of the various transitions within the configuration, all of which are rigorously forbidden for electric dipole radiation, have been calculated by Pasternack[4] and by Shortley, Aller, Baker, and Menzel,[5] henceforth abbreviated to "SABM." The lines joining ^2D and ^2P are allowed for electric quadrupole and magnetic radiation even in Russell-Saunders coupling. The transition $^4S-{}^2P$ is forbidden for such radiations in the ideal Russell-Saunders limit but is allowed as soon as one includes the first-order effect of the spin-orbit interaction. The λ 3727 pair of lines $^4S_{3/2}-{}^2D_{5/2}$, $^4S_{3/2}-{}^2D_{3/2}$, with which we are concerned, are more highly forbidden than the rest. Pasternack and SABM derive nonvanishing intensities for them by including the second-order effect of the spin-orbit coupling. However, their results for the intensities of this particular pair of lines, unlike those for the others, do not agree well with observation. The ratio r of the intensities is

$$r = \frac{I(^4S_{3/2} - {}^2D_{5/2})}{I(^4S_{3/2} - {}^2D_{3/2})}. \tag{1}$$

SABM calculate that this ratio is 0.033 for pure magnetic dipole, 2.33 for electric quadrupole, and 1.64 for both types simultaneously—the actual case. The observed value is $r = 0.49$. Pasternack obtained $r = 1.9$, in slightly worse disagreement with experiment than is the value 1.64 of SABM; Pasternack's estimate is probably the less accurate of the two, as he calculated the quadrupole moment (s_q in equation [4]) by an approximation based on screening constants rather than by means of Hartree wave functions. As Aller and Menzel[6] have emphasized, there is, apparently with either calculation, a very serious and baffling divergence between the results of theory and those of experiment.

The main thesis of the present paper is that the discrepancy is removed when one includes all the magnetic interaction between the various electrons. SABM computed the deviations from Russell-Saunders coupling by means of the conventional spin-orbit potential,

$$H_0 = -\frac{eh^2}{8\pi^2 m^2 c^2}\left(\frac{1}{r}\frac{dV}{dr}\right)\Sigma_i \boldsymbol{l}_i \cdot \boldsymbol{s}_i\,, \tag{2}$$

which couples the spin with its own orbit. Here V is the Hartree central potential, and $-dV/dr$ is thus equal to $(Z - \sigma(r))e/r^2$, where $-\sigma(r)e$ is the mean electronic charge, other than that of one $2p$ electron, interior to a radius r. Pasternack and SABM both omitted the magnetic interaction of the spins with each other, and also part of the interaction of the spin of one electron with the orbit of another. The explicit formula for the portion of the Hamiltonian which they omitted is[7]

$$\begin{aligned} H_1 = {} & \Sigma_{j\neq i}\frac{e^2 h}{2\pi m^2 c^2 r_{ij}^3}[\boldsymbol{r}_{ij} \times (\boldsymbol{p}_j - \tfrac{1}{2}\boldsymbol{p}_i)\cdot \boldsymbol{s}_i] \\ & + \Sigma_{j>i}\frac{e^2 h^2}{4\pi^2 m^2 c^2 r_{ij}^3} \times [\boldsymbol{s}_i \cdot \boldsymbol{s}_j - 3 r_{ij}^{-2}(\boldsymbol{s}_i \cdot \boldsymbol{r}_{ij})(\boldsymbol{s}_j \cdot \boldsymbol{r}_{ij})], \end{aligned} \tag{3}$$

[4] *Ap. J.*, **92**, 129, 1940. [5] *Ap. J.*, **92**, 178, 1940. [6] *Ap. J.*, **102**, 246, 1945.

[7] W. Heisenberg, *Zs. f. Phys.*, **39**, 499, 1926; or Condon and Shortley, *The Theory of Atomic Spectra* (Cambridge: At the University Press, 1935), p. 211. The factor $\frac{1}{2}$ in the term of eq. (3) proportional to $\boldsymbol{p}_i$ arises from the Thomas correction. In principle, we should add to eq. (3) a term $(e^2h^2/4\pi^2m^2c^2r^3)\sigma_{2p}(r)\Sigma_i$

where $\mathbf{r}_{ij} = \mathbf{r}_i - \mathbf{r}_j$. Here the first sum comes from the interaction of one spin with the orbit of another, while the second sum is the spin-spin interaction. The momentum operator $(h/2\pi i)$ grad $_j$ . . . of an electron is denoted by $\mathbf{p}_j$, and its spin, measured in multiples of $h/2\pi$, by $\mathbf{s}_j$. Thus the components of $\mathbf{s}_j$ are proportional to the usual Pauli matrices.

The contribution of the Hamiltonian (3) to the energy has been computed by a variety of authors,[8] though not explicitly in *O* II. In the present paper we shall be concerned with the effect of (3) on the magnetic dipole and electric quadrupole radiation. For this purpose it is, of course, necessary to calculate how the interactions (2) and (3) perturb the wave functions.

When the effect of (3) is included, we find that the intensity ratio (1) of the lines in question becomes 0.58, in more satisfactory agreement with the observational value 0.49. It may seem startling to the reader that the result is so significantly altered by the addition of (3) to (2), since usually (3) is a subordinate correction. The reason why the interaction (3) is abnormally important in our problem is that the spin-spin portion (second sum) of (3) affects the intensity of the lines in question in the first order, whereas the ordinary magnetic coupling (2) does so only in the second order.

In Section IV of this paper we shall examine the multiplet splittings of the $^2P_{1/2,\ 3/2}$ and $^2D_{3/2,\ 5/2}$ states. The question of multiplet widths is, of course, superficially a quite different one from that of intensities, but the same radial integrals are involved in both quantities. It is for this reason that it is instructive also to study the multiplet splittings. The first sum of equation (3), i.e., the portion which is caused by the interaction of one spin with the orbit of another electron, has no appreciable effect on the intensity ratio. On the other hand, only this part of (3) is of importance in connection with the multiplet intervals. Since the shell is only half-complete, the conventional spin-orbit interaction (2) does not contribute to the multiplet splitting except in the second and higher orders. This fact explains why the multiplet intervals are so small for the states in question.

We use Hartree wave functions[9] throughout. Eigenfunctions inclusive of exchange in the Fock approximation have been calculated by Hartree, Hartree, and Swirles;[10] but it was not thought that the small difference introduced by exchange would be significant for our purposes. The final results depend on the values of three integrals, viz.,

$$s_q = \left(\frac{2}{5}\right) e \int_0^\infty r^2 R_{2p}^2(r)\, dr\,, \tag{4}$$

$$\zeta = \frac{eh^2}{8\pi^2 m^2 c^2} \int_0^\infty r^{-1} \frac{-dV}{dr} R_{2p}^2(r)\, dr\,, \tag{5}$$

$$\eta = \frac{e^2 h^2}{16\pi^2 m^2 c^2} \int_0^\infty \int_0^{r_2} r_2^{-3} R_{2p}^2(r_1) R_{2p}^2(r_2)\, dr_1 dr_2\,. \tag{6}$$

$\mathbf{l}_i \cdot \mathbf{s}_i$, to allow for the fact that the interaction of a spin with the orbital magnetic moment of another electron has already been included in eq. (2) to the extent that the field from the other electron can be regarded as central, and, of course, it is erroneous to count the same effect twice. Here $\sigma_{2p}(r)$ denotes the fraction of the charge of a $2p$ electron, which is, on the average, interior to r. In our particular case of the configuration $2p^3$, however, this correction to eq. (3) is unnecessary to the degree of approximation under consideration, for we are interested only in a matrix element of (3) when the corresponding matrix element of (2), and hence the redundancy correction, are zero. In general, the term of eq. (3) proportional to $-\frac{1}{2}\mathbf{p}_i$ is equivalent to the corresponding screening portion of eq. (2), provided that the charge cloud of the jth electron is centrosymmetric, which, of course, it is not for a $2p$ electron. Because of an erroneous factor $\frac{1}{2}$, this equivalence is not brought out in the discussion on p. 212 of Condon and Shortley, as the factor which they give there as $Zr_1^{-3} - \frac{1}{2}r_{12}^{-3}$ should read $\frac{1}{2}Zr_1^{-3} - \frac{1}{2}r_{12}^{-3}$ (or, more accurately, $\frac{1}{2}Zr_1^{-3} - \frac{1}{2}\sigma(r_1)r_1^{-3}$, when Gauss's theorem is applied to the relevant portion of eq. [1], p. 211, with the assumption of central symmetry).

[8] G. Breit, *Phys. Rev.*, **36**, 383, 1930; **39**, 636, 1932; H. Wolfe, *Phys. Rev.*, **41**, 443, 1932; E. David, *Zs. f. Phys.*, **91**, 289, 1934; G. Araki, *Proc. Math. Phys. Soc. Japan*, **19**, 128, 1937; D. R. Inglis, *Phys. Rev.*, **61**, 297, 1942.

[9] D. R. Hartree and M. M. Black, *Proc. R. Soc. London, A*, **139**, 311, 1933.

[10] *Phil. Trans. R. Soc. London, A*, **238**, 229, 1939–40.

Here $R_{2p}(r)/r$ is the radial part of the $2p$ wave function, supposed normalized in the fashion

$$\int_0^\infty R_{2p}^2(r)\,dr = 1\,.$$

The expression (4) gives the second moment involved in the quadrupole strength. The radial integral in (5) is the usual one involved in the conventional spin-orbit interaction (2). The matrix elements of (3), on the other hand, are all proportional to the double integral (5). The way the various integrals are involved is best exhibited by giving the structure of the final formula for the transition probability, which turns out to be

$$A = [\alpha s_q^2\zeta^2 + \rho\zeta^4 + \gamma\zeta^2\eta + \delta\eta^2]\,. \tag{7}$$

Here α, β, γ, δ are constants which are, of course, different for the $^4S_{3/2}-{}^2D_{3/2}$ and $^4S_{3/2}-{}^2D_{5/2}$ transitions and which will be computed later in the paper in terms of known parameters, such as the $^4S-{}^2D$ and $^4S-{}^2P$ frequency intervals. Both SABM and Pasternack had only the part of equation (7) not involving η.

The integral ζ is best evaluated by extrapolation from the multiplet intervals in adjacent configurations, such as $2p^2$, $2p^4$, where the first-order effect of the spin-orbit interaction does not disappear because of half-completion of the shell. This extrapolation[11] gives $\zeta = 174$ cm^{-1}. Condon[12] has calculated s_q to be $0.70ea_H^2$ ($a_H = he/4\pi mc$) by means of Hartree wave functions. In Section IV we shall obtain the value 1.33 cm^{-1} for η.

II. THE MATRIX OF THE MAGNETIC INTERACTION

The matrix elements of the conventional spin-orbit interaction (2) have been calculated elsewhere in the literature, and so we shall not give details of how they are obtained.

In order to calculate the multiplet splittings, we shall need, in addition, the diagonal elements of the remainder (3) of the Hamiltonian. Also, in connection with the intensity problem, we shall require the matrix elements of (3) of the form $^4S_{3/2}-{}^2D_{3/2}$, since the intensities of the lines under consideration are very sensitive to this element. The only nonvanishing elements of the conventional spin-orbit interaction (2) are off-diagonal ones of the type $^4S-{}^2P$ and $^2P-{}^2D$. This interaction, when present, is much greater than the interelectronic magnetic coupling represented by the expression (3); in fact, the integral ζ is over one hundred times as large as η. Hence for our purposes it is pointless to calculate the matrix elements of (3) of the form $^4S-{}^2P$ or $^2P-{}^2D$, since they would be of much smaller order than the corresponding elements of (2). In other words, in our later secular determinant (15), entries involving η are carried only when nonconcurrent with ζ.

The Hamiltonian (3) involves the co-ordinates of two electrons. The matrix elements for the states in Russell-Saunders coupling in the *LSJ* system will be linear combinations of these two electron matrix elements. Hence, by expansion of the wave functions, the matrix elements for our three-electron system can be expressed in terms of those for a two-electron system, for which formulae have been given by Marvin.[13] The reduction of the three- to the two-electron problem is simplified by using the Slater method of diagonal sums,[14] together with certain deductions from group theory concerning the structure of the matrix elements. Considerations based on group theory or explicit calculation show that the only nonvanishing element of the second or spin-spin part of (3)

[11] Cf., e.g., H. A. Robinson and G. H. Shortley, *Phys. Rev.*, **52**, 713, 1937.

[12] *Ap. J.*, **79**, 219, 1939.

[13] *Phys. Rev.*, **71**, 102, 1947. The results of the present paper were obtained before Marvin's paper appeared and agree with those from his formulae.

[14] *Phys. Rev.*, **34**, 1293, 1929. For a good explanation of the general method which we use for calculating spectral terms by means of Slater determinants, see chaps. vi–viii of Condon and Shortley, *op. cit.*

is of the structure $^4S_{3/2}-{}^2D_{3/2}$. Furthermore, the diagonal elements of the first member of (3) are of the form

$$(LSJ\,|\,H_1\,|\,LSJ) = C\,[J\,(J+1) - L\,(L+1) - S\,(S+1)]\,, \tag{8}$$

where C is independent of J but depends on L and S. This structure is a group-theoretical consequence[15] of the fact that $r_{ij}^{-3}[(\boldsymbol{r}_i - \boldsymbol{r}_j) \times (\boldsymbol{p}_j - \tfrac{1}{2}\boldsymbol{p}_i)]$ transforms under a rotation of the orbital frame like the vector $\boldsymbol{L}$, and $\boldsymbol{s}_i$ under a rotation of the spin frame like the vector $\boldsymbol{S}$.

For $M = \frac{5}{2}$ there is the single Slater determinant, symbolized in the notation of Condon and Shortley by

$$^2D_{5/2} = |\,1^+1^-0^+\,|\,.$$

By following their *Theory of Atomic Spectra* (p. 171), one can express the corresponding diagonal matrix elements as the sum of twelve two-electron integrals of the typical form

$$\tfrac{1}{2}\int (1^+1^-)\,H_1\,(1^+1^-)\,.$$

These twelve integrals can be calculated by means of Marvin's formula (21). When they are summed algebraically with the proper sign, one finds

$$(^2D_{5/2}\,|\,H_1\,|\,^2D_{5/2}) = -\frac{37\eta}{5}\,, \tag{9}$$

with η as in equation (6). From (8), it follows immediately that

$$(^2D_{3/2}\,|\,H_1\,|\,^2D_{3/2}) = \frac{111\eta}{10}\,. \tag{10}$$

Furthermore, we have

$$(^4S_{3/2}\,|\,H_1\,|\,^4S_{3/2}) = 0\,, \tag{11}$$

since equation (8) vanishes when $J = L$ and $S = 0$.

For $M = \frac{3}{2}$ the Slater determinants in the zero-order scheme are

$$F = |\,1^+0^+ - 1^+\,|\,,\quad G = |\,1^+1^-0^-\,|\,,\quad H = |\,1^+1^- - 1^+\,|\,,\quad I = |\,1^+0^+0^-\,|\,.$$

The diagonal elements, found in the same way as above, are

$$\int F^*H_1F = 0\,,\quad \int G^*H_1G = \frac{37\eta}{5}\,,\quad \int H^*H_1H = -\frac{8\eta}{5}\,,\quad \int I^*H_1I = -\frac{23\eta}{5}\,.$$

Hence the invariance of the diagonal sum gives

$$(^2D_{5/2}\,|\,H_1\,|\,^2D_{5/2}) + (^2D_{3/2}\,|\,H_1\,|\,^2D_{3/2}) + (^2P_{3/2}\,|\,H_1\,|\,^2P_{3/2}) + (^4S_{3/2}\,|\,H_1\,|\,^4S_{3/2}) = \frac{6\eta}{5}\,.$$

Using equations (9), (10), and (11), we thus have

$$(^2P_{3/2}\,|\,H_1\,|\,^2P_{3/2}) = -\frac{5\eta}{2}\,, \tag{12}$$

and, by equation (8),

$$(^2P_{1/2}\,|\,H_1\,|\,^2P_{1/2}) = 5\eta\,. \tag{13}$$

The matrix element connecting $^4S_{3/2}$ and $^2D_{3/2}$ comes entirely from spin-spin interaction. It is calculated by using the Slater determinantal wave functions and noting that the linear combinations appropriate to the LSJ system are

$$^4S_{3/2} = F\,,\qquad ^2D_{3/2} = \frac{2\sqrt{2}G - H + I}{\sqrt{10}}\,.$$

[15] H. A. Kramers, *Kon. Akad. v. Wetensch. Amsterdam*, **34**, 965, 1931.

The matrix elements can be expressed in terms of those for the two-electron system by the same procedure as before. The relevant formula of Marvin is his equation (22) rather than (21), since now we are dealing with spin-spin coupling rather than with interaction of the orbit of one electron with the spin of another electron. The final result is

$$(^4S_{3/2}|\,H_1\,|^2D_{3/2}) = -\frac{6\eta}{\sqrt{5}}. \tag{14}$$

Before termination of the present section, there are two remarks that seem worth making about the calculation of the matrix elements for a two-electron system. One of these observations is that, in the calculation of the diagonal elements, one can omit entirely the application of the momentum operator $(h/2\pi i)$ grad . . . , to the radial factors in the wave functions. Such an application can give only zero, inasmuch as the radial factors are real; and so a nonvanishing result would give an imaginary diagonal element, impossible for a self-adjoint operator. This remark is based on the assumption that the wave function can be expressed as a simple Slater determinant. If one allows for polarization effects not included in the present paper, the decomposition into sums of products of one-electron functions, each separable into polar co-ordinates, is no longer possible, and the argument ceases to apply.

Our other remark is that the proportionality of the matrix elements given in equations (9)–(14) to the integral η may appear to the reader only an approximation contingent on the retention of terms of lowest nonvanishing order in the expansion of the Hamiltonian in the ratio of the smaller to the larger radius for a pair of electrons. Actually, the proportionality is rigorous for the $2p^3$ configuration or any other configuration of type $2p^z$ (neglecting polarization or, in other words, configuration interaction). This point is not mentioned by Marvin and is proved by the following reasoning not involving orbital co-ordinates. If k is an arbitrary vector not involving orbital co-ordinates, the function $(r_{ij}\cdot k)/r_{ij}^3$, regarded as a function either of the variables x_i, y_i, z_i, or x_j, y_j, z_j, is a solution of Laplace's equation, and so its expansion takes the form

$$\sum_{l=0}^{\infty}\sum_{m=-l}^{l} a_{lm}T_{lm}(\theta_<\phi_<)T_{l+1,-m}(\theta_>,\phi_>)\frac{r_<^l}{r_>^{l+2}}.$$

Consider, first, the case in which the momentum or gradient operator involved in the first part of equation (3) works on the inner electron. Then when we integrate over the co-ordinates of the outer electron, in $\int\Psi^*H_1\Psi$, the factor of $\Psi^*\Psi$ involving the outer electron will transform like the representation $D_1 \times D_1$ of the rotation group and so contains no representation higher than $l = 2$. Hence the orthogonality properties of different irreducible representations of the rotation group show that the integral over the outer $(>)$ electron vanishes when the above expansion of the first line of equation (3) is carried beyond $l = 1$. Furthermore, the integral vanishes when $l = 0$, as the factor $T_{l+1,\,-m}(>)$ is then odd, whereas the factor from $\Psi^*\Psi$ is even. Thus only the term with $l = 1$ persists. This is, of course, of the order of $r_>^{-3}$ corresponding to equation (6). To show that a similar result also obtains when the grad operator works on the outer electron, we note that the integrand now has as a factor Ψ^* grad Ψ, whose nonvanishing component transforms like the representation $l = 1$ of the rotation group, since grad Ψ is effectively an invariant if $\Psi = qf(r)$ $(q = x, y, z)$ and if only the application of the gradient operator to the q factor is relevant. Hence, because of the orthogonality, only the term $l = 0$ in the expansion makes a contribution, again of the order (6), since r^{-2} grad $\sim 1/r^3$. (This reasoning does not preclude the off-diagonal elements of the first part of [3] having terms of higher order than η in $1/r$; but such elements are of no importance for our problem, since we are not interested in elements of [3] of the type $[^2P|\,^4S]$ or $[^2P|\,^2D]$.) The expansion of the second or spin-spin part of equation (3) is of the form

$$\frac{\Sigma b_{lm}T_{lm}(<)T_{l+2,-m}(>)\,r_<^l}{r_>^{l+3}},$$

with coefficients b_{lm} involving the spin vectors. An analogous argument shows that integration over the outer electron gives a vanishing result except for the term $l = 0$ of the expansion.

III. PERTURBATION THEORY

The secular determinant may now be constructed from the results of the preceding section, along with the formulae for the matrix elements of the conventional spin-orbit interaction given on page 268 of Condon and Shortley. For $M = \frac{3}{2}$, the result is

$$\begin{vmatrix} E_0(^2\mathrm{D}) + \frac{111}{10}\eta - E & \frac{1}{2}\zeta\sqrt{5} & -\frac{6\eta}{\sqrt{5}} \\ \frac{1}{2}\zeta\sqrt{5} & E_0(^2\mathrm{P}) - \frac{5\eta}{2} - E & \zeta \\ -\frac{6\eta}{\sqrt{5}} & \zeta & E_0(^4\mathrm{S}) - E \end{vmatrix} \tag{15}$$

Here $E_0(^2\mathrm{D})$, for instance, denotes the energy of the ^{2}D state in the absence of any spin-orbit or magnetic coupling. The perturbation calculation is simple, since the system is nondegenerate. The second-order energies are as follows:

$$\begin{aligned} E(^2\mathrm{D}_{3/2}) &= E_0(^2\mathrm{D}) + \frac{111}{10}\eta - \frac{5\zeta^2}{4(PD)}, \\ E(^2\mathrm{P}_{3/2}) &= E_0(^2\mathrm{P}) - \frac{5\eta}{2} + \frac{5\zeta^2}{4(PD)} + \frac{\zeta^2}{(PS)}, \\ E(^4\mathrm{S}_{3/2}) &= E_0(^4\mathrm{S}) - \frac{\zeta^2}{(PS)}, \\ E(^2\mathrm{D}_{3/2}) &= E_0(^2\mathrm{D}) - \frac{37\eta}{5}, \\ E(^2\mathrm{P}_{1/2}) &= E_0(^2\mathrm{P}) + 5\eta, \end{aligned} \tag{16}$$

where $(PD) = E_0(^2\mathrm{P}) - E_0(^2\mathrm{D})$, etc. Here terms in η^2 have been neglected, since numerically η is of the order of magnitude of $\zeta^2/(PD)$. We have also included the formulae for the energies of the other states. It is not necessary to construct a secular determinant for them, since only one level has $J = \frac{5}{2}$ or $J = \frac{1}{2}$. The empirical values of the frequency denominators needed in connection with (16) are

$$(PD) = 13{,}642\ \mathrm{cm}^{-1}, \qquad (DS) = 26{,}828\ \mathrm{cm}^{-1}, \qquad (PS) = 40{,}470\ \mathrm{cm}^{-1}.$$

We prefer to use these values rather than to try to calculate them by means of the Slater F parameters, for the actual intervals do not have ratios in accord with the conventional first-order expressions for the electrostatic energy which does not include polarization. According to the formula of Slater, we should have

$$(PD) = 6F_2, \qquad (DS) = 9F_2,$$

where F_2 is a constant.

The perturbed wave functions corresponding to the approximation (16) for the $^2\mathrm{D}_{3/2}$ and $^4\mathrm{S}_{3/2}$ states are the following combinations of the unperturbed wave functions:

$$\begin{aligned} \Psi(^2\mathrm{D}_{3/2}) &= a\Psi^0(^2\mathrm{P}_{3/2}) + b\Psi^0(^4\mathrm{S}_{3/2}) + c\Psi^0(^2\mathrm{D}_{3/2}), \\ \Psi(^4\mathrm{S}_{3/2}) &= a'\Psi^0(^2\mathrm{P}_{3/2}) + b'\Psi^0(^4\mathrm{S}_{3/2}) + c'\Psi^0(^2\mathrm{D}_{3/2}). \end{aligned} \tag{17}$$

$$\begin{aligned} a &= -\frac{\zeta\sqrt{5}}{2(PD)}, \qquad a' = -\frac{\zeta}{(PS)}, \qquad b = -\frac{6\eta}{(DS)\sqrt{5}} - \frac{\zeta^2\sqrt{5}}{2(PD)(DS)}, \\ b' &= c = 1, \qquad c' = \frac{6\eta}{(DS)\sqrt{5}} + \frac{\zeta^2\sqrt{5}}{2(PS)(DS)}. \end{aligned} \tag{18}$$

Our notation for the various coefficients is the same as that of SABM, but their formulae differ from (18) in not including any of the terms proportional to η.

The line strengths can now be found from equations (11) and (12) of SABM, provided that we use the revised values (18) of the coefficients. The strengths for magnetic-dipole radiation are thus

$$S_m(^2D_{5/2}-{}^4S_{3/2}) = \frac{12c'^2}{5}\left(\frac{he}{4\pi mc}\right)^2, \qquad S_m(^2D_{3/2}-{}^4S_{3/2}) = \tfrac{4}{15}(10aa'+15bb'+6cc')^2\left(\frac{he}{4\pi mc}\right)^2. \tag{19}$$

The corresponding electric-quadrupole strengths are

$$S_q(^2D_{5/2}-{}^4S_{3/2}) = 14a'^2s_q^2, \qquad S_q(^2D_{3/2}-{}^4S_{3/2}) = (ac'+ca')^2 6s_q^2, \tag{20}$$

with s_q defined as in equation (4). Here and elsewhere terms involving powers of ζ and η higher than those given have been omitted.

The dipolar and quadrupolar transition probabilities are connected with the corresponding line strengths by the relations[16]

$$A_m = \frac{1}{2J+1}\frac{64\pi^4\nu^3}{3hc^3}S_m, \qquad A_q = \frac{1}{2J+1}\frac{32\pi^6\nu^5}{5hc^5}S_q, \tag{21}$$

where $2J+1$ is the statistical weight of the initial level. The contributions of the magnetic-dipole and electric-quadrupole radiation to the transition probability are additive. A similar additivity does not obtain for the line strengths themselves, since they are, rather artificially, defined in such a way as to make the proportionality factors different in the two relations of equations (21).

Equations (18), (19), (20), and (21) show that, when the dipolar and quadrupolar contributions to the transition probability are summed, the resultant depends on the parameters in the fashion (7). The quadrupole radiation is caused, to our approximation, only by the nondiagonal elements of the conventional spin-orbit interaction. On the other hand, the magnetic-dipole radiation depends on this interaction and the usually omitted spin-spin interaction both separately and in combination.

IV. EVALUATION OF THE RADIAL INTEGRAL η

Before a numerical estimate of the relative intensities can be made, it is necessary to know the value of the parameter η. This can be calculated by the evaluation of the integral (6) numerically with the Hartree and Black wave functions. This procedure gives $\eta = 1.33$ cm^{-1}.

As a test of the validity of the Hartree and Black wave functions for calculating η, the radial integral ζ of the conventional spin-orbit interaction was calculated numerically. The value of $-dV/dr$ to be used in equation (5), then, is

$$-\frac{dV}{dr} = er^{-2}\left\{8 - 2\int_0^r [R_{1s}(r)^2 + R_{2s}(r)^2 + R_{2p}(r)^2]\,dr\right\}. \tag{22}$$

When equation (22) is employed, the value of ζ turns out to be 198 cm^{-1}, which is larger than the presumably correct value 174 cm^{-1} obtained from the isoelectronic sequence. The lack of perfect agreement is not disquieting, for evaluation of ζ requires very accurate wave functions near the nucleus. The inner regions are weighted less strongly in the computation of η than in that of ζ, though still more heavily than in the calculation of electrostatic binding energies. The discrepancy between the empirical value of ζ and that calculated by the Hartree and Black wave functions suggests that possibly η should be reduced by a factor of 174/198 to the value 1.17 cm^{-1}, though this is probably an overcorrection.

[16] Cf. Condon and Shortley, *op. cit.*, pp. 98 and 100, eqs. (3) and (8).

If the value 1.17 cm^{-1} were used instead of 1.33, the intensity ratio defined in equation (1) would be increased by 10 per cent, and the agreement with experiment would be somewhat less satisfactory. If the value 198 rather than 174 cm^{-1} were employed for ζ, this ratio would be increased by 3.5 per cent. The relative transition probabilities are thus more sensitive to changes of η than to those of ζ.

V. MULTIPLET SPLITTINGS OF THE ^2P AND ^2D TERMS

Once the integrals η and ζ are known, the multiplet intervals in the ^2D and ^2P states can be calculated and compared with experiment. If we take $\eta = 1.33$ cm^{-1} and $\zeta = 174$ cm^{-1}, the values of the splittings obtained from equation (16) are

$$\Delta^2D = E(^2D_{5/2}) - E(^2D_{3/2}) = -21.8\ cm^{-1},$$

$$\Delta^2P = E(^2P_{3/2}) - E(^2P_{1/2}) = -16.4\ cm^{-1};$$

whereas the experimental values are[17]

$$\Delta^2D = -21.0, \qquad \Delta^2P = -15\ cm^{-1}.$$

The agreement between theory and experiment for Δ^2D is striking, and appears to confirm our evaluation of η. On the other hand, no reasonable choice of η will possibly remove the discrepancy for Δ^2P; the value $\eta = 0.57$ cm^{-1} would be required. The disagreement is probably caused by the neglect of polarization or, in other words, configuration interaction. The calculated values are probably quite sensitive to polarization corrections, as they may make the conventional spin-orbit coupling no longer quite disappear from the diagonal, even though the shell is half-complete. It is puzzling why these corrections are apparently so much larger for Δ^2P than for Δ^2D.

VI. THE TRANSITION PROBABILITIES

With the values of s_q, ζ, and η available, it is now possible to find numerical values for the strengths (19) and (20) and hence for the transition probabilities A. With $\zeta = 174$ cm^{-1} and $\eta = 1.33$ cm^{-1}, we find that[18]

$$A(^2D_{5/2} \rightarrow {}^4S_{3/2}) = (4.85 + .02 + 0.17 + 0.37) \times 10^{-5} = 5.41 \times 10^{-5}\ sec^{-1}, \quad (23)$$

$$A(^2D_{3/2} \rightarrow {}^4S_{3/2}) = (3.12 + 1.19 + 4.82 + 4.88) \times 10^{-5} = 14.01 \times 10^{-5}\ sec^{-1}. \quad (24)$$

Because of the statistical weight factor, the intensity ratio (1) is $\frac{3}{2}$ times the quotient of equation (23) by equation (24). The various terms in the sums show the breakdown in terms of the structure (7). By comparison of equations (23) and (24) with equation (7) it is seen that the spin-spin interaction contributes appreciably to the total transition probability both by itself in a term of the form η^2 and by combination with the conventional spin-orbit interaction in a term of the type $\eta\zeta^2$. In fact, the last two terms are the major part of the expression (24). On the other hand, the quadrupole member constitutes the bulk of (23).

With our choice of constants, the theoretical value of the ratio (1) of the intensities of the two components of the $^4S - {}^2D$ multiplet is $r = 0.58$. The observed values to be compared with this will be discussed in the next section.

[17] The values of the intervals which we quote are from *Atomic Energy Levels*, by Charlotte E. Moore, **1**, sec. 1, 48 (Circular 467 of the National Bureau of Standards). These values supersede the less accurate ones given in the older tables of Bacher and Goudsmit. We are much indebted to Mrs. Sitterly for informing us of the re-evaluation of the levels in advance of publication.

[18] Note that we use arrows in connection with transition probabilities but not in connection with line strengths, since the former, unlike the latter, are unsymmetric as regards interchange of initial and final indices.

VII. THE OBSERVED INTENSITY RATIO OF THE $^4S_{3/2}-{}^2D_{5/2}$ AND $^4S_{3/2}-{}^2D_{3/2}$ LINES OF *O* II

For comparison with the theoretical calculations, one of us (L. H. A.) decided to measure photometrically, in a number of representative planetary nebulae, the intensity ratio of the two multiplet components $^4S_{3/2}-{}^2D_{5/2}$ and $^4S_{3/2}-{}^2D_{3/2}$, which have wave lengths, respectively, 3729 and 3726 A. For ten such nebulae, observations were secured with the 82-inch reflector of the McDonald Observatory and the Cassegrain spectrograph equipped with quartz prisms and 500-mm camera, which gives a dispersion of 33 A/mm at λ 3727. A spot sensitometer and wedge-slit exposures with a lamp provided the photometric calibration. The data for NGC 7027 are taken from Mount Wilson

TABLE 1

INTENSITY RATIO λ 3729/λ 3726 IN THE PLANETARY NEBULAE

Nebula	α	δ	Plate No.	Date	No. of Points	r
NGC 40	$0^h\ 7^m6$	+71° 32′	CQ 4619	Sept. 1, 1945	4	0.85
			CQ 4625	Sept. 2, 1945	3	.82
NGC 2392	7 23.3	+21 7	CQ 5222	Apr. 10, 1947	1	.46:
IC 4593	16 7.0	+12 20	CQ 4593	Aug. 25, 1945	1	.67
NGC 6210	16 40.3	+23 59	CQ 4599	Aug. 26, 1945	2	.48
			CQ 4628	Sept. 3, 1945	1	.44
NGC 6543	17 58.6	+66 38	CQ 4600	Aug. 26, 1945	1	.46
			CQ 4637	Sept. 8, 1945	2	.52
NGC 6572	18 7.2	+ 6 50	CQ 4589	Aug. 24, 1945	1	.45
BD+30° 3639	19 30.8	+30 18	CQ 4642	Sept. 9, 1945	1	.46
NGC 6826	19 42.1	+50 17	CQ 4590	Aug. 24, 1945	1	.48:
IC 4997	20 15.6	+16 25	CQ 4639	Sept. 8, 1945	1	.36:
			CQ 4641	Sept. 9, 1945	1	.40:
NGC 7009	20 58.7	−11 46	CQ 4607	Aug. 31, 1945	2	.55
			CQ 4617	Sept. 1, 1945	2	.50
			CQ 4623	Sept. 2, 1945	4	.48
NGC 7027	21 3.3	+41 50	E 1730	July 31, 1946	2	.48
			E 1747	Aug. 23, 1946	1	.42
			E 1748	Aug. 24, 1946	2	.47
			E 1752	Sept. 4, 1946	2	0.50
Mean						0.49±0.01

spectrograms obtained by R. Minkowski in connection with a detailed spectrophotometric investigation of this object by Minkowski and Aller.

Table 1 gives the NGC number of the nebula, the position for epoch 1900, the plate number, the date of the observation, the number of points in the nebula at which the λ 3729/λ 3726 intensity ratio r was measured, and, finally, the intensity ratio itself.

With but three exceptions, this ratio comes out near 0.5. The ratio appears to be lower for IC 4997 and higher for IC 4593 and especially NGC 40. The discrepant ratio for NGC 40 appears to be real. Among the nebulae studied, this object has the lowest surface brightness and probably also the lowest density throughout most of its volume. It shows a pronounced filamentary structure, and much of the λ 3727 radiation may be contributed by regions of low density.

Our theoretical intensity ratio presupposes that the $^2D_{3/2}$ and $^2D_{5/2}$ levels are populated according to their statistical weights, i.e., in the ratio of 4 to 6. That is, the electron density is assumed sufficiently large for the relative populations of the excited levels to

be determined by collisional processes, i.e., collisional de-excitations of the ^2D term are assumed to be much more frequent than are radiative de-excitations.

Recent work[19] suggests that the target areas for collisional excitation of the ^2D term is so small that, in many gaseous nebulae, ions leave the metastable levels by radiation rather than by superelastic collisions. The exact theoretical value of the ratio, therefore, depends on the electron density, the electron temperature, and the cross-sections for collisional transitions between $^2D_{3/2}$, $^2D_{5/2}$, $^4S_{3/2}$, $^2P_{3/2}$, and $^2P_{1/2}$. The ratio, r, will be larger, the smaller the electron density, while with increasing electron density the intensity ratio should approach the theoretical value. The large value of the ratio for NGC 40, which presumably has the lowest density, and the small value for IC 4997, which is known to be the most dense of these nebulae, are in qualitative agreement with expectations.

Pending a complete treatment of the collisional cross-sections, we compare our theoretical value, 0.58, with the straight mean value 0.49 given by the observations, although it seems likely that the value 0.38 found from IC 4997 may turn out to be the value to be compared with the theoretical calculations.

In many instances the fluctuations in the ratio from nebula to nebula are probably real and arise from actual differences in electron density. Density fluctuations within a given nebula further complicate the problem.

VIII. CONCLUSION

The previous discrepancy between the observed and the calculated relative intensities for the 3729 and 3726 lines of *O* II is explained. The disagreement by about 20 per cent with the revised calculations is not disquieting, inasmuch as the Hartree and Black wave functions used to compute η and s_q may not be perfect and especially inasmuch as the calculation neglects polarization or configuration interaction.

The writers wish to thank Professor D. H. Menzel for his stimulating interest in this paper.

[19] L. H. Aller, *Pub. A.S.P.* (in press).

THEORETICAL CONTOURS OF ABSORPTION LINES

DANIEL L. HARRIS III
Yerkes Observatory
Received September 18, 1948

ABSTRACT

Theoretical contours for the sodium D_1 and D_2 lines are constructed for points on the solar disk corresponding to $\mu = 1.0$ (the center of the disk) and $\mu = 0.26$ ($r = 0.97R$). The contours have been constructed on the basis of the most reliable information that we have concerning the variation of the physical parameters (gas pressure, p; electron pressure, p_e; etc.) through the solar atmosphere, and allowing for the variation of the ratio of the line to the continuous absorption. A value of $\log N = 18.0$ predicts contours which are in substantial agreement with the observations.

Our knowledge of the basic physical processes operative in the solar atmosphere is now sufficiently complete that it is possible to undertake, along the lines of Strömgren's fundamental paper,[1] the construction of theoretical contours for at least the resonance lines. It is the object of this paper to illustrate how the current resources of the theory of model stellar atmospheres and of radiative transfer can be utilized for the purposes of interpreting observations. For this purpose the D lines of sodium in the solar spectrum would appear to provide an ideal test case, as we have fairly reliable knowledge of the relevant physical data and also the observations of Shane[2] and Allen.[3] More particularly, we shall construct theoretical line contours for the D_1 and D_2 lines at points on the solar disk corresponding to $\mu = 1.00$ and $\mu = 0.26$. In this connection reference should be made to the investigation of Merle Tuberg,[4] who has already considered the problem of the variation of line contours over the solar disk. However, in this paper we shall be concerned more with presenting a method of construction of line contours which might serve as an example for future comparisons between theory and observation.

I. DETERMINATION OF η

Defining η as the ratio of the line-absorption coefficient to the coefficient of continuous absorption at the frequency of the line, we shall write

$$\eta = \frac{\sigma_\nu}{\kappa_\nu} = \eta_0 H(a, v), \tag{1}$$

where

$$\eta_0 = \frac{\sqrt{\pi}\, e^2}{m c^2} \frac{\lambda^2}{\Delta\lambda_D} \frac{N_0 f}{n \bar{\kappa}}, \tag{2}$$

$$\Delta\lambda_D = \frac{\lambda}{c}\sqrt{\frac{2RT}{A_{Na}}}, \qquad n = \frac{\kappa_\nu}{\bar{\kappa}}, \tag{3}$$

and N_0 is the number of atoms per gram in the ground state.

[1] *Festschrift für Elis Strömgren* (Copenhagen: Einar Munksgaard, 1940).

[2] *Lick Obs. Bull.*, No. 507, 1941.

[3] *M.N.*, **100**, 10, 1939.

[4] *Ap. J.*, **103**, 145, 1946; see also B. Strömgren's earlier paper, *Ap. J.*, **86**, 1, 1937.

Taking $n = 0.75$[5] and evaluating the expressions for $\lambda = 5893$ A, we find

$$\Delta\lambda_D = 37.5\,\theta^{-1/2} m A\ , \tag{4}$$

$$\log \frac{N_0}{N} \approx \log \frac{N_0}{N_1} = 5.11\,\theta + 2.5 \log\ \theta - 8.78 + \log\ p_e\ , \tag{5}$$

and

$$\log \frac{\eta_0}{Nf} = -19.99 + 3 \log\theta + 5.11\,\theta + \log\ p_e - \log\ \bar{\kappa}\ . \tag{6}$$

TABLE 1

THE VARIATION OF (η_0/Nf) AND a WITH τ IN THE SOLAR ATMOSPHERE

τ	$(\eta_e/Nf)\times10^{18}$	$1/\Delta\lambda_D$	a		$(\eta_{1A}/Nf)\times10^{18}$	
			log $A = 3.8$	log $A = 3.4$	log $A = 3.8$	log $A = 3.4$
0.01	6.2×10^4	27.7 A^{-1}	0.005	0.004	0.23	0.18
0.02	5.8	27.6	.008	.006	.34	.26
0.04	5.4	27.4	.011	.008	.44	.32
0.08	4.1	27.2	.016	.011	.50	.34
0.12	3.4	26.9	.018	.013	.48	.35
0.20	2.3	26.5	.024	.017	.44	.31
0.32	1.6	26.0	.029	.020	.39	.27
0.60	8.1×10^3	25.1	.037	.026	.27	.19
1.0	4.4	24.3	.041	.031	.17	.13
1.4	2.8	23.6	.043	.036	.12	.10
2.0	1.5	22.9	.046	.036	.074	.058
3.0	7.8×10^2	22.0	.045	.036	.041	.033
4.0	4.7	21.4	.044	.035	.026	.020
5.0	2.9	20.9	.042	.034	.016	.013
6.0	2.0	20.4	0.040	0.033	0.011	0.009

Using Münch's model solar atmosphere[6] with log $A = 3.8$, we find the values of (η_0/Nf) given in the second column, and the values of $1/\Delta\lambda_D$ given in the third column, of Table 1. As $\bar{\kappa}$ is nearly proportional to p_e, the values of (η_0/Nf) are independent of log A within the computational uncertainties of the model atmospheres.

The function $H(a, v)$ has been tabulated by Hjerting,[7] and tables have been published by Harris[8] to facilitate its computation. Here v is the deviation from the center of the line in units of the Doppler width and a is the ratio of the effective natural line width to the Doppler width.

If we let $f_{\text{emission}} = \frac{1}{3}$, we find for the natural width

$$\Delta\lambda_N = \frac{\lambda^2}{c}\,\frac{4\pi e^2 \nu^2}{m c^3}\, f_{\text{em}} = 0.059 m A\ . \tag{7}$$

[5] *Ap. J.*, **102**, 385, 1945.

[6] *Ap. J.*, **106**, 217, 1947.

[7] *Ap. J.*, **88**, 508, 1938.

[8] *Ap. J.*, **108**, 112, 1948.

To evaluate the width due to collisions with neutral hydrogen, we use Lindholm's formula:[9]

$$\Delta\lambda_c = 8.43\,\frac{\lambda^2}{c}\,C^{2/5}\bar{v}^{3/5}N_e\,, \tag{8}$$

where

$$C = \frac{e^2 a}{h}\,\bar{R}_\kappa^2 = 2.65\times 10^{-32} \qquad \text{for} \qquad \bar{R}_\kappa^2 = 41\,a_0^2\,, \tag{9}$$

$$\bar{v} = \sqrt{\frac{8RT}{\pi}\left(\frac{1}{1}+\frac{1}{A_{Na}}\right)} = 1.055\times 10^6\,\theta^{-1/2}\,, \tag{10}$$

and

$$N_e = \frac{P\theta}{5040\,\kappa}\,. \tag{11}$$

We then find

$$\log \Delta\lambda_c = -4.67 + 0.7\log\,\theta + \log P\,, \tag{12}$$

where $\Delta\lambda_c$ is expressed in milliangstroms. Therefore, $a = (\Delta\lambda_c + \Delta\lambda_N)/\Delta\lambda_D$ will depend on the value of $\log A$ employed. The fourth and fifth columns of Table 1 give the values of a for $\log A = 3.8$ and $\log A = 3.4$, while the corresponding values of (η/Nf) for $\Delta\lambda = 1.0$ A are given in the sixth and seventh columns.

In the remaining part of this paper we shall consider only the value $\log A = 3.8$. The value of A can be determined by comparison of a weak and a strong line of the same metal atom in the same state of ionization, or from a weak line of a neutral metal and a strong line of the same metal in the singly ionized state, but not from a single line (or doublet).

Table 2 gives the values of (η/Nf) for $\Delta\lambda = 1.0, 0.8, \ldots, 0.2$, and 0.1 A. Therefore, each column corresponds to a constant value of $\Delta\lambda$, the required value of v being found from $v = \Delta\lambda/\Delta\lambda_D$, where the denominator varies with τ.

If we write for $H(a, v)$ the first term in its asymptotic expansion, we find that

$$\eta = \text{Constant}\,\frac{1}{\Delta\lambda_D}\,\frac{\Delta\lambda_N+\Delta\lambda_c}{\Delta\lambda_D}\cdot\frac{1}{v^2}$$

or that

$$\eta = \text{Constant}\,(\Delta\lambda_N+\Delta\lambda_c)\,(\Delta\lambda)^{-2}. \tag{13}$$

Therefore, we can use the column of (η/Nf) for $\Delta\lambda = 1.0$ A to determine the values of (η/Nf) for another value of $\Delta\lambda > 1.0$ from equation (13).

II. SOLUTION OF THE EQUATION OF TRANSFER

The equation of transfer,

$$\mu\,\frac{dI_\nu}{dt_\nu} = I_\nu - \tfrac{1}{2}\,(1-\lambda_\nu)\int_{-1}^{+1} I_\nu\,d\mu - \lambda_\nu B_\nu\,, \tag{14}$$

has been solved exactly[10] under the assumptions that η is constant with optical depth and

[9] *Über die Verbreiterung und Verschiebung von Spektrallinien* (Uppsala: Almquist & Wiksells, 1942). The constant 8.43 results from the evaluation of

$$\int_0^\infty \sin^2\left(\frac{1}{x^5}\right)x\,dx = (\tfrac{1}{2})^{8/5}\Gamma(\tfrac{3}{5})\sin\left(\frac{3\pi}{10}\right) = 0.3975\,,$$

instead of by numerical integration (Chandrasekhar, unpublished).

[10] S. Chandrasekhar, Paper XX, *Ap. J.*, **106**, 145, 1947.

that B_ν is a linear function of the optical thickness in $(\sigma_\nu + \kappa_\nu)$. The exact solution for the case $\epsilon = 0$ is

$$I(0, \mu) = \lambda^{3/2} B^{(1)} H(\mu) \left\{ \mu + \frac{B^{(0)}}{\lambda B^{(1)}} + \frac{1-\lambda}{2\lambda^{1/2}} \alpha_1 \right\}. \quad (15)$$

The problem of a variable η has been solved in the first, second, and third approximations by Merle Tuberg,[4] assuming that B_ν is a linear function of t_ν.

If we let $B_\nu = B^{(0)} + B^{(1)}\tau_\nu$, then, in the continuum,

$$I^{\text{cont}}(0, \mu) = B^{(0)} + B^{(1)}\mu ; \quad (16)$$

and we have the law of darkening,

$$\phi(\mu) = \frac{I(0, \mu)}{I(0, 0)} = \frac{\mu + \beta}{1 + \beta} \qquad \left(\beta = \frac{B^{(0)}}{B^{(1)}}\right). \quad (17)$$

TABLE 2

VALUES OF $(\eta/Nf) \times 10^{18}$

τ	$\Delta\lambda$					
	1.0 A	0.8 A	0.6 A	0.4 A	0.2 A	0.1 A
0.01	0.23	0.36	0.64	1.4	6.0	59
0.02	.34	.54	0.96	2.2	9.1	74
0.04	.44	.69	1.24	2.8	11.7	89
0.08	.50	.79	1.40	3.2	13.3	95
0.12	.48	.75	1.33	3.0	12.6	92
0.20	.44	.70	1.24	2.8	11.7	83
0.32	.39	.60	1.08	2.5	10.3	71
0.60	.27	.42	0.75	1.7	7.1	58
1.0	.17	.27	0.48	1.1	4.6	38
1.4	.12	.19	0.34	0.77	3.3	28
2.0	.074	.12	0.21	0.47	2.0	.....
3.0	.041	.064	0.11	0.26	1.1	.....
4.0	.026	.040	0.07	0.16	0.7	.....
5.0	.016	0.025	0.04	0.10	0.4	.....
6.0	0.011	.....	.....	.....	.....	.....

Figure 1 gives the law of darkening observed by Abbot (1913)[11] for $\lambda = 5955$ A. The full line is the linear relation adopted with $\beta = 0.718$.

Figure 2 gives the run of β with λ determined from the observed values of $\phi(\mu)$ at $\mu = 1.00$ and $\mu \approx 0.35$. The open circles are from observations by Canavaggia and Chalonge (1943);[12] the filled circles and plus signs are from observations by Abbot (1906–1908 and 1913);[11] and the crosses are from observations by Raudenbusch (1937).[11] For the D lines a value of $\beta = 0.725$ would seem to be appropriate (represented by a filled square).

We should also be able to determine β from the theory of the continuous spectrum. However, as Münch[5] has shown, the predicted center-limb contrast is greater than that observed. Using $n = 0.75$ and the tables provided in Chandrasekhar and Frances Breen's Paper XVIII,[13] we find $\beta = 0.462$ (open square). A change of ± 0.05 in n changes β by ± 0.016 only. This linear relation is shown in Figure 1, labeled *I*.

[11] Quoted by Chalonge and Kourganoff, *Ann. d'ap.*, **9**, 69, 1946.

[12] *Ann. d'ap.*, **9**, 143, 1946.

[13] *Ap. J.*, **105**, 461, 1945.

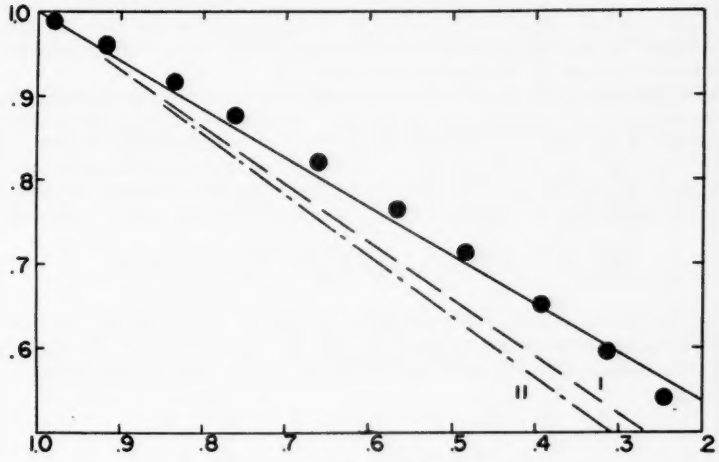

FIG. 1.—Law of darkening at $\lambda = 5955$ A

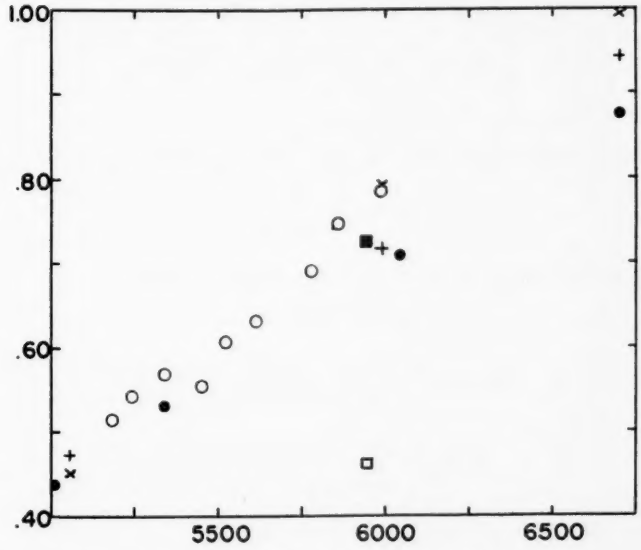

FIG. 2.—Variation of β with wave length

By developing $B(T)$ in a Taylor expansion about τ_0 and using the temperature distribution, $T^4 = T_0^4(1 + \frac{3}{2}\tau)$, we obtain $\beta = 0.378$. This is shown in Figure 1, labeled *II*.

This later method cannot be extended to the temperature distribution given by Chandrasekhar[14] in higher approximations because $B_\nu(T)$ cannot be represented by a polynomial in τ because of the logarithmic singularity at $\tau = 0$.

Owing to the theoretical complications that arise in the problem of the law of darkening in the continuum, it appears best to use the observed value of β at the present time. A comparison of the results obtained from the use of the theoretically derived value of $\beta = 0.462$ and the observed value of $\beta = 0.725$ will be found at the end of the paper.

In view of this uncertainty, we shall adopt the following procedure for solving the equation of transfer for the case of variable η. Instead of equation (15), we shall write

$$I(0, \mu) = \bar{\lambda}^{3/2} B^{(1)} H(\mu) \left\{ \mu + \frac{\beta}{\bar{\lambda}} + \frac{1-\bar{\lambda}}{2\bar{\lambda}^{1/2}} \alpha_1 \right\} + \Delta I(\bar{\lambda}), \tag{18}$$

where the first part is what the exact solution gives for $\lambda = \bar{\lambda} =$ Constant and the second part, $\Delta I(\lambda)$, is a correction term to allow for the variation of λ from $\bar{\lambda}$. We shall assume that we can evaluate ΔI in the first approximation at $\mu_1 = 0.577$. In this case,[15]

$$\Delta I = \frac{B^{(0)}/\sqrt{\bar{\lambda}} - B^{(1)}\sqrt{\bar{\lambda}}/\sqrt{3}}{(1+\sqrt{\bar{\lambda}})^2} \bar{\delta}_2 + \frac{2B^{(1)}/\sqrt{3}}{1+\sqrt{\bar{\lambda}}} \bar{\delta}_1 \tag{19}$$

depends on the evaluation of the two weighted means,

$$\bar{\delta}_1 = \int_0^\infty \delta\lambda \, e^{-\sqrt{3/\bar{\lambda}}\, n\tau} d(\sqrt{3/\bar{\lambda}}\, n\tau), \tag{20}$$

$$\bar{\delta}_2 = \int_0^\infty \delta\lambda \, e^{-2\sqrt{3/\bar{\lambda}}\, n\tau} d(2\sqrt{3/\bar{\lambda}}\, n\tau), \tag{21}$$

where

$$\delta\lambda = \lambda - \bar{\lambda}. \tag{22}$$

So far we have left $\bar{\lambda}$ unspecified. We shall now choose $\bar{\lambda}$ so that $\bar{\delta}_2 = 0$; then

$$\Delta I = \frac{2}{\sqrt{3}} \frac{B^{(1)} \bar{\delta}_1}{1+\sqrt{\bar{\lambda}}}. \tag{23}$$

Dividing by $I^{(\mathrm{cont})}(0, \mu)$, we obtain, for the residual intensity,

$$r(\mu) = r(\mu) + \Delta r(\mu), \tag{24}$$

where

$$r(\mu) = \frac{\bar{\lambda}^{3/2} H(\mu)}{\mu + \beta} \left\{ \mu + \frac{\beta}{\bar{\lambda}} + \frac{1-\bar{\lambda}}{2\bar{\lambda}^{1/2}} \alpha_1 \right\} \tag{25}$$

and

$$\Delta r(\mu) = \frac{2\bar{\delta}_1}{\sqrt{3}(\mu+\beta)(1+\sqrt{\bar{\lambda}})}. \tag{26}$$

To evaluate $\bar{\delta}_1$ and $\bar{\delta}_2$, we may use the formulae[13]

$$\bar{\lambda} + \bar{\delta}_2 = \sum_1^5 q_i \lambda(\tau_{2i}) \qquad \text{and} \qquad \bar{\lambda} + \bar{\delta}_1 = \sum_1^5 q_i \lambda(\tau_{1i}), \tag{27}$$

[14] *Ap. J.*, **100**, 76, Table 1, 1944.

[15] M. Tuberg, *Ap. J.*, **103**, 145, 1946, eqs. (63), (64), and (65).

where

$$\tau_{2i} = \frac{x_i \sqrt{\lambda_0}}{2n\sqrt{3}} \quad \text{and} \quad \tau_{1i} = \frac{x_i \sqrt{\lambda_0}}{n\sqrt{3}}. \tag{28}$$

The appropriate weights and subdivisions are given in the accompanying tabulation.

i	x_i	τ_{2i}	τ_{1i}	q_i
1.....	0.26356	$0.101\sqrt{\bar{\lambda}}$	$0.202\sqrt{\bar{\lambda}}$	0.5218
2.....	1.4134	0.542	1.085	.3987
3.....	3.5964	1.380	2.761	.0759
4.....	7.0858	2.720	5.440	.0036
5.....	12.6408	4.852	9.705	0.00002

The function $r(\mu)$ was computed from the tables in Chandrasekhar and Frances Breen's Papers XIX[16] and XX[17] for $\mu = 1.00$ and $\mu = 0.26$ and using $\beta = 0.725$. The results are shown in Table 3.

TABLE 3

THE FUNCTION $r(\mu)$ FOR $\beta = 0.725$

λ	$r(\mu=1.0)$	$r(\mu=0.26)$	λ	$r(\mu=1.0)$	$r(\mu=0.26)$
1.0.....	1.0000	1.0000	0.2.....	0.4378	0.5253
0.9.....	0.9405	0.9674	0.15.....	0.3837	0.4588
0.8.....	0.8796	0.9306	0.10.....	0.3197	0.3772
0.7.....	0.8168	0.8880	0.075.....	0.2810	0.3274
0.6.....	0.7515	0.8391	0.050.....	0.2345	0.2674
0.5.....	0.6831	0.7819	0.025.....	0.1721	0.1891
0.4.....	0.6100	0.7139	0.000.....	0.0000	0.0000
0.3.....	0.5299	0.6310			

The correction term is then found to be

$$\Delta r(\mu) = \frac{0.67\,\bar{\delta}_1}{1+\sqrt{\bar{\lambda}}} \quad \text{for} \quad \mu = 1.00, \tag{29}$$

$$\Delta r(\mu) = \frac{1.17\,\bar{\delta}_1}{1+\sqrt{\bar{\lambda}}} \quad \text{for} \quad \mu = 0.26. \tag{30}$$

III. COMPUTATION OF THE PROFILE

The construction of a profile then proceeds as follows:

1. For an assumed value of Nf and a given value of $\Delta\lambda$, we must first know the run of η with τ (Table 2).

2. Selecting a preliminary value of $\bar{\lambda}$, we evaluate $\bar{\lambda} + \bar{\delta}_2$; a second computation starting with $\bar{\lambda} + \bar{\delta}_2$ in place of the preliminary value of λ will generally make $\bar{\delta}_2$ equal to zero.

3. We next evaluate $\bar{\delta}_1$.

4. Using $\bar{\lambda}$ and $\bar{\delta}_1$, we then evaluate $r(\mu)$ and $\Delta r(\mu)$, and the residual intensity follows.

[16] *Ap. J.*, **106**, 143, Table 1, 1947. [17] *Ibid.*, p. 145.

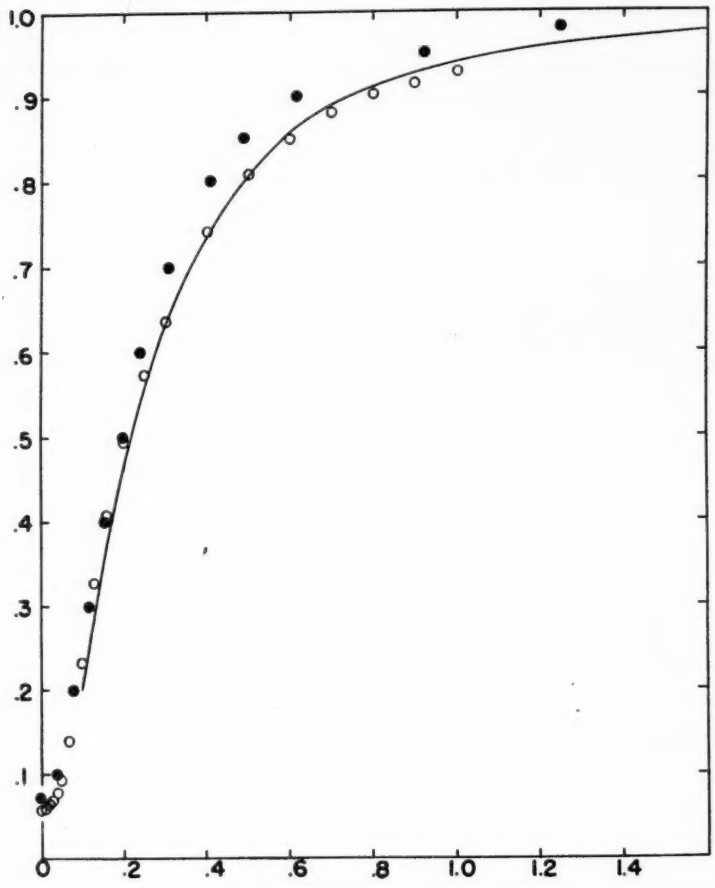

FIG. 3.—Contour of D_1 line at $\mu = 1.00$

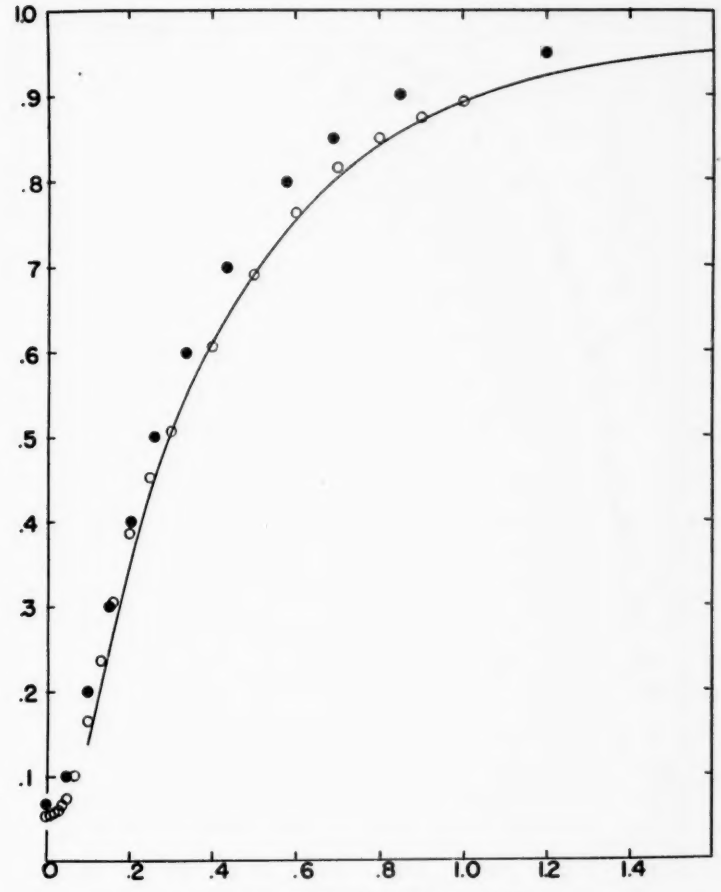

FIG. 4.—Contour of D_2 line at $\mu = 1.00$

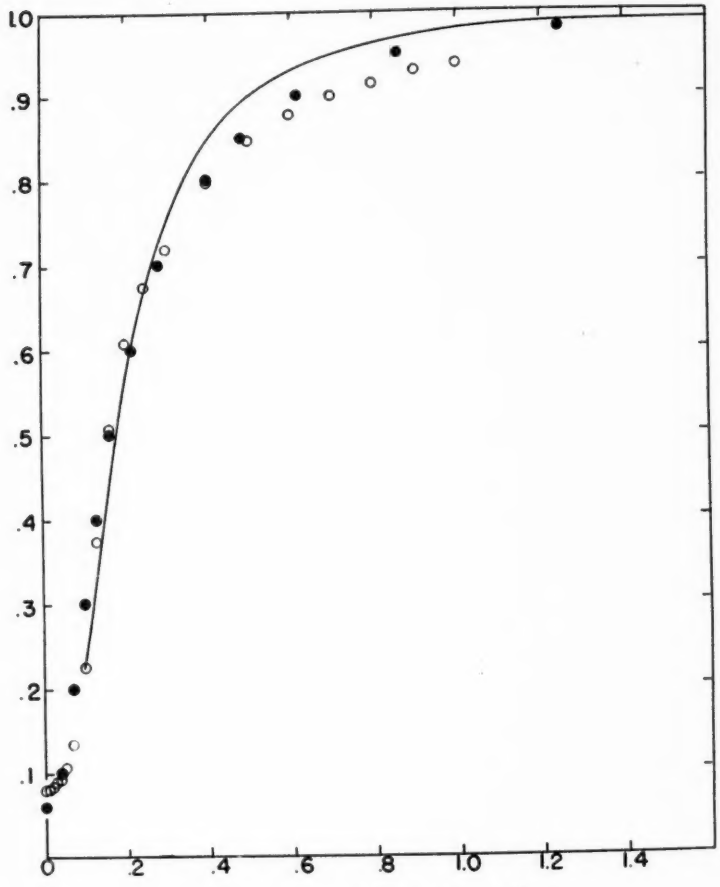

FIG. 5.—Contour of D_1 line at $\mu = 0.26$

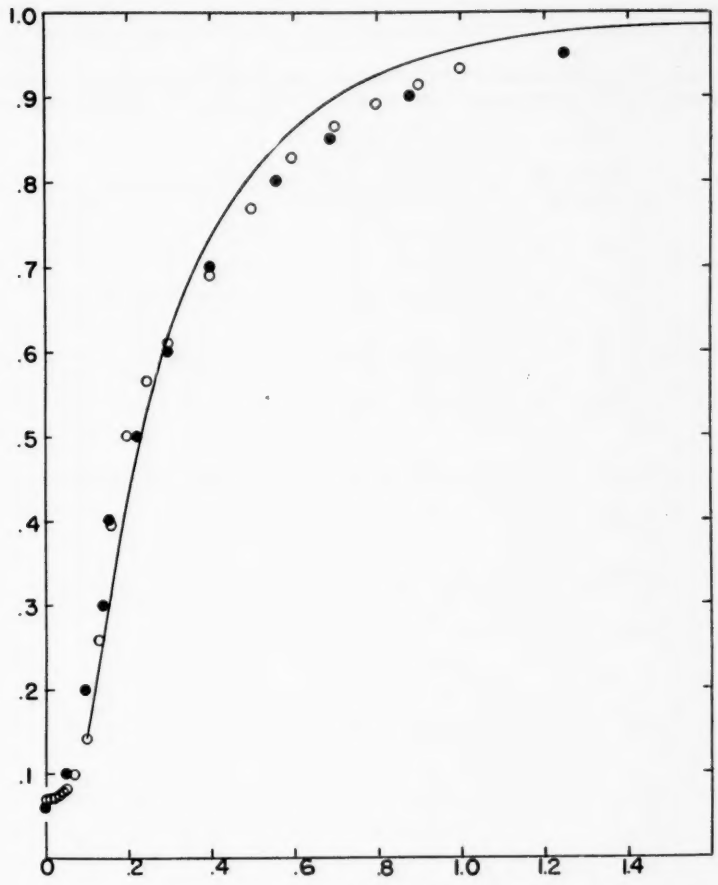

FIG. 6.—Contour of D_2 line at $\mu = 0.26$

IV. APPLICATION OF THE METHOD TO THE D_1 AND D_2 LINES

Figures 3–6 give the comparison of the observations by Shane (*open circles*) and by Allen (*closed circles*) with the theoretical contours. The theoretical contours illustrated have been obtained with $N = 10^{18}$ atoms per gram, $\beta = 0.725$, and the assumed f-values of $\frac{1}{3}$ and $\frac{2}{3}$.

No attempt has been made to determine a definitive value of the abundance of sodium in the solar atmosphere. However, the difference between log $N = 18.0$ used above and

TABLE 4

THE EFFECT OF ABUNDANCE ON THE COMPUTED CONTOURS

$\Delta\lambda$	$N = 10^{18}$ $r(\mu)+\Delta r(\mu)=\Gamma(\mu)$	μ	$N = 5\times10^{17}$ $r(\mu)+\Delta r(\mu)=\Gamma(\mu)$
0.4 A.....	0.714+0.024=0.738	1.00	0.822+0.018=0.840
	.808+ .041= .849	0.26	.892+ .032= .924
0.6.....	.839+ .017= .856	1.00	.908+ .011= .919
	.903+ .029= .932	0.26	.949+ .019= .968
0.8.....	.899+ .012= .911	1.00	.946+ .006= .952
	.942+ .021= .963	0.26	.970+ .011= .981
1.0.....	.933+ .008= .941	1.00	.964+ .005= .968
	0.963+0.014=0.977	0.26	0.981+0.008=0.989

TABLE 5

THE EFFECT OF DIFFERENT LAWS OF DARKENING IN THE CONTINUUM ON THE THEORETICAL LINE CONTOURS

$\Delta\lambda$	$\beta = 0.725$ $r(\mu)+\Delta r(\mu)=\Gamma(\mu)$	μ	$\beta = 0.462$ $r(\mu)+\Delta r(\mu)=\Gamma(\mu)$
0.4 A.....	0.714+0.024=0.738	1.00	0.680+0.028=0.708
	.808+ .041= .849	0.26	.801+ .056= .857
0.6.....	.839+ .017= .856	1.00	.819+ .020= .839
	.903+ .029= .932	0.26	.901+ .040= .941
0.8.....	.899+ .012= .911	1.00	.886+ .014= .900
	.942+ .021= .963	0.26	.941+ .029= .970
1.0.....	.933+ .008= .941	1.00	.925+ .009= .934
	0.963+0.014=0.977	0.26	0.962+0.019=0.981

the value of log $N = 17.65$ found by Strömgren is due to the use of $n = 0.75$ instead of 1.0 and to the use of Münch's model solar atmosphere instead of the one computed by Strömgren.

We have separated the discussion into two parts, the first dealing with the determination of η and the second involving the equation of transfer and the value of β. In Table 4 we show the effect of varying η by comparing the values of $r(\mu)$ and $\Delta r(\mu)$ obtained with $N = 10^{18}$ and with $N = 5 \times 10^{17}$. It should be emphasized that a change in n and/or f would produce the same effect as a change in N, while a change in the model solar atmosphere assumed would produce a somewhat similar effect.

We also show in Table 5 the effect of using the theoretical value of $\beta = 0.462$ instead of the observed value of 0.725. It will be noted that the center-limb contrast is about 34 per cent larger for the smaller value of β. On the other hand, the center-limb contrast for the continuum is only about 18 per cent greater for the theoretical and observed β ($\mu = 1.0$ to $\mu = 0.26$).

If we let $\bar{\tau}$ be the optical depth corresponding to the value of λ, we find the values from the computation with $N = 10^{18}$, as shown in the accompanying tabulation.

$\Delta\lambda$	$\bar{\tau}(D_1)$	$\bar{\tau}(D_2)$	$\Delta\lambda$	$\bar{\tau}(D_1)$	$\bar{\tau}(D_2)$
0.1 A.....	0.20	0.22	0.8.....	0.32	0.31
0.2.....	.24	.28	1.0.....	.33	.33
0.4.....	.30	.27	1.6.....	0.33	0.32
0.6.....	0.32	0.29			

It is possible that the remaining deviations of the observations from the theoretically predicted contours are due to the neglect of noncoherent scattering, as discussed by Zanstra[18] and Houtgast.[19] However, in view of the agreement already obtained, we should expect that the inclusion of this effect would not change our results by more than a few per cent.

I wish to express my appreciation to Dr. S. Chandrasekhar for his assistance and encouragement in carrying out the above discussion.

[18] *M.N.*, **106**, 225, 1946.

[19] *The Variations in the Profiles of Strong Fraunhofer Lines along a Radius of the Solar Disc* (Utrecht: Schotanus & Jens, 1942).

EXACT CURVES OF GROWTH FOR THE FORMATION OF ABSORPTION LINES ACCORDING TO THE MILNE-EDDINGTON MODEL
I. TOTAL FLUX

MARSHAL H. WRUBEL
Yerkes Observatory
Received November 9, 1948

ABSTRACT

Curves of growth have been computed for six values of the damping from $\log a = -3.0$ to $\log a = -1.0$ and four values of $B^{(0)}/B^{(1)}$ from $\frac{1}{3}$ to $\frac{1}{9}$, using Chandrasekhar's exact solution of the equation of transfer for the Milne-Eddington model and Hjerting's tabulation of the line-absorption coefficient.

NOTATION

κ_ν: Continuous absorption coefficient at frequency ν (replaced by κ_{ν_0} in the neighborhood of an absorption line);
$\bar{\kappa}$: Mean continuous absorption coefficient;
σ_ν: Scattering coefficient at frequency ν;
σ_{ν_0}: Fictitious scattering coefficient at the center of the line;[1]
t_ν: Optical depth in total absorption: $dt_\nu = -(\kappa_\nu + \sigma_\nu)\rho ds$;
τ_ν: Optical depth in the continuum: $d\tau_\nu = -\kappa_\nu \rho ds$;
η: Ratio of scattering coefficient to continuous absorption coefficient: $\eta = \sigma_\nu/\kappa_\nu$;
η_0: Ratio of the fictitious scattering coefficient at the center of the line to the continuous absorption coefficient at the center of the line: $\eta_0 = \sigma_{\nu_0}/\kappa_{\nu_0}$;
λ: Ratio of continuous to total absorption: $\lambda = \kappa_\nu/(\kappa_\nu + \sigma_\nu) = (1 + \eta)^{-1}$;
b: Doppler width; in frequency units: $b^{(\nu)} = (\nu/c)\sqrt{(2kT/Am_0)}$;
v: Deviation from the center of the line in units of the Doppler width: $v = (\nu - \nu_0)/b^{(\nu)}$;
W: Equivalent width or area of absorption line;
$B_\nu(T)$: Planck function for frequency ν and temperature T [$= B_\nu(T_0)$ at boundary of atmosphere];
$B^{(0)}/B^{(1)}$: Ratio of coefficients in linear expansion of $B_\nu(T)$ (see eq. [3]); equivalent to the reciprocal of β in Unsöld's notation and $8n/3x_0$ in Strömgren's;
a: Ratio of effective natural line width to Doppler width (same as Hjerting's notation);
$I_\nu(\tau, \mu)$: Specific intensity at depth τ and in a direction making an angle of cosine μ with the normal;
$r_\nu(\mu)$: Ratio of intensity at a point in the line to the continuous intensity;
R_ν: Ratio of the flux at a point in the line to the continuous flux;
$H(\mu)$, α_1, α_2: Functions and moments involved in the exact solution of the equation of transfer.

INTRODUCTION

The last two decades have witnessed the growth of the quantitative analysis of stellar spectra. Although the ultimate aim of such research remains the determination of abundances by the analysis of absorption-line contours, much progress has been made by considering the equivalent width or area of the line as a whole.

[1] F. Hjerting, *Ap. J.*, **88**, 508, eq. (8), 1938.

Various methods have been used to compute theoretical curves of growth giving the functional relation between the equivalent width and abundance. The broad features of such curves are noticeable even in the elementary case of an absorption tube:[2] for weak lines the equivalent width is primarily due to Doppler effect, and for strong lines it is due to damping. Early attempts to construct curves appropriate for stellar atmospheres were admittedly only qualitative (for example, D. H. Menzel[3] used an expression for the absorption coefficient constructed by adding two asymptotic forms, and a solution for the Schuster-Schwarzschild model wrong by 20 per cent in the residual intensity). More recent curves still had the disadvantage of being based upon approximate solutions for the residual intensity; yet the success of K. O. Wright and R. B. King,[4] J. L. Greenstein,[5] and others in using these curves seems to indicate that effort spent in improving the theoretical curves is not effort wasted.

As more accurate methods were employed, it became apparent that the so-called "Milne-Eddington model" was more appropriate than the Schuster-Schwarzschild model (the specific formulation of the former will be found in the following section). This advance was primarily due to B. Strömgren, who showed that the Milne-Eddington model was quite satisfactory when a representative point for the formation of the absorption line could be chosen in the atmosphere.[6]

The following calculations were undertaken not merely to add still another set of curves of growth to the number already in existence but rather to provide, for the first time, a set based upon the exact solution for the residual intensity, as found by S. Chandrasekhar.[7]

STATEMENT OF THE PROBLEM

It is generally assumed that the absorption in a stellar atmosphere is due to two components—one the continuous absorption, which varies slowly with frequency, and the other the line absorption, which has a strong frequency dependence. We represent the continuous portion by the coefficient κ_ν; and in the neighborhood of an absorption line (at most a few angstroms wide) we can replace this by the constant κ_{ν_0}, the value of this coefficient at the center of the line. If we consider a resonance line, the absorption in the line is due to pure scattering, that is, the same frequency is re-emitted as is absorbed; and we can represent it by the scattering coefficient σ_ν.

We denote the ratio of the scattering coefficient to the continuous absorption coefficient by η and let

$$\lambda = \frac{\kappa_\nu}{\kappa_\nu + \sigma_\nu} = \frac{1}{1+\eta}, \tag{1}$$

or the ratio of the continuous to the total absorption; λ is equal to 0 if σ_ν is very large, as in the center of a strong line, and equal to 1 in the adjacent continuum. With these substitutions the equation of transfer takes the following form:

$$\mu \frac{dI_\nu}{dt_\nu} = I_\nu - \tfrac{1}{2}(1-\lambda_\nu) \int_{-1}^{+1} I_\nu(t_\nu, \mu')\, d\mu' - \lambda B_\nu(T), \tag{2}$$

where t_ν is the optical depth measured in the total absorption and $B_\nu(T)$ is the Planck function for the frequency ν at the appropriate optical depth, t. For problems in line

[2] A. Unsöld, *Physik der Sternatmosphären* (Berlin: J. Springer, 1938), pp. 264–269.

[3] *Ap. J.*, **84**, 462, 1936.

[4] *Ap. J.*, **106**, 224, 1947.

[5] *Ap. J.*, **107**, 151, 1948.

[6] *Ap. J.*, **86**, 1, 1937; see particularly M. Tuberg, *Ap. J.*, **103**, 145, 1946, and D. L. Harris, *Ap. J.*, **109**, 53, 1949, for the manner of selecting the representative point.

[7] *Ap. J.*, **106**, 145, 1947.

formation it is generally sufficient to expand $B_\nu(T)$ as a linear function of τ_ν, the optical depth in the continuum:

$$B_\nu(T) = B^{(0)} + B^{(1)}\tau_\nu . \tag{3}$$

If the linear expansion of $B_\nu(T)$ is chosen as a Taylor expansion about the boundary temperature, T_0, it follows that

$$B_\nu(T) = B_\nu(T_0)\left[1 + \frac{3}{8}\frac{e^{h\nu/kT_0}}{e^{h\nu/kT_0}-1}\frac{h\nu}{kT_0}\frac{\bar{\kappa}}{\kappa_{\nu_0}}\tau_\nu\right], \tag{4}$$

where $\bar{\kappa}$ is an appropriately chosen mean continuous absorption. By assuming that λ is independent of depth, we can write τ_ν as λt_ν; and the equation of transfer takes the form appropriate for the Milne-Eddington model,

$$\mu\frac{dI_\nu}{dt} = I_\nu - \tfrac{1}{2}(1-\lambda_\nu)\int_{-1}^{+1} I_\nu(t,\mu')\,d\mu' - \lambda\left[B^{(0)} + \lambda B^{(1)}t\right]. \tag{5}$$

There have been numerous approximate solutions to this equation. The usual procedure has been to use the Eddington approximation $K = \frac{1}{3}J$; but Chandrasekhar[6] has solved this equation exactly, without any approximations of any sort, and has found the angular distribution of the emergent radiation to be

$$I(0,\mu) = \lambda^{3/2}B^{(1)}H(\mu)\left(\mu + \frac{B^{(0)}}{\lambda B^{(1)}} + \frac{1-\lambda}{2\lambda^{1/2}}\alpha_1\right), \tag{6}$$

where the functions $H(\mu)$ have been tabulated by Chandrasekhar and Frances Breen[8] for a wide range of λ and μ. From this solution it follows that the ratio of the intensity at a point in the line to the continuous intensity is

$$r_\nu(\mu) = \frac{\lambda^{3/2}}{\mu + \dfrac{B^{(0)}}{B^{(1)}}}H(\mu)\left(\mu + \frac{B^{(0)}}{\lambda B^{(1)}} + \frac{1-\lambda}{2\lambda^{1/2}}\alpha_1\right), \tag{7}$$

and the ratio of the flux at a point in the line to the continuous flux is

$$R_\nu = \frac{\lambda^{3/2}}{\dfrac{1}{3} + \dfrac{1}{2}\dfrac{B^{(0)}}{B^{(1)}}}\left(\alpha_2 + \frac{B^{(0)}}{\lambda B^{(1)}}\alpha_1 + \frac{1-\lambda}{2\lambda^{1/2}}\alpha_1^2\right), \tag{8}$$

where α_1 and α_2 are tabulated first and second moments of $H(\mu)$.

The scattering coefficient, σ_ν, is a function of the so-called "fictitious scattering coefficient" for the center of the line,[1] σ_{ν_0}; and we define $\eta_0 = \sigma_{\nu_0}/\kappa_{\nu_0}$. The relation between the area of an absorption line, W (its equivalent width), and η_0 is called a "curve of growth." It is more convenient to measure distances from the center of a line in terms of v $(=[\nu - \nu_0]/b^{(\nu)}$, where $b^{(\nu)}$ is the Doppler shift), and in constructing curves of growth the quantity

$$\frac{W}{b} = \int_{-\infty}^{+\infty}(1-R)\,dv \tag{9}$$

is computed as a function of η_0.

Curves have been computed for six values of the damping, running from $\log a = -3.0$ to $\log a = -1.0$ in intervals of 0.4 and for $B^{(0)}/B^{(1)}$ equal to $\frac{1}{3}$, $\frac{2}{3}$, $\frac{4}{3}$, and $\frac{10}{3}$. The results are given in Table 1. They are further illustrated in Figures 1–4. It should be emphasized that these curves refer to the integrated flux. Curves for the intensity at the center of the disk will be forthcoming in the near future.

[8] *Ap. J.*, **106**, 143, 1947.

TABLE 1

log η_0	log a					
	−1.0	−1.4	−1.8	−2.2	−2.6	−3.0
	log W/b for $B^{(0)}/B^{(1)}=\frac{1}{3}$					
−2.8	−2.766	−2.766	−2.766	−2.766	−2.766	−2.766
−2.4	−2.367	−2.367	−2.367	−2.367	−2.367	−2.367
−2.0	−1.968	−1.968	−1.969	−1.969	−1.969	−1.969
−1.6	−1.572	−1.572	−1.572	−1.573	−1.573	−1.573
−1.2	−1.180	−1.180	−1.181	−1.181	−1.182	−1.182
−0.8	−0.800	−0.802	−0.804	−0.805	−0.805	−0.805
−0.4	−0.444	−0.450	−0.453	−0.454	−0.455	−0.455
0.0	−0.131	−0.144	−0.150	−0.152	−0.153	−0.154
+0.4	+0.124	+0.101	+0.091	+0.086	+0.085	+0.084
+0.8	*+0.325*	+0.288	+0.271	+0.264	+0.261	+0.260
+1.2	+0.490	*+0.433*	+0.406	+0.394	+0.389	+0.387
+1.6	+0.641	+0.558	*+0.514*	+0.493	+0.485	+0.481
+2.0	+0.796	+0.681	+0.611	*+0.576*	+0.561	+0.554
+2.4	+0.964	+0.817	+0.713	+0.655	*+0.627*	+0.614
+2.8	+1.145	+0.974	+0.835	+0.742	+0.692	*+0.668*
+3.2	+1.335	+1.150	+0.983	+0.852	+0.768	+0.724
+3.6	+1.531	+1.337	+1.154	+0.992	+0.868	+0.791
+4.0	+1.728	+1.532	+1.339	+1.157	+1.000	+0.883
+4.4	+1.927	+1.728	+1.533	+1.341	+1.161	+1.008
+4.8	+2.127	+1.927	+1.729	+1.534	+1.343	+1.165
+5.2	+2.327	+2.127	+1.927	+1.730	+1.534	+1.344
+5.6	+2.527	+2.327	+2.127	+1.927	+1.730	+1.534
+6.0	+2.727	+2.527	+2.327	+2.127	+1.927	+1.730
	log W/b for $B^{(0)}/B^{(1)}=\frac{2}{3}$					
−2.8	−2.845	−2.845	−2.845	−2.845	−2.845	−2.845
−2.4	−2.446	−2.446	−2.446	−2.446	−2.446	−2.446
−2.0	−2.047	−2.047	−2.047	−2.047	−2.047	−2.047
−1.6	−1.651	−1.651	−1.651	−1.651	−1.651	−1.651
−1.2	−1.258	−1.258	−1.259	−1.259	−1.260	−1.260
−0.8	−0.877	−0.880	−0.881	−0.882	−0.882	−0.882
−0.4	−0.519	−0.525	−0.528	−0.529	−0.530	−0.530
0.0	−0.202	−0.214	−0.220	−0.222	−0.223	−0.223
+0.4	+0.060	+0.038	+0.028	+0.024	+0.022	+0.021
+0.8	*+0.268*	+0.233	+0.217	+0.210	+0.207	+0.206
+1.2	+0.439	*+0.386*	+0.360	+0.349	+0.345	+0.343
+1.6	+0.595	+0.516	*+0.475*	+0.456	+0.449	+0.445
+2.0	+0.750	+0.641	+0.576	*+0.544*	+0.531	+0.525
+2.4	+0.917	+0.776	+0.680	+0.626	*+0.600*	+0.589
+2.8	+1.096	+0.930	+0.799	+0.713	+0.667	*+0.646*
+3.2	+1.284	+1.102	+0.941	+0.819	+0.742	+0.703
+3.6	+1.478	+1.287	+1.107	+0.953	+0.838	+0.769
+4.0	+1.675	+1.479	+1.290	+1.113	+0.963	+0.855
+4.4	+1.874	+1.676	+1.480	+1.292	+1.118	+0.973
+4.8	+2.073	+1.874	+1.677	+1.481	+1.294	+1.123
+5.2	+2.273	+2.073	+1.874	+1.677	+1.482	+1.296
+5.6	+2.473	+2.273	+2.073	+1.874	+1.677	+1.482
+6.0	+2.673	+2.473	+2.273	+2.073	+1.874	+1.677

TABLE 1—*Continued*

LOG η_0	LOG a					
	−1.0	−1.4	−1.8	−2.2	−2.6	−3.0
	log W/b for $B^{(0)}/B^{(1)}=\frac{4}{3}$					
−2.8	−2.942	−2.942	−2.942	−2.942	−2.942	−2.942
−2.4	−2.542	−2.542	−2.542	−2.542	−2.542	−2.542
−2.0	−2.143	−2.143	−2.144	−2.144	−2.144	−2.144
−1.6	−1.746	−1.746	−1.747	−1.747	−1.747	−1.747
−1.2	−1.353	−1.353	−1.354	−1.354	−1.355	−1.355
−0.8	−0.971	−0.973	−0.975	−0.976	−0.976	−0.976
−0.4	−0.610	−0.615	−0.618	−0.619	−0.620	−0.620
0.0	−0.287	−0.298	−0.303	−0.306	−0.307	−0.307
+0.4	−0.016	−0.037	−0.046	−0.050	−0.051	−0.052
+0.8	*+0.202*	+0.170	+0.155	+0.149	+0.146	+0.145
+1.2	+0.382	*+0.333*	+0.309	+0.299	+0.295	+0.293
+1.6	+0.542	+0.470	*+0.432*	+0.416	+0.409	+0.406
+2.0	+0.699	+0.597	+0.539	*+0.510*	+0.498	+0.493
+2.4	+0.863	+0.731	+0.642	+0.595	*+0.573*	+0.563
+2.8	+1.039	+0.880	+0.758	+0.682	+0.642	*+0.623*
+3.2	+1.225	+1.048	+0.895	+0.783	+0.715	+0.681
+3.6	+1.418	+1.229	+1.055	+0.909	+0.805	+0.745
+4.0	+1.614	+1.420	+1.233	+1.062	+0.923	+0.826
+4.4	+1.812	+1.615	+1.422	+1.236	+1.069	+0.935
+4.8	+2.012	+1.812	+1.616	+1.423	+1.239	+1.076
+5.2	+2.211	+2.012	+1.812	+1.617	+1.424	+1.242
+5.6	+2.411	+2.211	+2.012	+1.812	+1.617	+1.424
+6.0	+2.611	+2.411	+2.211	+2.012	+1.812	+1.617
	log W/b for $B^{(0)}/B^{(1)}=\frac{10}{3}$					
−2.8	−3.066	−3.066	−3.066	−3.066	−3.066	−3.066
−2.4	−2.666	−2.666	−2.666	−2.666	−2.666	−2.666
−2.0	−2.267	−2.267	−2.267	−2.267	−2.267	−2.267
−1.6	−1.870	−1.870	−1.870	−1.871	−1.871	−1.871
−1.2	−1.476	−1.476	−1.477	−1.477	−1.478	−1.478
−0.8	−1.091	−1.093	−1.094	−1.094	−1.095	−1.095
−0.4	−0.724	−0.730	−0.732	−0.733	−0.733	−0.733
0.0	−0.392	−0.402	−0.407	−0.409	−0.410	−0.410
+0.4	−0.109	−0.127	−0.134	−0.138	−0.139	−0.140
+0.8	*+0.125*	+0.096	+0.083	+0.077	+0.075	+0.074
+1.2	+0.316	*+0.272*	+0.252	+0.243	+0.239	+0.237
+1.6	+0.482	+0.418	*+0.385*	+0.371	+0.365	+0.362
+2.0	+0.640	+0.548	+0.497	*+0.473*	+0.463	+0.458
+2.4	+0.802	+0.680	+0.602	+0.561	*+0.543*	+0.535
+2.8	+0.975	+0.824	+0.714	+0.647	+0.614	*+0.599*
+3.2	+1.157	+0.986	+0.843	+0.744	+0.686	+0.658
+3.6	+1.348	+1.162	+0.996	+0.861	+0.770	+0.719
+4.0	+1.543	+1.351	+1.167	+1.005	+0.877	+0.794
+4.4	+1.741	+1.544	+1.353	+1.172	+1.014	+0.893
+4.8	+1.940	+1.741	+1.545	+1.355	+1.177	+1.023
+5.2	+2.139	+1.940	+1.741	+1.546	+1.357	+1.181
+5.6	+2.339	+2.139	+1.940	+1.741	+1.546	+1.357
+6.0	+2.539	+2.339	+2.139	+1.940	+1.741	+1.546

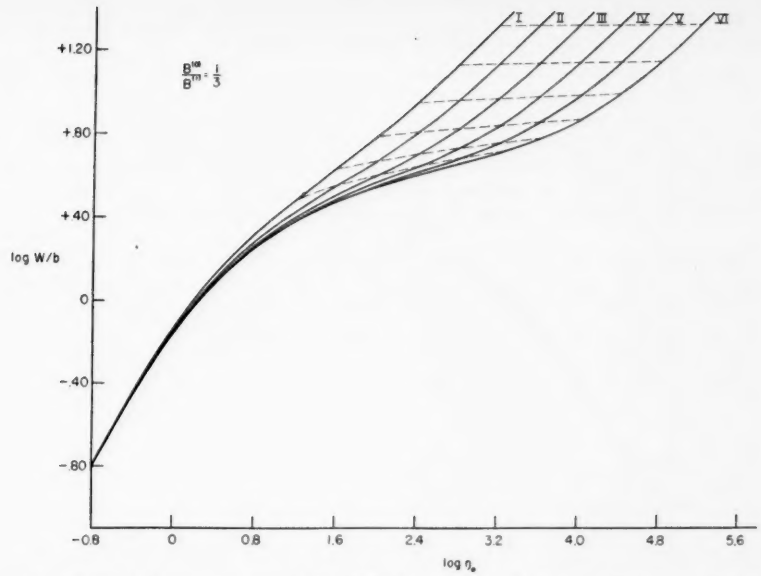

FIG. 1.—Theoretical curves of growth for $B^{(0)}/B^{(1)} = \frac{1}{3}$: curve *I*, log $a = -1.0$; curve *II*, log $a = -1.4$; curve *III*, log $a = -1.8$; curve *IV*, log $a = -2.2$; curve *V*, log $a = -2.6$; curve *VI*, log $a = -3.0$.

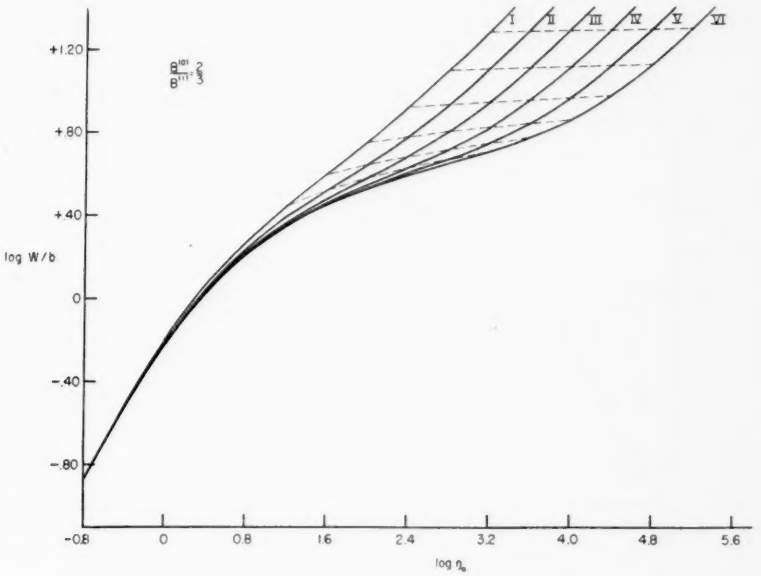

FIG. 2.—Theoretical curves of growth for $B^{(0)}/B^{(1)} = \frac{2}{3}$: same notation as Fig. 1

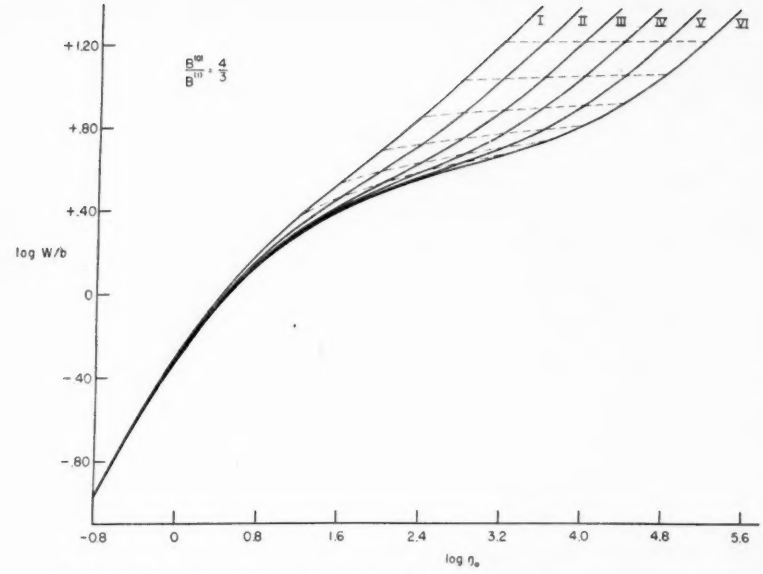

FIG. 3.—Theoretical curves of growth for $B^{(0)}/B^{(1)} = \frac{4}{3}$: same notation as Fig. 1

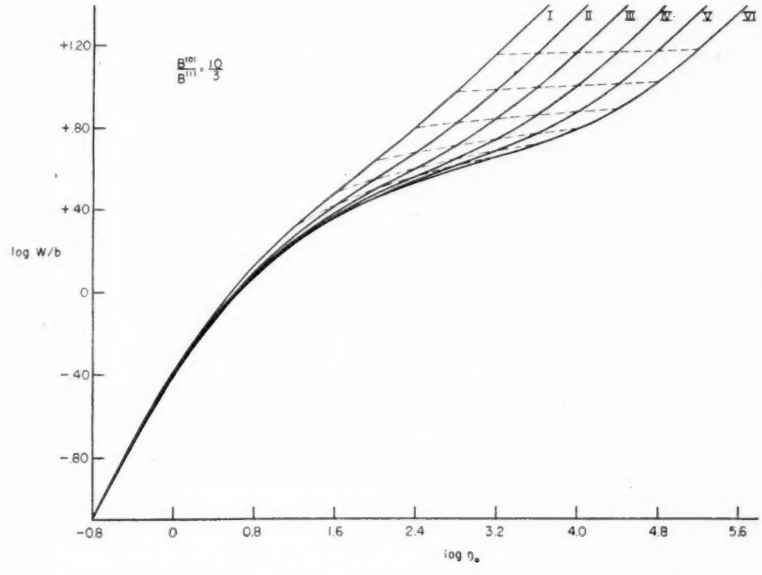

FIG. 4.—Theoretical curves of growth for $B^{(0)}/B^{(1)} = \frac{10}{3}$: same notation as Fig. 1

CONSTRUCTION OF TABLES

From Hjerting's tables of the absorption coefficient,[1] η was found as a function of v for every combination of η_0 and damping a. These values were used to compute $1 - \lambda$ as a function of v. The quantity R_ν was calculated for those values of λ for which Chandrasekhar and Breen have published the H-functions and moments; and, by interpolation in $R - \sqrt{\lambda}$, a table was constructed for each value of $B^{(0)}/B^{(1)}$, giving R as a function of $1 - \lambda$. Since $1 - \lambda$ was already known as a function of v, R was found as a function of v by using these tables. The equivalent width was then computed by numerical integration.

This method was used out into the wings of the line until $1 - \lambda$ fell below 0.20 and the contribution from the rest of the line was small by comparison. Beyond that point $1 - R$ was expressed as a quadratic function of $1 - \lambda$, and η was approximated by the asymptotic series.[9] The resulting expression was integrated from the value of v, at which numerical integration stopped, out to infinity. This method was checked frequently by comparison with the equivalent widths calculated numerically much farther out into the wings. In no case was numerical integration stopped before $v = 5$.

USE OF TABLES

Interpolation in log a *for constant* $B^{(0)}/B^{(1)}$.—For moderate values of η_0, interpolation for different values of the damping may easily be done directly across Table 1. For values of W/b lying below the value in italics, it is more convenient to interpo'ate along lines of constant $a\eta_0$. In Figures 1–4, which accompany the tables, the dotted lines are lines of constant $a\eta_0$.

Interpolation in $B^{(0)}/B^{(1)}$ *with log* a *and log* η_0 *constant.*—It follows directly from the form of R that there is a constant difference between numerical values of W/b (not the logarithms) for the four values of $B^{(0)}/B^{(1)}$ tabulated, provided that log a and log η_0 are constant. In order to find W/b for intermediate values of $B^{(0)}/B^{(1)}$, it is only necessary to multiply this difference by a numerical factor m and add it to the initial value. Table 2 gives the value of W/b for $B^{(0)}/B^{(1)} = \frac{2}{3}$, as well as the difference D; further,

$$\left(\frac{W}{b}\right)_{B^{(0)}/B^{(1)}} = \left(\frac{W}{b}\right)_{2/3} + m\,D\,, \tag{10}$$

$$m = \frac{3\left(\dfrac{3B^{(0)}}{B^{(1)}} - 2\right)}{3\dfrac{B^{(0)}}{B^{(1)}} + 2}\,. \tag{11}$$

It follows that m is -1, 1, and 2 for $B^{(0)}/B^{(1)}$ equal to $\frac{1}{3}$, $\frac{4}{3}$, and $\frac{10}{3}$, respectively.

Reduction to a single curve of growth.—In order to compare data from different parts of the spectrum with a single curve of growth, it is necessary to be able to reduce all values of $B^{(0)}/B^{(1)}$ to a single value. If log W/b and log a are kept constant, a correction, Δ log η_0, may be added to η_0 to reduce all observations to a single curve for $B^{(0)}/B^{(1)} = \frac{2}{3}$. These corrections, obtained by interpolation in Table 1, are given in Table 3.

In conclusion, I wish to express my indebtedness to Dr. S. Chandrasekhar for his advice and encouragement, to Dr. B. Strömgren for many detailed discussions during the early stages of the calculation, and to Dr. J. L. Greenstein for his explanation of the observational point of view. Particular thanks are due to my wife for drawing the accompanying figures.

[9] Hjerting, *op. cit.*, eq. (7).

TABLE 2

LOG η_0	LOG $a=-3.0$		LOG $a=-2.6$		LOG $a=-2.2$	
	$(W/b)_{2/3}$	$-D$	$(W/b)_{2/3}$	$-D$	$(W/b)_{2/3}$	$-D$
−0.8	0.1313	0.0256	0.1312	0.0255	0.1313	0.0255
−0.4	0.2951	0.0552	0.2955	0.0554	0.2958	0.0555
0.0	0.5974	0.1043	0.5981	0.1045	0.5993	0.1046
+0.4	1.0500	0.1628	1.0519	0.1630	1.0561	0.1641
+0.8	1.607	0.211	1.612	0.212	1.622	0.214
+1.2	2.201	0.237	2.211	0.239	2.234	0.243
+1.6	2.787	0.242	2.809	0.247	2.860	0.256
+2.0	3.347	0.237	3.393	0.245	3.503	0.265
+2.4	3.885	0.229	3.985	0.248	4.225	0.292
+2.8	4.430	0.228	4.650	0.269	5.166	0.363
+3.2	5.045	0.249	5.527	0.338	6.595	0.527
+3.6	5.869	0.316	6.887	0.498	8.966	0.849
+4.0	7.168	0.475	9.185	0.819	12.96	1.42
+4.4	9.400	0.793	13.11	1.39	.....	.....
+4.8	13.27	1.37	.....	.....	.....	.....
+5.2	19.77	2.30	.....	.....	.....	.....
+5.6	30.42	3.79	.....	.....	.....	.....
+6.0	47.57	6.14	.....	.....	.....	.....

LOG η_0	LOG $a=-1.8$		LOG $a=-1.4$		LOG $a=-1.0$	
	$(W/b)_{2/3}$	$-D$	$(W/b)_{2/3}$	$-D$	$(W/b)_{2/3}$	$-D$
−0.8	0.1316	0.0256	0.1319	0.0255	0.1328	0.0259
−0.4	0.2966	0.0555	0.2985	0.0560	0.3029	0.0573
0.0	0.6028	0.1056	0.6106	0.1076	0.6283	0.1116
+0.4	1.0663	0.1664	1.0906	0.1716	1.1474	0.1844
+0.8	1.648	0.219	1.710	0.232	1.854	0.260
+1.2	2.293	0.255	2.432	0.280	2.751	0.340
+1.6	2.985	0.279	3.281	0.333	3.931	0.448
+2.0	3.770	0.314	4.374	0.421	5.627	0.630
+2.4	4.781	0.391	5.970	0.592	8.254	0.955
+2.8	6.290	0.558	8.506	0.917	12.46	1.51
+3.2	8.739	0.882	12.64	1.48	19.23	2.43
+3.6	12.80	1.45	.....	.....	30.07	3.89
+4.0	.....	.....	.....	.....	47.34	6.21
+4.4	.....	.....	.....	.....	74.79	9.88
+4.8	.....	.....	.....	.....	118.4	15.7
+5.2	.....	.....	.....	.....	187.5	24.9
+5.6	.....	.....	.....	.....	297.1	39.4
+6.0	.....	.....	.....	.....	470.7	62.4

TABLE 3

log W/b	log a					
	−1.0	−1.4	−1.8	−2.2	−2.6	−3.0
	$\Delta \log \eta_0$ for $B^{(0)}/B^{(1)}=\frac{1}{3}$					
−0.8	+0.08	+0.09	+0.08	+0.08	+0.08	+0.08
−0.6	+ .09	+ .09	+ .09	+ .09	+ .09	+ .09
−0.4	+ .09	+ .09	+ .09	+ .09	+ .09	+ .09
−0.2	+ .10	+ .10	+ .10	+ .10	+ .10	+ .10
0.0	+ .11	+ .11	+ .11	+ .11	+ .12	+ .12
+0.2	+ .12	+ .13	+ .13	+ .13	+ .14	+ .14
+0.4	+ .13	+ .14	+ .15	+ .16	+ .16	+ .16
+0.6	+ .12	+ .13	+ .14	+ .15	+ .17	+ .18
+0.8	+ .11	+ .11	+ .11	+ .11	+ .11	+ .11
+1.0	+ .11	+ .11	+ .11	+ .10	+ .10	+ .10
+1.2	+ .11	+ .11	+ .11	+ .10	+ .10	+ .10
+1.4	+ .11	+ .11	+ .11	+ .11	+ .11	+ .11
+1.6	+ .11	+ .11	+ .11	+ .11	+ .11	+ .11
+1.8	+ .11	+ .11	+ .11	+ .11	+ .11	+ .11
+2.0	+0.11	+0.11	+0.11	+0.11	+0.11	+0.11
	$\Delta \log \eta_0$ for $B^{(0)}/B^{(1)}=\frac{4}{3}$					
−0.8	−0.10	−0.10	−0.10	−0.10	−0.10	−0.10
−0.6	− .11	− .11	− .11	− .11	− .11	− .11
−0.4	− .11	− .11	− .11	− .11	− .11	− .12
−0.2	− .12	− .12	− .12	− .12	− .12	− .12
0.0	− .13	− .13	− .13	− .13	− .13	− .13
+0.2	− .14	− .14	− .15	− .15	− .15	− .15
+0.4	− .14	− .15	− .16	− .16	− .17	− .16
+0.6	− .14	− .14	− .14	− .15	− .16	− .18
+0.8	− .13	− .13	− .13	− .12	− .12	− .12
+1.0	− .13	− .12	− .12	− .12	− .12	− .12
+1.2	− .12	− .12	− .12	− .12	− .12	− .12
+1.4	− .12	− .12	− .12	− .12	− .12	− .12
+1.6	− .12	− .12	− .12	− .12	− .12	− .12
+1.8	− .12	− .13	− .13	− .13	− .13	− .13
+2.0	−0.12	−0.12	−0.12	−0.12	−0.12	−0.12
	$\Delta \log \eta_0$ for $B^{(0)}/B^{(1)}=\frac{1.0}{3}$					
−0.8	−0.23	−0.23	−0.24	−0.23	−0.23	−0.23
−0.6	− .24	− .24	− .24	− .24	− .24	− .24
−0.4	− .25	− .25	− .25	− .25	− .25	− .25
−0.2	− .26	− .27	− .27	− .27	− .27	− .27
0.0	− .27	− .28	− .29	− .29	− .29	− .29
+0.2	− .29	− .30	− .31	− .31	− .31	− .31
+0.4	− .29	− .31	− .32	− .33	− .34	− .33
+0.6	− .29	− .29	− .30	− .31	− .32	− .33
+0.8	− .27	− .27	− .27	− .27	− .27	− .27
+1.0	− .27	− .26	− .26	− .26	− .26	− .26
+1.2	− .27	− .27	− .27	− .26	− .26	− .26
+1.4	− .26	− .26	− .26	− .26	− .27	− .27
+1.6	− .27	− .27	− .27	− .27	− .27	− .27
+1.8	− .27	− .27	− .27	− .27	− .27	− .27
+2.0	−0.27	−0.27	−0.27	−0.27	−0.27	−0.27

THE WOLF-RAYET SPECTROSCOPIC BINARY HD 190918*

O. C. WILSON
Mount Wilson Observatory
Received October 8, 1948

ABSTRACT

The emission and absorption components of this star are of types close to WN5 and B0, respectively. Many observations made in 1946, 1947, and 1948 have been combined by graphical methods to yield approximate spectrographic orbits. Only the λ 4686 band of *He* II was measured in the W spectrum, while five or six absorption lines due to the B-type component were regularly used. Derived constants of the system are: $\gamma_B = -21.8$ km/sec, $K_B = 10.0$ km/sec; $\gamma_W = +88$ km/sec, $K_W = 38$ km/sec; $(m_B + m_W) \sin^3 i = 0.986\ \odot$.

Since the spectra of the components of HD 190918 are not very different from those of HD 193576, whose minimum total masses are 35 ⊙, it is probable that the value of i for HD 190918 does not exceed 18°. It is concluded, therefore, that the red shift of the λ 4686 *He* II band in WN stars is probably independent of the orientation of the polar axes of the stars with respect to the line of sight and that its origin is to be sought in processes occurring within the WN atmospheres.

The spectrum of HD 190918 is composite. A broad emission at λ 4686 and weaker, rather poorly defined bands near λ 4605 and λ 4619 lead to a classification of about WN5 for the emission component. A slightly later type, somewhere between WN5 and WN6, might be preferred, as there are indications of some faint band structure between λ 4619 and λ 4686.

The absorption-line spectrum corresponds closely to type B0. Ionized helium, represented by λ 4542 and λ 4200, seems not to be present. The lines λ 4089 *Si* IV and λ 4097 *N* III are strong, as are λ 4471 *He* I and the Balmer series. Strong interstellar H and K are, of course, present.

Since the absorption lines are relatively prominent and the emission bands have a "submerged" appearance, one may probably conclude that, in the photographic region at least, the continuous spectrum of the B-type component is stronger than that of the W star.

It now seems probable that all spectra of this general type, i.e., broad emission and relatively narrow absorption, arise from binary stars. Accordingly, spectrographic observations were begun in the summer of 1946 and have been continued through the observing seasons of 1947 and 1948 for the purpose of determining the orbit of the system. Previous observations[1] showed that the velocity range was small; it was hoped that the period would also prove to be sufficiently short to provide at least reasonable assurance of a small orbital inclination.

Five absorption lines were measured on nearly all the spectrograms and a sixth, λ 4116 *Si* IV, on some of them. Only λ 4686 *He* II was measured in the W spectrum, since the other bands were too weak and poorly defined on most of the spectrograms to be reliable. This was due partly to the inherent weakness of the bands and partly to the fact that the spectrograms were purposely made rather dense in order to increase the accuracy of measurement of the somewhat diffuse absorption lines. Wave lengths for the lines used, all taken from Miss Moore's tabulation,[2] are in Table 1.

Radial velocities of the two components from individual plates are in Table 2. A number of the spectrograms were taken consecutively in pairs; moreover, several series

* *Contributions from the Mount Wilson Observatory, Carnegie Institution of Washington*, No. 755.

[1] J. S. Plaskett, *Pub. Dom. Ap. Obs., Victoria*, **2**, 287, 1924.

[2] *Contr. Princeton U. Obs.*, No. 20, 1945.

of plates were taken on successive nights. These pairs and series provide evidence that the probable error of a velocity from a single plate is fairly large, as would be expected from the nature of the spectra.

The period was found by trial and error, and the adopted value—85.0 days—is not of extreme accuracy. In fact, since the errors of measurement are fairly large in comparison with the semi-amplitudes of both stars, simple graphical methods have been used throughout.

Normal points, calculated with $P = 85.0$ days, are given in Table 3, while Figure 1 shows the normals assembled on sine-curves whose semi-amplitudes were derived by trial and error. Phases are to be calculated from the formula JD = 2429831.2 + 85.0E, the zero point of phase being that corresponding to the time of closest approach of the W star to the observer. Orbital eccentricity was assumed to be zero, since there is no evidence for large deviation from this value and small values of e could hardly be determined with accuracy.

TABLE 1

ADOPTED WAVE LENGTHS OF LINES IN HD 190918

λ	Element	λ	Element
4026.217	*He* I	4340.468	*H*
4088.863	*Si* IV	4471.508	*He* I
4097.31	*N* III	4685.682	*He* II
4116.104	*Si* IV		

Constants of the system are in Table 4. The very small minimum mass is almost certainly to be attributed to the influence of sin i. The two components of HD 190918 are spectroscopically not very different from those of HD 193576; for the latter a total mass of 35 ⊙ is probably not far from the truth.[3] If it is assumed that the total mass in the present instance is also 35 ⊙, one finds $i = 18°$. Hence it seems fairly certain that in the system HD 190918 the polar regions of the stars are directed toward the observer.

This latter point is probably of some importance. In HD 193576, which is an eclipsing binary, the line of sight must lie close to the orbit plane, whereas in HD 190918 it is not far from perpendicular. Nevertheless, in both systems the γ-axis of the W component is shifted toward positive values by considerable amounts.[3] These facts seem to leave no doubt, therefore, that the red shift of the λ 4686 band of *He* II in the WN stars does not depend appreciably upon the aspect of the star to the observer. Whatever the origin of the shift may be, it is probably to be sought in processes occurring within the atmosphere itself.

E. S. Keeping[4] has questioned the writer's conclusion that the γ-axis of the W star in HD 193576 is shifted 90 km/sec positive with respect to that of the other component. In Table 6 of Keeping's paper, the mean for λλ 4686, 4619, 4603—the same emission bands used by me—is $\gamma_W = +77$ km/sec, compared to my value of +56 km/sec. The difference is thus not to be found in disagreement concerning the emission bands. Apparently, it lies largely in the assumed wave lengths of the absorption lines of the other component. By far the best absorption lines are those of the Balmer series. As I pointed out,[3] it is very important to decide in such a case whether the Pickering series of *He* II is of sufficient strength to justify the adoption of a blended wave length. Inspection of many plates convinced me that in HD 193576 the Pickering series was too weak with respect to the Balmer lines to cause appreciable distortion. Nevertheless, in Table 1 of Keeping's

[3] O. C. Wilson, *Mt. W. Contr.*, No. 623; *Ap. J.*, **91**, 379, 1940.

[4] *Pub. Dom. Ap. Obs., Victoria*, Vol. **7**, No. 23, 1947.

TABLE 2

RADIAL VELOCITIES OF HD 190918

(Km/Sec)

PLATE	JD*	RADIAL VELOCITY	
		Absorption	Emission
C 7522	2429827.67	−32.9	.....
C 7555	864.74	−15.4	.....
γ 23782	30269.62	−34.1	+137.2
27766	2008.70	+ 4.3	+ 21.8
767	2008.70	−19.3	+ 78.3
772	2009.70	+ 5.2	+ 62.4
773	2009.70	−10.9	.....
782	2010.98	− 8.3	.....
783	2010.98	−12.5	.....
894	2049.68	−21.7	.....
895	2049.68	−34.1	+ 70.1
896	2049.68	−32.7	+124.7
903	2050.64	−16.4	+ 47.9
904	2050.64	−39.0	+148.7
911	2051.66	−39.3	+161.0
912	2051.66	−24.6	.....
926	2070.66	−21.9	.....
927	2070.66	−28.8	.....
936	2071.87	−34.9	+154.9
937	2071.87	−35.3	+ 86.1
939	2072.64	−25.0	+133.0
940	2072.64	−42.0	+192.7
28022	2100.68	−22.7	.....
023	2100.68	−21.3	.....
030	2101.65	+ 5.6	.....
031	2101.65	− 7.1	.....
138	2128.66	−22.3	+162.0
151	2131.62	−12.0	.....
176	2163.60	.....	+ 69.9
177	2163.60	.....	+ 66.7
188	2164.59	.....	+117.1
199	2167.58	.....	+127.4
226	2171.57	−18.0	+143.6
503†	2312.95	−35.7	+ 89.9
509	2313.91	−30.9	+171.6
513	2314.94	−38.3	+159.2
515	2315.94	−35.8	+ 96.1
519	2317.88	−24.6	+111.9
531	2333.91	−12.0	.....
537	2334.97	−12.4	+ 66.4
541	2337.96	− 8.0	+ 94.2
676	2373.74	−20.7	+ 40.6
680	2374.72	−16.4	+ 59.3
685	2375.73	−21.3	+ 30.8
689	2376.72	−20.5	+ 74.6
693	2377.74	− 7.3	+ 52.2
874	2430.67	−31.6	.....
880	2431.65	−23.7	.....
886	2432.67	−12.1	.....
891	2433.65	− 9.3	.....
919	2452.64	−12.4	+ 57.1
924	2453.64	− 6.2	.....
930	2454.61	−28.9	.....

* Tabulated JD's for plates taken consecutively are the means for the group. Exposure times seldom exceeded 1 hour per plate.

† Beginning with γ 28503, the spectra were widened about twice as much as for the earlier plates. In forming normal places, fully widened spectra were given weight 1, the others weight ½.

TABLE 2—*Continued*

Plate	JD*	Radial Velocity	
		Absorption	Emission
29146	2432514.59	−30.1	+ 74.3
149	2515.58	−39.7	+115.2
155	2516.58	−25.3	.....
451	2655.96	.....	+116.9
460	2657.94	.....	+ 57.4
526	2685.88	−18.0	+ 14.3
527	2685.88	− 2.6	+ 67.7
528	2685.88	−21.3	+ 89.7
553	2692.94	− 9.2	.....
554	2692.94	− 8.4	.....
555	2692.94	+ 2.5	+ 54.4
559	2693.94	−14.1	+ 32.4
560	2693.94	− 2.6	+ 73.3
579	2697.96	−12.6	.....
580	2697.96	−26.0	+ 54.0
585	2698.96	− 9.3	+ 66.7
586	2698.96	−23.8	+139.1
591	2714.96	− 3.9	+ 4.4
592	2714.96	−24.1	.....
626	2719.98	−14.1	.....
632	2720.96	−23.7	.....
685	2727.98	−18.6	.....
723	2747.94	−29.2	+167.2
724	2747.98	−24.7	+132.4
725	2748.74	.....	+ 69.8
726	2748.74	.....	+ 60.2
727	2748.88	−28.8	+135.4
728	2749.73	−42.1	+154.6
729	2749.73	−36.8	+182.6

TABLE 3

NORMAL POINTS FOR $P=85.0$ DAYS

No.	Absorption			Emission		
	Phase	Vel. (Km/Sec)	Wt.*	Phase	Vel. (Km/Sec)	Wt.*
1	0.100	−25.3	4	0.109	+110.5	5
2	.212	−33.3	6	.220	+105.0	8
3	.326	−32.3	5	.325	+128.9	7
4	.368	−27.3	4	.366	+141.7	4
5	.481	−12.6	4	.472	+ 97.8	7
6	.604	−19.3	10	.603	+ 70.5	5
7	.677	−12.0	14	.665	+ 65.7	9
8	.853	−15.8	3	.841	+ 57.1	1
9	.937	−17.3	5	0.948	+ 60.5	7
10	0.987	−20.0	7	.....	.....	.....

* The weights for the absorption velocities are the numbers of plates included, except as modified by the statement of n. † to Table 2. For emission, all spectra have unit weight.

paper it is apparent that he has adopted the mean wave lengths of *H* and *He* II lines for *Hβ*, *Hγ*, *Hδ*, and *Hε*. Thus, in effect, he has shifted the wave lengths of his best absorption lines nearly an angstrom toward the violet. The natural consequence of this procedure, for which I can see no justification, is that the major portion of the difference in γ-velocities disappears. Fortunately, in the case of HD 190918 this question cannot

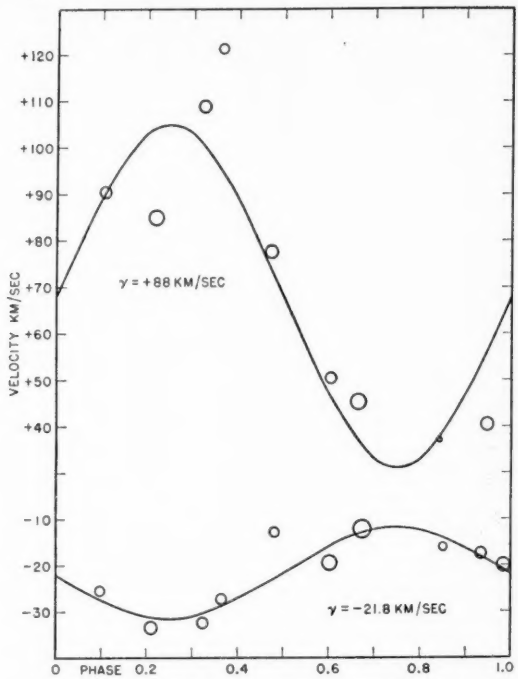

FIG. 1.—Radial-velocity curves of HD 190918

TABLE 4

ORBITAL CONSTANTS OF HD 190918

$\gamma_B = -21.8$ km/sec		$a_B \sin i$	$= 1.2 \times 10^7$ km
$K_B = 10.0$ km/sec		$a_W \sin i$	$= 4.4 \times 10^7$ km
$\gamma_W = +88$ km/sec		$\frac{m_B}{m_W}$	$= 3.7$
$K_W = 38$ km/sec		$(m_B + m_W) \sin^3 i$	$= 0.986 \odot$

arise. The Pickering series is either absent altogether or, if present at all, is barely visible on only the most favorable spectrograms.

As shown in Table 2, variations in velocity from month to month appear definitely to exclude the possibility of a period much longer than 85 days. There is always the chance that some shorter period might satisfy the observations, although considerable effort led to no results in this direction. If, however, a shorter period were found to be correct, our conclusion that the line of sight makes a small angle with the normal to the orbit plane would be strengthened because, in order to maintain reasonable total mass for the system, the value of *i* would necessarily be even smaller than that adopted.

HIGH-DISPERSION SPECTROGRAMS OF T CORONAE BOREALIS*

ROSCOE F. SANFORD
Mount Wilson Observatory
Received October 15, 1948

ABSTRACT

Velocities from absorption lines.—Coudé spectrograms of T CrB, when it is fainter than 9 mag., show an absorption-line spectrum of class gM3, associated with nova-like emission lines, just as before the February, 1946, outburst. The variable velocities from the gM3 source are represented by a sine-curve with a semi-amplitude of 21 km/sec, a period of 230.5 days, and a systemic velocity of −29 km/sec (see Fig. 1).

Velocities from bright lines.—The emission lines associated with the nova source also give a systemic velocity of −29 km/sec but show no certain velocity variation. Neither orbital motion nor pulsation seems adequate to explain a velocity variation for the gM3 source and a lack of variation in the velocities from the emission-line source; but no other explanation is at hand.

Structure of the bright lines.—Curves, photometric tracings, and reproductions of the spectrograms serve to illustrate a variety of structural changes in the bright lines.

Intensities of the bright lines in relation to the light-curve are summarized in Table 5 and Fig. 7.

T Coronae Borealis was discovered to have risen from magnitude 9.8 to 3.0 on February 9, 1946, by Norman F. H. Wright, of Bedford Park, England, and by Armin J. Deutsch, at the Yerkes Observatory, 3 months less than 80 years after J. Birmingham had discovered a similar rise to magnitude 2 on May 12, 1866. It is, therefore, without question, a recurrent nova. The light-changes following the 1866 outburst were diligently observed by various observers.[1]

Several astronomers have recorded the light-changes since the outburst in February, 1946. Edison Pettit has compared his light-curve with that after the 1866 outburst.[2] The curves agree closely for the 9 months following each outburst.

Pettit's observations (Fig. 6) show the light-variation to be divided roughly into the following four parts: (1) the rapid waning from 3.0 mag. on February 9, to 9.3 mag. on March 12, 1946; (2) the slower decline from 9.3 to 9.8 mag. between March 12 and May 17, 1948; (3) the secondary maximum, which began about May 17, reached its peak of 7.9 mag. in early July, and ended by October 10, 1946; and (4) the relatively quiescent stage since October 10, 1946, during which the variable has hovered around 9.5 mag.

Except for the major outbursts in 1866 and 1946 and the secondary maxima which followed each by about $3\frac{1}{2}$ months, the variations of T CrB have been relatively minor. From 1334 estimates made on Harvard plates, Cecilia Payne-Gaposchkin and Frances W. Wright[3] showed the extreme range to have been $1\frac{1}{2}$ photographic magnitudes over the interval of 13 years preceding the outburst of February, 1946. Their results represent typical behavior during the relatively quiescent stages away from primary and secondary maxima.

The pre-outburst spectrograms of this variable obtained at Mount Wilson (some as early as 1921) have already been discussed.[4, 5, 6, 7, 8] Also, the spectral changes from February 10, 1946, to February 8, 1947, have been described.[9]

* *Contributions from the Mount Wilson Observatory, Carnegie Institution of Washington*, No. 756.

[1] See Campbell and Shapley, *Harvard Circ.*, No. 247, 1923.

[2] *Pub. A.S.P.*, **58**, 361, 1946.

[3] *Ap. J.*, **104**, 75, 1946.

[4] Adams and Joy, *Carnegie Inst. Washington Year Book*, No. 20, pp. 230 and 274, 1921; and No. 21, p. 234, 1922.

[5] Adams and Joy, *Pub. A.S.P.*, **33**, 263, 1921.

[6] M. L. Humason, *Mt. W. Contr.*, No. 596; *Ap. J.*, **88**, 228, 1938.

[7] A. H. Joy, *Pub. A.S.P.*, **50**, 300, 1938.

[8] R. Minkowski, *Pub. A.S.P.*, **55**, 101, 1943.

[9] R. F. Sanford, *Pub. A.S.P.*, **58**, 158, 1946; **59**, 87, 1947.

The work of Adams and Joy in 1921 and of Joy in 1938 revealed that the spectrum contained not only the emission lines characteristic of a nova but also the absorption lines of a class gM3 spectrum corresponding to a star of absolute magnitude about 0. Approximately the same value is derived if we take the apparent and the absolute magnitude of nova T CrB at maximum as +3 and −7 (about the accepted absolute magnitude of ordinary novae at maximum), respectively, and the class M3 spectrum as belong-

TABLE 1

RADIAL VELOCITIES OF T CRB

Plate	U.T.	Mag.	Spectral Region	Absorption Lines (gM3)	Emission Lines (Nova)
	1946				
Ce 4189	Mar. 16.464	9.4	Ph_2	−45.6 (19)	−14.3 (17)
4213	Apr. 15.372	9.6	Ph_2; vis.	−33.8 (19)	−23.2 (6)
4270	May 14.385	9.9	Ph_2; vis.	−21.4 (19)	.....
4274	17.285	9.9	Ph_2	−11.8 (13)	−25.6 (8)
4276	June 9.325	8.5	Ph_1	.....	.....
4278	10.212	8.5	vis.	.....	.....
4279	10.297	8.5	Ph_2; vis.	.....	−25.9 (10)
4283	12.226	8.4	Ph_2; vis.	.....	−24.9 (8)
4339	July 21.216	8.1	Ph_2; vis.	.....	−25.2 (6)
4345	22.206	8.1	Ph_2; vis.	.....	.....
4348	Aug. 10.181	8.3	Ph_2; vis.	.....	−42.0 (7)
4358	12.184	8.3	vis.	.....	.....
4388	Sept. 7.188	9.1	Ph_2; vis.	−45.4 (18)	−34.6 (12)
	1947				
4535	Jan. 9.542	9.7	Ph_2; vis.	−13.0 (16)	−32.4 (8)
4541	10.507	9.7	Ph_1; vis.	− 7.6 (13)	−33.9 (5)
4592	Feb. 8.476	9.4	Ph_2; vis.	− 4.8 (26)	−32.0 (6)
4619	Mar. 12.457	9.5	Ph_1; vis.	−18.2 (12)	−33.3 (4)
4630	14.446	9.5	Ph_2; vis.	−18.0 (28)	−32.2 (11)
4645	Apr. 11.326	9.6	Ph_2; vis.	−35.4 (18)	−29.1 (9)
4661	May 1.469	9.7	Ph_2; vis.	−42.1 (10)	−30.1 (4)
4673	4.325	9.6	Ph_2; vis.	−49.9 (38)	−28.2 (8)
4714	June 7.257	9.5	Ph_2; vis.	−50.4 (31)	−26.7 (12)
4740	July 4.303	9.8	Ph_2	−37.8 (16)	−22.1 (8)
4802	Aug. 7.219	9.8	Ph_2; vis.	−16.0 (36)	−31.7 (8)
	1948				
γ 29352	Feb. 19.476	9.8	Ph	−41.6 (10)	−23.4 (10)
29433	Mar. 23.378	9.8	Ph	.....	−28.3 (4)
29523	Apr. 28.287	9.8	Ph	−11.7 (10)	−27.1 (7)
29546	May 17.328	9.8	Ph; vis.	+ 0.9 (5)	−26.7 (9)
Ce 5191	May 24.387	9.8	Ph_2; vis.	−10.7 (33)	−33.7 (6)

ing to a star of apparent magnitude 10.2. Pettit's diagram[2] contains the light-curve for the nova that results from correcting his observed light-curve for the effect of blending with a gM3 star of constant magnitude 10.2. The radial velocities from the class gM3 lines, although derived with comparatively low dispersion before 1946, showed a range beyond the uncertainties of measurement.

Our first observations of the spectrum with high dispersion after the 1946 outburst were made on February 10.438, 1946 U.T. By the time the variable had waned to the ninth magnitude, the class M3 spectrum again became prominent; and it was soon evident that the velocities, derived for the first time with high dispersion, were indeed variable. Hence it seemed worth while to continue to observe with high dispersion as long as practicable. It has turned out to be possible to obtain fair exposures even at the

faintest magnitudes by using a slit 75 per cent wider than normal. The advantage of high dispersion lies in greater accuracy of velocity determinations and better resolution of detail in the emission lines.

The present *Contribution* is based almost entirely on coudé spectrograms obtained with the 100-inch telescope on Mount Wilson from March, 1946, to May, 1948 (see Table 1). The spectral regions covered by each spectrogram are given in the fourth column, where "Ph_2" and "Ph_1" indicate the photographic region in the second (10 A/mm) and first (20 A/mm) orders, respectively, and "vis." indicates the visual region in the first order (20 A/mm). The four prismatic spectrograms included have a dispersion of 36 A/mm at $H\gamma$.

ABSORPTION LINES

M-type spectrum.—The band head of *TiO* at λ 4957 which characterizes a class M spectrum "was definitely present on the Yerkes spectrograms of February 16, 1946," according to Armin J. Deutsch.[10] Our spectrograms, which include some lower-dispersion plates not listed in Table 1, showed no *TiO* band until February 20, when, as the star reached the eighth magnitude, a trace of the head at λ 4957 could be discerned. No

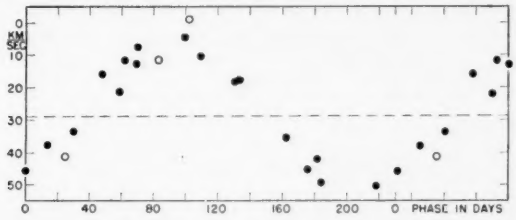

FIG. 1.—Radial velocities from class M lines. Phases are reckoned from March 16, 1946, with P = 230.5 days. *Solid circles*, coudé velocities; *open circles*, one-prism velocities; *broken line*, systemic velocity. Ordinates are negative.

coudé spectrogram was obtained between February 18 and March 16, 1946. On the latter date T CrB, having waned to 9.5 mag., showed not only the band at λ 4957 but others as well and much detail of the band structure of *TiO* in the region of λ 4600. Coudé spectrograms in April and May provided radial velocities from measures of M-type lines in the photographic and/or the visible region of the spectrum. In June, July, and August, 1946, when the secondary maximum of T CrB occurred, the class gM3 spectrum was so overpowered by the nova spectrum that satisfactory measures of velocity were impossible even in the visible region. Thereafter, all the spectrograms were obtained when T CrB was 9 mag. or fainter and the class M spectrum lines could again be measured on all spectrograms suitably exposed. Three of the four prismatic spectrograms were likewise suitable for measurement.

The class M3 velocities derived from these spectrograms are listed in the fifth column of Table 1. Their plot with time revealed a definite variation in a period of 230.5 days, according to which all the velocities have been assembled in Figure 1. Phases are counted from March 16, 1946. The velocities, extending over an interval of 774 days, or more than 3 periods, can be represented by a simple sine-curve with a systemic velocity of −29 km/sec and a semi-amplitude of 21 km/sec.

If this velocity variation is caused by orbital motion, the source of the class gM3 spectrum was receding most rapidly about June 28, 1946; February 3 and September 21, 1947; and May 8, 1948. It was approaching most rapidly about October 6, 1946; June 3,

[10] *Pub. A.S.P.*, **60**, 122, 1948.

1947; and January 19, 1948. Nearest approach would have occurred about April 19 and December 5, 1946; July 23, 1947; and March 9, 1948.

Shell spectrum.—Spectrograms obtained in June, just after the start toward secondary maximum, showed pronounced absorption lines accompanying the emission lines of *H*, *Ti* II, and *Mg* I. Weaker lines accompanied emission lines of *Fe* II and *Fe* I. The absorption lines of *Ti* II, *Mg* I, *Fe* II, and *Fe* I were well resolved, and the *H* lines of quantum number greater than 6 barely resolved into doublets (see doublet absorption lines marked with arrows and heavy absorption components of *H* series for June 10 in Fig. 2). In July and August the double *H* absorption lines, though weaker, had much the same displacements as in June. Those of *Ti* II, *Fe* II, and *Mg* I were still double but had undergone a shift to the violet from their positions in June. In August, all except the *H* lines were single. In September, 1946, and January, February, March, and April, 1947, these absorption lines, if present, were very weak; but in May, June, and July, 1947, they strengthened but were not resolved into components. The appearance of these absorption lines was similar to the absorption lines in so-called "shell stars." One possible explanation for them is, therefore, the absorption produced in the gaseous shell about T CrB.

TABLE 2

SHELL-LINE VELOCITIES

(Km/Sec)

DATE	HYDROGEN			*Mg* I, *Fe* II, *Fe* I, *Ti* II	
	Quant. No. <7	Quant. No. >7			
1946 June 10	−37	−21	+16	−25	+ 8
July 21	−37	−30	+27	−54	−16
Aug. 11	−45	−39	+11	....	−12
1947 May 4	....	....	+ 7	....	+14
June 7	+37	....	+17	....	+14
July 4	+33	....	+12	....	+20

The velocities from these lines, hereafter referred to as "shell lines," are summarized in Table 2.

Only the higher members of the Balmer series show the two absorption components just discussed. There are, however, shortward absorption components of *Hδ*, *Hγ*, *Hβ*, *Hα*, and H and K of *Ca* II, for which the mean displacement, −84 km/sec, is definitely less algebraically than the displacements given in Table 2. The lines listed in this paragraph are relatively much weaker than the lines in Table 2 but may also be shell lines.

Absorption lines of Ca II and Na I.—Sharp absorption lines of H and K of *Ca* II have appeared on all suitably exposed spectrograms. These may be single or accompanied by one or more less sharp components. The velocity displacements for all these lines are given in Table 3 (See Fig. 3).

The computed interstellar velocity for T CrB is about −16 km/sec. This assumes the accepted values of solar motion; differential galactic rotation; a distance of 1000 parsecs; and a light-path within the interstellar gas stratum only about one-quarter of its length from observer to star. This last assumption was made because of the high galactic latitude (+46°) of this star.

The mean observed velocity for the sharp H and K components (−24.7 ± 1.5 km/sec) is 8.7 km/sec smaller algebraically than is the computed interstellar value. Although this difference is quite appreciable, it can hardly be taken as infallible evidence that the measured velocity is not wholly interstellar; for the computed velocity is, at best, valid only statistically and then probably just for objects of low galactic latitude. No certain

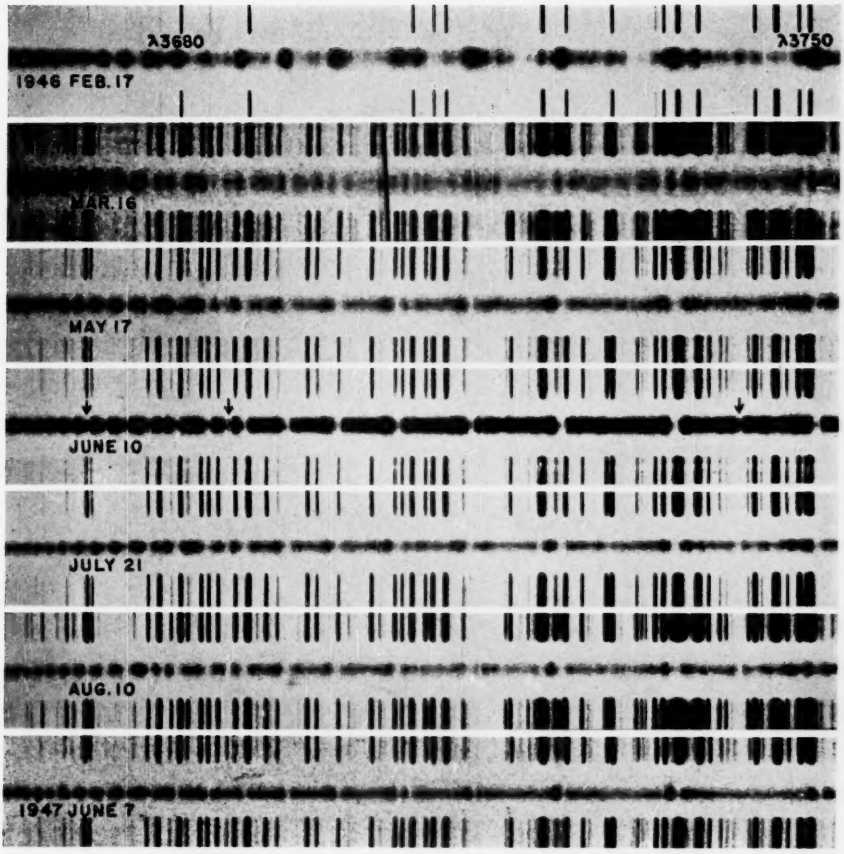

FIG. 2.—Spectrum of T CrB between λ 3660 and λ 3750

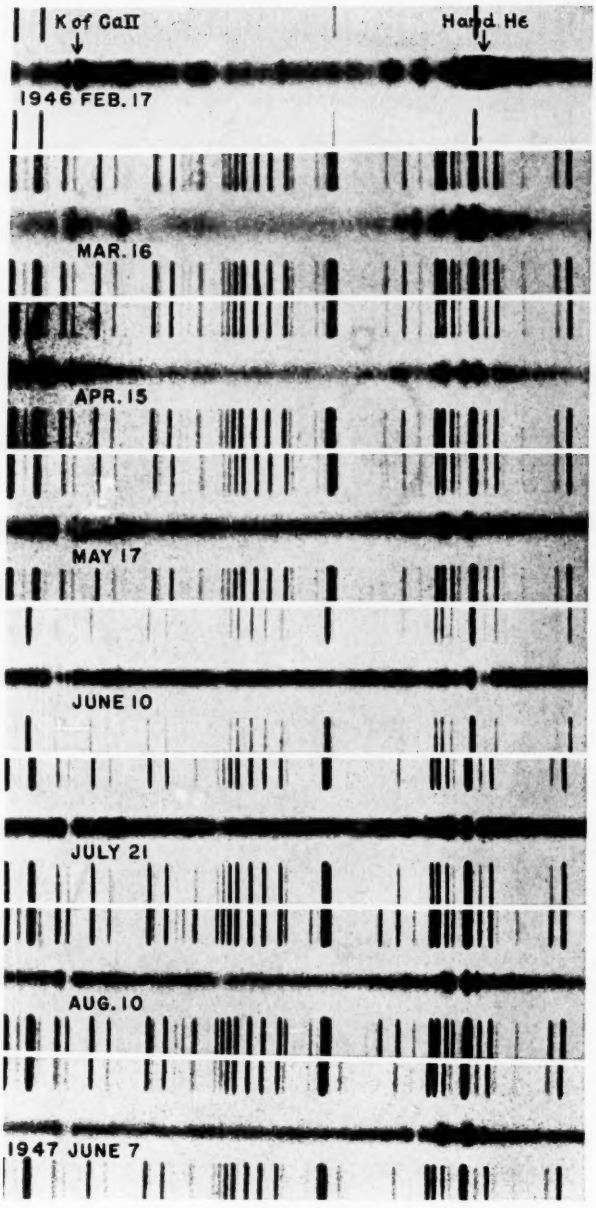

FIG. 3.—Spectrum of T CrB; region of H and K of *Ca* II

significance is, therefore, attached to the difference. At the same time, it may be well to have in mind that the observed velocity from the sharp H and K lines, −24.7 km/sec, is very nearly the simple mean of the computed interstellar velocity, −16 km/sec, and the systemic velocity of T CrB, −29 km/sec. Perhaps the observed line is a blend of circumstellar and interstellar components.

The velocity displacement of the longward absorption component of H and K (Table 3) and that of the longward shell-line component, *Ti* II, *Mg* I, etc., of Table 2, are roughly the same, but it is not certain that they belong together.

TABLE 3

VELOCITIES FROM H AND K, AND D1 AND D2 ABSORPTION LINES

(Km/Sec)

Plate Ce	H and K			D1 and D2	M-Type Velocities
4146		−23.4			
4148				−22.6	
4150		−23.9			
4157				−21.3	
4166				−24.1	
4179		−20.9			
4189	−77.4	−20.8			
4213	(−74.8)	(−33.4)	(+23.7)		
4274	−80.4	−26.0			
4279	−91.5	−27.0	+20.2	−14.8	− 9
4283	−91.0	−25.8	+17.1	−17.3	− 9
4339		−24.2	+13.2	−23.7	−20
4345				−17.4	−20
4348		−26.0			
4388		−24.4			
4535		−31.2		−21.0	−13
4541				−15.9	− 8
4592		−25.1		−13.4	− 5
4619				−17.0	−18
4630		−23.0		−17.3	−18
4645		−22.8		−31.7	−35
4673		−22.1	+10.7	−25.3	−50
4714		−19.5	+12.9	−31.3	−50
4740		−28.9	+ 4.5		
4802		−28.7			

Absorption lines of D1 and D2 of *Na* I have the velocity displacements given in the next-to-last column of Table 3. The first three entries are from plates upon which the nova-like spectrum predominated and for the interval when H and K were single absorption lines that gave displacements in agreement with these three *Na* I velocities. The remaining D-line velocities of Table 3 show some evidence of variability. It is, therefore, probably significant that they have a fair correlation with the M-type velocities given in the last column of Table 3, which have simply been repeated from Table 1 except for Ce 4279, 4283, 4339, and 4345. For these four plates, M-type velocities have been read from Figure 1. This correlation suggested that *Na* I absorption lines with velocities like those of the sharp H and K lines are always present but have their positions somewhat displaced when blended with stellar *Na* I lines of the class M spectrum.

Absorption of He λ 3889.—During 1946 the emission lines of *He* I in the photographic region were evidently divided by minima or absorption; but only at λ 3889 was the emission strong enough to show structure clearly. Evidently absorption and emission of λ 3889 *He* I and *Hζ* combined to produce a varied structure until September, 1946, after

which a stabilized pattern persisted. The left-hand column of Figure 4 shows the sequence of structure at λ 3889 by means of photometric tracings. The stabilized pattern finally reached in September, 1946, and represented by the tracing for June, 1947, is one of emission approximately bisected by a strong absorption line whose reduced wave length is λ 3889.01 ± 0.03. Since the hydrogen lines have no such conspicuous absorption component, this one must belong with λ 3889.65 of *He* I, from which it is displaced by −49.4 ± 2.3 km/sec. This helium absorption line is presumably favored by low density in T CrB, as in shell stars.

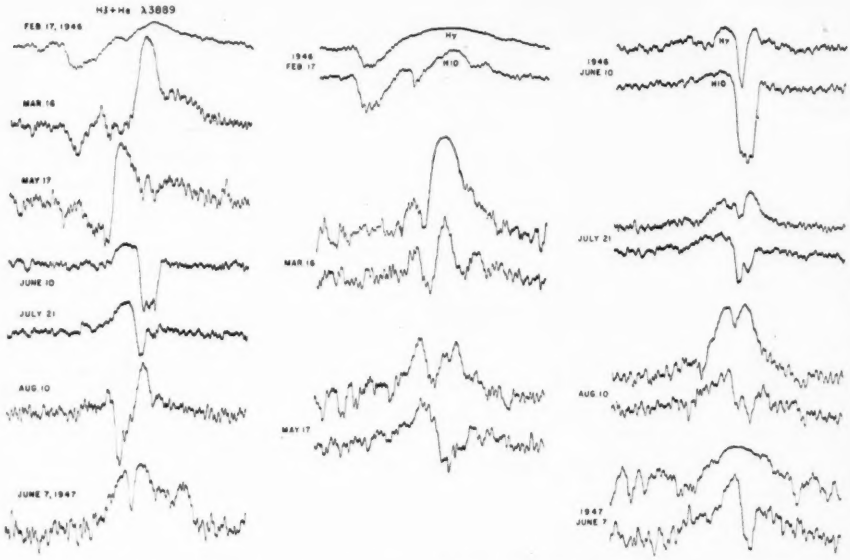

FIG. 4.—Column 1, microphotometer tracings of the blend of $H\zeta$ and *He* λ 3889. Columns 2 and 3, pairs of tracings of $H\gamma$ (*above*) and *H* 10 (below) on each date to illustrate marked difference in their structure.

EMISSION LINES

The line *H* 10, taken as typical of *H* lines of high quantum number, had two emission components from March to May, 1946, and from March to July, 1947. It was single the rest of the time. Bright $H\gamma$, typical of $H\delta$ and $H\beta$, was double from March to August, 1946, and single thereafter. The line $H\alpha$ was a double emission line throughout 1946 and single in 1947 and 1948. Up to May, 1946, the displacements of the longward components of these three bright *H* lines were identical within the errors of observation. During June and July the longward components of $H\gamma$ and $H\alpha$ persisted, and their displacements were the same as those of the longward component of the shell absorption lines already discussed. Quantitative values will be given later.

The decrement of the Balmer series to which longward emission components of $H\gamma$ and $H\alpha$ belonged in July seemed to be very large, since this component was very strong at $H\alpha$, moderately strong at $H\gamma$, and absent at *H* 10. Hence, for hydrogen lines of quantum number greater than 9, emission no longer interfered. Then the shell, which produced the longward absorption components of *Ti* II, *Mg* I, *Fe* II, and *Fe* I, also produced an absorption component of these *H* lines.

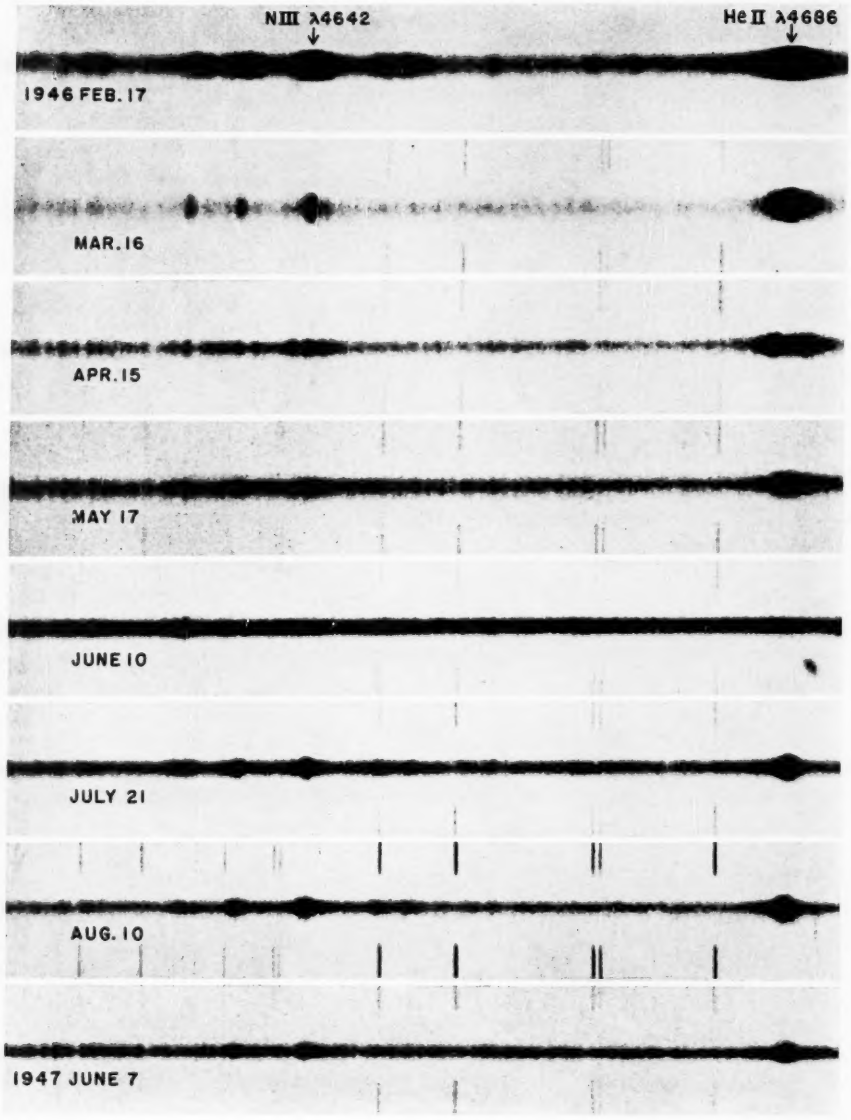

FIG. 5.—Spectrum of T CrB; region of λ 4642 *N* III and λ 4686 *He* II

The second and third columns of Figure 4 contain pairs of photometric tracings from coudé spectrograms, $H\gamma$ above and H 10 below in each pair, the tracings having been lined up by the systemic velocity (−29 km/sec). The scale in km/sec for H 10 has been made the same as that of $H\gamma$. From these tracings may be judged the relative intensities of the components within an emission line and also the relation of the intensities of components in H 10 to those in $H\gamma$ and the relative position of emission and absorption in the two lines. The replacement of emission in $H\gamma$ by the absorption in H 10 may be seen by comparing the tracings of these two lines in June and July, 1946.

As previously stated, the helium emission lines in the photographic region, although evidently complex, were too weak to define the structure during 1946, except for λ 3889. After that time, single emission components appeared on nine spectrograms.

H and K of *Ca* II in emission showed a varied structure, but the emission was so weak that it served only as a background upon which absorption components were brought out (see Fig. 3).

Other prominent emission lines, belonging to *O* III, *N* III, *He* II, *Fe* II, [*O* III], [*Ne* III], [*Ne* V], and [*Fe* II], are single (see Fig. 5 for *N* III, λ 4642, and *He* II, λ 4686, as examples of these lines).

Emission-line intensities.—The intensities of the emission lines have been derived by eye estimates by comparing them with the emission line of *He* II λ 4686, on spectrogram Ce 4535, which is simple and symmetrical and to which an intensity of 10 was arbitrarily assigned. An effort has been made to allow for the effects of a considerable spread in effective exposures. Spectrograms of lower dispersion have been used when necessary. The structure of the hydrogen lines made intensity estimates difficult. I have tried to sum up the contribution of the components and thus arrive at estimates, fully realizing that only rough qualitative results can be so obtained.

For conciseness and ease of reference, most of these data are presented in curves. Preliminary plots showed that the general run of intensity was so similar for *O* III and *N* III that a combined curve would serve for both. Likewise, a single curve for [*O* III], [*Ne* III], and [*Ne* V] could be used and one for *H* and *He* I. These and the curves of intensity for a number of other emission lines are shown in Figure 6. The abscisssae are the logarithms of the number of days after JD 2431860, a time scale that is open near the beginning, when changes are most rapid, and compact later on, when changes are slower. For the curves of *H*, *He* I, *He* II, and [*Fe* X] the scale is reduced to one-fourth that for the other curves, in order to make the figure more compact.

The meager data for the intensities of some of the weak emission lines do not serve for curves, but some of these data are mentioned in Table 4, which summarizes, among other things, pertinent data on line intensities that may be read from the curves of Figure 6.

The coronal lines of [*Fe* XIV] and [*Fe* X] appeared in the interval during which the magnitude fell from about 4.5 to 9.5. In September, 1946, after the decline from secondary maximum had started, the coronal line λ 6374 of [*Fe* X] was again present and persisted until February, 1947, when the variable reached magnitude 9.7. Thereafter, T CrB varied only slightly from 9.5 mag. until May, 1948, when last observed. The coronal lines, therefore, developed during the decline from the maxima and disappeared when the variable had reached the beginning of an extended quiescent minimum. Two other recurrent novae, RS Oph[11] and T Pyx,[12] have likewise exhibited coronal lines during the declining phase.

Ever since the emission lines of *O* III, *N* III, *He* II, [*O* III], [*Ne* III], and [*Ne* V] first appeared, they have always been present whenever spectra were obtained, except in early June, 1946. The interval during which the lines are absent extends, at the most,

[11] Adams and Joy, *Pub. A.S.P.*, **45**, 301, 1934.

[12] A. H. Joy, *Pub. A.S.P.*, **57**, 171, 1945.

from May 15 to July 17, 1946, judged by our observations. This is during the rising branch of the secondary maximum.

The three emission lines of [*O* III], λλ 4363, 4959, and 5007, seem to vary in relative intensity. The ratio λ 5007/λ 4363 was approximately as given in the accompanying tabulation.

April–August, 1946, incl.	1
September, 1946, and January–August, 1947, incl.	3
February–May, 1948, incl.	2

Emission-line velocities.—Whenever possible, hydrogen-line velocities from each plate were derived (1) from *Hα*, (2) from suitable hydrogen lines between *Hζ* and *Hβ* (designated by *Hγ*+), and (3) from hydrogen lines of quantum number higher than 8 (desig-

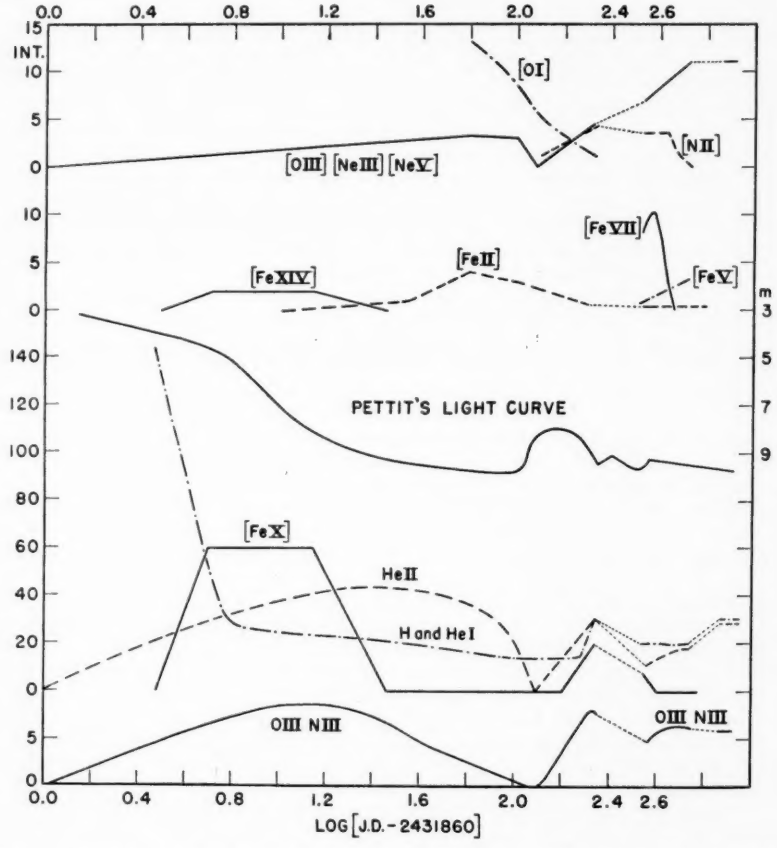

FIG. 6—Curves of intensity for emission lines in T CrB. Abscissae are logarithms of the number of days after JD2431860. Ordinates are intensities by comparison with *He* 4686 of Ce 4535, assigned intensity 10. Curves for [*Fe* X], *He* II, *H*, and *He* I have ordinates compressed to one-quarter the scale of the other curves. Dotted lines join successive observing seasons. The magnitude scale for Pettit's light-curve is on the right.

nated *H* 10+). On account of the low accuracy of these three kinds of velocities for individual plates, only mean values, for intervals that seem significant, are given in Table 5.

During the interval March–May, 1946, the range in the velocity values of the longward component for the three sets of hydrogen lines is probably too small to establish a

TABLE 4

EMISSION-LINE INTENSITY DATA

Date	Maximum	Minimum
1946 Feb. 9	*H*, *He* I	.....
Feb. 16	[*Fe* XIV], [*Fe* X], *Na* I, *Mg* II, *Si* II, *Ca* II, *Sc* II, *Ti* II, *Sr* II, [*S* II]	.....
Feb. 22	*O* III, *N* III	.....
Mar. 8	*He* II	.....
Apr. 13	[*O* I], [*Fe* II], [*O* III], [*Ne* III], [*Ne* V]	.....
May 20	Secondary light max. starts	.....
June 8	.....	*H* and *He* I; no lines of *O* III, *N* III, *He* II, [*O* III], [*Ne* III], [*Ne* V], [*N* II]
Sept. 7	[*Fe* X]	.....
1947	[*N* II], [*Fe* V], [*Fe* VII], [*O* III], [*Ne* III], [*Ne* V], max. higher than in April, 1946; *H*, *He* I, and *He* II stronger than at the end of 1946 season	.....
1948	Intensities for 1948 not significantly different from those in 1947, except that lines of [*Fe* VII], [*O* I], and [*N* II] are not seen	.....

TABLE 5

HYDROGEN EMISSION-LINE VELOCITIES

(Km/Sec)

	1946				1947		1948
	March–May		June–August				
Hα	− 7	(−101)*	+13	−165	....	(−87)	(−47)
Hγ+	−13	−140	+ 9	−104	....	−48	−39
H 10+	+ 2	−127	....	− 87	+27	−51	−36

* Very weak values are in parentheses.

real difference between them. Likewise, *Hα* does not show a velocity significantly different from *Hγ*+ for the longward component in the interval June–August. Reference has already been made (p. 86) to the longward emission components of the *Hγ* group and of *Hα* for June and July as occupying approximately the position of the longward shell component of the *H* 10 group of lines. The data for the longward components in the third column of Table 5 are in harmony with that hypothesis.

For the shortward components in both these intervals there is some evidence that the displacements tend to larger negative values with decreasing quantum number. It is conceivable that this might arise because the shortward components are less steep on their shortward sides and thus yield different displacements, depending on the density.

But such an explanation seems inadequate from measures of the components of *Hα* with exposures of 30 and 100 minutes (Ce 4339). The shorter exposure showed both components of *Hα* and hardly any continuous spectrum; in the longer exposure, *Hα* overlay a fully exposed continuous spectrum. Nevertheless, the shortward components have measured displacements differing by only 2 km/sec and the longward components by only 5 km/sec, respectively.

The separate velocities for *Hα*, *Hγ*, and *H* 10, when these are single emission lines, increase algebraically with quantum number, although the differences are possibly too small to be significant.

The displacements for helium emission lines are given in Table 6. The values display differences which seem larger than the probable errors. The displacement already obtained for the absorption component of λ 3889 has been added to Table 6, since it is similar to the displacement of the emission components of the helium lines in the photographic region.

The radial velocities from the emission lines of *N* III, *O* III, *He* II, *Fe* II, [*O* III], [*Ne* III], [*Ne* V], and [*Fe* II] are in accord with one another and have therefore been used to obtain a mean velocity for each spectrogram. These are given in the sixth column of Table 1. The simple mean of all these velocities is −28.8 km/sec, agreeing closely with

TABLE 6

HELIUM-LINE DISPLACEMENTS

λ 3889	(abs)	−49±2 km/sec
Helium lines in photographic region	(em)	−45±7
	(abs)	+15
λ 5875	(em)	−21±6
λ 6678	(em)	−38±8

the systemic velocity, −29 km/sec, given by the class gM3 lines. Only two of these emission-line velocities have residuals from the systemic velocity as large as 14 km/sec; the rest have residuals of less than 10 km/sec. There appears to be no evidence of a velocity variation for these emission lines in the period of 230.5 days to which the velocities from gM3 lines conform.

Since the gM3 source gives radial velocities with a definite periodic variation and the emission-line source does not, it is difficult to assume that they are a binary system unless the emission-line source is much more massive than the other source. This assumption would undoubtedly lead to difficulties in other respects. No satisfactory explanation is at hand for the periodic velocity variations for the one source and constant velocity for the other.

The two spectrograms Ce 4592 and Ce 4714 have the absorption velocities −4.8 and −50.5 km/sec and the emission velocities −32 and −27 km/sec, respectively. Evidently, if these two spectrograms are aligned by means of their absorption lines, the emission lines cannot be aligned. In Figure 7, *b* these spectrograms and the spectrum of *α* Ori in the region λλ 4300–4420 are aligned by the absorption lines. The lack of alignment of the emission lines of *Hγ* and λ 4363 [*O* III] is consistent with the velocities given above; also the general similarity of the absorption-line spectrum of T CrB to that of *α* Ori is evident.

Among the emission lines of T CrB in the visible, a line of [*Fe* VII] was measured on eight spectrograms. The mean of the eight after correction for the velocity shift of the forbidden lines is λ 6086.83 ± 0.04. P. W. Merrill[13] had derived λ 6086.9 from measures of spectrograms of Z Andromedae.

[13] *Mt. W. Contr.*, No. 728; *Ap. J.*, **105**, 122, 1947.

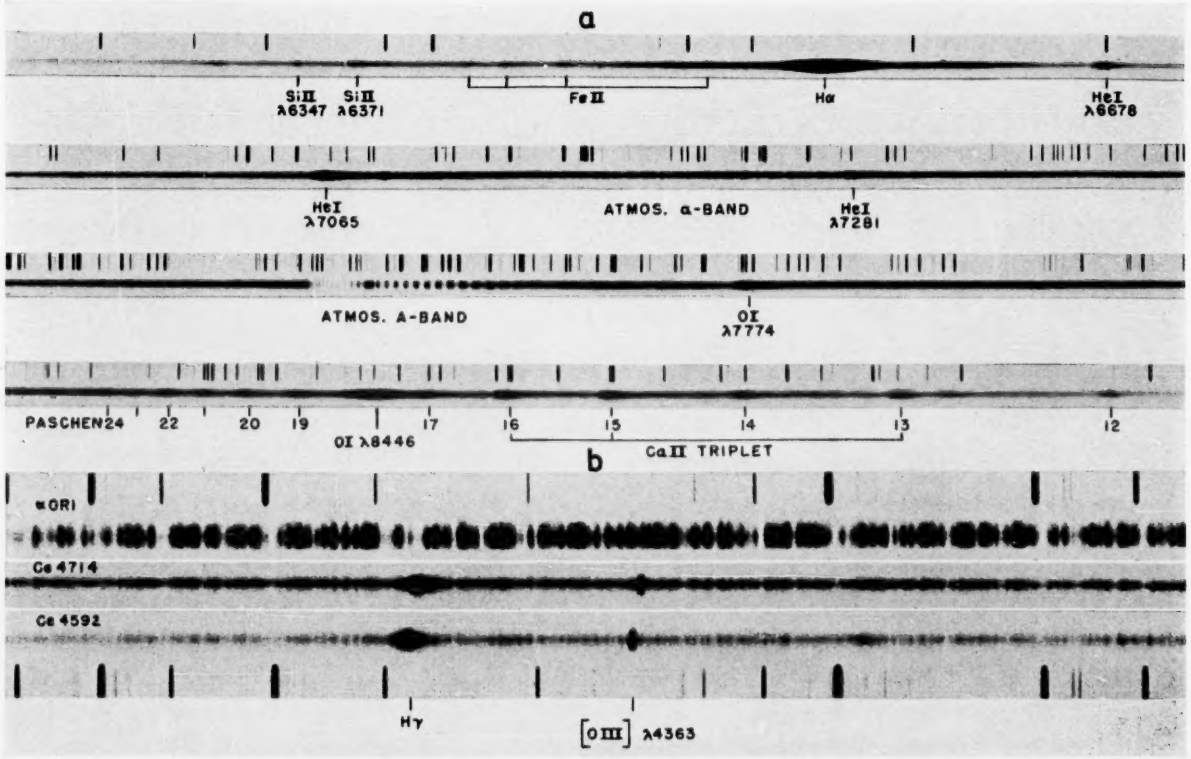

FIG. 7.—Spectrum of T CrB: (*a*) Portions of the spectrogram Ce 4166 of February 14, 1946, including the infrared. (*b*) Region of $H\gamma$ on Ce 4714 and Ce 4592, with that of α Ori. The staggered positions of the emission lines in the two plates result from lining up two spectrograms of T CrB with very different class M radial velocities.

INFRARED SPECTRUM

Figure 7, *a* shows portions of the infrared spectrogram of T CrB, Ce 4155, photographed February 14, 1946, with a dispersion of 20 A/mm. The more outstanding emission lines have been labeled. Few observations of novae have been made in this spectral region.

A. J. Deutsch[14] has published a concise description of three infrared spectrograms (48 A/mm), obtained on February 12, 16, and 18, 1946; the Mount Wilson plate, Ce 4166, midway between his first and second spectrograms, confirmed the sequence of changes described by him. There was definite absorption on the shortward sides of the emission lines of the *Ca* II triplet and perhaps also on the shortward sides of the Paschen lines and of the helium lines λ 6678 and λ 7065. Shortward absorption components of *Hα* and *O* I were not certainly observed.

[14] *Pub. A.S.P.*, **60**, 120, 1948.

STELLAR SPECTRA WITH EMISSION LINES IN THE OBSCURING CLOUDS OF OPHIUCHUS AND SCORPIUS*

OTTO STRUVE AND MOGENS RUDKJØBING
Yerkes and McDonald Observatories
Received September 8, 1948

ABSTRACT

Six dwarf stars situated in the densest part of the obscuring clouds in Ophiuchus and Scorpius are found to have spectra with strong emission lines of hydrogen and calcium. The great intensity of *Ca* II H seems to indicate that the excitation of the emission spectrum is due to collisions, the principal source of energy perhaps being the potential energy of the surrounding nebula. In addition, three faint early-type stars were found.

Joy's[1] remarkable discovery of forty stars having strong emission lines in the vicinity of the great obscuring cloud of Taurus has inspired a study of the faint stars in the region of the dark nebulae in Ophiuchus and Scorpius. With the 82-inch telescope of the McDonald Observatory the authors have observed the spectra of twenty-six stars in this region. The Cassegrain spectrograph with quartz prisms and the $f/1$ Schmidt camera was used for all the stars with the exception of the two brightest, for which the glass prisms and the $f/2$ camera were used. On the chart (Fig. 1), a print made from a Ross *Atlas* plate, the stars are marked by arrows and by numbers indicating the order in which their spectra were taken. Of these stars, those having the numbers 5, 6, 7, 14, 16, 17, 18, 19 are situated outside the densest part of the nebula. Of the eighteen that are seen on the background of the optically thick part of the cloud, six were found to have emission lines. These are all of photographic magnitudes between 12 and 15. Nearly all stars in this densest part of the cloud and in this range of magnitudes have been observed. One of the emission-line stars (No. 13 in our list) is a variable star with a range of at least 1.5 mag. It is brighter than stars 9, 11, and 12 on Plate 2 in the Ross *Atlas of the Milky Way*, fainter than 9 on Plate 3, and fainter than 9, 11, and 12 on Plate 5.

These six stars range in spectral type, as estimated from the absorption features, between A and M. With the exception of one, No. 22, which is of early type, they are K and M stars and are thus similar to the majority of Joy's stars in Taurus, presumably belonging to the main sequence and having, in addition, a superimposed spectrum of strong emission lines, which make them stand out among the ordinary dMe and dKe stars which are occasionally found among ordinary stellar populations. A short description of these stars is given in Table 1.

An interesting feature of stars 9, 12, and 13 is the great strength of the blend of *Ca* II H and $H\epsilon$, which seems to be abnormal, since it exceeds the sum of the intensities to be expected in the two blended components. This may be explained as an effect of excitation of the Ca^+ ions by transfer of excitation from colliding hydrogen atoms, which in the process of collision make the transition corresponding to the $H\epsilon$ line. Because the excited Ca^+ ions have to send out more than 90 per cent of the excitation energy in the H line,[2] while the hydrogen atoms before the collision process had the approximately equal probabilities of emitting light both in a Lyman line, in the Balmer line in question, and in some infrared lines, the result is an increase in intensity of the H blend. The opposite process, which in thermodynamical equilibrium would balance the one mentioned, will in a diluted radiation field occur less frequently because it involves the collision of two atoms, both of which must be in excited states.

* *Contributions from the McDonald Observatory, University of Texas*, No. 158.

[1] *Pub. A.S.P.*, **58**, 244, 1946.

[2] D. R. Hartree and W. Hartree, *Proc. Roy. Soc. London, A*, **164**, 167, 1938.

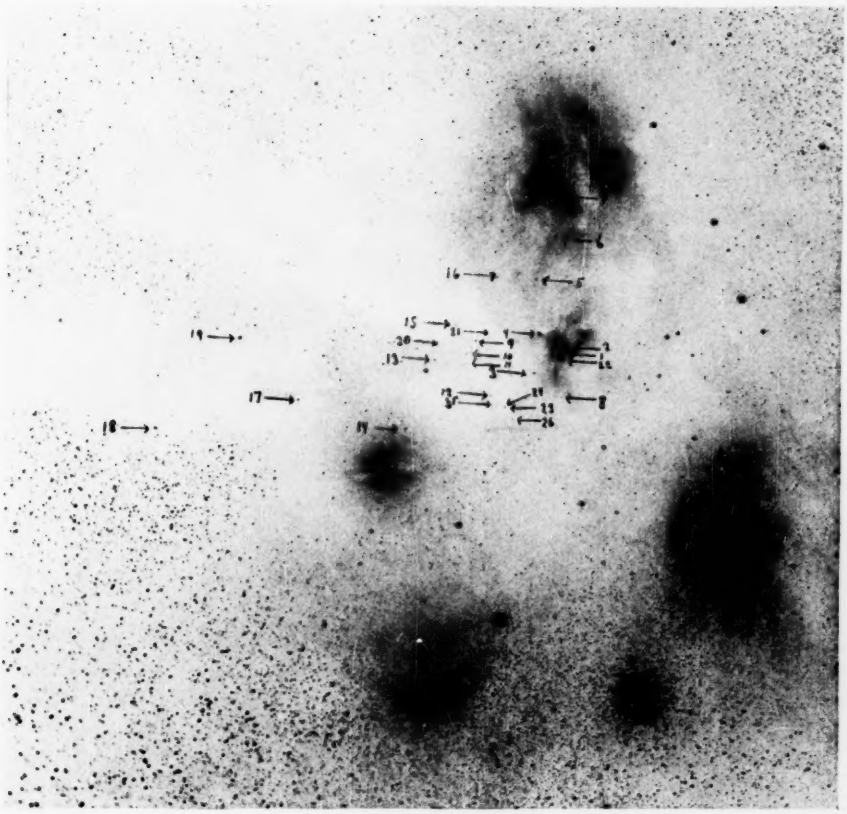

FIG. 1.—Region of the obscuring nebulosity in Scorpius and Ophiuchus. The numbers of the stars observed correspond to those given in Tables 1 and 2.

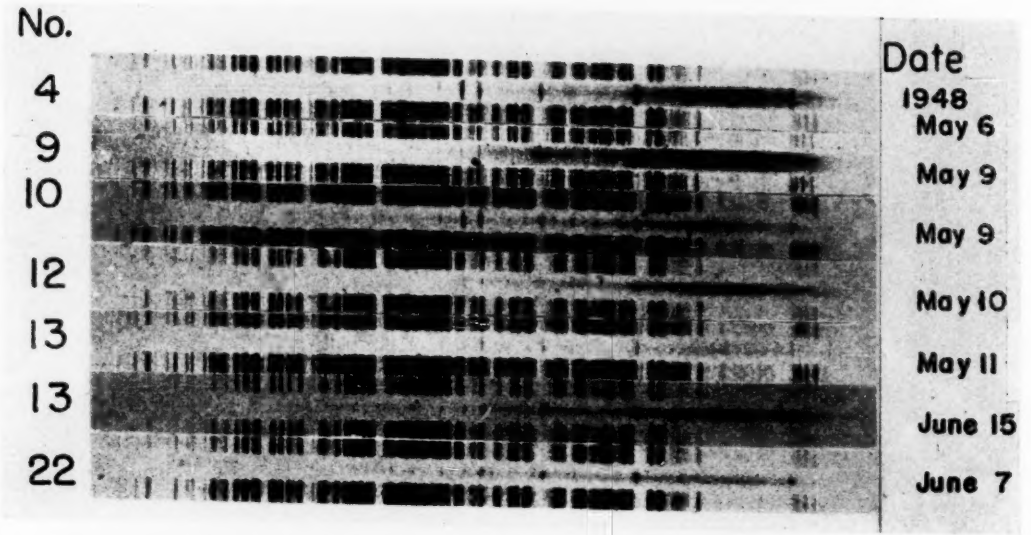

FIG. 2.—The spectra of six emission-line stars in Scorpius and Ophiuchus

That the extra intensity is really found in the *Ca* II line and not in the hydrogen line is suggested by one of Joy's[3] spectra, which has a greater dispersion than ours and which shows the same effect (the spectrum *c* on his Pl. XIV), being the only one of his spectra in which the *Ca* II lines are not too strong or too faint in comparison with the hydrogen lines to show the effect. It looks as if a strong *Ca* II H line is accompanied by a fainter hydrogen line.

The occurrence of dwarf stars with strong emission lines in cosmic dust clouds again raises the problem of the origin of their peculiar spectra. A computation based upon Hoyle's[4] expression for the accretion of mass of a star which rests within a nebula leads

TABLE 1

EMISSION-LINE STARS

No.	α(1948)	δ(1948)	Mag.	Sp.	Description
4	$16^h22^m.8$	−24°13′	13	K5	Very strong *H* and *Ca* II and perhaps weak *He* I; the absorption lines are systematically weaker than normal
9	16 24.5	−24 14	12.5	K2	Fairly strong and very broad *H*, strong and sharp *Ca* II; *Ca* II H very much stronger than *Ca* II K
10	16 24.7	−24 16	15	K?	Very strong *H* and *Ca* II, moderately strong *Fe* II; spectral type estimated from the continuous spectrum because the emission lines overlie the absorption features
12	16 24.1	−24 34	13.5	M	Moderate *H* and *Ca* II, perhaps weak *Fe* II; *Ca* II H very much stronger than *Ca* II K; has *TiO* absorption bands
13	16 25.6	−24 20	12.5 / −14.0	K	Very strong *H* and weak *Ca* II; *H*+*Ca* II H is much stronger than *Hδ*
22	16 22.3	−24 22	15	A?	Strong *H* and *Ca* II
	Faint Stars of Early Type without Emission Lines				
3	16 23.0	−24 28	13	A0	Fairly sharp absorption of *H*
5	16 22.9	−23 50	13	A5	Diffuse lines of *H*
16	16 23.8	−23 50	13.5	A	Very weak and shallow absorption lines of *H*

to the following ratio of the energy released by the infall of particles to the radiation energy emitted by the star:

$$\alpha = 16\pi \frac{(GM)^3}{RL} N m_H \left(\frac{3\bar{R}T}{\mu}\right)^{-3/2}.$$

Here R, M, and L denote the radius, mass, and luminosity of the star in question, N the number of atoms per unit volume, m_H the mass of the hydrogen atom, $\bar{R}$ the gas constant, and T and μ the temperature and molecular weight of the gas surrounding the star. This expression was derived from Hoyle's formula for the accretion of mass by multiplying the amount of matter gained per second by the potential energy GM/R per unit mass released during the motion of the matter toward the star. (There seems to be a small error in Hoyle's formula [17].) With the values of M, R, and L which Kuiper has given for the dwarf K0 star, 70 Oph A (Table 34*a* in Chandrasekhar's *Stellar Structure*), we find the following value for α (μ has been put equal to 1):

$$\alpha = 10^{-4.95} \cdot N \left(\frac{T}{10^3}\right)^{-3/2}.$$

[3] *Ap. J.*, **102**, 168, 1945.

[4] *M.N.*, **106**, 412, 1946.

Thus an ordinary dwarf star, like the one considered here, could produce enough emission to be observed only if the number of atoms per cubic centimeter of the cloud is of the order of 10^3 or 10^4 for a temperature of the gas of the order of 10^4 degrees. However, too much stress must not be laid on this formula, first, because it is derived as a very rough approximation by Hoyle and, second, because much of the interstellar matter in the cloud is probably in the form of dust to which the formula does not apply.[5]

We should, according to the above mechanism, have emission lines only in those cases in which the pressure of radiation from the stars is not strong enough to drive away the gas. Thus an early-type star will have this kind of emission lines only if it has a small radius, giving it a great gravitational potential at the surface. Our star 22 is perhaps

TABLE 2

STARS WITHOUT EMISSION LINES

Star No.	Spectral Type
1	B3 (as in *HD Catalogue*)
2	G8
3	A
5	A
6	K0
7	G5
8	K2
11	K5
14	G5
15	(Underexposed)
16	A
17	K2
18	K0
19	G (overexposed)
20	M
21	K0
23	K5
24	(Underexposed), a double star
25	K5
26	Early-type star, F0?

such a case. It is situated near the eighth-magnitude star, HD 147889, which is our No. 1 and whose spectral type is given by the *Henry Draper Catalogue* as B3. This star is imbedded in the nebula, as is indicated by the brightness of the nebular matter around it. Number 22 is 7 or 8 mag. fainter, and, being of early type, it is almost certainly underluminous.

In addition to the six emission-line stars, three faint stars of type A were found within the nebula. Their data are given in Tables 1 and 2. These spectra have no emission lines, and only No. 16 looks abnormal because of the weakness of its hydrogen absorption lines. This may be an underluminous A star or possibly even a white dwarf. The rest of the stars have normal spectra of types G, K, and M. Most of them are probably foreground stars, while a few, outside the densest part of the nebula, may be distant objects shining through the thinner portions of the cloud. Table 2 gives the estimated spectral types of the stars without emission lines. The emission-line spectra are reproduced in Figure 2. Of the variable star, No. 13, two spectra are given, the first taken in the beginning of May and the second in the middle of June, 1948. They do not suggest that any spectral changes have taken place during this interval of time.

[5] Dr. Hoyle has very kindly verified our computations, in a slightly different manner. His results and ours are in essential agreement.

SPECTROGRAPHIC OBSERVATIONS OF TW ANDROMEDAE*

W. A. HILTNER, BURKE SMITH, AND O. STRUVE
Yerkes and McDonald Observatories
Received November 8, 1948

ABSTRACT

The orbital elements lead to $K = 30.0$ km/sec and $\gamma = -46.0$ km/sec. The eccentricity is close to zero. The intensities and profiles of the H lines seem to change with the phase.

The eclipsing binary TW And was discovered as a variable by A. Kopff in 1909.[1] It is listed by Schneller,[2] whose epoch of principal minimum and period is the same as that given by Dugan.[3] These elements are repeated in the new catalogue by Kukarkin and Parenago:

$$\text{JD } 2420051.620 + 4.122745E .$$

N. L. Pierce's finding list (1947) gives the spectral class as dF0 + G6 and the magnitude variation as 9.0–11.0. Only one spectrum is visible, that of the F0 star, except during total eclipse, when the spectrum of the fainter star may be seen. The present investigation is based on the measurement of ten spectrograms with glass prisms and 180-mm camera taken in 1946 and twenty-one spectrograms with quartz prisms and 500-mm camera taken in 1947, all with the standard Cassegrain spectrograph attached to the 82-inch McDonald telescope. The dispersions were 76 A/mm at $H\gamma$ for the former (Gf/2) and 55 A/mm at $H\gamma$ for the latter (CQ). The emulsion used was Eastman 103a-O. The list of star lines is given in Table 1. A single plate (Gf/2 8419) was taken during total eclipse, at phase 0.001, and shows the spectrum of the faint star as being later than G6—probably K0.

Table 2 shows, for each plate, the date, phase as determined from Dugan's minimum, number of lines measured, and plate velocity. The probable errors are about ± 3 km/sec for the Gf/2 series and also for the CQ series. Since the probable errors and the numbers of lines measured are approximately the same for both sets of plates, it appears that the accuracy of the velocity measurements is substantially the same for either type of plate. In determining the orbital elements, equal weights were given to all plates. Figure 1 shows a plot of the observed velocities and a velocity-curve based on the individual observations. The normal points are shown in Figure 2 and were determined from a preliminary curve, with the observations grouped as shown in Table 3. The velocity of plate Gf/2 8362 at phase 0.025 was omitted in computing the normal velocities, as the residual for this point is abnormally large, although the plate is of good quality. It is of interest to note that M. B. Shapley[4] found an apparent variation in light during totality, which would include phase 0.025.

The period, as determined from the spectrograms, is in close agreement with that given by Dugan.[3] Plate Gf/2 8419, taken during totality (phase 0.001), shows only the spectrum of the fainter component, while the next preceding and following plates (phases 0.968 and 0.025), show the spectrum of the brighter star. However, the velocity-curve,

* *Contributions from the McDonald Observatory, University of Texas*, No. 160. The spectrograms were obtained by Mr. Struve and Mr. Hiltner, while the measurements were made by Mr. Smith.

[1] *A.N.*, **182**, 61, 1909.

[2] *Berlin Babelsberg Katalog für 1940.*

[3] *Contr. Princeton U. Obs.*, No. 14, 1933.

[4] *Ap. J.*, **56**, 439, 1922.

TABLE 1

LIST OF STAR LINES

Element	λ	Element	λ	Element	λ
Fe I	3849.97	*Ni* II	4067.05	*Fe* I	4250.79
Fe I	3856.37	*Fe* I	4071.74	*Fe* I	4260.48
Fe I	3878.58	*Sr* II	4077.71	*Fe* I	4299.24
Fe I	3902.95	*Hδ*	4101.74	*Sc* II	4314.08
Ti II	3913.46	*Fe* I	4143.50	*Fe* I	4325.76
Ca II	3933.67	*Mg* I	4167.27	*Hγ*	4340.47
Cr II	4003.33	*Sr* II	4115.52	*Fe* II	4351.76
Fe I	4005.25	*Ca* I	4226.73	*Fe* I	4404.75
Fe I	4045.82	*Fe* II	4233.17	*Mg* II	4481.23
Fe I	4063.60				

TABLE 2

RADIAL VELOCITIES OF TW ANDROMEDAE

Plate	Date	U.T.	Phase from JD 2432077.667		Lines Measured	Velocity (Km/Sec)
			Days	Decimals		
	1946					
Gf/2 8362	Sept. 13	6:30	0.103	0.025	23	−10.8
8380	17	6:31	3.099	.752	23	−13.2
8412	22	5:32	3.940	.956	23	−25.0
8413	22	6:08	3.968	.962	23	−29.2
8414	22	6:48	3.990	.968	23	−30.6
8419	22	10:00	0.004	.001	19	−31.0
8444	24	5:28	1.813	.440	25	−40.8
8454	25	6:21	2.851	.692	20	−23.0
8455	25	6:59	2.877	.698	27	−13.8
8467	27	7:15	0.768	.186	18	−75.0
	1947					
CQ 5353	June 5	11:06	0.441	.107	22	−59.0
5364	6	9:39	1.377	.334	27	−81.9
5379	7	10:38	2.420	.587	24	−39.0
5395	8	10:44	3.420	.830	23	−21.2
5452	11	10:33	2.290	.556	24	−42.8
5506	16	10:40	3.171	.770	26	−20.0
5645	26	9:55	0.775	.188	23	−75.7
5646	26	10:51	0.817	.198	23	−73.0
5672	28	10:50	2.813	.683	19	−40.7
5733	July 3	11:01	3.702	.897	23	−36.2
5782	5	10:54	1.570	.381	25	−50.8
5795	6	3:52	2.279	.553	24	−31.7
5796	6	4:51	2.320	.563	23	−34.5
5813	7	10:22	3.549	.861	23	−34.1
5838	8	10:02	0.412	.100	20	−61.0
5839	8	10:56	0.449	.109	23	−46.9
5863	9	10:01	1.399	.342	29	−77.9
5864	9	10:44	1.442	.350	26	−66.5
5902	12	10:50	0.321	.078	25	−47.8
5922	13	10:28	1.306	.317	26	−66.0
5957	15	9:11	3.256	0.790	24	−19.6

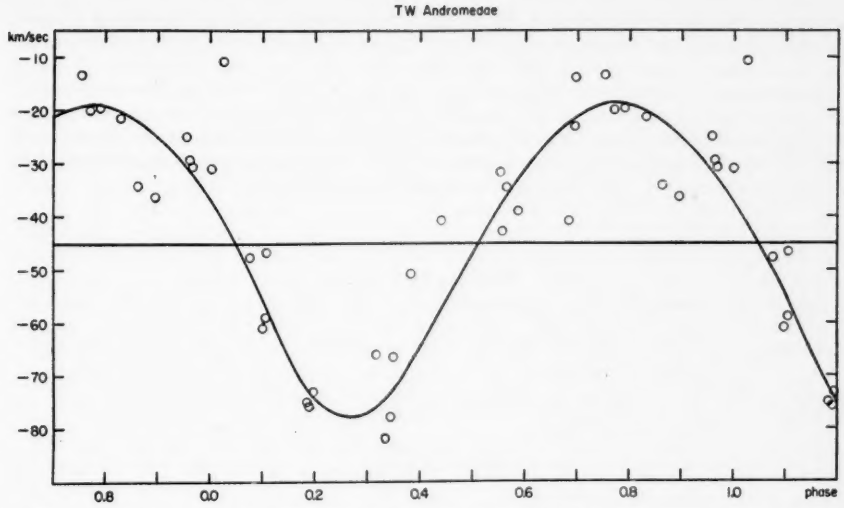

FIG. 1.—Velocity-curve of the TW Andromedae, showing the individual observations. The curve is that obtained with the elliptical elements.

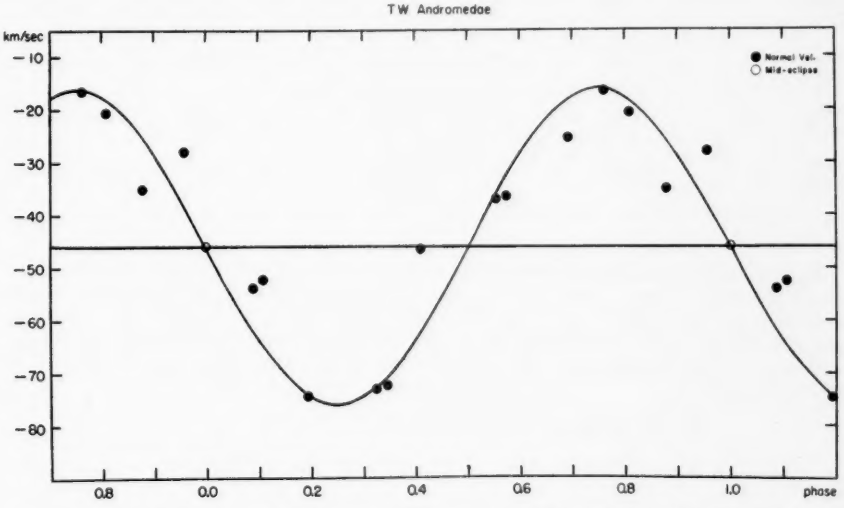

FIG. 2.—Velocity-curve of TW Andromedae. The normal points have been plotted; the curve is that corresponding to the circular elements. The small circle at phase zero was assumed.

as determined from the normal points, does not cross the γ-axis at the epoch of total eclipse. Based on the velocity-curve in Figure 1, one would expect the principal minimum to occur about phase 0.050 (0.206) days later than the time computed from Dugan's light-elements. The evidence from the spectrogram at phase 0.001 is, however, conclusive proof that the total eclipse was not shifted to phase 0.050, so that we cannot attribute the large residual at phase 0.025 to a normal rotation effect (otherwise the direction of rotation would be opposite to that of orbital motion); and we are inclined to believe that the departure may be caused by the uncertainty of the velocity-curve.

TABLE 3

NORMAL VELOCITIES

Plate	Average Phase (in Decimals)	Normal Velocity (Km/Sec)	Plate	Average Phase (in Decimals)	Normal Velocity (Km/Sec)
5902, 5838	0.089	−54.0	5796, 5379	0.575	−36.5
5353, 5839	.108	−52.5	5672, 8454, 8455	.691	−25.2
8467, 5645, 5646	.191	−74.5	8380, 5506	.761	−16.5
5922, 5364	.325	−73.0	5957, 5395	.810	−20.5
5863, 5864	.346	−72.3	5813, 5713	.879	−35.0
5782, 8444	.410	−46.5	8412, 8413	.959	−28.0
5795, 5452	0.555	−37.0	8414, 8419	0.984	−31.0

Orbital elements were computed by the method of Lehmann-Filhes from the velocity-curve shown in Figure 1, assuming a period of 4.122745 days and the epoch of principal minimum not at Dugan's minimum (JD 2432077.667), but at JD 2432077.873, which is phase 0.050 counting from Dugan's minimum. This curve represents the best fit, taking into account all observations except the one at phase 0.025, which was omitted. The solution gives:

$$K = 29.5 \text{ km/sec}, \qquad \omega = 178^\circ,$$

$$\gamma = -45.0 \text{ km/sec}, \qquad T = \text{JD } 2432079.068,$$

$$e = 0.12, \qquad a \sin i = 1{,}660{,}000 \text{ km}.$$

In view of the discrepancy between the observed velocity from plate G*f*/2 8419 at phase 0.0 (−31.0 km/sec) and the velocity obtained from the curve where it crosses the γ-axis (−45.0 km/sec), another velocity-curve was drawn, assuming zero phase at Dugan's minimum. This curve is based on Table 3, except that the normal point at phase 0.984 (Pls. G*f*/2 8414 and 8419) was omitted and the curve was assumed to pass

through the point of intersection of the axis and the epoch of total eclipse. Figure 2 shows the curve as drawn, using circular elements. This gives for the orbital elements,

$$K = 30.0 \text{ km/sec}, \qquad \gamma = -46.0 \text{ km/sec}.$$

In view of the small difference between the two solutions and the fact that the one observation at total eclipse shows a large residual, we believe that the second solution more nearly represents the true values of the elements.

A variation in the appearance of the hydrogen lines with phase was suspected. These lines are generally strong and broad. It was possible to measure both $H\gamma$ and $H\delta$ on most plates. At certain phases these lines show a sharp central core superimposed on a broader underlying line. In measuring the velocity of the H lines the setting was always made on the core, if visible, rather than on the middle of the underlying line. The velocity of the core shows no systematic deviation with phase from the mean plate velocity, and both they and the wings must come from the F0 star, since the H lines in the fainter component are barely visible at primary eclipse and are rather narrow.

The suspected effect may be summarized as follows: preceding primary eclipse (phases 0.770–0.000), a sharp core is generally visible in one or both of the hydrogen lines, $H\gamma$ and $H\delta$, and is superimposed on a broad underlying line. Following primary eclipse (phases 0.000–0.186), the H lines are narrower and a core is not generally visible.

RADIAL-VELOCITY OBSERVATIONS WITH THE BRUCE SPECTROGRAPH

DANIEL M. POPPER
Department of Astronomy, University of California, Los Angeles
Received October 25, 1948

ABSTRACT

Some results of observations obtained with the Bruce spectrograph in 1946 and 1947 are reported.

μ Orionis.—The large eccentricity of the orbit of μ Ori AB is confirmed. The discrepancy between the masses and luminosities noted by Alden remains, unless μ Ori B is an M star.

4 Sextantis.—Preliminary elements are $K_1 = 100$ km/sec, $K_2 = 105$ km/sec, $P = 3.056$ days. A discussion by Shajn of Yerkes and Simeis observations has appeared in Russia.

α Ophiuchi.—On the assumption that the spectrum is that of a single star, a velocity of $+9 \pm 2$ km/sec is found.

V 380 Cygni.—Orbital elements in good agreement with those of an earlier orbit of Harper are obtained. The line of apsides does not appear to be rotating so rapidly as has been predicted.

V 505 Sagittarii.—Circular elements for this A-type eclipsing binary of period 1.2 days are $K = 104$ km/sec, $\gamma = -6$ km/sec.

INTRODUCTION

The Bruce spectrograph of the 40-inch refractor of the Yerkes Observatory has been used in one-prism form almost exclusively for a number of years.[1] A camera of focal length 12 inches, half that formerly employed, was designed by Henyey and Greenstein and installed during December, 1945. The resulting dispersion was 51.5 A/mm at $H\gamma$. In August, 1946, an improved prism, ground in the Yerkes optical shop by Mr. Fred Pearson, was installed. The dispersion was reduced to 63.5 A/mm at $H\gamma$. Plates with the older prism are numbered 1SR 672–1SR 762; those with the new prism, 1SR 763——. The plateholder is so designed that up to fifteen spectrograms may be exposed on a single plate. The performance of the Bruce spectrograph, even with improved optics, is not completely satisfactory. A continuous check on systematic and accidental errors was obtained through eighty spectrograms of standard-velocity stars (principally ε Ori, η Leo, ζ Cas, and 102 Her) on forty-five plates. The results of the measures of the standard-star spectrograms are shown in the accompanying tabulation. By d is designated the

Plates	1SR 672–762	1SR 763–817
Number of spectrograms	56	24
Correction	$+0.9 \pm 0.6$ km/sec	$+5.1 \pm 0.8$ km/sec
d	4 km/sec	7 km/sec

average difference between two velocities of the same standard star on the same plate. In addition to these corrections, there is some evidence, particularly for the earlier plates, that the correction varies systematically with wave length. The corrections, +1 km/sec and +5 km/sec, have been applied to all measures included in this paper.

The spectrograms discussed here were obtained in the interval January, 1946—April, 1947. Miss Anne Underhill and Messrs. John Phillips and Arne Slettebak shared the observing duties equally with the writer. To Dr. Struve I am indebted for suggesting that μ Ori and α Oph be placed on the observing program. Some results of this program are presented in the following sections.

[1] Frost, Barrett, and Struve, *Ap. J.*, **64**, 1, 1926.

MU ORIONIS[2]

By combining visual observations of the system μ Ori AB with astrometric measures of A, Alden was able to obtain a value of the mass ratio.[3] His result is that component B, which is estimated to be 2.3 mag. fainter than component A, has a mass approximately equal to that of A, an apparent contradiction of the mass-luminosity relation. In order to compute the mass ratio, however, it was necessary for Alden to obtain the semi-major axis of the relative orbit, a'', by combining with the double-star observations the orbital eccentricity, e, found spectrographically. The value of e used by Alden is 0.76; he points out that, if the true value were considerably smaller, a'' would be greater and consequently the relative mass of B would be less.

The spectrographic observations of μ Ori A have been discussed by Bourgeois.[4] Star A is a spectroscopic binary with one spectrum visible. Its orbit is circular and has a period of 4.45 days and a velocity amplitude, K_A, of 29 km/sec. The center of mass velocity, γ_A, is variable, as was first pointed out by Frost and Struve.[5] From the variation of γ_A, Bourgeois obtained the eccentricity 0.76. The period of variation found is 17.5 years, and the amplitude, K_{AB}, 14.9 km/sec. Alden notes that the value of e depends on a large value of γ_A obtained at a single epoch (1928.9) at Yerkes and that confirmation of the large eccentricity by checking this value of γ_A is much to be desired.

According to Bourgeois's orbit, during most of the cycle of 17.5 years γ_A varies gradually from +37 to +45 km/sec. In a short interval of time near periastron, however, γ_A rises rapidly to a maximum of +66 km/sec and then quickly drops again. Predicted values of γ_A according to Bourgeois's elements are given in the accompanying tabulation. Even

Date...	1944.0	1945.0	1946.0	1946.25	1946.50	1946.75	1947.0
γ_A.....	+48.4	+52.0	+59.7	+63.0	+66.4	+62.5	+50.6

the relatively low precision of the current Bruce spectrograms should suffice to check the reality of the rapid change of γ_A.

A series of thirteen plates was obtained between 1946.07 and 1946.24. Six more were obtained in the interval 1946.85–1947.25. The observations are listed in Table 1. Of the nineteen plates, fourteen contain two spectrograms each. The average velocity difference of the two spectrograms on a plate is 4.9 km/sec. All plates are given equal weight in the discussion. The stellar wave lengths adopted were compiled from the tabulations of Harper[6] and of Morgan.[7] Lines giving consistently high or low residuals were eliminated in the velocity reductions, leaving an average of ten lines per spectrogram.

In the discussion of the observations of μ Ori A, Bourgeois's values of P, K_A, e, and T were first assumed:

$$P = 4.44746 \text{ days}, \qquad e = 0,$$

$$K_A = 29.0 \text{ km/sec}, \qquad T_{\text{min vel}} = \text{JD } 2423862.224.$$

Then the thirteen earlier observations of mean epoch 1946.13 were solved for γ_A and for δT. The results are

$$\gamma_A = +49.1 \pm 0.8 \text{ km/sec}; \qquad \delta T = +0.38 \pm 0.03 \text{ days}.$$

[2] HD 40932; mag. 4.3; Sp. A2; $\alpha = 5^h56^m9$; $\delta = +9°39'$ (1900).

[3] *A.J.*, **50**, 73, 1942.

[4] *Ap. J.*, **70**, 256, 1929.

[5] *Ap. J.*, **60**, 192, 1924.

[6] *Trans. I.A.U.*, **4**, 188, 1932.

[7] *Pub. Yerkes Obs.*, Vol. **7**, Part III, 1934.

TABLE 1

RADIAL VELOCITIES OF μ ORIONIS A

Plate	U.T.	Julian Day	Phase*	Velocity (Km/Sec)	O−C
	1946	2,430,000+			
1SR 674.....	Jan. 26.224	1846.724	0P920	+41	0
676.....	27.035	1847.535	.392	+69	− 2
685.....	29.079	1849.579	.851	+31	0
690.....	Feb. 1.223	1852.723	.558	+76	− 1
693.....	2.174	1853.674	.772	+44	− 1
696.....	3.149	1854.649	.991	+16	− 5
699.....	4.018	1855.518	.186	+39	+ 1
701.....	25.071	1876.571	.920	+16	− 7
703.....	28.217	1879.717	.627	+59	−10
705.....	Mar. 1.117	1880.617	.830	+40	+ 5
708.....	3.102	1882.602	.276	+57	+ 4
717.....	27.118	1906.618	.676	+68	+ 6
720.....	28.142	1907.642	.906	+30	+ 5
797.....	Nov. 6.501	2131.001	.128	+41	+12
800.....	22.388	2146.888	.700	+69	+11
803.....	23.447	2147.947	.938	+42	+20
	1947				
815.....	Jan. 22.270	2207.770	.389	+83	+12
817.....	23.277	2208.777	.616	+91	+21
823.....	Apr. 3.078	2278.578	0.310	+75	+20

* Zero phase refers to minimum radial velocity.

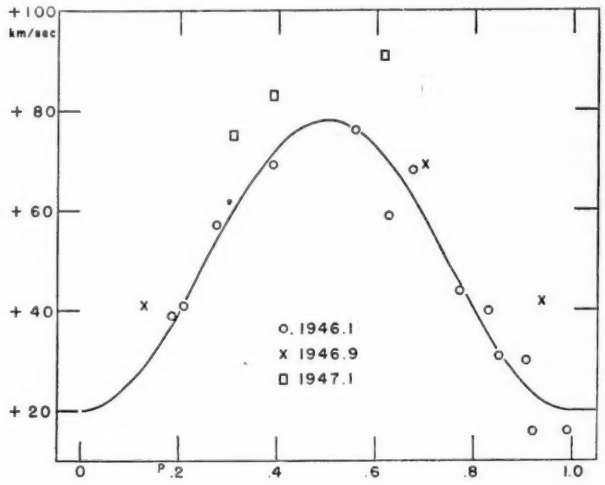

FIG. 1.—Radial velocities of μ Orionis. The curve represents the observations of epoch 1946.1

The residuals of Table 1 and the curve of Figure 1 were computed with these values of the elements. Zero phase corresponds to minimum velocity. Bourgeois found variations in $T_{\text{min vel}}$ greater than could be accounted for by light-time variations. The variation, $\delta T = 0.38$ days, found here is outside the range observed previously.

With this value of δT and with P, K, and e as adopted, the later observations were also solved for γ_A. The results are shown in the accompanying tabulation. All the observations are shown in Figure 1. The residuals within the first epoch also show a systematic increase with time.

Epoch	No. of Plates	γ_A	Epoch	No. of Plates	γ_A
1946.13.....	13	+49	1947.06.....	2	+65
1946.88.....	3	+63	1947.25.....	1	+69

The conclusion to be drawn from these results is that, although it took place about a year later than predicted, the rapid rise of γ_A to a value near +66 km/sec and hence a large eccentricity for the orbit of μ Ori AB are verified. The apparent discrepancy in the mass ratio noted by Alden remains. It should be pointed out, however, that, if star B is of spectral type M, its bolometric correction could be 2 mag. greater than that of star A, so that the bolometric luminosities of the stars could be equal.

The period of revolution of the system AB appears to be somewhat greater than that derived by Bourgeois. The observations are not numerous enough to justify a redetermination of the spectroscopic elements. The correction to the period is of the order of magnitude of +1 year.

4 SEXTANTIS[8]

G. A. Shajn discovered 4 Sex to be a double-lined spectroscopic binary,[9] the maximum separation of the component lines corresponding to a velocity difference of approximately 200 km/sec. He was unable to derive a period from twenty-three spectrograms with double lines obtained at the Simeis Observatory. The individual velocities were not published.

This star was placed on the Bruce program in January, 1946. Sixty-seven spectrograms were obtained on twenty-four nights between January 27 and April 22. Double lines are measurable on thirty-eight spectrograms.

Although the lines in the spectrum of 4 Sex are sharp, they are very numerous, so that blending is severe. In order to increase the homogeneity of the measured velocities, the positions of the lines on thirteen spectrograms with single lines were used as reference positions. The zero point of the velocities depends on the adopted wave lengths of nine of these lines. The agreement among the nine zero points corresponds to a probable error of ± 1.6 km/sec.

Inspection of the measured velocities led to the following preliminary circular elements:

$$\gamma = +17 \text{ km/sec},$$

$$K_1 = 100, \qquad P = 3.056 \text{ days},$$

$$K_2 = 105, \qquad \text{Epoch of minimum velocity of}$$

$$m_1 \sin^3 i = 1.4\odot, \qquad \text{component 1} = \text{JD } 2431847.95.$$

$$m_2 \sin^3 i = 1.3\odot,$$

[8] HD 85217; mag. 6.2; Sp. F5; $\alpha = 9^h45^m3$; $\delta = +4°49'$ (1900).

[9] *Pulkova Obs. Circ.*, **2**, 11, 1932.

Dr. Shajn visited the Yerkes Observatory in the spring of 1946. It was agreed that the Simeis and Yerkes material should be discussed together in a joint paper to be published in Russia. The discussion by Dr. Shajn has now been published.[10]

The spectral type of the mean component of 4 Sex is F6 V on the Yerkes system. Figure 2 shows two spectrograms obtained at the McDonald Observatory, one having been exposed near each nodal passage.

ALPHA OPHIUCHI[11]

The broad, diffuse lines in the spectrum of α Oph make it a difficult object for radial-velocity determination. Frost[12] and Lee[13] were of the opinion that the lines showed doubling, with velocity ranges of 200–300 km/sec. Although no orbit has ever been published for this bright star, its record in the astronomical literature[14] is that of a probable spectroscopic binary. In lines as broad and diffuse as those in this spectrum, doubling of the kind reported by the early Yerkes observers is very difficult to ascertain. The present tendency is to exclude such stars from the binary category unless the evidence is stronger than in the case of α Oph.

In order to determine whether the spectrum, considered as that of a single star, shows appreciable velocity variations, a series of twenty-seven spectrograms of α Oph was obtained on sixteen nights. The spectrograms were usually strongly exposed, so that the wings of the *H* lines would be filled in, making for easier measurement. Only the $H\delta$ and $H\gamma$ lines were measured. Using night means, the two spectrograms of a single night having been exposed in rapid succession, I find for the mean velocity

$$+9.3 \pm 1.6 \text{ km/sec} .$$

The probable error of a single velocity is ± 6.2 km/sec. This corresponds to about 2 μ on the plate, which is satisfactory, considering the small number and poor quality of the lines. Hence, from the evidence presented here, the velocity of the star may be considered constant. The mean value adopted in the *General Catalogue*[14] is $+15 \pm 2$. Because precise velocities are difficult to obtain for α Oph, it is not a promising object in which to look for radial-velocity variations correlated with reported motion in an astrometric orbit.[15]

V 380 CYGNI[16]

V 380 Cyg has been included in discussions[17, 18] of the distribution of matter in stellar interiors as one of the systems for which apsidal rotation has been established. The evidence in favor of apsidal rotation, first noted by Luyten,[19] is the change in phase at which secondary eclipse occurs, as shown by the Madison photoelectric observations.[20, 21] The

[10] D. Popper and G. Shajn, *Pub. Crimean Ap. Obs.*, Vol. **2**. A brief communication from Dr. Shajn to Dr. Struve tells of the publication of this paper and also mentions a systematic run in the velocity residuals. Although I am listed as co-author of the paper, owing to difficulties in communication I have taken no part in its preparation, except by making available to Dr. Shajn the results of my measurements. The present account is given here because it contains additional information concerning the Yerkes observations not in Dr. Shajn's possession and because it appears desirable to announce the approximate elements of the system.

[11] HD 159561; mag. 2.1; Sp. A5; $\alpha = 17^h30^m3$; $\delta = +12°38'$ (1900).

[12] *A.N.*, **177**, 174, 1908.

[13] *Ap. J.*, **39**, 47, 1914.

[14] *A General Catalogue of Radial Velocities* (*Pub. Lick Obs.*, Vol. **18**, 1932).

[15] N. E. Wagman, *A.J.*, **52**, 50, 1946; **53**, 137, 1948.

[16] HD 187879; mag. 5.6; Sp. B2; $\alpha = 19^h47^m2$; $\delta = +40°20'$ (1900).

[17] H. N. Russell, *Ap. J.*, **90**, 650, 1939.

[18] Z. Kopal, *Harvard Circ.*, No. 443, 1940.

[19] *B.A.N.*, **8**, 271, 1938.

[20] G. E. Kron, *Ap. J.*, **82**, 225, 1935.

[21] Z. Kopal, *Harvard Circ.*, No. 441, 1940.

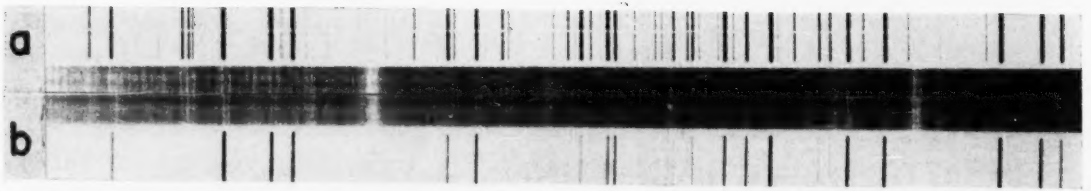

FIG. 2.—McDonald spectrograms of 4 Sextantis near nodal passages. *a*, JD 2432304.74, 0.542 phase; *b*, JD 2432309.61, 0.136 phase. These phases are based on Shajn's improved period of 3.05459 days. Zero phase is the time of minimum velocity of component 1.

change amounts to 0.1 day in the interval 1924–1928. The orbital period is 12.4 days. The rate of change is subject to an uncertainty amounting to a large fraction of its value and is in need of verification.

Spectrographic orbits of V 380 Cyg (B 5070) have been published by Harper. The individual observations have not appeared. For our discussion, the important elements are e, the orbital eccentricity, and ω, the angle between ascending node and periastron. Harper's first orbit[22] gave

$$e = 0.20\,, \qquad \omega = 120°.$$

The second,[23] which used the same twenty-one observations as the first and included eight later ones, gave

$$e = 0.22\,, \qquad \omega = 116°.$$

The mean epochs are about 1920.6 for the first set and 1932.9 for the added observations. If the rate of apsidal rotation is as given by Luyten and by Kopal, ω should have increased about 18° between 1926 and 1946. With an eccentricity as large as 0.2, this change should be detectable with observations of the accuracy of those used here. Photometric observations should give a more accurate result but do not appear to have been made.

Twenty-three plates of V 380 Cyg were obtained with the Bruce spectrograph at a mean epoch of 1946.8. Of these, twenty contain two spectrograms per plate. The mean difference of velocity of the two spectrograms per plate is 3.3 km/sec. The lines in the spectrum of V 380 Cyg are relatively sharp, though only those of *H* and *He* could be measured. The results of the measures are contained in Table 2. A least-squares solution for the orbital elements was carried out with the accompanying results; those of Harper's second solution are tabulated for comparison:

	Yerkes	Victoria
P	12.426 days (assumed)	
γ	-4 ± 3 km/sec	-4 km/sec
K	94 ± 2 km/sec	94 km/sec
e	0.21 ± 0.02	0.22
ω	$118°\pm6°$	116°
T	JD 2432161.47 ± 0.22	
$f(m)$	$1.01\odot$	

Residuals from the Yerkes orbit are also given in Table 2. The phases are fractions of the period computed from periastron passage.

The two sets of spectroscopic elements are in excellent agreement. It appears that the line of apsides of the orbit of V 380 Cyg cannot be advancing at the rate assumed by Russell and by Kopal. Whether there is any advance or not remains to be settled by future observations, preferably of the phase of secondary minimum.

Kron's epoch of primary minimum is

$$\mathrm{JD}_{\min} = 2423587.145\,.$$

His period, based on a 7-year interval, is 12.4262 days. Harper's, based on a 12-year interval, is 12.4255 days. These periods, combined with Kron's epoch, predict minima at

[22] *Pub. A.A.S.*, **4**, 219, 1920.

[23] *Pub. Dom. Ap. Obs., Victoria*, **6**, 244, 1935.

JD 2432161.22 and 2432160.74, respectively, whereas my spectroscopic elements predict a minimum at 60.85 ± 0.3 days. A period of 12.4257 days is indicated, although an uncertainty of a few units in the last place remains.

The spectrum of this star has been classified on the Yerkes program of spectroscopic parallaxes. The result, kindly made available to me by Dr. Morgan, is

$$\text{Sp.} = \text{B1} \; ; \qquad M_{pv} = -3.6 \; .$$

That the luminosity of V 380 Cyg is in no way exceptional for a B1 star has been pointed out previously. The large masses and luminosities adopted by Kopal in his discussion of the system[21] appear open to question.

TABLE 2

RADIAL VELOCITIES OF V 380 CYGNI

Plate	U.T.	Julian Day	Phase*	Velocity (Km/Sec)	O−C
	1946	2,430,000+			
1SR 752	June 19.276	1990.776	0P2633	−78	−11
753	July 11.407	2012.907	.0442	−88	0
755	12.328	13.828	.1184	−118	−10
758	13.285	14.785	.1954	− 99	− 6
765	Aug. 7.183	39.683	.1991	− 90	+ 2
769	10.322	42.822	.4517	+ 4	− 8
770	12.145	44.645	.5984	+ 58	− 2
773	16.150	48.650	.9207	+ 9	− 3
776	19.131	51.631	.1606	− 87	+16
784	26.099	58.599	.7213	+ 89	+ 9
786	Sept. 30.132	93.632	.5406	+ 34	−10
787	Oct. 1.123	94.623	.6204	+ 67	+ 2
789	12.117	2105.617	.5051	+ 32	0
790	13.126	06.626	.5863	+ 55	− 2
792	27.084	20.584	.7096	+ 76	− 4
796	Nov. 6.081	30.581	.5141	+ 44	+ 9
802	23.117	47.617	.8851	+ 42	+ 4
805	Dec. 6.047	60.547	.9256	+ 3	− 5
806	7.009	61.509	.0030	− 56	+ 4
809	23.002	77.502	.2901	− 48	+ 7
	1947				
820	Mar. 19.467	2263.967	.2483	− 81	− 8
822	20.463	64.963	.3285	− 25	+13
825	Apr. 3.452	78.952	0.4543	+ 20	+ 7

* Zero phase refers to periastron passage.

V 505 SAGITTARII[24]

V 505 Sgr is one of the few eclipsing binaries within reach of the Bruce spectrograph for which no spectrographic orbit has been published. The light-curve has been analyzed by Slonim,[25] who finds the hotter component to possess 0.95 of the total luminosity of the system. The depth of the primary minimum is 0.8 mag., the eclipse being partial.

Sixteen spectrograms have been obtained. The spectral type is A1 V. The only lines which could be measured reliably were K, $H\delta$, $H\gamma$, and *Mg* II 4481. The measured velocities, together with the residuals from the orbital elements given below, are contained in

[24] HD 187949; mag. 6.4; Sp. A2; $\alpha = 19^h47^m5$; $\delta = -14°51'$ (1900).

[25] *A.N.*, **253**, 367, 1934.

Table 3. The phases were computed from the elements listed in the 1940 issue of Schneller's *Katalog und Ephemeriden:*

$$JD_{min} = 2425501.376 + 1.1828711E .$$

With the assumptions that these light-elements are valid and that the orbit is circular, the observations yield

$$\gamma = -2 \pm 2 \text{ km/sec}, \qquad K = 104 \pm 2 \text{km/sec} .$$

The measures and computed orbit are shown in Figure 3. The assumptions employed appear to be justified.

TABLE 3

RADIAL VELOCITIES OF V 505 SAGITTARII

Plate	U.T.	Julian Day (Helioc.)	Phase*	Velocity (Km/Sec)	O−C
	1946	2,432,000+			
1SR 753.....	July 11.351	012.856	0P809	+ 94	− 2
755.....	12.281	013.786	.596	+ 42	−16
757.....	13.204	014.710	.377	− 74	0
759.....	14.275	015.780	.281	−104	− 1
767.....	Aug. 9.190	041.695	.190	− 96	+ 2
770.....	12.174	044.679	.713	+ 92	− 7
776.....	19.175	051.680	.631	+ 74	0
784.....	26.135	058.640	.515	+ 26	+18
786.....	Sept. 30.094	093.596	.067	− 37	+ 7
787.....	Oct. 1.053	094.555	.878	+ 47	−23
789.....	12.072	105.573	.192	− 91	+ 8
790.....	13.085	106.586	.049	− 38	− 5
792.....	27.023	120.522	.830	+ 84	− 5
792.....	27.048	120.547	.851	+ 98	+16
796.....	Nov. 6.001	130.499	.265	−118	−13
802.....	23.010	147.507	0.643	+101	+21

* Zero phase refers to primary minimum.

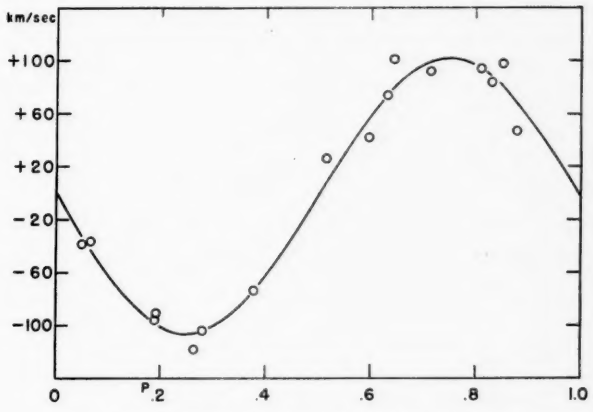

FIG. 3.—Radial velocities of V505 Sagittarii

From the elements of the spectroscopic orbit we obtain

$$a_1 \sin i = 1.69 \times 10^6 \text{ km} = 2.43 \text{ solar radii}, \qquad f(m) = 0.137 \odot .$$

According to Slonim's analysis of the light-curve, i is 82°.5, which gives us

$$a_1 = 2.46 \text{ solar radii}; \qquad \frac{m_2^3}{(m_1 + m_2)^2} = 0.141 \odot .$$

IDENTIFICATION OF A MOLECULAR BAND AT λ 3682 IN THE SPECTRA OF LATE-TYPE STARS*

GEORGE H. HERBIG†

Received August 18, 1948

ABSTRACT

A molecular band with head at λ 3682, discovered by Merrill in R Andromedae (Se), occurs also in a number of M-type stars. The band has been observed by Miss F. Lowater in an arc containing zirconium oxide. It was found independently by the writer on a spectrogram, taken by R. B. King, of the zirconium arc in air. The electronic transition involved has been identified, from the rotational structure of the band, as $^1\Sigma - {}^1\Sigma$. Both this fact and the observed enhancement of λ 3682 in S-type stars are in agreement with a *ZrO* identification. If this is correct, the band is probably the (0, 0) head of a new system. The identity of the ground term of the *ZrO* molecule accordingly becomes uncertain.

The first published mention of a well-marked molecular band with head near λ 3682 in the spectra of S- and late M-type stars was made by P. W. Merrill in his description of the spectrum of R Andromedae.[1] He later published measurements of the wave length of the head and about thirty band lines.[2] The band was observed also by A. H. Joy in the course of his investigation of the absorption features in and near the *H* 17 (λ 3697) and *H* 18 (λ 3691) emission lines in *o* Ceti.[3] The λ 3682 band is degraded longward and, in R Andromedae, can be traced to about λ 3710. The wave lengths measured by Merrill and by Joy are given in Table 4.

The stellar spectrograms employed in the present study were obtained by Drs. Adams, Joy, and Merrill with the plane-grating spectrograph at the coudé focus of the 100-inch telescope. For all the variable stars the dispersion was 10 A/mm in the photographic region and the ultraviolet, 20 A/mm in the visual region. For *o* Ceti several spectrograms of dispersion 2.9 and 5.8 A/mm in those spectral regions were also available. The spectrograms of β Pegasi and α Herculis were entirely of the higher dispersions.

Table 1 summarizes the observations of the band at λ 3682 and of a weak feature near λ 3571 on coudé plates of nine long-period variables and two bright M giants. The eye estimates of band strengths given in Table 1 specify only the amount of the discontinuity in the continuous spectrum on either side of the position of the band head and do not include any estimate of the intensity of the resolved line structure.

For most of the long-period variables in Table 1, only a few coudé plates are sufficiently exposed in the λ 3682 region. For *o* Ceti, however, there are eighteen good spectrograms taken in 1945–1948 during four successive cycles. In *o* Ceti the λ 3682 band clearly behaves as do the *TiO* bands with respect to the brightness of the variable at any particular maximum. On plates exposed throughout the two cycles which included low maximum magnitudes (January, 1946, 4.1 mag.; and December, 1946, 4.3 mag.), the estimates of the intensity of λ 3682 ranged from medium through strong, while on plates taken through the two cycles having high maxima (January, 1945, 2.9 mag.; and October, 1947, 3.1 mag.), the estimates ranged from weak to medium.[4] The possibility of

* *Contributions from the Mount Wilson Observatory, Carnegie Institution of Washington*, No. 754.

† Fellow of the National Research Council.

[1] *Mt. W. Contr.*, No. 730; *Ap. J.*, **105**, 360, 1947.

[2] *Mt. W. Contr.*, No. 743; *Ap. J.*, **107**, 303, 1948.

[3] *Mt. W. Contr.*, No. 737; *Ap. J.*, **106**, 288, 1947.

[4] I am indebted to Mr. Leon Campbell, of the Harvard College Observatory, for these maximum magnitudes.

similar fluctuations in the band strength for the other variable stars must be kept in mind when drawing any conclusions from Table 1. There is no conspicuous tendency for the strength of λ 3682 to vary with the phase in *o* Ceti.

Miss F. Lowater, in the course of her vibrational analysis of the α, β, and γ systems of *ZrO*,[5] stated:

> In the ultraviolet region there is a system differing in general appearance from α, β, γ for the bands are much weaker and the triplets not easily recognizable. Comparison of these less conspicuous bands with those of titanium oxide and of hafnium oxide measured by Meggers and by King shows that they are not due to these oxides, which might be present as impurities.

That the λ 3682 band cannot be due to *YO* is demonstrated by its absence on plates of the yttrium arc in air, kindly loaned by Dr. R. B. King, and by the fact that evidence

TABLE 1

ESTIMATED INTENSITIES OF BAND HEADS AT λ 3682 AND λ 3571 IN M- AND S-TYPE STARS

STAR	TYPE	ESTIMATED STRENGTH	
		λ 3682	λ 3571
β Peg	M2	Absent	.....
α Her	M5	Weak	.....
R Hya	M6e	Weak	Invisible
o Cet	M6e	Variable*	Weak
R Cas	M7e	Medium	.....
R Ser	M7e	Medium?	.....
R Aql	M7e	Very weak	Very weak
U Ori	M8e	Very weak	.....
R Leo	M8e	Very weak	Very weak
χ Cyg	M6e, Se	Very strong	Medium
R And	Se	Strong	Weak

* See text.

to be presented below indicates that the band arises from a transition involving singlet electronic terms rather than the even multiplicities to be expected of *YO*.

The wave lengths of the ultraviolet bands measured by Miss Lowater are given in Table 2, together with the arc intensities as listed in the *M.I.T. Wave Length Tables*.

The source employed by Miss Lowater for the production of these bands was an iron or copper arc in air, on one pole of which was placed chemically pure ZrO_2.

The λ 3682 band was found by the writer, quite independently, on a first-order grating spectrogram of dispersion 3.7 A/mm, taken by Dr. R. B. King. The source was the envelope of a carbon arc in air, one pole of which was charged with metallic zirconium. In this source the λ 3682 band was much weaker than the familiar *ZrO* bands in the blue, being comparable in intensity with the R_b head of the (2, 0) band of the α system at λ 4313. Nevertheless, the rotational structure was clearly resolved. The band lines have been measured out to the point where they become confused with lines of the *CN* $\Delta v = 0$ sequence (λ 3883, λ 3871, etc.). The wave length of the band head was measured as λ 3682.19.

The laboratory wave lengths of the band lines are given in Table 3; they were obtained by the use of the M.I.T. wave lengths of *Fe* and *Zr* lines appearing on the spectrogram.

[5] *Proc. Phys. Soc.*, **44**, 51, 1932.

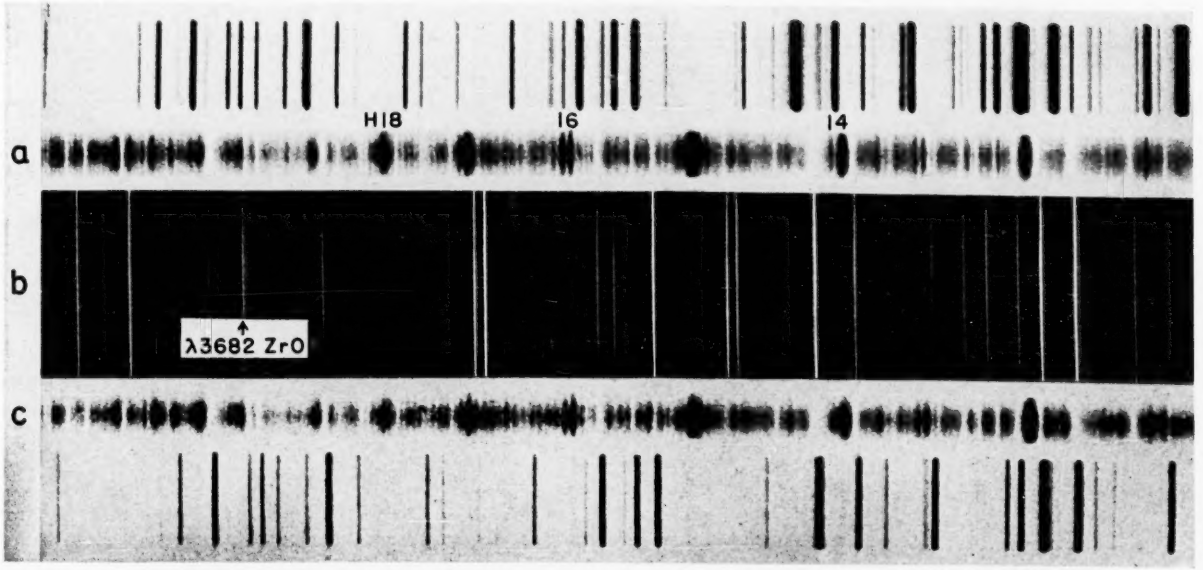

FIG. 1.—The λ 3682 band in: (*a*) *o* Ceti, plate Ce 4576, 1947 February 5; (*b*) laboratory spectrogram of the zirconium arc in air; (*c*) χ Cygni, plate Ce 3762, 1945 April 28.

All the approximately 130 lines can be arranged in two branches. The head-forming branch is, of course, an *R*, while the other is probably a *P* branch, since if it were a *Q*, the intensity would be greater than that of the *R* (assuming singlet states), which is not observed to be the case. Furthermore, the absence of a *P* branch would have to be explained. The presence of a single *R* and a single *P* branch characterizes a $^1\Sigma - {}^1\Sigma$ transition. Although only transitions involving triplet electronic terms have thus far been identified in the spectrum of *ZrO*, $^1\Sigma$ terms are among those in the term manifold which arises from a combination of unexcited *Zr* and *O* atoms. Accordingly, there is no obvious theoretical or experimental evidence in conflict with the assignment of the λ 3682 band to *ZrO*. The absence of any vibrational isotope effect, as well as the absence of near-by bands of comparable or greater strength, suggests that we are dealing with the (0, 0) band of a new system. If this is the case, the interesting question arises: Since both systems are found in absorption in late-type stars, is the $^1\Sigma$ or the $x^3\Pi$ term (the latter being the lower term of the α, β, and γ systems) the ground term of *ZrO*? None of the other bands listed in Table 2 are well enough seen on the laboratory spectrogram to permit detailed examination.

TABLE 2

BAND HEADS IN THE ULTRAVIOLET, MEASURED BY MISS LOWATER

λ	*I*(Arc)	λ	*I*(Arc)	λ	*I*(Arc)	λ	*I*(Arc)
3472.43.....	20	3506.22.....	20	3515.79.....	2	3598.92.....	2
3491.84.....	20	3508.24.....	20	3589.81.....	5	3682.43.....	30
3491.97.....	30	3511.93.....	2	3593.07.....	2	3726.31.....	5

The close agreement of the laboratory wave lengths of the stronger band features with those measured by Merrill and Joy in R Andromedae and *o* Ceti (reproduced in Table 4; see also Fig. 1) leaves no reasonable doubt regarding the identification of the stellar feature with the band observed in the *Zr* arc. The enhancement of λ 3682 in stars with S-type characteristics (see Table 1) is in harmony with the *ZrO* identification.

Bands of *ZrO* are found in the spectra of ordinary M-type stars which are not considered to show any general inclination toward S-type characteristics: β Pegasi (M2), α Herculis (M5), and *o* Ceti (M6–M8). In the last two stars, where the blue-green system of *TiO* is very strong, the *ZrO* α (blue) system is not present. It is likely that this is due to a considerable extent to the heavy opacity in that region contributed by *TiO*, since the persistence of λ 3682 in the last two stars demonstrates that *ZrO* actually is present. In β Pegasi, the *TiO* bands are by no means so heavy, and the strongest *ZrO* heads are visible.[6] The red (γ) system of *ZrO* appears in moderate strength in all three stars.

The open structure of λ 3682 should make the band a promising means of temperature determination when a rotational analysis becomes available.

Two broad unidentified absorption features are present in the ultraviolet region of the spectra of *o* Ceti, R Andromedae, and several other long-period variables. The first of these was measured by Merrill[2] in R Andromedae. It is a wide, shallow absorption band which causes a minimum in the continuous spectrum near λ 3578, although there is a feature resembling a head at λ 3571. Feeble absorption may extend to about λ 3565. The absorption can be traced longward as far as λ 3595. It resembles a weak molecular band, perhaps with a multiple head, degraded longward. A possible identification is with

[6] D. N. Davis, *Mt. W. Contr.*, No. 733; *Ap. J.*, **106**, 28, 1947.

TABLE 3

WAVE LENGTHS OF LINES IN λ 3682 BAND

R BRANCH		*P* BRANCH	
λ	Intensity	λ	Intensity
3682.877	3	3686.198	1
82.989	4	86.443	1
83.108	4	86.707	2
83.231	3	86.964:	2
83.357	4	87.251	2
83.491	3	(87.53)*	———
83.644	3	87.820	2
83.815	3	88.129	2
83.968	3	88.427	2
84.158	3	88.755	2
84.340	3	89.079	2
84.515	3	89.399	2
84.712	3	89.741	2
84.924	4	90.098	2
85.148:	3	90.456	2
85.356	3	90.821	2
85.580	3	91.189	2
85.840	4	91.550	2
86.067	3	91.952	2
86.324	3	92.339	2
86.585	4	92.752	2
86.823	3	93.151	2
87.124	4	93.568	2
(87.41)*	———	94.014	2
87.701	4	94.439	2
87.992	3	94.889	2
88.301	3	95.332	2
88.617	3	95.786	3
88.937	3	96.255	3
89.272	3	96.743	3
89.622	3	97.186 B	4
89.950	3	97.692 b	3:
90.318	3	(98.20)*	———
90.694	3	98.701 b	3
91.059	3	99.173 B	3
91.435	3	99.713 B	3
91.826	3	3700.223 B	5
92.228	3	00.774 B	4
92.633	3	01.340 B	4
93.039	3	01.894 B	4
93.467	3	02.456 B	4
93.880	3	03.026 B	6
94.334	3	03.614 B nv	6
94.792	3	04.213 B nv	5
95.243	3	04.824 B nv	5
95.697	3	05.430 B nv	6:
96.158	3	06.037 B nv	5
96.646	3	(06.65)*	———
97.186 B	4	07.288 B nv	4
97.617 b	3:	07.902 B nv	4
(98.12)*	———	08.576 B nv	3
98.615 b	3	(09.23)*	———
99.173 B	3	09.879 B nnv	3
99.713 B	3	10.530 B nn	2
3700.223 B	5	11.219 B nn	3

TABLE 3—*Continued*

R Branch		*P* Branch	
λ	Intensity	λ	Intensity
3700.774 B	4	3711.915 b	3
01.340 B	4	12.588 B nn	2
01.894 B	4	13.325 b	2
02.456 B	4	(14.03)*	——
03.026 B	6	(14.74)*	——
03.614 B nv	6	15.447 n	1
04.213 B nv	5	16.192 b	1
04.824 B nv	5	16.914 n	2
05.430 B nv	6:	17.684	2
06.037 B nv	5	18.470	4
(06.65)*	——	19.236	2
07.288 B nv	4	(20.00)*	——
07.902 B nv	4	20.777	2
08.576 B nv	3	21.581	1
(09.23)*	——	22.382	2
09.879 B nnv	3	23.204	2
10.530 B nn	2	24.008	1
11.219 B nn	3	24.812	1
12.015 b	2	25.680	1
12.588 B nn	2	26.532	1:
13.433 b	1		
(14.16)*	——		
(14.90)*	——		
15.641	0.5		
16.415	0.5		
17.152	1		
17.908	1		
18.730	0.5		
19.497	1		
(20.31)*	——		
21.109	0.3		
21.909	0.5		
(22.73)†	——		
23.562	0.3		

NOTES TO TABLE 3

Symbols used in Table 3:

( ) * Predicted wave length; molecular line masked by atomic line.

( ) † Predicted wave length; actual line not seen.

B Unresolved blend of two band lines.

b Blended with another line but measurable separately.

n Diffuse.

nn Very diffuse.

nv Diffuse on shortward side.

TABLE 4

COMPARISON OF STELLAR AND LABORATORY WAVE LENGTHS OF LINES IN λ 3682 BAND

R And (Merrill)		o Cet (Joy)		Laboratory	
λ	*I*	λ	*I*	λ	*I*
3690.31 (+*V* 3690.28)	1			3690.318	3
				90.456?	2
90.75	0.5	3690.762 (+*Fe* 3690.730)	1	90.694	3
				90.821	2
91.12	0.5	91.136	1	91.059	3
				91.189	2
91.53	0.5	91.509	1	91.435	3
				91.550	2
91.91	0	91.888	1	91.826	3
				91.952	2
92.27 (+*V* 3692.22)	1.5	92.263 (+*V* 3692.225)	3	92.228	3
				92.339	2
92.68	1			92.633	3
				92.752	2
93.09	0			93.039	3
				93.151	2
93.52	0.5			93.467	3
				93.568	2
93.94 (+*Ni* 3693.93 *Sm* II 3693.99)	1.5			93.880	3
				94.014	2
94.30	1			94.334	3
				94.439	2
94.86	0.7			94.792	3
				94.889	2
95.29	0.6			95.243	3
				95.332	2
95.86 (+*V* 3695.86)	1.6			95.697	3
				95.786	3
96.24	0			96.158	3
				96.255	3
96.68	0.5	96.685	1	96.646	3
				96.743	3
97.19	0	97.172	1	97.186	4
97.73 (+*Gd* II 3697.73)	2.5	97.657	2	97.617	3:
				97.692	3:
98.18	0			(98.12)	—
				(98.20)	—
98.70	0.5			98.615	3
				98.701	3
99.18	0.5			99.173	3
99.68	0.7			99.713	3
3700.22	0.6			3700.223	5
00.87	0			00.774	4
01.44	0			01.340	4
01.91	0.5			01.894	4
02.34	2			02.456	4
02.99	1			03.026	6
03.57 (+*V* 3703.58)	2			03.614	6
04.19	1.5			04.213	5

the (0, 0) band of OH^+.[7] In the spectra of R Andromedae, R Leonis, and *o* Ceti a broad, weak absorption sets in rather abruptly at about λ 3525 and shades shortward with some indication of a weaker head at about λ 3515.

I wish to express my appreciation to the National Research Council for their grant of a Fellowship for 1948–1949; to Dr. A. H. Joy and Dr. P. W. Merrill for helpful discussions and the opportunity to use their coudé spectrograms; and to Dr. R. B. King for the loan of several of his laboratory spectrograms.

[7] F. W. Loomis and W. H. Brandt, *Phys. Rev.*, **49**, 55, 1936.

SPECTROGRAPHIC OBSERVATIONS OF THE ECLIPSING VARIABLE RS SAGITTARII

JORGE SAHADE
Observatorio Astronómico de Córdoba, Argentina
Received October 22, 1948

ABSTRACT

Spectrograms of RS Sagittarii at maximum light show a spectrum of B5 type. Around principal mid-eclipse this spectrum is blended with one of a type not later than A2. The orbital elements are: $K = 85.1$ km/sec; $\omega = +41°$; $e = 0.09$; T = phase 2.09 days; $\gamma = +6.0$ km/sec; $a \sin i = 2.8 \times 10^6$ km; $f(m) = 0.15\odot$. The eccentricity agrees with the one from Roberts' photometric observations, but there is a discrepancy in the value of ω.

In April, 1946, an investigation of the spectra of southern eclipsing variables was started at the Córdoba Observatory with the 60-inch reflecting telescope. The spectrograph attached at the Cassegrain focus (31.5 meters of equivalent focal length) is a Wood-grating one of a novel design by Gaviola,[1] built at the observatory shops. It allows a dispersion of about 40 A/mm in the first order. At present, it is the only spectrograph that we have at our disposal.

The writer's observing program includes primarily stars south of declination $-30°$; in some special cases stars located north of declination $-30°$ are also included. This paper is the first one in a series to present the results being obtained.

PREVIOUS DATA ON RS SAGITTARII

The star RS Sagittarii[2] was suspected by Gould[3] to be a variable, and the variability was confirmed by Roberts,[4] who concluded, from his eye estimates, that the system is of the Algol type and is formed by "two stars almost exactly equal in size, but one of which is at least twice brighter than the other," and, furthermore, that "the orbit is eccentric, the amount of the eccentricity being 0.245."[5] In his classical paper on orbits of eclipsing binaries, Shapley[6] rediscusses Roberts' observations and is led to a different value of the eccentricity, namely, $e = 0.091$, and to $\omega = 261°$. Shapley's darkened solution indicates that "both eclipses must be considered partial" and that "the duration of the primary is 6^h44^m and of the secondary is 5^h31^m." He remarked that "there seems to be no evidence of ellipticity or reflection in the maximum light observations, but further photometric work is needed to decide the matter definitely."

Dugan and Wright[7] included RS Sgr in their investigation on "certain eclipsing binaries for variation of period," and the conclusion was that "there seems to be a variation, though its course is not at all sure." They added that "an accurate light curve and a complete velocity curve are much to be desired."

[1] *Rev. d'opt.*, **27**, 178, 1948; *Rev. Astr.*, **14**, 231, 1942.

[2] $\alpha = 18^h14^m3$; $\delta = -34°8'$ (1950.0). CD−34°12673 (7.4 mag.) = CPD−34°7719 (7.0 mag.) = L. 7646 = Ch. 6546 = HD 167647 (Sp. B5).

[3] *Uranometria argentina*, p. 288, 1879.

[4] *A.J.*, **15**, 101, 1895.

[5] *A.J.*, **16**, 97, 1896.

[6] *Contr. Princeton U. Obs.*, No. 3, 1915.

[7] *Contr. Princeton U. Obs.*, No. 19, 1939.

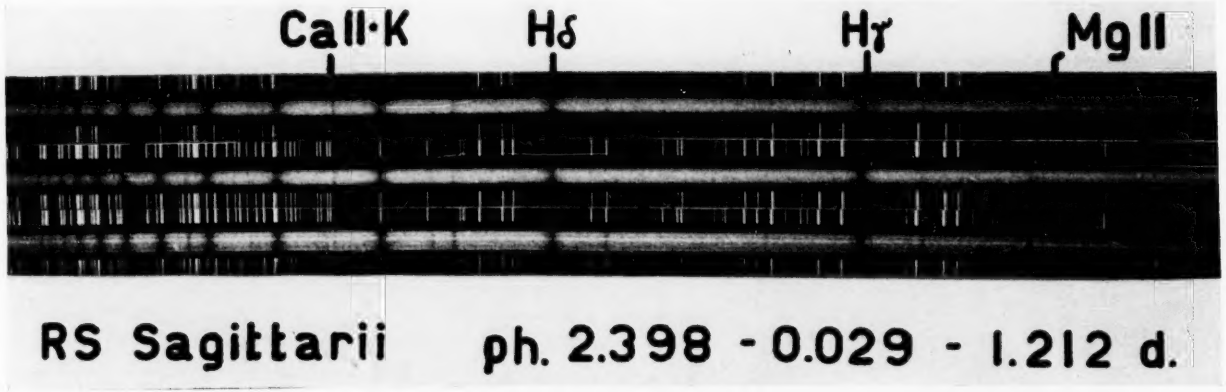

FIG. 1.—Positive enlargements of RS Sagittarii

The last photometric study of this star belongs to Redman,[8] whose photographic light-curve by the Fabry method gives

$$M = 6.0 \text{ mag.}, \qquad A_1 = 0.97 \text{ mag.}, \qquad A_2 = 0.22 \text{ mag.}$$

Redman's published light-curve shows a certain amount of ellipticity and again a duration of principal eclipse longer than that of the secondary. The secondary minimum falls a little before half a period.

Spectrographic observations for radial velocity have been previously made at the former Lick Observatory station in Santiago, Chile, by G. F. Paddock and R. E. Wilson;[9] and, although a complete velocity-curve was not determined, the conclusion was that "the eccentricity and the velocity of the system with respect to the Sun are approximately zero and the amplitude about 150 km."[10] The fourteen radial velocities obtained at Santiago[11] have been recently discussed by Colacevich,[12] who, assuming Roberts' values for the epoch of the principal minimum and the period and Shapley's values for e and ω, obtained

$K = 70$ km/sec, $\qquad a_1 \sin i = 2.32 \times 10^6$ km,
$\gamma = +14$ km/sec, $\qquad f(m) = 0.085\ \odot$.
$T =$ Phase 1.135 days,

THE OBSERVATIONS AT BOSQUE ALEGRE

The spectrograms secured at Bosque Alegre are forty-nine in number. Forty-four of them were taken during the months of May, June, July, and August, 1946, either on Eastman 103-O or 103-F emulsion.[13] The rest of the material was obtained on Eastman 103*a*-O emulsion, one plate in October, 1946, and four in June, 1948. The equivalent slit-width for the 1946 spectrograms was 1.5 A, the one for the 1948 spectrograms 1.2 A. The exposure times are indicated for each plate in Table 2, which lists the radial velocities. The phases have been computed from the light-elements suggested by Dugan and Wright,[7] namely,

$$\text{Princ. Min.} = \text{JD } 2423477.968 + 2^d.41568\, E\,.$$

THE SPECTRUM

At maximum light, the spectrum of RS Sagittarii (Fig. 1) is of type B5, with a weak and sharp *Ca* II K line of interstellar origin. Around central phase of principal eclipse, the *He* I lines weaken, and *Ca* II K and *Mg* II 4481 strengthen, the latter becoming at least as strong as *He* I 4471. *He* I is present on all our spectrograms, suggesting a partial eclipse, in agreement with the photometric data. The strength of *Ca* II K relative to *Ca* II H + *He* ϵ around mid-eclipse indicates that the type of the spectrum blended with the one from the B5 star is not later than A2. Except at principal minimum, our spectrograms do not show noticeable changes with phase or with cycle.

THE RADIAL VELOCITIES

The radial velocities have been derived by measuring the lines of *H*, *He* I, *Mg* II, and *Ca* II, in the wave-length interval λλ 3788–4495, which are listed in Table 1. It has been possible to measure *Mg* II 4481 only on a very few spectrograms.

[8] *M.N.*, **105**, 219, 1945.
[9] G. F. Paddock, *Lick Obs. Bull.*, **9**, 39, 1916.
[10] *Ibid.*, p. 71, 1917.
[11] *Pub. Lick Obs.*, **16**, 265, 1928.
[12] *Mem. della Soc. astr. italiana*, Vol. XIII, No. 3, 1940.
[13] The plates were very old, and therefore the background was rather heavy. Because of wartime conditions, we had not been able to receive fresh plates during several years, until October, 1946.

The radial velocities from *Ca* II K are indicated in Table 2 and are shown in Figure 2. They suggest that the line is not purely interstellar but slightly blended with the stellar line.

As for the other elements, since the radial velocities derived from them follow the same trend, their mean value for each plate has been considered for deriving the orbital elements. These mean values are also listed in Table 2 and shown in Figure 3.

The orbital elements have been determined from a least-squares solution by applying the method of Schlesinger with the modification by Sterne;[14] they are shown in Table 3, together with their mean errors, and the corresponding velocity-curve is drawn in Figure 3. For the least-squares solution the individual values were grouped in ten normal

TABLE 1

WAVE LENGTHS USED IN THE DETERMINATION OF THE RADIAL VELOCITIES OF RS SAGITTARII

H	*He* I	*Ca* II	*Mg* II
3797.90	3819.64	3933.67	4481.23
3835.39	4009.27		
4101.74	4026.22		
4340.47	4143.76		
	4387.93		
	4471.51		

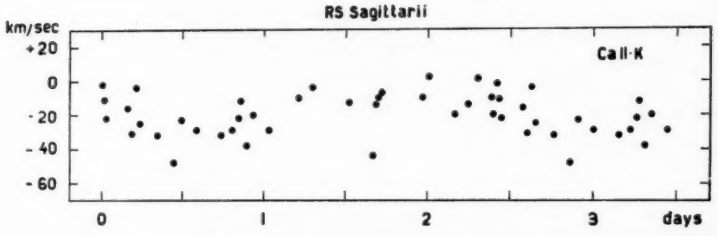

FIG. 2.—Radial velocities from *Ca* II K

places, and each one was given a weight equal to the square root of the number of individual values considered. The preliminary elements were derived by following the Wilsing-Russell method. In our determination of the orbital elements we have disregarded the radial velocity from plate I-171, at phase 2.396 days, which gives +52 km/sec. This spectrogram is rather underexposed and only three *H* lines are measurable; nevertheless, the individual values for the lines are very consistent and have practically repeated themselves in two measures.

The orbital eccentricity obtained from the present spectrographic study agrees with the one derived by Shapley from Roberts' photometric observations. Our value of ω, however, is quite different from the one indicated by the photometry of the system. The inspection of our spectrograms and the distribution of the individual radial velocities according to phase do not show any peculiarity which could account for the discrepancy, and therefore we are unable to explain it. Perhaps spectrograms of much better quality than those on which we have based this work would clarify the question, and, with this purpose in mind, a new set of plates will be obtained next year in Bosque Alegre.

[14] *Proc. Nat. Acad. Sci.*, **27**, 175, 1941.

TABLE 2

RADIAL VELOCITIES

PLATE	DATE	U.T.	EMULSION	EXPOSURE TIME (MINUTES)	PHASE (DAYS)	RADIAL VELOCITIES (KM/SEC)	
						Ca II K	All Lines except *Ca* II K*
I 170	1948 June 25	1:50	103*a*-O	11	2.385	−10	+ 4
S 208	1946 June 19	7:22	103-O	48	2.398	−20	0
I 173	1948 June 25	2:38	103*a*-O	11	0.003	− 2	+ 6
174	June 25	2:55	103*a*-O	14	0.015	+11	+ 4
S 209	1946 June 19	8:29	103-O	72	0.029	−22	− 17
123	May 14	5:20	103-O	30	0.133	.....	− 36
124	May 14	5:58	103-O	30	0.160	−16	− 45
125	May 14	6:38	103-O	25	0.187	−31	− 43
126	May 14	7:14	103-O	31	0.212	− 4	− 53
127	May 14	7:50	103-O	22	0.237	−25	− 37
128	May 14	8:19	103-O	22	0.258	.....	− 35
129	May 14	8:46	103-O	18	0.276	.....	− 51
130	May 14	9:12	103-O	14	0.294	.....	− 44
334	Oct. 16	0:57	103*a*-O	16	0.346	−32	− 47
187	June 17	7:58	103-F	65	0.423	.....	− 70
282	July 21	4:10	103-F	45	0.445	−48	− 69
188	June 17	8:53	103-F	20	0.461	.....	− 79
283	July 21	5:18	103-F	78	0.493	−23	− 77
296	Aug. 7	5:24	103-O	17	0.585	−29	− 87
95	May 12	9:10	103-O	13	0.708	.....	− 63
96	May 12	9:30	103-O	15	0.722	.....	− 58
97	May 12	9:52	103-O	14	0.738	−32	− 82
169	June 15	7:09	103-F	52	0.805	−29	− 57
170	June 15	8:07	103-F	48	0.845	−22	− 73
217	June 20	4:24	103-F	40	0.859	−12	− 68
218	June 20	5:14	103-F	49	0.894	−38	− 56
219	June 20	6:12	103-F	58	0.934	−20	− 30
220	June 20	8:32	103-F	90	1.031	−29	− 27
195	June 18	2:22	103-O	13	1.190	.....	− 6
196	June 18	2:54	103-O	42	1.212	−10	+ 13
198	June 18	4:59	103-F	62	1.299	− 4	+ 12
301	Aug. 8	3:48	103-O	29	1.520	−13	+ 60
302	Aug. 8	4:56	103-F	97	1.567	.....	+ 73
108	May 13	8:12	103-O	14	1.668	−44	+ 67
109	May 13	8:34	103-O	16	1.684	−14	+ 69
110	May 13	8:58	103-O	18	1.700	−10	+ 87
111	May 13	9:26	103-O	18	1.720	− 7	+ 86
159	May 18	8:46	103-F	46	1.860	.....	+107
227	June 21	5:14	103-F	43	1.894	.....	+ 93
160	May 18	9:42	103-F	43	1.899	.....	+117
228	June 21	6:06	103-F	51	1.930	.....	+111
229	June 21	7:01	103-F	48	1.968	−10	+103
230	June 21	7:54	103-F	49	2.005	+ 2	+ 70
79	May 11	10:06	103-O	13	2.163	−20	+ 78
201	June 19	1:53	103-O	20	2.170	.....	+ 45
80	May 11	10:18	103-O	4	2.172	.....	+ 40
203	June 19	3:40	103-O	20	2.242	−16	+ 49
204	June 19	4:15	103-O	42	2.268	.....	+ 47
205	June 19	5:02	103-O	42	2.301	+ 1	+ 34
I 171	1948 June 25	2:06	103*a*-O	11	2.396	.....	+ 52

* The groups indicated by the braces correspond to each normal place.

The velocity-curve in Figure 3 strongly suggests that the maximum is narrower than the minimum. If the photometric value of ω is reliable, then there are two possible explanations: either a change in the orientation of the line of apsides or a distortion of the velocity-curve of the kind frequently encountered in spectroscopic binaries which results in a tendency of the values of ω to cluster[15] between 0° and 90°.

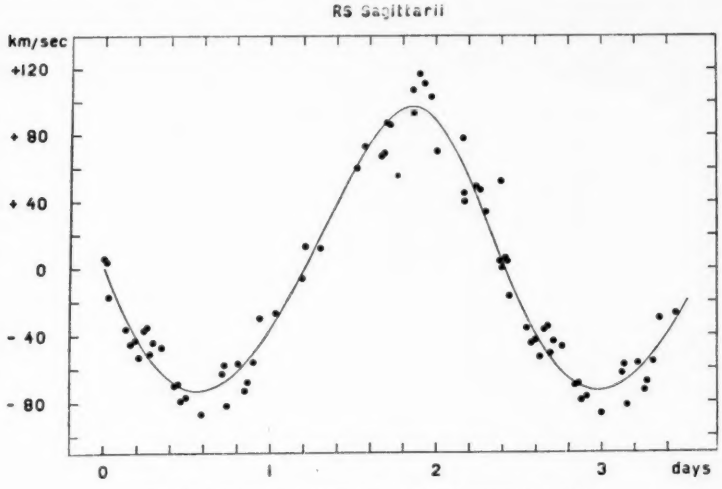

FIG. 3.—Radial velocities from all lines except *Ca* II K

TABLE 3

ORBITAL ELEMENTS AND MEAN ERRORS

$P = 2.41568$ days (assumed)	$T_0 =$ Phase 1.82 ± 0.018 days
$K = 85.1 \pm 3.7$ km/sec	$T =$ Phase 2.09 ± 0.61 days
$\omega = +41° \pm 27°$	$\gamma = +6.0 \pm 5.1$ km/sec
	$a \sin i = 2.8 \times 10^6$ km
$e = 0.09 \pm 0.025$	$\dfrac{m_2^3 \sin^3 i}{(m_1 + m_2)^2} = 0.15 \odot$

The time of principal mid-eclipse, from the spectrographic orbital elements, is phase −0.05 days, in excellent agreement with the photometric data.

I am indebted to Messrs Héctor Bobone, Jr., and Julio Albarracín for help during the process of reduction of the plates.

[15] O. Struve, *Pop. Astr.*, **56**, 348, 1948.

ANALYSIS OF THE METALLIC-LINE STARS. II*

JESSE L. GREENSTEIN†
Yerkes and McDonald Observatories
Received September 13, 1948

ABSTRACT

The general properties of the metallic-line stars are reviewed. Measures of radial velocity for different elements in the spectroscopic binary, ζ Lyr A, are used to show the singleness of that metallic-line star. The metallic-line stars are F stars near the main sequence which show a number of apparent peculiar abundances of the elements. No substantial effect of dilution is found. The high-dispersion spectrophotometric analysis of τ UMa already published is supplemented by lower-dispersion measures of *Si, Al, Na.* Line intensities are interpreted in terms of the total number of atoms and ions present and show that *Ca, Sc, Ti, Zr, V,* and *Mg* are definitely abnormal. No simple dependence of abundance deficiencies on atomic number is found.

The reduced amount of neutral and singly ionized atoms of the above elements can be a true abundance effect or an effect of excess second ionization. This excess is found to be definitely localized, since all elements with reduced abundances have ionization potentials between 12 and 16 electron-volts, i.e., close to hydrogen, 13.54 volts. Various possible mechanisms for excess second ionization near the Lyman lines and continuum are reviewed. All depend on a deviation from equilibrium in the sense of excessively ionized hydrogen producing emission lines or selectively ionizing the metals directly by charge transfer. This latter collisional effect is of a resonance character, with protons the source of excess second ionization. Its rate of occurrence may be very large compared to that of radiative ionization. Since the atmosphere of the dwarf, τ UMa, shows unexpectedly large turbulence and low surface gravity, it is possible that the dynamics of its atmosphere are responsible for the apparent abundance deficiencies.

THE METALLIC-LINE STARS

In Papers I[1] and III[2] of this series I have shown that the spectroscopic features of a group of five F stars of a wide range of luminosity can be quantitatively accounted for, in detail, by the specification of the physical parameters of their atmospheres, i.e., the electron pressure, P_e, and the ionization temperature, T_{ion}, at a representative optical depth, the excitation temperature, T_{exc}, and the turbulent atomic velocity, V. The chemical composition of the atmospheres, as determined with the proper values of these physical parameters, proved to be substantially the same as that of the sun. Table 12 of Paper I gave the abundances of the individual metals so determined; Paper I, Table 14, gave that of hydrogen. Only the star τ UMa showed outstandingly different abundances from the normal F stars. This object is a member of a rather numerous group of "metallic-line stars" discussed by Morgan, Keenan, and Kellman[3] and by Roman, Morgan, and Eggen.[4] These metallic-line stars form an appreciable fraction of the stars classified as of type A on very low dispersion; on moderate dispersion they are often characterized by two spectral types, one—say, A3—according to the weak K-line intensity and the other—say, F5—from the great strength of the metallic lines. Several recent investigations have shown that, according to color,[4, 5] these stars are not A stars but are, in fact, F stars. They often appear in galactic clusters, e.g., the Hyades, Coma, and the Ursa Major cluster; in clusters their apparent magnitude puts them near the

* *Contributions from the McDonald Observatory, University of Texas,* No. 159.

† Now at the California Institute of Technology.

[1] Greenstein, *Ap. J.*, **107**, 151, 1948.

[2] Greenstein and Hiltner, *Ap. J.* (in press).

[3] *An Atlas of Stellar Spectra* (Chicago: University of Chicago Press, 1943).

[4] *Ap. J.*, **107**, 107, 1948.

[5] Morgan and Bidelman, *Ap. J.*, **104**, 245, 1946.

main-sequence branch of the cluster HR diagram, if they are classified by their metallic lines.[6, 7] They would be underluminous if classified by their K line. Dr. O. J. Eggen kindly informs me that his unpublished photoelectric colors in galactic clusters show the metallic-line stars to be slightly overluminous for their color indices, as compared to the main-sequence cluster stars. The lack of a unique relation between spectral type and color and the absence of information on the masses makes this observation difficult to interpret. However, it is an interesting further additional phenomenon connected with the appearance of other false high-luminosity characteristics, which we shall discuss later. Thus many preliminary lines of evidence had indicated a close relation of these stars to F stars in color and luminosity and probably in radius and mass.

If the only peculiarity were the weakness of the K line, various explanations might be advanced. A preliminary investigation in 1941 on spectra of dispersion 30 A/mm, however, showed so many interesting peculiarities that a detailed study was initiated. Rotational broadening was visible even on low-dispersion spectra in many stars, and the following objects were proved to have poor lines on coudé spectra (3 A/mm dispersion): ζ Lyr A, ζ UMa (faint), α^2 Lib, ϵ Ser, 15 UMa, α Gem (faint). The star 63 Tau seems to have sharp lines even at 18 A/mm but is too faint (5.7 mag.) for the McDonald coudé. The star 60 Leo may also have sharp lines. Of all the stars observed, only τ UMa has proved suitable for a detailed investigation. Unfortunately, it is not a member of the Ursa Major cluster and has no trigonometric parallax. Its color has been given in unpublished measures of Stebbins[4] as $C_1 = +0.16$ mag., corresponding to that of a normal dF6 star. According to the *Atlas of Stellar Spectra*,[3] it is one of the more extreme cases, in that it has a large difference between the spectral types indicated on low dispersion by the K line (A3) and the metallic lines (F6 II). From the spectrophotometric measures of central intensities of the absorption lines, in Paper I, it was clear that the spectrum was that of a single star. It has been called a spectroscopic binary[8] of small range, 9 km/sec, but no detailed evidence has been recently obtained; the present data did not include velocity measurements.

The star τ UMa is HD 78362,3 and has apparent magnitude 4.74; its proper motion is large, 0".122 in p.a. 123°; it is given as A7211, with a 10.6 mag., common-proper-motion companion at about 57" in p.a. 48°. If τ UMa has, in fact, a physical companion 6 mag. fainter, the latter should be an M dwarf of absolute magnitude near +9. Two spectra were obtained in November, 1947, which showed that τ UMa (faint) was a G0 star and probably a normal dwarf. If the stars are physically connected, τ UMa (bright) would have an absolute magnitude near −1, and be a bright giant! This paradox, fortunately, has been resolved by Strand,[9] who measured τ UMa on plates taken with the 40-inch refractor. Combining these with the older visual measurements, he finds that the stars do *not* show common proper motion and that the pair is optical, with the fainter dwarf G star more distant and nearly stationary. It is most probable that τ UMa is no different in luminosity from other metallic-line stars, such as 63 Tau, which it very closely resembles.

The motion of τ UMa in the v-direction, is −0".010; in the τ-direction it is 0".119. Thus the peculiar motion is appreciable. If we assume[4] a luminosity $M = +2.7$, the parallax is 0".040, and the τ-component motion corresponds to 14 km/sec. Since the radial velocity is −6 km/sec, there is no evidence for high-velocity characteristics, the total space motion being of the order of 25 km/sec. If the star were as luminous as would have been required by the false common-proper-motion companion, the space motion would have been abnormally high, i.e., about 140 km/sec.

The metallic-line star ζ Lyr A gives an interesting opportunity to test the singleness

[6] Titus and Morgan, *Ap. J.*, **92**, 256, 1940.

[7] Weaver, *Pub. A.S.P.*, **58**, 246, 1946.

[8] Moore and Burns, *Lick. Obs. Bull.*, **4**, 68, 1906.

[9] Results very kindly communicated in advance of publication.

of a metallic-line star. This is a single-lined spectroscopic binary; an orbit by Jordan[10] shows a total range of 102 km/sec in a period of 4.3 days. It is improbable that in such a close system the observed spectrum could arise from a star which is itself a double. Spectroscopically, ζ Lyr A is classified[4] as of metallic-line type, A4 + F0; on coudé plates the lines show large rotational broadening. I measured three Process plates of ζ Lyr A, dispersion 30 A/mm, in the region λλ 3670–4101 and two of τ UMa. The latter were used for identification and also to check the singleness of τ UMa; from sixteen good *Fe* I lines I find a velocity of −3 km/sec for τ UMa, and from four (partially blended) *Ca* II lines, −4 km/sec. The plates of ζ Lyr A give the data in Table 1; eight hydrogen lines (somewhat blended), 4 *Ca* II and 12 *Fe* I lines were used. Note that, in spite of a variation of 65 km/sec, there is good agreement in the velocities shown by *H*, *Ca* II, and *Fe* I; thus all lines originate in a single star.

TABLE 1

VELOCITIES OF ζ LYRAE A (KM/SEC)

1942 Date	*H*	*Ca* II	*Fe* I	Mean
May 9	+ 1.8	+ 2.8	+ 5.3	+ 3.3
11	−41.9	−40.6	−40.1	−40.8
12	−63.8	−61.6	−60.5	−61.8

TABLE 2

SPECTRAL TYPES FROM DIFFERENT ELEMENTS

STAR	SPECTROPHOTOMETRIC		ESTIMATED		ESTIMATED METALLIC LINES
	Ca II	Hydrogen	*Ca* II	Hydrogen	
τ UMa	A3	A9	A5	F0	F6 II
15 UMa	A3	A9	A2	F0	F5 IV
ζ Lyr A	A4	A4	A4	A7	F0

Table 3, of Paper I, contained measured equivalent widths of the hydrogen lines and of the K line, in several metallic-line stars and in normal stars. The data can be used to obtain "measured" spectral types; while only of moderate precision, such information helps confirm features suspected on low-dispersion spectra. From the observed relations between equivalent widths and spectral type for the normal dwarfs, the equivalent spectral types given under "Spectrophotometric" in Table 2 are obtained. No attempt was made to classify quantitatively the numerous metallic lines. The data in the last three columns under "Estimated" are from the work of Roman, Morgan, and Eggen.[4] The general results are accordant and clearly show that the hydrogen lines indicate a spectral type intermediate between that of the K line and the hydrogen lines. It was shown in Paper I that the estimated spectral type F6 II is a remarkably good representation of the metallic lines in τ UMa.

Figure 1 shows enlargements of spectra (30 A/mm) of the two metallic-line stars, τ UMa and 63 Tau, and also of θ UMa, F6 III. The weakness of the K line is conspicuous, as is the strength of the hydrogen lines in the metallic-line star. The blend of

[10] *Pub. Allegheny Obs.*, **1**, 115, 1909.

H and $H\epsilon$ is strange in appearance, in that the two lines are well resolved. In a normal A3 star $H\epsilon$ is too strong for H to appear, while in normal F stars, H is the dominant line. A theoretical detailed prediction of the contour of the blend would provide an insight into the height in the atmosphere at which the lines are formed. Note that the metallic lines are the same in τ UMa and in 63 Tau and that, in general, they are stronger than in θ UMa. Such lines as λ 4077 of *Sr* II are much enhanced, as they are in supergiants, as compared to θ UMa. The high-dispersion spectra showed that the metallic-line star had many strong enhanced lines of the ionized metals and rare earths, which are relatively weak in α CMi, and which resemble the lines in ρ Pup (F6 II) remarkably well. Figure 2 contains enlargements of McDonald coudé spectra, with some of the interesting lines marked. The neutral lines are of about the same intensity in all F stars, except for *Ca* I, *Mg* I, and *Ti* I, which are weak in τ UMa. Certain ions are also seen to be weakened in τ UMa; they are *Ca* II, *Ti* II, *Sc* II, *Zr* II. The details of these weakenings will be discussed later. A study of another metallic-line star, such as 63 Tau, would be valuable to ascertain whether the same elements are weakened as in τ UMa; such a study is being made by Dr. Harold A. Weaver. Less extreme stars should also be studied.

I will not attempt to discuss further the general statistical properties of the metallic-line stars. An analysis of their space motions and parallaxes is to be desired when a fuller list becomes available. In galactic research they have been the source of a false "space-reddening" among groups of near-by A stars, as classified on low-dispersion spectra. Their relation to types of stellar population needs clarification. Weaver[7] pointed out their appearance in galactic clusters of Trumpler's type 2, i.e., those with red-giant stars and no high-luminosity B stars. It would also be of interest to explore their relationship, by studies of space motions and distribution in the galaxy, to Baade's population types.

DILUTION EFFECTS

The strength of large numbers of metallic lines in what were originally considered to be A stars leads naturally to the suggestion that the lines might be formed in a detached shell or envelope around an A star. Spectra like those of the shell of Pleione or of 14 Com might also be interpreted as evidences of composite spectral type. However, if lines of the observed great strength are to be produced in a shell, an extended atmosphere with large effects of dilution would be required. The spectrum of *Fe* I provides a simple test of this hypothesis, since it contains many lines arising from excited metastable and normal levels. Of the *Fe* I lines measured in Paper I, Table 2, half with excitation potential greater than 2 volts arise from nonmetastable levels. If there were any dilution, the population of these normal levels would be less than that predicted by the Boltzmann distribution, approximately in proportion to the dilution, while the metastable levels would have populations nearly unaffected by the dilution. From the curve of growth and the equivalent widths, I determined the observed effective absorption coefficient, proportional to the number of atoms of *Fe* I contributing to form a given line; let us call this quantity $\log X_f'''$, as read from the curve of growth. In originally forming the curve of growth, I had predicted values of the effective absorption coefficient, $\log X_f''$; these are based on the observed solar curve of growth and on the difference of excitation temperature between the star and the sun. The difference was then formed,

$$S_i \equiv \log_{10} X_f''' - \log_{10} X_f'' \; ; \tag{1}$$

and the average value of S_i was determined for normal and metastable lines separately. Such systematic shifts as exist are given in Table 3, together with a final estimated average deviation of the systematic difference; in parentheses are given the number of *Fe* I lines used. A negative residual, in the sense of normal *minus* metastable, indicates the logarithmic deficiency in the population of a normal level in the star as compared to the population predicted from solar data.

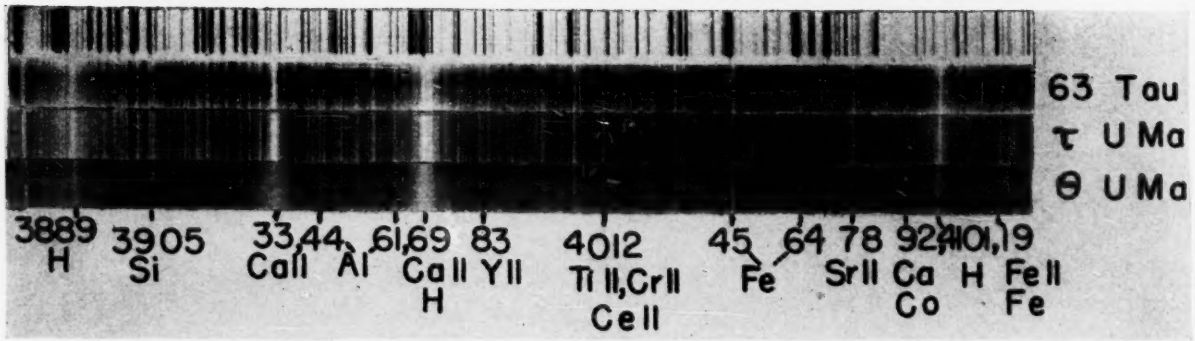

FIG. 1.—Two metallic-line stars, 63 Tau and τ UMa compared to the F6 III star, θ UMa. Original dispersion 20 A/mm. The lines of the neutral elements are about the same, but most ions are appreciably strengthened in the metallic-line stars. Note the weakness of the λ 3933 line of *Ca* II, and the strength of the hydrogen lines.

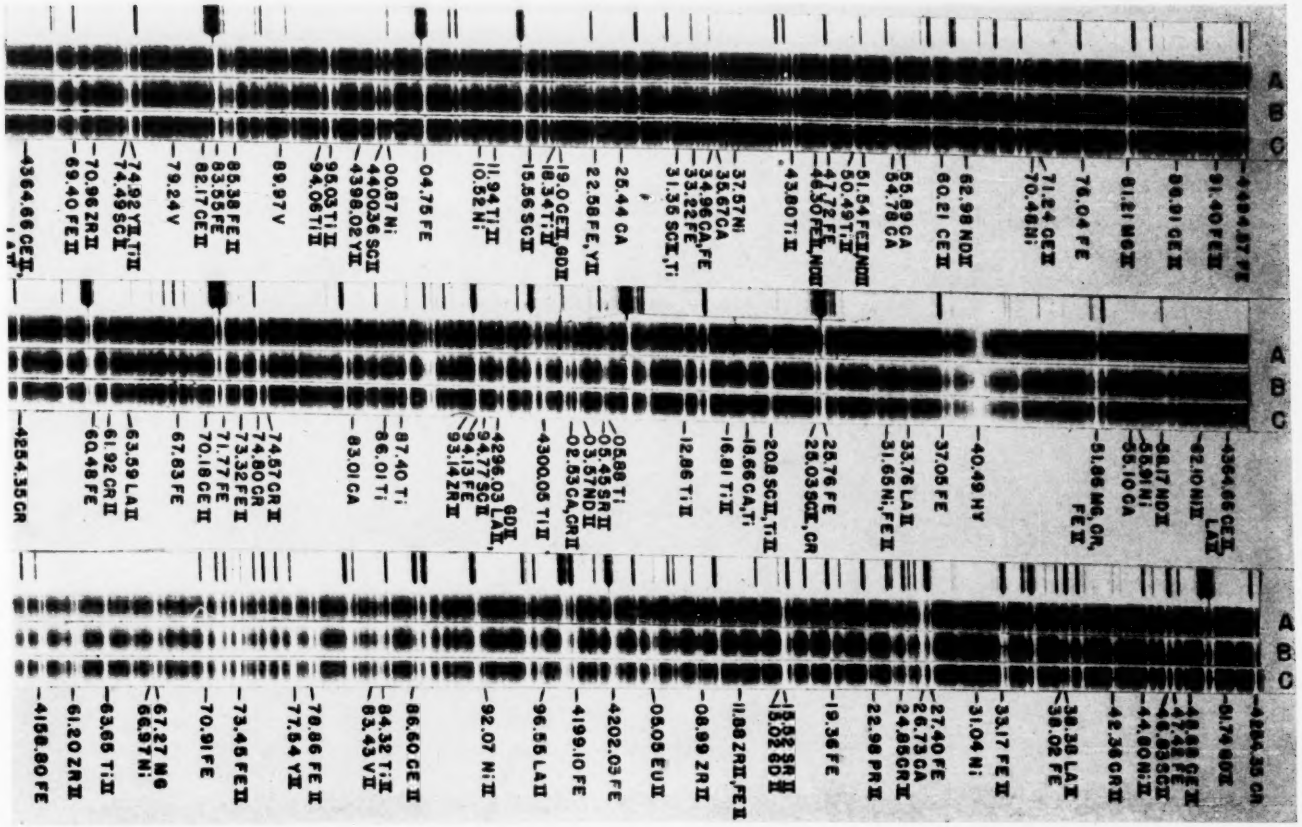

FIG. 2.—Enlargements of sections of coudé spectra of θ UMa = A; of ρ Pup = B, type F6 II; and of the metallic-line star τ UMa = C, A3 + F6 II. Original dispersion 3 A/mm. Comparison spectrum that of *Fe* arc. The spectra of ρ Pup and τ UMa are very similar in the general strength of the ions, as compared to θ UMa; the metallic-line star shows many pseudo-high-luminosity effects. Lines of *Ni*, *La*, and the rare earths are strengthened, particularly in τ UMa: those of *Ca*, *Sc*, *Zr*, *Mg*, and *Ti* are weakened.

There is slight evidence for a negative relative shift, S_i, in all stars, amounting to about -0.11 in the logarithm. This is equivalent to a population of excited normal levels 80 per cent of that predicted by the Boltzmann distribution, if we assume that the metastable levels are populated exactly according to the latter. The effects are near the limit of observational accuracy, and it is uncertain whether τ UMa shows a larger than average effect. The differences between the F stars and τ UMa are so small that it is very unlikely that the strength of the *Fe* I lines could be accounted for if they had their origin in a shell surrounding an A star (the effective number of *Fe* I atoms in the atmosphere of τ UMa is about one hundred times larger than in an A star).

The origin of the slight systematic underpopulation of the excited normal levels may be in effects of stratification, either in the sun or in the F stars. There is probably also an appreciable contribution to the strength of excited metastable lines from atoms at high levels in the stellar chromosphere. Stars may have stream motions, outward flow, or a systematic increase of turbulent velocity outward. A small effective increase of the mean velocity of the atoms with height will produce a relatively large effect in the equivalent width, because of curve-of-growth effects.

TABLE 3

S_i, DEVIATIONS FROM THE CURVES OF GROWTH FOR *Fe* I

Star	Metastable Lines	Normal Lines	Normal *minus* Metastable
τ UMa	+0.08 (35)	−0.11 (35)	−0.19±0.06
ρ Pup	+ .04 (27)	− .08 (29)	− .12± .06
α Per	.00 (20)	+ .06 (18)	+ .06± .08
θ UMa	.00 (31)	− .17 (35)	− .17± .07
α CMi	+0.03 (35)	−0.11 (34)	−0.14±0.04

QUANTITATIVE ANALYSIS OF τ UMA

It has been found that an excellent correlation exists between the turbulent velocity and the luminosity of the star in types B, A, and F. Disregarding the complication introduced by rotation (which seems small in F supergiants), the apparent line contour seen on high dispersion is also well correlated with luminosity. The broad U-shaped lines of an F supergiant are easily recognized; there is some evidence that their width may exceed that predicted from the turbulence measured by the curve of growth. Conversely, in F dwarfs of small rotation, the true line contours[2] are narrow and indicate a velocity not far above the thermal motion of the atoms. The curve of growth of even the sun gives a velocity of 2.2 km/sec, which is somewhat larger than the thermal 1.5 km/sec. The turbulent velocity and the apparent line width indicated for τ UMa are unusual for a dwarf star; the well-determined value of 4.0 km/sec (Paper I, Table 7) is far above any previously suggested for a dwarf. For supergiants I find 5.0 km/sec (ρ Pup, F6 II, $M = -3$) and 6.3 km/sec (α Per, F5 Ib) and for the fainter stars 2.8 km/sec (α CMi, F5 IV, and θ UMa, F6 III). Although τ UMa is almost certainly of lower luminosity than α CMi and θ UMa, it has a larger turbulence. This unexpected result accounts for many spectral peculiarities of τ UMa; thus Morgan[3] noted, even on low dispersion, the spectral similarity of τ UMa and ρ Pup, in spite of the difference of luminosity of 6 mag.

The detailed analysis, in Paper I, leads also to a low opacity, κ_ν, and therefor to a low electron pressure, P_e, in τ UMa. Thus $\log \kappa_\nu = -1.62$, which is lower than the opacity in the three F stars studied (e.g., ρ Pup, -1.36) and rivals that in α Per (-1.64). The deduced electron pressures are found to be $\log P_e = 0.0$ for τ UMa, $+0.4$ for

ρ Pup, and +0.1 for α Per. Thus the electron pressure is comparable to that in a supergiant. This totally unexpected result is required by the great strength of the lines of most of the ionized metals; it indicates that some fundamental new physical mechanism is operative in the metallic-line star. The deduced effective surface gravity is $\log g_e = +1.6$ (the gravitation value should be near +4); thus g_e is lower than in all stars except α Per, which gave +1.2. The reduction of surface gravity is not unexpected, since turbulence is present; the effective gravity has often been found to be below the expected value in supergiants. We shall later inquire as to whether the observed peculiar abundances of certain metals are correlated with the turbulence. It would be of great importance to establish the existence of large turbulence in all other metallic-line stars. However, the strength of the ionized lines observed with low dispersion, e.g., *Sr* II, *Fe* II, *Cr* II, indicates the similarity of most of these stars (see Fig. 1 for the detailed resemblance of τ UMa and 63 Tau).

TABLE 4

ADDITIONAL LINE INTENSITIES IN F STARS
($-\log_{10} W/\lambda$)

STAR	λ 3905 *Si* I	λ 3933 *Ca* II	λ 3944 *Al* I	λ 3961 *Al* I	λ 5890 *Na* I	λ 5896 *Na* I	PLATES	
							Violet	Yellow
τ UMa	4.02	3.14	4.07	4.03	4.00	4.06	2 II*a*-O, 1 103*a*-F	3 103*a*-F, 1 III-F
ρ Pup	4.04	2.76	4.06	4.07	4.01	4.05	2 IV-O, 1 III-F	1 103*a*-F, 2 III-F
θ UMa	.....	2.74	4.03	4.08	4.06p	4.28p	2 II*a*-O	1 III-F
α CMi	4.14	2.76	4.11	4.12	4.13p	4.24p	2 IV-O	2 III-F
α Per	4.01	2.61	4.07	4.05p	4.03	4.05	2 IV-O	3 III-F

THE ABUNDANCES OF THE ELEMENTS

In Paper I, Table 12, I have given a résumé of the final derived abundances in τ UMa as compared to those in the sun; eight of the twenty elements were observed in two stages of ionization. Such quantitative results involve a large number of simplifications of the theoretical problem of the interpretation of line intensities. The methods used were the same in all stars, and the abundances are in units of the solar abundance. The validity of the results for τ UMa can be supported by the reasonableness of the results for the normal F stars. The normal stars showed no well-established differences, larger than a factor of 2, of the abundance of any element as compared to the solar value. In contrast, τ UMa showed deficiencies by a factor of 10 in four elements and by a factor of 3 in two other elements.

One apparent systematic trend appeared to be that the elements showing large deficiencies in τ UMa were those of low atomic weight. Unfortunately, the important light elements *He*, *C*, *N*, and *O* are unobservable in this region of the spectrum (a program of infrared observation is planned). While *H* proved to be normally abundant, data were lacking for certain other light elements, *Na*, *Al*, *Si*, which might prove of interest. Their lines occurred in spectral regions not covered by the coudé plates. In November, 1947, spectra were obtained with the McDonald Cassegrain spectrograph (CG series), with a dispersion ranging from 16 A/mm at λ 3900 to 77 A/mm at λ 5890. Separate exposures were taken for the *Na* lines (103*a*-F and III-F emulsions), where the dispersion is low and the errors large, and for the *Al* and *Si* lines (II*a*-O and IV-O emulsions). Additional measures of the K line were also obtained. The calibration was provided by a tube photometer with suitable filters. A résumé of the data is given in Table 4.

The reduction of the new measures proceeded as in Paper I; from the old curves of growth, the number of atoms in the given state were obtained and the differences of effective abundances, $\Delta \log \zeta_i$ (Paper I, Table 7):

$$\Delta \log \zeta_i \equiv \log \frac{\dfrac{N_i(*)}{\kappa_\nu(*)}}{\dfrac{N_i(\odot)}{\kappa_\nu(\odot)}} = \log \frac{\eta_{0,i}(*)}{\eta_{0,i}(\odot)} + \log \frac{V(*)}{V(\odot)}. \qquad (2)$$

From the temperature, pressure, opacity, and velocity previously determined (Paper I, Table 7) it is possible to compute the actual abundance in the form of the ratio of the number of atoms of the element, i, in all stages of ionization, per gram of stellar material, as compared to the number in the sun, $\log z_i(*)/z_i(\odot)$. Tables 5 and 6 give the final

TABLE 5

APPARENT ABUNDANCES OF NEUTRAL ATOMS IN THE F STARS
($\Delta \log \zeta_i$)

Element	τ UMa	ρ Pup	θ UMa	α CMi	α Per
Na I.....	+0.15 (2)	+0.02 (2)	−0.15 (2:)	−0.12 (2:)	−0.54 (2)
Al I.....	− .37 (2)	− .55 (2)	−0.19 (2)	− .29 (2)	−1.05 (2)
Si I.....	−0.30 (1)	−0.44 (1)	.....	−0.35 (1)	−0.67 (1)

TABLE 6

CORRECTED RELATIVE ABUNDANCES OF THE ELEMENTS
($\log z_i[*]/z_i[\odot]$)

Element	Z	τ UMa	ρ Pup	θ UMa	α CMi	α Per	Qual.	I.P. (Volts)	
Na.....	11	+0.44	+0.36	+0.09	+0.11	−0.12	c	5.12	47.10
Al.....	13	−0.02	−0.12	+0.10	0.00	−0.53	b	5.96	18.75
Si.....	14	+0.18	+0.13	.....	+0.02	0.00	d	8.11	16.27
S.....	16	−0.53	−0.05	−0.14	−0.35	−0.08	c	10.31	23.3

determinations of abundances for the additional elements; they also include a determination of rather low weight for *S* I, which was available in Paper I, Table 7, but was not then considered of sufficient weight to be included in Paper I, Table 12. The new Table 6, together with Paper I, Table 12, presents the final abundance determinations in the F stars.

If we form the mean for the supergiants (ρ Pup, α Per) and for the two fainter stars (θ UMa, α CMi), we derive the difference $\Delta \log z_i'$ (Paper I, Table 13), +0.02 *Na*, −0.37 *Al*, +0.04 *Si*, +0.18 *S*. These abundance differences are of the same order as those previously found for all other elements; the large residual for *Al* may well be completely accidental error. Figure 3 is a plot of the abundance difference, $\log z_i(*)/z_i(\odot)$, against atomic number Z. In the first discussion of the results of Paper I, there had been a tendency for the light elements to show abundance deficiencies in τ UMa. If we suppress the entries for *Na*, *Al*, and *Si*, there is a general negative residual for all elements, $Z \leqslant 23$; this trend has now disappeared, since all three new light elements have normal abundances (Table 6). However, even with the older data, the large deficiency for *Zr* ($Z = 40$) was peculiar. Plotted against Z, the residuals now are definitely erratic in character. The great difference between τ UMa and the normal F

stars is clearly shown in the lower half of Figure 3, where θ UMa and α CMi are compared to the sun. Over the whole range of Z there is no systematic trend and no large residual.

A more interesting regularity exists in Figures 4 and 5, where the log $z_i(*)/z_i(\odot)$ are plotted against ionization potential (I.P.). The choice of which I.P. is used in such a presentation depends on a hypothesis as to the cause of the abundance deficiencies in τ UMa. Elements doubly ionized are not observed in F stars, and it is therefore impossible to decide whether an element is deficient because it suffers from an abnormal excessive second ionization or from a true abundance deficiency. Consider the typical case of *Ca;* an abnormal second ionization caused by an excess of ultraviolet radiation beyond 11.8 volts could reduce the number of *Ca* II ions. The ratio *Ca* I/*Ca* II, however, is determined by radiation just beyond 6.1 volts, which may be normal. Then the numbers of atoms of both *Ca* II and *Ca* I are reduced by the same factor, and the same low abun-

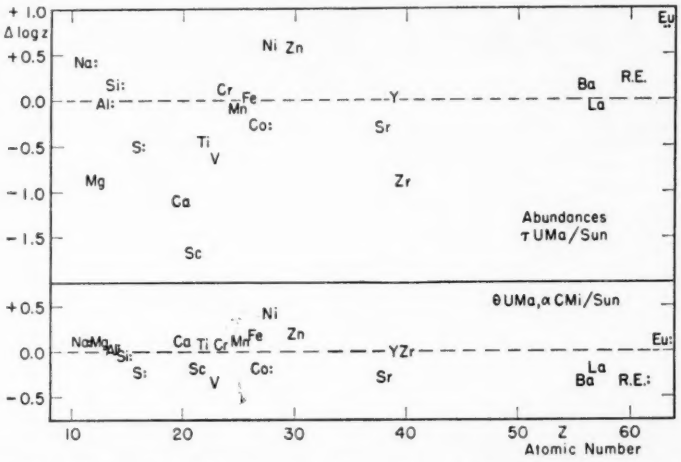

FIG. 3.—The differences of the logarithms of the abundances, by numbers of atoms, Δ log z, as a function of atomic number, Z. A colon represents an uncertain determination.

dance would be derived from both stages of ionization. In F stars and in the sun, most elements exist nearly completely in the singly ionized state (if we disregard possible abnormal second ionizations). Thus it is the *second I.P.* that is relevant to most of the metallic lines. Nearly all first I.P.'s lie close together, from 5.1 to 8.1 volts. We shall see that the possible excess radiation lies near 13 volts and probably does not strongly affect the first ionization, except possibly of *S* I (10.3 volts) and *Zn* I (9.3 volts). All elements are plotted in Figures 4 and 5 at their second I.P., except *S*, a slightly ambiguous case, for which I assume that it is the ratio *S* I/*S* II that may be affected. The importance of the newly observed elements (*Na, Al, Si*) is that they have small atomic number but fortunately have large second I.P.; thus *Na* II has an I.P. of 47 volts while *Ca* II has 11.8 volts.

The bottom section of Figure 4 shows that θ UMa and α CMi have little or no systematic abundance difference from the sun; the slight negative trend at low I.P. might indicate that the ionization temperature has been taken slightly too low. The two upper sections compare the supergiants with the sun or with the fainter F stars. There is a real, but small, systematic effect here; all elements for which the I.P. lies between 12 and 16 volts show *negative* residuals. These elements—*Ca, Sc, Ti, Zr, V,* and *Mg*—are rela-

tively well-determined cases, some observed in two stages of ionization. Figure 5, however, compares τ UMa with the sun and also with the F supergiants. A comparison with θ UMa and α CMi would not be different from that with the sun. Again the negative residuals occur for I.P. between 11.8 and 16 volts and are much larger than in Figure 4. A few critical cases may be mentioned, *V* II is fairly well observed, with five lines. Its second I.P. is 12.3 volts, which exceeds that of *Ca* II (11.8 volts); nevertheless, *V* II seems to show a normal abundance in τ UMa. The rare earths, labeled *R.E.* in the diagram, all have second I.P.'s near 11.4 volts and are quite strong in τ UMa. Thus some

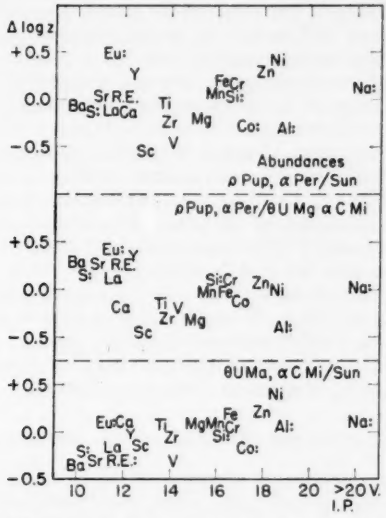

FIG. 4.—The abundance differences, $\Delta \log z$, as a function of second ionization potential in electron volts (I.P.). Note the deficiencies in the supergiants between *12* and *16 V*.

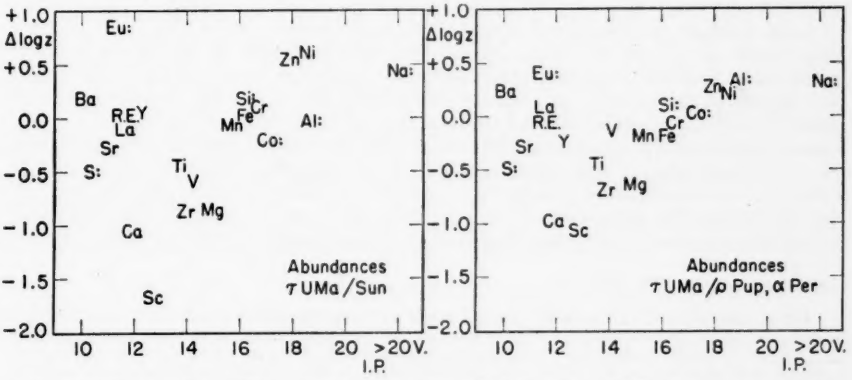

FIG. 5.—The abundance differences, $\Delta \log z$, for the metallic-line star τ UMa, when compared to the sun, and to the F supergiants. Note the large deficiencies between *12* and *16 V*. The scatter, and the range of the deficiencies is much reduced in the comparison with the supergiants.

peculiar phenomenon must occur very close to 12 volts. It sets in abruptly, since the largest deficiencies are observed at 13 volts, and decreases more slowly toward larger I.P., since the metals between 14 and 16 volts form a rather regular sequence as they approach normal abundances. No positive residual occurs in Figure 5 (left-hand side) between 12.5 and 16.0 volts or in Figure 5 (right-hand side) between 11.8 and 16.2 volts. The deficiencies are smaller and the scatter less when τ UMa is compared with the supergiants than when compared with the sun. The smaller scale arises from the tendency in Figure 4 for the supergiants to show somewhat the same pattern of deficiencies as does τ UMa. The smaller scatter arises because the spectrum of τ UMa resembles that of a supergiant and is very different from that of the sun. Systematic and accidental errors introduced by blending, as well as by the method of analysis, are more completely eliminated by a comparison with the supergiants.

There are two ways of interpreting the observed apparent abundance deficiencies in τ UMa. Theories of the origin of the elements from thermonuclear reactions in a dense, hot, primal source have predicted certain systematic trends in the relative abundance of the heavy and the light elements. Changes of initial conditions would yield systematic changes of this ratio, slowly varying with atomic number. The erratic abundance deficiencies observed in τ UMa do not show any simple systematic run with Z. Secondary results of changes in the abundance of the heavy elements may still provide an explanation; for example, nuclear fission of the transuranic (or other peculiar, unstable nuclei) results in fission products near the middle of the periodic table. Unfortunately for considerations of nuclear abundances, we lack information on isotope abundances and on the important light elements, *He*, *C*, *N*, and *O*. If we consider improbable the hypothesis that true erratic abundance differences are caused by fission, we must consider more seriously the possibility that a "spectroscopic accident," such as the presence of excess ionizing radiation, has produced spurious abundance defects.

DEVIATIONS FROM THE ELEMENTARY THEORY OF IONIZATION

Struve and Swings[11] suggested that emission by the Lyman-β line of hydrogen might account for an excess ionization of *Ca* II. Their hypothesis was limited to the case of *Ca* II and was directed toward an explanation of the intensity variations of *Eu* II/*Ca* II in peculiar A stars like α^2 CVn. The more complete data, now available for the first time for a peculiar F star, show that the excess ionization (if it is real) persists over a considerable range of energy; further, I find the new result that *Ca* I shares the peculiarity of *Ca* II. Further laboratory and stellar data on the doubly ionized metals is of great importance. It will be extremely difficult to trace the details of the effects of excess radiation on the ionization of different elements.[12] The ionization probability is a complex and at present unknown function of distance beyond the series limit. For elements with many low-lying metastable levels, ionization from excited states will be important; only a small fraction of the atoms are in the ground state in a typical singly-ionized rare earth. Such elements would be influenced by radiation of lower energy than the resonance I.P. Other ions which are partially ionized by radiation of less energy than their resonance I.P. are *Ca* II, *Sc* II, *V* II, *Cr* II, *Fe* II, *Ni* II, *Y* II, *Zr* II, *Ba* II, and *La* II. In simple hydrogenic atoms the ionization cross-section decreases as ν^{-3} shortward of the series limit; however,

[11] *Observatory*, **64**, 291, 1942.

[12] It is unfortunate that the doubly ionized atoms are probably unobservable in the F stars. They would provide an obvious crucial test as to whether the changes of line intensity are true abundance deficiencies or excessive ionizations. The elements here of interest—*Mg* III, *Ca* III, *Sc* III, and *Zr* III—all probably will have lines of very high excitation potentials. In the case of *Eu* III which does not affect the problem of τ UMa, Swings (*Ap. J.*, **100**, 132, 1944) found that *Eu* III and *Eu* II varied in phase in α^2 CVn; it is obvious that all abundance changes cannot be explained by excess second ionizations. See also Struve, *Proc. Amer. Phil. Soc.*, **85**, 357, 1942.

Page[13] and Bates,[14] in their résumés of the data for complex atoms and ions, find some cross-sections to be constant or even to increase shortward of the series limit. The available energy density, according to the Planck formula, always decreases steeply toward larger energies; this provides the ultimate limitation to the width of the band of radiation by which an atom is ionized, perhaps 1 or 2 volts near the series limit. Nevertheless, exceptions may exist if the ionization continua are peculiar. If specific line emissions are to contribute appreciably to ionization, they must represent over their limited frequency range as high an energy density as is contained within 1 or 2 volts of the continuum. The Lyman emission lines are Ly-α, 10.16 volts; Ly-β, 12.04 volts; Ly-γ, 12.69 volts; the continuous limit is at 13.54 volts. Shortward of the Lyman limit, if the pure recombination emission spectrum of hydrogen were present, the intensity would decrease as $\exp(-h\nu/kT)$. Thus, if Lyman emission lines and continua existed, they might produce about the correct energy distribution to account for the sudden increase in second ionization, apparently indicated for τ UMa near 12 volts, and the slow decrease, which disappears by 16 volts.

There is a grave observational objection to the hypothesis of excess emission in the Lyman series and continuum. If Ly-α alone were in emission, we might expect excess ionization near 9–11 volts and possibly excess population of the second level. The latter would be interesting in view of the strength of the hydrogen lines; however, in Paper I, Table 14, the abundance of hydrogen determined from the population of the second level was found to be normal or slightly above normal. But if Ly-β and the continuum are also in emission, observable effects in the Balmer line intensities would occur, in the form of either high residual intensities or emission, especially at $H\alpha$. The residual intensities are low, and there is no trace of $H\alpha$ emission. The emission excess in the Lyman lines thus cannot extend to the surface or be in an envelope or shell.

The existence of Lyman emission within a normal stellar atmosphere also seems improbable theoretically. The great abundance of neutral hydrogen results in an enormous absorption coefficient in the lines and in the continuum (about 10^7 cm^2/gm at the series limit). The problem of radiative transfer for such an emission line within a stellar atmosphere has not been theoretically considered, but the general outline of the theory can be obtained from a consideration of an absorption line. Thus we may ask what is the effect of the normally present Lyman absorption lines on the energy available for ionization inside an atmosphere in which the hydrogen and the metals are well mixed. At the boundary, absorption lines are observed in the outward flux of radiation; at an optical depth, τ, in the continuum the optical depth in a line, τ_ν, is $(\eta_\nu + 1)\tau$. We thus approach conditions of local thermodynamic equilibrium very rapidly inside a Lyman line. The net flux, F_ν, becomes small and the mean intensity, J_ν, approaches $B_\nu(T_\tau)$, the Planck function at the local temperature, T_τ; the radiation is nearly isotropic. Since most metallic lines are formed near $\tau = 0.1$, $\tau_\nu \approx 10^6$, and the radiation available for ionization is that of a black body at the boundary temperature of the star. The ionization depends on the energy density, or on J_ν, rather than on the flux. It is thus difficult to see how any peculiar ionization effects can be associated with the Lyman lines, either in absorption or in emission.

1. We shall first compute the J_ν in an unstratified case. We assume that the integrated Planck emission is a linear function of optical depth; hence

$$B_\nu = a_\nu + b_\nu \tau \,. \tag{3}$$

In the usual degree of approximation,

$$\frac{b_\nu}{a_\nu} = \frac{3}{8}\frac{h\nu}{kT_0}. \tag{4}$$

[13] *M.N.*, **99**, 385, 1939.

[14] *M.N.*, **106**, 423, 432, 1946.

We adopt the approximation $K_\nu = \frac{1}{3}J_\nu$ and also $F_\nu = 2J_\nu$ at the boundary. Assume that the line is formed completely by pure scattering ($\epsilon = 0$). The solution is

$$\frac{J_\nu - B_\nu}{B_\nu} = \frac{2\,\frac{b_\nu}{a_\nu} - q^2}{q^2 + 2q}\,\frac{e^{-q\tau}}{1 + \frac{b_\nu}{a_\nu}\,\tau}, \tag{5}$$

$$q^2 = 3\,(1 + \eta)\,. \tag{6}$$

The deviation of the actual mean intensity, J_ν, from the thermal emission, B_ν, in units of B_ν, given by equation (5), and evaluated at $\tau = 0.1$ is shown in Table 7, for various line strengths, η. The approach to the equilibrium value is rapid, i.e., as $\exp(-q\tau)$ as τ increases, with $q \approx 10^4$ in the Lyman lines and continuum. More interesting cases arise if there is stratification in the formation of a strong absorption line. Eddington[15] pointed out that there may be a damming-up of radiation if a strong line is formed near the top of an atmosphere. Swings and Chandrasekhar[16] have also considered such stratified atmospheres.

2. If we assume hydrogen completely neutral at the top of the atmosphere, then $\eta = \eta_1$ for $\tau \leqslant \tau_1$; $\eta = 0$ for $\tau > \tau_1$. This model would be of interest if hydrogen were abnormally ionized (other elements being normal) at the bottom of an atmosphere, for example, because of rising currents from the convective zone. This model seems physically implausible on an elementary theory, since the second I.P. of the metals lies close to that of hydrogen. However, if there were abnormal effects on hydrogen due to the convection, hydrogen might conceivably be almost completely ionized while normal metallic ions could still have their lines formed at optical depths greater than τ_1. We are interested only in the solutions for $\tau \geqslant \tau_1$,

$$J_\nu - B_\nu = \gamma\, e^{-\sqrt{3}\tau}\,. \tag{7}$$

By continuity of J_ν and F_ν with the values given by the solution valid at $\tau < \tau_1$, we determine

$$\gamma = \frac{b_\nu}{q_1}\; e^{\sqrt{3}\tau_1}\,\frac{\eta_1(q_1+2) + 2\left(2 - \frac{a_\nu}{b_\nu}\,q_1^2\right)\,e^{-q_1\tau_1} - (q_1-2)\,\eta_1\,e^{-2q_1\tau_1}}{(q_1+2)\left(\frac{q_1}{\sqrt{3}}+1\right) - (q_1-2)\left(\frac{q_1}{\sqrt{3}}-1\right)\,e^{-2q_1\tau_1}}. \tag{8}$$

If τ_1 remains finite and η_1 becomes large, we find that

$$\frac{J_\nu - B_\nu}{B_\nu} \to \frac{\frac{b_\nu}{a_\nu}\,e^{-\sqrt{3}(\tau-\tau_1)}}{\sqrt{3}\left(1 + \frac{b_\nu}{a_\nu}\,\tau\right)}. \tag{9}$$

In Table 7, I give the results of computation with equation (8) or equation (9) for the case $\tau_1 = 0.1$, i.e., evaluating $J_\nu - B_\nu/B_\nu$ at a depth in the atmosphere where ordinary metallic lines are formed but at a wave length in the far ultraviolet, so that we are considering radiation governing the second ionization of the metals. The decrease with increasing depth is slow, i.e., as $\exp(-\sqrt{3}\tau)$. The deviations from thermal emission are now large for a strong line, J_ν being about four times as large as B_ν.

[15] *M.N.*, **89**, 620, 1929. [16] *M.N.*, **97**, 24, 1936.

3. If we take the opposite type of stratification, we have the case in which hydrogen is completely ionized above a point τ_2; then

$$\eta = 0\,, \qquad \tau < \tau_2\,; \qquad \eta = \eta_2\,, \qquad \tau \geqslant \tau_2\,.$$

The metallic lines are considered to be formed completely *above* the Lyman lines. Then we find

$$\gamma = -\frac{b_\nu}{q_2}\, e^{q_2\tau_2} \times \frac{(1+\tfrac{2}{3}\sqrt{3})\,\eta_2 - 2\sqrt{3}\,(1+\eta_2)\left(\frac{2}{3}-\frac{a_\nu}{b_\nu}\right) e^{-\sqrt{3}\tau_2} - (1-\tfrac{2}{3}\sqrt{3})\,\eta_2\, e^{-2\sqrt{3}\tau_2}}{(1+\tfrac{2}{3}\sqrt{3})\left(\frac{q_2}{\sqrt{3}}+1\right)+(1-\tfrac{2}{3}\sqrt{3})\left(\frac{q_2}{\sqrt{3}}-1\right) e^{-2\sqrt{3}\tau_2}}. \quad (10)$$

The results of the computation of $J_\nu - B_\nu/B_\nu$ at $\tau_2 = 0.1$ are given in the last column of Table 7; below τ_2 this quantity decreases rapidly, as exp $(-q_2\tau)$.

TABLE 7

DEVIATIONS FROM THERMAL EMISSION

$\left(\frac{J_\nu - B_\nu}{B_\nu}$ at $\tau = 0.1$; $\frac{b_\nu}{a_\nu} = 10\right)$

η for Metal	Eq. (5) Unstratified $\eta_1 = \eta_2$	Eq. (8) $\eta_2 = 0$	Eq. (10) $\eta_1 = 0$
0	+1.11	+1.11	+1.11
1	+0.50	+1.23	+0.41
10	−0.082	+1.78	−0.41
100	−0.074	+2.56	−0.75
300	−0.023	+2.67	−0.80
∞	0.00	+2.89	−0.86

In Table 7 when $\eta = 0$ we see that the mean intensity exceeds the thermal value by a factor of 2; this arises from the large value of b_ν/a_ν in the ultraviolet. In the unstratified model and in that in which the hydrogen absorption line is formed *below* the metallic lines, the excess rapidly disappears as the hydrogen-line absorption coefficient increases, and there may be *less* than thermal intensity. We normally expect such a deficiency because a line decreases the flux at the boundary. Only when the hydrogen line is produced *above* the other elements does an *excess* appear from the damming-up of radiation. For a strong line, $\eta = \infty$, case 2 gives four times as much radiation as the unstratified case 1 and twenty-eight times as much as the oppositely stratified case 3. Our conclusion is that the presence of stratification of the level of origin of the hydrogen Lyman absorption lines may produce small but observable effects on the ionization of other elements with I.P. near that of hydrogen.

Let us return, briefly, to the possible existence of emission lines of hydrogen within the lower layers of a stellar atmosphere. It has been suggested by Menzel and Struve, in personal communications, that the atmosphere of a giant (or unstable dwarf) star may have an essentially filamentary structure, resembling prominence activity on a large scale. Let there be local fluctuations of density and temperature; since recombination emission depends on the square of the density, there may be considerable difference between adjacent regions with regard to emission and absorption lines. If the filaments

are small enough and relatively transparent, a considerable deviation from thermodynamic equilibrium may occur. The dynamics of such filaments, their lifetimes against dissipation by expansion or radiation, and their penetration of a resisting medium have not yet been investigated. The maintenance of such filaments at dwarf-star pressures seems difficult. We might consider that the filaments are caused by an instability at the top of the hydrogen convective zone and that the metallic-line stars are particularly unstable objects. We might thus also obtain selective ionization effects by Lyman emission lines even deep within an atmosphere. A further somewhat related effect of stratification is discussed below.

COLLISIONAL IONIZATION

Collisional ionization has seldom been considered in stellar atmospheres. If the kinetic energy of the colliding particle is the source of the ionization energy, the number of fast collisions decreases rapidly with increasing energy in the same manner as does the number of high-energy quanta. Collisions with protons of normal thermal velocities are negligible sources of ionization as compared to electron collisions. The requirement of conservation of momentum gives this result. Classically, for a head-on collision of a particle with mass, m_1, with a bound electron of mass, m_e, the kinetic energy, t, required to ionize the atom of I.P. $= I$, is

$$t \geqslant \frac{(m_1 + m_e)^2 I}{4 m_1 m_e}. \tag{11}$$

For proton collisions, $t \geqslant 460I$, and for electron collisions $t \geqslant I$. It is found[17] that such collisions have a cross-section of 10^{-16}–10^{-17} cm^2, at their maximum efficiency. If electron collisions were a source of ionization, they would produce no selective effects.

One type of collisional process, however, exists which can transfer considerable ionization energy, even when the kinetic energy is small. Such a phenomenon is the *Umladung* or "charge-transfer," in which an electron is exchanged between an ion and a neutral particle (or between a singly and a doubly ionized particle). Mott and Massey[18] review the theory and some laboratory observations of this interesting process. Either excitation or ionization is observed when a collision occurs between two different particles which have nearly the same excitation or ionization energies. Many laboratory sources of emission from highly excited levels of an atom depend on this phenomenon, which in this case transfers the excitation of a metastable atom of *He*, *A*, and *Ne* to the nonmetastable atom being excited. The near-equality of the ionization energies of two different particles results in a quantum-resonance which yields large cross-sections for the charge-transfer process. In our case we are interested in reactions of the form

$$H^+ + M + t \rightleftarrows H + M^+ + t' . \tag{12}$$

Here M is a metal whose second I.P. is near that of hydrogen, H, while t and t' are the initial and final kinetic energies. If $I(M) > I(H)$, higher kinetic energies are required; and therefore such a process will be less efficient in ionizing M, the reverse process of neutralization dominating. However, the kinetic energies required are small, depending only on $|I(M) - I(H)|$. The resonance need not be completely sharp in any case, because of the finite width of the levels in quantum theory. Morse and Stueckelberg[19] outline the theory, but unfortunately not in a form which would permit simple calculation of the type of process that we require, e.g., $H^+ + Ca^+ \rightarrow H + Ca^{++}$. Laboratory data are also confined to processes like proton interaction with H_2, N_2, *He*, *Ne*, and *A*. A few generalizations are possible. When conditions for resonance transfer of ionization are fulfilled,

[17] Kallmann and Rosen, *Phys. Zs.*, **32**, 540, 1931.

[18] *The Theory of Atomic Collisions* (Oxford: Clarendon Press, 1933), chap. xiii.

[19] *Ann. d. Phys.*, **9**, 579, 1931; *Helv. phys. acta*, **5**, 370, 1932.

the cross-sections are found to be near, or even to exceed, the gas-kinetic cross-section; values of $\sigma(MH^+) \approx 10^{-15}$ cm^2 occur. The cross-sections will drop rapidly, in a fashion similar to a typical quantum-resonance curve, as $|I(M) - I(H)|$ increases; the width of the resonance will be several electron-volts at stellar temperatures. Thus charge transfer may be a source of deviations of ionization from that predicted on the simple theory.

From the known conditions inside a stellar atmosphere we can determine whether collisional ionizations occur sufficiently frequently to be of importance. For simplicity, I omit the encounters with photons and the recombinations with electrons and first determine merely the rate of occurrence of specifically collisional effects. If the hypothesis here advanced should prove plausible, the simultaneous equilibria between collisional, radiative, and recombination processes will have to be discussed. Let there be $n(H)$ total particles of hydrogen and $n(M)$ particles of metal, M (the latter being the number in the singly ionized state); $n(H) \gg n(M)$. Let the number of protons be $Xn(H)$, and let V be the velocity of the protons (we shall neglect the motions of the heavy M particles). The number of ionized particles of M^+ produced per cubic centimeter per second is

$$n(M)\, n(H)\, \sigma(MH^+)\, X V\ , \tag{13}$$

where $\sigma(MH^+)$ is the cross-section for ionization of M by a proton. The converse collisional recombination, $M^+ + H \rightarrow M + H^+$, occurs at the rate

$$n(M^+)\, n(H)\, \sigma(M^+H)\, (1 - X)\, V\ . \tag{14}$$

In a steady state,

$$\frac{n(M^+)}{n(M)} = \frac{\sigma(MH^+)}{\sigma(M^+H)}\, \frac{X}{1 - X}. \tag{15}$$

The cross-sections are similar if $I(M)$ is near $I(H)$, so that the ionization of M tends toward that of H. If hydrogen is highly ionized, the collisional ionization may prove of importance in producing excess ionization over a narrow band of ionization potentials near that of hydrogen.

For simplicity, consider the rate of production of M^+, from equation (13); this rate can be computed if we take $n(H)$, X, and V from the model stellar atmospheres of B. Strömgren.[20] We adopt the equilibrium values of $n(H)$ and V:

$$n(H) = \frac{P_g}{kT}, \tag{16}$$

$$V = \left(\frac{2kT}{m_H}\right)^{1/2}. \tag{17}$$

It is possible that both the above values and the ionization of hydrogen, X, may require correction in abnormal regions of some stars. The number of ionizing collisions per cubic centimeter per second is

$$\frac{dn(M^+)_{\text{coll}}}{n(M)} = X P_g \sigma(MH^+) \left(\frac{2}{m_H kT}\right)^{1/2}. \tag{18}$$

The number of radiative ionizations of M depends somewhat on the nature of the ionization continuum from the ground state. If we write, approximately, the continuous absorption coefficient beyond the series limit, a_ν as

$$a_\nu = a_0 \left(\frac{\nu_0}{\nu}\right)^n, \tag{19}$$

[20] *Pub. Københavns Obs.*, No. 138, 1944.

we find the number of radiative ionizations per cubic centimeter per second from

$$\frac{dn(M^+)_{\text{rad}}}{n(M)} = 4\pi \int_{\nu_0}^{\infty} \frac{B_\nu a_\nu d\nu}{h\nu}. \tag{20}$$

The thermal emission, B_ν, can be approximated at these temperatures and energies by

$$B_\nu = \frac{2h\nu^3}{c^2}\, e^{-h\nu/kT}. \tag{21}$$

If we write

$$x_0 = \frac{h\nu_0}{kT}, \tag{22}$$

we find

$$\frac{dn(M^+)_{\text{rad}}}{n(M)} = \frac{8\pi a_0 \nu_0^n}{c^2}\left(\frac{kT}{h}\right)^{3-n} \int_{x_0}^{\infty} x^{2-n} e^{-x} dx. \tag{23}$$

The integral proves quite insensitive to n for reasonable values; for either $n = 2$ or $n = 3$, equation (23) reduces to

$$\frac{dn(M^+)_{\text{rad}}}{n(M)} = \frac{8\pi a_0 \nu_0^2 kT}{hc^2}\, e^{-h\nu_0/kT}. \tag{24}$$

Most of the contributions to radiative ionization come from the region near the series limit. Finally, we write the ratio of the number of collisional to radiative ionizations as follows:

$$\frac{dn(M^+)_{\text{coll}}}{dn(M^+)_{\text{rad}}} = \frac{\beta\sigma(MH^+)}{a_0}, \tag{25}$$

where

$$\beta = 0.0145\, XP_g\, e^{h\nu_0/kT} T^{-3/2}. \tag{26}$$

Collisional effects dominate when P_g is large and X approaches unity. The ratio $\sigma(MH^+)/a_0$ can be as large as 100 if the resonance is favorable, since a_0 seldom exceeds 10^{-17}.

Computations of X and β for some model atmospheres[20] are contained in Table 8; the abundance of hydrogen adopted was $\log A = 3.8$, and the second I.P. of the metal, M, was taken equal to that of hydrogen, 13.54 volts. The surface gravity, $\log g = 3.5$, is near that of a giant, and $\log g = 4.5$ near that of a dwarf. Models for supergiants or for a star with low effective gravity like τ UMa were not available. It can be seen that there are two conflicting effects; β increases but X decreases as the temperature decreases. Collisional ionization may become the overwhelmingly frequent process in cooler stars (10^6 more frequent than radiative ionization); but the level of second ionization of M could not then be very high, according to equation (15), since the reverse process dominates. The pressure dependence is not large. In the model with $\theta_0 = 0.8$, which is close to a dwarf F star, computations were made at three optical depths; β decreases with depth but X increases. Below $\tau = 1$, hydrogen is appreciably ionized, and there probably would be appreciable excess collisional ionization, even though β is not very large (i.e., collisional rate 10^4 times radiative rate).

We have not included the possibility of deviations of physical conditions in the star from a static normal model. It has often been suggested there may be an excess of rapidly moving protons entering the lower layers of an atmosphere from the hydrogen-convective zone. Such a model would result in quite complex changes of the ionization equilibrium of the atmosphere, but it would also particularly increase the effectiveness of collisional

ionization. The pattern of abundance deficiencies produced by resonance collision with hydrogen would bear a marked resemblance to that presented in Figures 4 and 5, i.e., the deficiencies would disappear as $|I(M) - I(H)|$ increases.

TURBULENCE AND SURFACE GRAVITY

We have indicated a possibility that the abundance deficiencies in τ UMa may depend sensitively on the peculiarities of the ionization of hydrogen in the star. Supergiants have somewhat unstable atmospheres, large turbulence, and mass motions; many have slightly variable radial velocity. The supergiants α Per and ρ Pup show in smaller degree the apparent low abundances of the same elements as τ UMa. If convection produces a greater than normal instability in the atmosphere of a dwarf star, it might also be responsible for the turbulence and such apparent abundance deficiencies in τ UMa.

Extensive work on the curves of growth of supergiants shows that there is a correlation (perhaps even a unique relation) between turbulence and increasing luminosity. Few dwarfs have as yet been investigated; Be and Ae stars have turbulence in their shells, but the turbulence in the sun is only about 1 km/sec. The turbulent velocity is apparently well determined from the curves of growth; it remains an arbitrary parameter out-

TABLE 8

RATIO OF RESONANCE COLLISION TO RADIATIVE IONIZATIONS

τ	1		0.1	1		5	1		1	
θ_0	0.7		0.8	0.8		0.8	0.9		1.0	
log g	3.5	4.5	4.5	3.5	4.5	4.5	3.5	4.5	3.5	4.5
log X	−0.72	−1.06	−2.81	−1.60	−1.95	−0.70	−2.42	−2.76	−3.15	−3.48
log β	+2.34	+2.81	+4.29	+3.18	+3.55	+2.41	+3.94	+4.15	+4.55	+4.81

side the theory of normal stellar atmospheres. The thermal velocity for a metal of atomic weight $\mu = 60$ is 1.3 km/sec at 6000°; in τ UMa the total velocity from the average curve of growth of the metals is 4 km/sec (Paper I, Table 7). The turbulent velocity is then 3.8 km/sec; to my knowledge it is the only dwarf with appreciable turbulence. The mean kinetic energy for a metal is thus nine times as large as expected, and a kinetic temperature of 54,000° is indicated. If this were a true kinetic temperature a light element, for example, *Ca* I, should show a velocity $(139/40)^{1/2}$, or 1.9 times greater than a heavy element, such as *La* II. Such an effect should be visible as a raising of the nearly flat part of the curve of growth of *Ca* (Paper I, Fig. 2) by about 0.25 in log W/λ with respect to that of *La* II. While the curves are not well enough defined to exclude this, such an increase in V seems improbable; furthermore, it would result in an apparent systematic increase in the abundance of the light elements as compared to the heavy elements in a star with turbulence. This is opposite to the small systematic effect observed. The test from line contours is not possible because of an apparent slight rotational broadening of the lines of τ UMa. The turbulence in the sun may possibly be large enough to permit a more critical examination of the dependence of line contour and curve of growth on atomic weight.

We should not conclude from the apparent high kinetic temperatures of the heavy elements alone that the turbulent motions contribute much to the total kinetic-energy content of the atmosphere. If the turbulence is of the normal type,[21] with hydrogen also having a turbulent motion of only 3.8 km/sec, this turbulence is negligible in comparison to the thermal motion of hydrogen, which is 10 km/sec. Because of the enormous abun-

[21] McCrea, *M.N.*, **89**, 718, 1929.

dance of hydrogen,[22] the total kinetic energy of the atmosphere is dominated by the normal thermal motion of hydrogen. It would be very important to obtain reliable line contours of the *O* and *N* lines in a supergiant F star of large turbulence, since they might clearly show whether the velocities depend on the atomic weight. There may be some true local heating at the interface between turbulent elements, which may appear in the form of diluted high-temperature radiation and excitation, if a sufficiently large fraction of the atmosphere is so heated. In the picture of normal turbulence, however, there will not be a complete degeneration of the turbulence into high-temperature thermal motion and atomic excitation. Shock waves or noise originating from the turbulent motion of the granules has been suggested as a source of the excitation of the solar chromosphere and corona.[23] Such a superficial heating as an indirect result of lower-level turbulence may account for part of the support of the outer envelope of a star. Such support may be correlated with another phenomenon common to F supergiants and τ UMa, the reduction of the effective surface gravity, g_e. The density gradient in an atmosphere is given by $\exp(-\mu m_H g h/kT)$. Since the observed motions of the heavy elements correspond to a mean kinetic energy nine times the thermal value (kT), the value of g_e might be about one-ninth the expected gravitational value, g. The problem is again complicated by the unknown dependence of the mean kinetic energy per particle on its atomic weight. In the turbulent motions of prominences there is no separation of heavy and light elements because of the diffusion drag of hydrogen on the heavy elements. It is quite reasonable to ascribe the reduction of g_e, at least in part, to turbulence. According to Paper I, Table 7, $g_e/g = 0.004$ in τ UMa and about 0.1 in the two supergiants. Radiative support or large-scale motions may also exist. If, as a working hypothesis, we ascribe atmospheric instability to the convective layer of the star, we may ask whether τ UMa does not owe its low surface gravity, its turbulence, and its peculiar abundances of the elements all to the same cause—the disturbance of its lower atmosphere by currents of ionized gas.

[22] I am indebted to Dr. Martin Schwarzschild for this argument.

[23] Biermann, *Naturwiss.*, **33**, 118, 1946; M. Schwarzschild, *Ap. J.*, **107**, 1, 1948.

VARIATIONS IN THE STELLAR LUMINOSITY FUNCTION
II. A REGION IN ORION

S. W. McCUSKEY
Warner and Swasey Observatory, Case Institute of Technology
Received October 13, 1948

ABSTRACT

An analysis of the galactic structure in Orion (R.A. 6^h14^m; Dec. $+14°0$) by means of spectra, photographic magnitudes, and colors indicates a slight excess of stars with $-1 < M < 1$ and a deficiency of stars with $M > 1$, as compared to the standard van Rhijn luminosity function, at distances less than 400 parsecs. The deficiency among the intrinsically fainter stars is 0.3 in log $\varphi(M)$ on the average. On the other hand, an excess of 0.5 in log $\varphi(M)$ for $M < +2$ and an excess of 0.2 for $M > +2$ is indicated at 600 parsecs. The photographic absorption in the region amounts to 2.8 mag. at 2500 parsecs.

INTRODUCTION

This analysis of the galactic structure in the northern part of Orion, based upon spectral types, photographic magnitudes, and colors, is a continuation of the work outlined in a preceding issue of the *Astrophysical Journal*.[1] The field, labeled "LF8," center R.A. 6^h14^m; Dec. $+14°$; $l = 165°$; $b = +1°$, is near the boundary of Orion, Monoceros, and Gemini and includes Selected Area 74 in its northeastern portion. The study is part of a large-scale program, now under way at the Warner and Swasey Observatory, to improve our knowledge of the fluctuations in the stellar luminosity function in the Milky Way. In the first paper of the series, McCuskey and Seyfert[1] presented results for regions in Aquila (LF1) and Cygnus (LF2). It was found in those two regions that the observed values of log $\varphi(M)$[2] exceeded the values given by the standard van Rhijn luminosity function by about 0.3 in the range $-2 < M < +1$. A deficiency of about the same amount was indicated in the magnitude range $+2 < M < +4$.

OBSERVATIONAL DATA

Spectral types have been determined for some sixteen hundred stars in LF8. Both 4° and 2° prisms attached to the 24-inch Burrell telescope were used to obtain the spectra on Eastman II*a*-O plates. Primary classification of spectra was obtained from the plates taken with the 4° prism arrangement, the 2° dispersion being used to resolve overlaps. The spectra were classified on from four to six plates, in order to make the survey as complete and the classification as accurate as possible. As shown by the distribution in Table 1, very few stars brighter than $m_{pg} = 12$ were omitted, while between magnitudes 12 and 12.5 there are 111 stars for which no classification could be made. A few stars fainter than magnitude 12.5 were observed but are not included in the table. The spectral types, photographic magnitudes, and colors for individual stars will be published in the near future in a separate paper.

Luminosity classes on the Morgan, Keenan, and Kellman[3] system have been given for nearly all stars of type F0 and later and brighter than $m_{pg} = 11.0$. Giant (III) and dwarf (V) classes have been assigned for fainter stars of class G5 and later, where the

[1] *Ap. J.*, **106**, 1, 1947.

[2] The quantity $\varphi(M)$ is the number of stars per cubic parsec in the neighborhood of the sun with absolute magnitudes between $M - \frac{1}{2}$ and $M + \frac{1}{2}$.

[3] *An Atlas of Stellar Spectra* (Chicago: University of Chicago Press, 1943).

TABLE 1

OBSERVED SPECTRAL DISTRIBUTION IN LF8

(Area 17.3 Sq. Deg.)

m_{pg}*	B0	B2	B3	B5	B8	B9	A0	A2, 3	A5	F0 III	F0 V	F2 III	F2 V	F5 III	F5 V	F8 III	F8 IV	F8 V	G0 III	G0 IV	G0 V
≤ 6.00	0	0	1	0	3	0	2	0	0	0	0	0	1	0	0	0	0	0	0	0	0
6.25	0	0	0	0	1	0	0	0	0	1	0	0	0	0	0	0	0	0	0	0	0
6.75	0	0	0	1	1	0	0	0	0	0	0	0	0	0	0	0	0	0	0	0	0
7.25	0	0	0	1	4	0	2	0	0	0	0	1	0	0	0	0	0	1	0	1	0
7.75	0	1	0	0	3	1	1	0	0	0	0	0	0	0	0	0	0	0	0	0	0
8.25	0	0	0	2	1	6	1	3	0	1	0	0	0	0	1	0	0	1	0	1	0
8.75	0	0	1	6	5	0	7	3	1	2	0	1	2	0	0	0	0	2	0	1	0
9.25	1	0	0	4	7	4	1	7	1	0	2	0	1	0	2	0	0	0	2	0	1
9.75	0	0	1	5	22	5	4	8	1	0	0	0	2	0	0	0	0	3	0	0	1
10.25	2	0	0	6	5	8	5	6	3	1	3	1	2	1	1	0	0	3	0	0	3
10.75	1	0	0	6	11	15	9	16	1	1	5	0	8	0	6	0	1	7	0	1	6
11.25	0	1	1	5	24	32	46	15	12	13		11		9		20			32		
11.75	1	2	0	7	19	22	49	19	9	16		11		13		18			58		
12.25	0	1	0	3	44	32	69	37	8	16		7		5		22			90		
Total	5	5	4	46	150	125	196	114	36	61		48		38		78			197		

m_{pg}*	G2 III	G2 IV	G2 V	G5† III	G5† IV	G5† V	G8 III	G8 IV	G8 V	K0 III	K0 IV	K0 V	K2, 3 III	K2, 3 IV	K2, 3 V	K5–M8† III	K5–M8† V	Unclassified‡	All Stars
≤ 6.00	0	0	0	0	0	0	0	0	0	0	0	0	0	0	0	0	0	0	7
6.25	0	0	0	0	0	0	0	0	0	0	0	0	0	0	0	0	0	0	2
6.75	0	0	0	0	0	0	0	0	0	0	0	0	0	0	0	0	0	1	3
7.25	0	0	0	0	0	0	1	0	0	1	0	0	0	0	0	1	0	1	14
7.75	0	0	0	0	0	0	1	0	0	1	0	0	0	0	0	0	0	0	8
8.25	0	0	0	0	0	0	0	0	0	2	0	0	0	0	0	0	0	2	21
8.75	0	1	0	0	0	0	0	2	0	4	2	0	0	0	0	0	0	1	41
9.25	0	0	0	1	1	1	0	1	0	7	0	1	1	0	0	0	0	3	49
9.75	0	3	0	5	0	0	2	4	0	7	1	0	1	0	2	0	0	1	78
10.25	0	0	1	1	2	1	3	0	0	2	2	0	1	0	0	0	1	3	67
10.75	0	1	1	2	2	5	5	4	0	5	4	1	1	0	1	0	0	6	132
11.25		4		3	2	11	4	7	8	12	3	3	3	(1)	1	1	0	11	295
11.75		6		3	(6)	9	5	4(2)	3	5	(2)	2	3	(1)	0	1	0	13	309
12.25		6		0	(24)	5	6	(21)	1	6	(14)	1	0	(3)	1	(3)	0	111	536
Total		23			84			84			88			20			7	153	1562

* The entries under m_{pg} are representative of half-magnitude intervals, e.g., 7.01–7.5, 7.51–8.0, etc.

† Parentheses around entries for faint groups of spectral classes G5 to M8 indicate the number of stars to which luminosity classes could not be assigned.

‡ Included under the heading "Unclassified" are: double stars too close together to show separate spectra; stars showing composite spectra or peculiar spectra; sixteen stars of the cluster NGC 2169; stars with spectra unclassifiable because of overlap.

spectrum was sufficiently exposed to warrant it. Criteria for the detailed luminosity classification have been published by Nassau and van Albada.[4] For $m_{pg} > 12$, the recognition of giants and dwarfs becomes uncertain in most cases.

A comparison of the spectral types assigned here with those of the *Henry Draper Catalogue* indicates a tendency for the HD classes to be slightly later than ours at A0 and at K0. This trend, however, is not pronounced. Ninety-eight stars were available for the comparison.

Photographic magnitudes for all stars brighter than 12.5 were measured on four plates. The required sequence was established in SA 74 by means of double-exposure plates, with the North Polar Sequence for calibration. The part of the sequence which could be checked by comparison with photographic magnitudes given by Seares, Kapteyn, and van Rhijn[5] showed no striking systematic difference between the two. The average probable error of a final blue magnitude for a field star is ± 0.05 mag.

Photored magnitudes of some seven hundred stars of early spectral type have been obtained in order to study the interstellar reddening in the region. Eastman 103*a*-E plates with a No. 22 Wratten filter were used. The effective wave length of the combination is about λ 6200. In this case, also, a sequence was established by comparison with the NPS on multiple-exposure plates. Red magnitudes for the NPS stars were taken from a paper by Nassau and Burger[6] and were corrected slightly at the faint end of the sequence by means of unpublished material supplied by the same authors. The probable error of a final red magnitude, based on the measurement of four plates, is ± 0.04. All the photometry, blue and red, was done with a graduated scale of stellar images on plates taken with the Burrell telescope.

Counts of faint stars have been made on an Eastman 103*a*-O plate of 10 minutes' exposure time. Calibration of the counts was effected with the magnitudes published for SA 74 in the *Mount Wilson Catalogue of Selected Areas*. The counts extend to $m_{pg} = 17$, the sky covered being 1.15 square degrees in four areas symmetrically situated with respect to the center of the field.

SUMMARY OF DATA FOR ANALYSIS

Table 1 contains a statistical summary of the spectral distribution as a function of photographic magnitude for LF8. The grouping has been made somewhat more detailed than usual, in order that the material might be more useful to others. In forming the functions log $A'(m)$[7] for analysis, several spectral classes have been grouped together. The area of the sky covered by LF8 is 17.3 square degrees.

For the stars with $m_{pg} \leqslant 7.0$, values of log $A'(m)$ derived from Seydl's[8] counts of *Henry Draper Catalogue* data have been used. These are published, for suitable spectral groups, in the first paper[9] of this series (hereafter called "Paper I"). These counts refer to the galactic-latitude zones 0° to $\pm 10°$ at all longitudes.

In the magnitude range $6.5 < m < 9.0$, the data for analysis are strengthened by counts according to spectral type and apparent magnitude made in the *Henry Draper Catalogue* for an area of 100 square degrees centered at LF8. These data are presented in Table 2.

The average observed red indices (R.I.) for LF8 are given in Table 3. The number in parentheses following a tabular entry indicates the number of stars involved in the average. Data for thirty-one late-type stars are included for a check of the zero point of

[4] *Ap. J.*, **106**, 20, 1947.

[5] *Mount Wilson Catalogue of Photographic Magnitudes in Selected Areas 1–139.*

[6] *Ap. J.*, **103**, 25, 1946.

[7] $A'(m)$ is the number of stars per 100 sq. deg. with magnitudes between $m - \frac{1}{4}$ and $m + \frac{1}{4}$.

[8] *Pub. Obs. Nat. Prague*, No. 6, 1929.

[9] *Ap. J.*, **106**, 5, 1947.

the color system. Since very few dwarfs of types G8 and later were found among the stars brighter than the eleventh magnitude, data for these groups have not been included. Normal red indices and mean absolute magnitudes required in computing the color excess–distance relation are given in the second and third columns. These values are the same as those adopted in Paper I. Twelve stars of types earlier than B5 have also been measured for color. In the analysis which follows, they will be used individually to strengthen the conclusions relative to interstellar reddening in this region. The probable error of a red index is ± 0.06 mag.

TABLE 2

DISTRIBUTION OF SPECTRAL TYPES FROM THE *Henry Draper Catalogue* FOR THE REGION SURROUNDING LF8

(Area 100 Sq. Deg.)

m_{pg}	Spectral Type									All Stars
	B0–B2	B5	B8–A0	A2–A5	F0–F5	F8–G0	G5	K0–K2	K5–M	
6.51–7.00	0	1	7	1	1	0	0	1	0	11
7.01–7.50	1	3	17	0	3	3	4	7	2	40
7.51–8.00	1	5	35	16	9	0	3	8	0	77
8.01–8.50	0	2	58	16	12	4	7	10	0	109
8.51–9.00	0	1	62	16	20	15	13	21	3	151

TABLE 3

AVERAGE OBSERVED RED INDICES IN LF8

Spectrum	Norm.	$\bar{M}$	m_{pg}							
			8.01–9.00	9.01–10.00	10.01–10.50	10.51–11.00	11.01–11.50	11.51–12.00	12.01–12.50	12.51–13.00
B5	−0.53	−1.0	−0.42(9)	−0.20(10)	+0.05(5)	+0.11(7)	+0.16(6)	+0.40(6)	+0.39(3)	.....
B8	− .46	−0.5	− .23(7)	− .22(29)	+ .01(5)	+0.15(12)	+ .20(25)	+ .26(16)	+ .44(40)	+0.50(10)
B9	− .32	0.0	− .17(4)	− .14(9)	− .18(8)	+0.04(15)	+ .22(30)	+ .33(22)	+ .45(30)	+ .46(17)
A0	− .20	+0.5	− .16(8)	− .14(4)	+ .01(5)	+0.15(8)	+ .28(43)	+ .31(49)	+ .46(61)	+ .55(30)
A2, 3	− .07	+1.5	− .01(5)	− .08(15)	+ .10(6)	+0.30(16)	+ .39(15)	+ .42(19)	+ .52(36)	+ .54(19)
A5	.00	+1.7	.....	+ .18(2)	+ .17(3)	.....	+0.43(11)	+0.47(8)	+0.56(5)	+0.67(2)
F8V	+ .40	.....	+0.58(3)	+ .27(3)	+ .61(3)	+0.55(5)	.....	.....	.....	.....
G0V	+ .46	.....	.....	+ .12(1)	+ .59(3)	+0.62(4)	.....	.....	.....	.....
G2V	+ .60	.....	.....	.....	+ .45(1)	+1.03(1)	.....	.....	.....	.....
G5V	+0.84	.....	.....	+0.45(1)	+0.36(1)	+0.68(5)	.....	.....	.....	.....

ANALYSIS OF THE OBSERVATIONAL DATA

COLOR EXCESSES AND PHOTOGRAPHIC ABSORPTION

Color excesses of the late-type dwarf stars deduced from Table 3 indicate that the red indices are too large by about 0.03 mag. If the stars of class G5 V are omitted, however, this zero-point difference amounts to 0.10 mag. Since these stars are near by, such an excess presumably cannot be ascribed to interstellar reddening. A similar trend is shown by the A stars with $m_{pg} < 10.0$. This is evident from the plot of color excess (E_r) against uncorrected distance modulus, shown in Figure 1.

Whether this excess is inherent in the color indices as measured or results from an assumption of too blue an intrinsic index for these stars is uncertain. Morgan and Bidelman[10] have presented some evidence that the normal blue-yellow color indices for stars of classes A0, A2–3, and A5 should be −0.04, 0.00, and +0.07, instead of −0.15, −0.04,

[10] *Ap. J.*, **104**, 245, 1946.

and 0.00, which have been used here as a basis for deriving normal red indices. On the other hand, in the analyses of color data for LF1 and LF2, color excesses of +0.14 and +0.03 mag., respectively, for the late-type dwarfs were found. In view of the wide divergence of zero point in measures presumably made as nearly as possible in the same way, we shall accept the intrinsic red indices as given in Table 3. In computing, therefore, the run of photographic absorption (A_{pg}) from the values of E_r provided by the curve of Figure 1, a zero-point correction of −0.1 mag. has been applied. The variation of A_{pg} with true distance is shown in Figure 2. A factor $A_{pg}/E_r = 2.6$ was used to convert color excesses into total absorption. This ratio is the same as that adopted in Paper I.

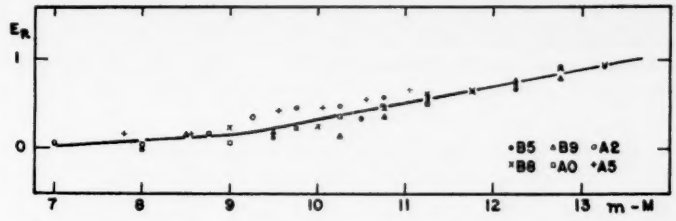

FIG. 1.—Red color excess, E_r, as a function of uncorrected distance modulus for early-type stars

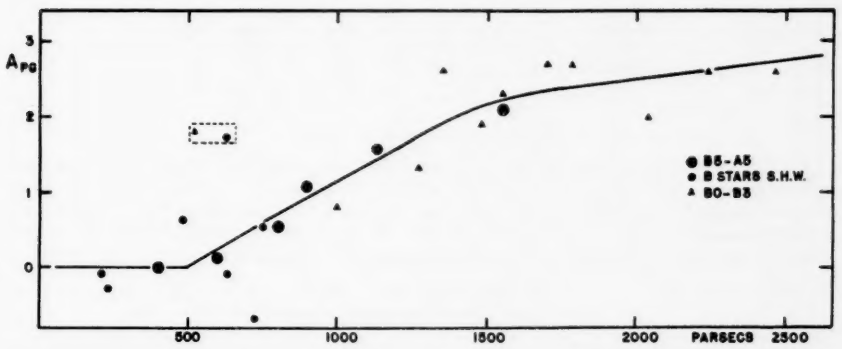

FIG. 2.—Total photographic absorption, A_{pg}, as a function of true distance. Large filled circles represent points obtained from B5–A5 color-excess data given in Fig. 1. Small circles represent color data of Stebbins, Huffer, and Whitford. Triangles represent A_{pg} (from red color-excess data for faint stars earlier than B5 as determined in the present survey. The box indicates star HD 44637.

Eight early-type B stars, measured for color photoelectrically by Stebbins, Huffer, and Whitford,[11] lie within LF8. These are shown in Figure 2 and confirm the fact that little or no absorption occurs in this region out to 500 parsecs. The one unusually reddened star, HD 44637 B3e, provides a comparison between the photoelectric colors and ours. The other stars are too bright to be measured in the routine photometry here. A factor of 9 was used to convert E_1 on the photoelectric scale to A_{pg}.

Twelve fainter B0–B3 stars for which red indices were obtained from our plates yielded values of A_{pg}, which have been plotted individually in Figure 2.

We conclude that in this region the absorption sets in at about 500 parsecs, reaches 2.2 mag. at 1500 parsecs, and is 2.8 mag. at 2500 parsecs. These results agree with those

[11] *Ap. J.*, 91, 20, 1940.

of Bok, Boutelle, and Olmsted,[12] who have studied the space reddening and absorption at $l = 165°$, $b = 0°$, and have found 1.2 mag. per kiloparsec for A_{pg}.

SEPARATION OF GIANTS AND DWARFS

In the absence of a sufficient number of brighter stars in any one of the "luminosity-function" regions, little can be said, from our data alone, about the percentages of giant and dwarf stars. For the most part, therefore, a separation of these two groups has been made in the same manner as that described in Paper I, viz., by relying on the published results of others and by adjusting the percentages for the fainter stars so that the computed numbers of giants and dwarfs agree reasonably well with the observed numbers from our data. Again the G5 stars have been treated as a group by themselves because of the rapidly changing giant-dwarf ratio at this class. Table 4 gives the adopted percentages of dwarf stars. The K5–M8 stars were not included, since they are so scarce in this region.

TABLE 4

ADOPTED PERCENTAGES OF DWARF STARS

SPECTRAL GROUP	m_{pg}		
	$\leqslant 8.5$	8.5–10.5	>10.5
F8–G2	30	45	60
G5	20	40	70
G8–K3	4	10	35

ADOPTED VALUES OF LOG $A'(m)$

After grouping the entries of Table 1 according to the same subdivisions as those used in Paper I and expanding these numbers to refer to 100 square degrees of the sky, plots of the resulting log $A'(m)$ against m were made for each spectral group. Freehand smooth curves through the points were used to obtain the values of log $A'(m)$ at half-magnitude intervals necessary for density analyses. The adopted values of log $A'(m)$ are given in Table 5.

COMPUTED DENSITY FUNCTIONS

The number of stars per 1000 cubic parsecs as a function of distance for each spectral group is exhibited in Table 6. An (m, log π) tabular analysis was used to obtain these densities. In order to insure uniformity of treatment with the previously published results for LF1 and LF2, the same mean absolute magnitudes and dispersions have been used here. They are given in Paper I, Table 12. The density values of Table 6 have been corrected for interstellar absorption according to the curve presented in Figure 2.

One may summarize the results of these computations as follows:

1. The B8–A0 stars, which form a large percentage of the whole, decrease very slowly in space density to a distance of 1000 parsecs from the sun, with an indication of clustering at 600 parsecs. In the next 500 parsecs they become 2.5 times as numerous; and this higher density persists to the limit of the survey, 2000 parsecs. A similar trend is evident in the space density of gF8–G2 stars. There appears to be a concentration of these objects at about 1500 parsecs distance.

2. Both the gG5 and the gG8–K3 stars decrease in numbers with distance until, at 1000 parsecs, the density is about 0.1 of that near the sun. Beyond that point, however,

[12] *A.J.*, **53**, 197, 1948.

the density of gG5 stars remains constant at a low level, while the density of the gG8–K3 group increases to a value at 1500 parsecs nearly equal to that in the neighborhood of the sun.

3. Both the A2–A5 and the F0–F5 stars decrease rapidly in numbers in the first 500 parsecs to a density about 0.2 that near the sun. Between 500 and 1000 parsecs there is some evidence for a secondary maximum in the numbers of F0–F5 stars.

4. The dwarf stars of classes G5 and G8–K3 decrease rapidly in number with distance within the first 500 parsecs. Beyond that point the data are incomplete. On the other

TABLE 5

ADOPTED VALUES OF LOG $A'(m)$ FOR REGION LF8

m_{pg}	B5	B8–A0	A2–A5	F0–F5	F8–G2		G5		G8–K3	
					g	d	g	d	g	d
4.0	9.12	9.00	9.28	8.90	9.10	8.70	8.40	7.80	9.27	7.90
4.5	9.20	9.40	9.46	9.17	9.10	8.73	8.70	8.10	9.50	8.15
5.0	9.32	9.75	9.66	9.42	9.12	8.78	9.00	8.39	9.74	8.40
5.5	9.50	0.10	9.85	9.70	9.21	8.83	9.30	8.69	0.02	8.69
6.0	9.75	0.47	0.08	9.98	9.40	9.03	9.62	8.98	0.30	8.92
6.5	0.00	0.80	0.31	0.23	9.70	9.34	9.94	9.27	0.55	9.16
7.0	0.29	1.11	0.60	0.50	9.98	9.64	0.20	9.56	0.78	9.38
7.5	0.59	1.40	0.90	0.78	0.25	9.94	0.45	9.85	0.92	9.58
8.0	0.89	1.60	1.16	1.02	0.50	0.23	0.65	0.11	1.07	9.80
8.5	1.17	1.77	1.30	1.25	0.74	0.52	0.82	0.40	1.26	0.19
9.0	1.38	1.88	1.44	1.40	0.95	0.80	1.00	0.63	1.58	0.60
9.5	1.48	2.00	1.58	1.40	1.16	1.02	1.12	0.90	1.76	0.88
10.0	1.50	2.10	1.71	1.48	1.36	1.30	1.22	1.13	1.82	1.10
10.5	1.52	2.24	1.86	1.90	1.56	1.60	1.30	1.39	1.90	1.33
11.0	1.52	2.47	2.01	2.19	1.80	1.94	1.38	1.62	1.96	1.56
11.5	1.52	2.70	2.18	2.29	2.15	2.30	1.44	1.85	2.10	1.76
12.0	1.52	2.90	2.32	2.30	2.43	2.60	1.50	2.05	2.26	1.97
12.5	1.54	3.16	2.50	2.30	2.69	2.91	1.60	2.23	2.40	2.20

TABLE 6

DENSITY FUNCTIONS IN LF8

(Number of Stars per 1000 Cubic Parsecs)

DISTANCE (PARSECS)	SPECTRAL GROUP										ALL
	B5	B8–A0	A2–A5	F0–F5	dF8–G2	dG5	dG8–K3	gF8–G2	gG5	gG8–K3	
100	0.010	0.08	0.40	1.0	1.0	4.0	4.0	0.08	0.10	0.40	11.07
200	.005	.08	.20	1.0	0.8	2.0	5.0	.05	.08	.40	9.62
300	.005	.08	.17	0.5	0.8	1.3	0.8	.03	.06	.20	3.95
400	.005	.10	.10	0.1	0.8	1.0	0.1	.03	.04	.16	2.44
500	.003	.09	.10	0.1	1.0	1.0	0.5	.03	.02	.08	2.92
600	.005	.17	.10	0.2	2.4	2.4	3.8	.07	.02	.13	9.30
800	.008	.08	.09	0.5	5.9	.....	.....	.05	.02	.08	6.73
1000	.017	.05	.10	0.4	.....	.....	.....	.10	.02	.05	0.74
1200	.010	.10	.21	0.2	.....	.....	.....	.41	.002	.10	1.03
1400	.003	.22	0.13	.....	.....	.....	.....	.57	.01	.25	1.18
1600	.002	.28	.....	.....	.....	.....	.....	0.36	0.02	0.40	1.06
1800	.0004	.26	.....	.....	.....	.....	.....	.....	.....	.....	0.26
2000	0.0005	0.28	.....	.....	.....	.....	.....	.....	.....	.....	0.28

hand, the dF8–G2 stars remain sensibly constant in density in the first 500 parsecs and thereafter increase rapidly. At 750 parsecs they appear to be nearly five times as numerous as near the sun.

5. Finally, attention should be drawn to the probable concentration of B5 stars at a distance of 1000 parsecs. There the high density follows a rapid decline in numbers within the first 500 parsecs; at 500 parsecs the density is about one-third, while at 1000 parsecs it is 1.7 times as large as the density in the solar neighborhood. The concentration appears to be real and is reflected in the relatively large number of ninth- and tenth-magnitude B5 stars shown in Table 1.

DENSITY DISTRIBUTION FROM GENERAL STAR COUNTS

Star counts to $m_{pg} = 17.0$ in four areas symmetrically situated with respect to the center of LF8 furnish the data for a more general density analysis based on the standard van Rhijn luminosity function.[13] The total area of the sky involved in these samples is 1.15 square degrees. Calibration for the fainter stars was obtained from the magnitudes published for SA 74 in the *Mount Wilson Catalogue of Photographic Magnitudes in Selected*

TABLE 7

LOG $N(m)$ FROM STAR COUNTS IN LF8

m_{pg}	LF8 Counts	A.C.R. Counts	GP43 (Table 10)
9	0.71	0.85	0.58
10	1.11	1.18	1.09
11	1.46	1.53	1.49
12	1.82	1.82	1.84
13	2.20	2.15	2.19
14	2.53	2.47	2.58
15	2.83	2.79	2.94
16	3.14	3.12	3.26
17	3.45	3.45	3.56

Areas 1–139. These magnitudes tie in satisfactorily with the sequence established for the brighter stars described in a preceding paragraph.

Table 7 contains the observed values of log $N(m)$, where $N(m)$ is the number of stars brighter than magnitude m. For comparison I have included in the third column values already published[14] in the course of another survey. Two of the "Anticenter Regions" (A.C.R.), in which counts were made four years ago, Nos. 6 and 7, lie within LF8. The area of these two regions is 1.55 square degrees, in which a total of 7989 stars was counted. The last column of Table 7 gives the smoothed values of log $N(m)$ for the appropriate latitude and longitude taken from the work of van Rhijn, *Groningen Publications*, No. 43, Table 10. In general, the agreement between these sets of values is good, the only departures being in the numbers provided by GP43 for the faintest stars.

The relative density, $D(r)$, has been computed from the data of the second column of the table. An (m, log π) tabular analysis was used, with absorption corrections taken from Figure 2. The required table for $b = +1°$ was obtained by interpolation from those given by Bok and MacRae,[15] which are based on the van Rhijn luminosity function, corrected for changes with height above the galactic plane.

[13] *Groningen Pub.*, No. 47, p. 17, 1936.

[14] McCuskey, *Ap. J.*, **102**, 32, 1945.

[15] *Ann. New York Acad. Sci.*, **42**, 252 ff., 1941.

Table 8 contains in the second column the relative density so computed. The third column gives the density relative to that at 100 parsecs obtained by summing the results for the various spectral groups in LF8 (Table 6). The striking difference between these two functions is sufficient evidence for a considerable departure of the actual luminosity function in this region from the standard function usually employed in star-count analysis. In the last column of Table 8 are given the densities published previously [14] for A.C.R. regions 6 and 7. The marked differences between the second and fourth columns arise from the very low absorption value, 0.4 mag. per kiloparsec, used in the previous computation. While over the broad longitude range 160°–173° the Stebbins, Huffer, and Whitford B-star data indicate such a low value of the absorption, in LF8 the local reddening appears to be considerably greater. Hence the revised densities given in the second column are considered to be more representative of this local area. The differences illustrate clearly the disagreeable uncertainties arising in this type of analysis due to fluctuations in the absorption.

TABLE 8

RELATIVE DENSITY FUNCTIONS IN LF8

Distance (Parsecs)	$D(r)$ (Counts)	$D(r)$ (Spectra)	$D(r)$ (A.C.R. Counts)
100	1.50	1.00	1.00
200	1.40	0.87	1.45
300	1.00	0.36	1.30
400	0.80	0.22	1.00
500	0.56	0.26	0.85
600	0.40	0.84	0.70
800	0.50	.....	0.45
1000	0.70	.....	0.20
1500	0.82	.....	0.14
2000	0.90	.....	0.11

VARIATIONS IN THE LUMINOSITY FUNCTION

As in Paper I, the luminosity function, $\log \varphi_s(M)$, has been computed for distances 100, 200, 400, and 600 parsecs from the densities given in Table 6. At a given distance the density for each spectral group has been distributed about the mean absolute magnitude, M_0, with a dispersion σ_0. Summation for each M over all the spectral groups yielded the total population between $M - \frac{1}{4}$ and $M + \frac{1}{4}$. Corrections to reduce these numbers to a volume of 1 cubic parsec and to an interval of 1 mag. were then applied to obtain $\log \varphi_s(M)$. Table 9 shows the resulting luminosity functions, together with the standard van Rhijn function for comparison.

If we allow $\varphi(M) \cdot D(r)$ to be the number of stars per cubic parsec of absolute magnitude $M \pm \frac{1}{2}$ at distance r, as predicted by the use of the van Rhijn function, the difference, $\log R = \log \varphi_s(M) - \log \varphi(M) \cdot D(r)$, measures the departure of the form of the observed functions from the standard. The value $D(r)$ is given in Table 8, second column. Values of $\log R$ plotted against M are shown in Figure 3.

From an inspection of Table 9 and Figure 3, it is apparent that strong fluctuations in the luminosity function with distance occur in LF8. There appears to be a general deficiency of stars with $+1 < M < +7$ in the entire space as far as 500 parsecs. This is particularly evident at 400 parsecs and is clearly due to the dearth of dwarf G5 and K stars as compared to the number near the sun. On the other hand, there appears to be a slight excess of stars with $-1 < M < +1$ within the same region. Beyond 500 parsecs the

rapidly increasing numbers of dwarf stars plus the maximum in the B8–A0 group (Table 6) create a large excess in the observed log $\varphi_s(M)$ over nearly the whole range in M.

The order of magnitude of the differences in $\varphi_s(M)$ found in LF8 is the same as those found in LF1 (Aquila) and LF2 (Cygnus), the exception being that the excess of intrinsically bright stars is not so marked in LF8. When all the observations of the LF regions are completed, the galactic-longitude effects in $\varphi_s(M)$ can be examined in more detail.

TABLE 9

VARIATION OF LUMINOSITY FUNCTION LOG $\varphi_s(M)$ IN LF8

M	DISTANCE (PARSECS)				STANDARD
	100	200	400	600	
−2	4.58	4.41	4.48	4.62	4.75
−1	5.26	5.17	5.21	5.40	5.07
0	5.94	5.86	5.73	5.89	5.68
+1	6.48	6.38	6.07	6.16	6.34
+2	6.75	6.66	6.23	6.33	6.77
+3	6.81	6.76	6.26	6.56	6.86
+4	6.96	6.89	6.46	6.94	7.19
+5	7.27	7.15	6.72	7.25	7.35
+6	7.44	7.32	6.78	7.37	7.50
+7	7.34	7.29	6.52	7.27	7.53

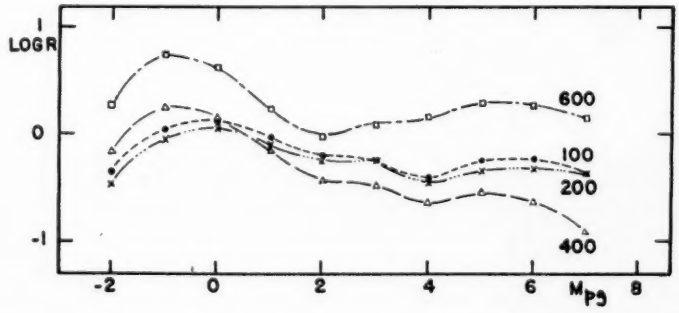

FIG. 3.—Variation in the departures of the observed luminosity functions from the standard van Rhijn function. Ordinates are values of log R = log $\varphi_s(M)$ − log $\varphi(M) \cdot D(r)$; abscissae are photographic absolute magnitudes.

THE OSCILLATIONS OF A ROTATING STAR

T. G. Cowling and R. A. Newing
University College, Bangor, North Wales
Received September 11, 1948

ABSTRACT

Rayleigh's principle is generalized to give approximately the periods of oscillation of a rotating star when those of the corresponding nonrotating star are known. Ledoux's formula for the fundamental period of radial oscillation follows from ours if his approximations are made. More exact numerical results for the fundamental period are obtained in certain cases, and the error involved by making Ledoux's approximations is shown to be not small. Formulae applying to oscillations of the overtone radial and nonradial types are also derived.

I

In 1941, Pekeris and Ledoux[1] applied Rayleigh's principle to derive approximate values for the fundamental period of radial oscillation of a nonrotating star. They showed that quite good approximations to the period could be obtained by assuming simple formulae for the displacement during the oscillation; in many cases an adequate approximation is found by assuming a dilation and compression which are uniform throughout the star. Some of their results were later derived independently by Bhatnagar.[2]

Ledoux and others[3] have also considered the "radial" oscillations of rotating stars (i.e., oscillations such that, in the absence of rotation, the displacement would be wholly radial). Their methods did not depend on Rayleigh's principle, which requires generalization before application to rotating systems.[4] Ledoux's methods were based on certain other general principles of dynamics; in applying them he again assumed a uniform dilation and compression, a little modified by the effect of rotation. Other workers operated by less accurate methods.

In this paper Rayleigh's principle will be applied to the oscillations of rotating stars. The discussion is not limited to "radial" oscillations, though numerical applications are, perforce, made only for these. Ledoux's results obtained by assuming uniform dilation are shown to be identical with those obtained by Rayleigh's principle, with a similar assumption. The error involved in making such an assumption is, however, found to be larger in the rotating than in the nonrotating case.

II

We proceed, first, to rederive Rayleigh's principle in a form suitable for use here. Oscillations of a rotating mass are a special case of oscillations about steady motion: we therefore consider, first, oscillations about steady motion for a dynamical system possessing a finite number of degrees of freedom. Suppose that the system is specified by $n + N$ generalized co-ordinates $q_1, q_2, \ldots, q_n, Q_1, Q_2, \ldots, Q_N$, of which the Q-co-ordinates are cyclic. The equations of motion of the system can be specified in terms of the Routhian function, R; this is connected with the kinetic energy, T, by the equation

$$R = T - \sum_s \dot{Q}_s P_s , \tag{1}$$

[1] *Ap. J.*, **94**, 124, 1941.

[2] *Proc. Nat. Inst. Sci. India*, **11**, 25, 1945.

[3] Ledoux, *Ap. J.*, **102**, 143, 1945; Bhatnagar, *Bull. Calcutta Math. Soc.*, **38**, 93, 1946.

[4] For one type of generalization see Lamb, *Hydrodynamics* (6th ed.; Cambridge: At the University Press, 1932), pp. 313–315.

where P_s is the (constant) generalized momentum corresponding to the co-ordinate Q_s, and R is expressible in the form

$$R = \tfrac{1}{2}\sum_r \sum_s a_{rs}\dot{q}_r\dot{q}_s + \sum_r \alpha_r \dot{q}_r + W, \tag{2}$$

where α_r and W are, respectively, linear and quadratic functions of the P's, and otherwise the quantities a_{rs}, α_r, and W depend only on the variables q_r. When R has been expressed in form (2), the equations of motion are

$$\frac{d}{dt}\left(\frac{\partial R}{\partial \dot{q}_r}\right) - \frac{\partial R}{\partial q_r} = -\frac{\partial V}{\partial q_r}, \tag{3}$$

where V is the potential energy.

In the usual way, each q_r is supposed to vanish in the undisturbed steady motion. The steady motion itself is such that

$$\frac{\partial V}{\partial q_r} = \frac{\partial R}{\partial q_r} = \frac{\partial W}{\partial q_r}. \tag{4}$$

The equations of small oscillation about the steady motion are

$$\sum_s (a_{rs}\ddot{q}_s + c_{rs}\dot{q}_s + b_{rs}q_s) = 0, \tag{5}$$

where

$$b_{rs} = \frac{\partial^2}{\partial q_r \partial q_s}(V - W) = b_{sr}, \tag{6}$$

$$c_{rs} = \frac{\partial \alpha_r}{\partial q_s} - \frac{\partial \alpha_s}{\partial q_r} = -c_{sr}. \tag{7}$$

In equation (5) the values of a_{rs}, b_{rs}, and c_{rs} are supposed to be those characteristic of the steady motion. In an oscillation of period $2\pi/\sigma$ we can put $\dot{q}_s = \iota\sigma q_s$, $\ddot{q}_s = -\sigma^2 q_s$, and get

$$\sum_s (-\sigma^2 a_{rs} + \iota\sigma c_{rs} + b_{rs})\, q_s = 0. \tag{8}$$

We are now in a position to state the modified form of Rayleigh's principle: it is as follows: Let $2\pi/\sigma$ be a period of oscillation and let q_r be any set of values of the generalized co-ordinates, not necessarily those in the oscillation considered; let q_r^* be the complex conjugate of q_r. Then

$$\sum_r \sum_s (-\sigma^2 a_{rs} + \iota\sigma c_{rs} + b_{rs})\, q_s q_r^* = 0, \tag{9}$$

correct to the first order of small quantities, if q_r differs only slightly from its value q_r^0 in the oscillation of period $2\pi/\sigma$. That is, equation (9), regarded as a quadratic in σ, gives a very good approximation to the true value of σ if q_r is a moderately good approximation to q_r^0.

To prove the result stated, put $q_r = q_r^0 + \delta q_r$ and neglect squares and products of the δq terms. Then

$$\sum_r \sum_s (-\sigma^2 a_{rs} + \iota\sigma c_{rs} + b_{rs}) q_s q_r^*$$

$$= \sum_r \sum_s (-\sigma^2 a_{rs} + \iota\sigma c_{rs} + b_{rs}) (q_s^0 q_r^{0*} + q_s^0 \delta q_r^* \delta q_s q_r^{0*})$$

$$= \sum_r (q_r^{0*} + \delta q_r^*) \left\{ \sum_s (-\sigma^2 a_{rs} + \iota\sigma c_{rs} + b_{rs}) q_s^0 \right\}$$

$$+ \sum_s \delta q_s \left\{ \sum_r (-\sigma^2 a_{sr} - \iota\sigma c_{sr} + b_{sr}) q_r^{0*} \right\}.$$

The expressions in the brackets both vanish, by the use of equation (8) and its complex conjugate.

The modified form of Rayleigh's principle becomes recognizably the same as the ordinary form when $c_{rs} = 0$. In this case

$$\frac{\sum_r \sum_s b_{rs} q_s q_r^*}{\sum_r \sum_s a_{rs} q_s q_r^*} \tag{10}$$

is equal to σ^2 to the first order of small quantities, if q_r differs only slightly from its value in the oscillation of period $2\pi/\sigma$. The case arises when the total kinetic energy is the sum of two separate parts, one depending only on the "palpable" velocities, $\dot{q}_r$, and the other only on the cyclic velocities, $\dot{Q}_s$. In this case $a_r = 0$, and the equations of motion are those of a system specified by co-ordinates q_r only, moving with kinetic energy $\frac{1}{2}\Sigma\Sigma a_{rs}\dot{q}_r\dot{q}_s$ and potential energy $V - W$. The usual arguments are here available to show that equation (10) is a minimum when q_r is the displacement in the gravest mode of oscillation.

The above statement and proof of the modified form of Rayleigh's principle refer to a system with a finite number of degrees of freedom. It is, however, easy to generalize them to apply to any dynamical system. To do so, it is simply necessary to note that equation (9) is the ordinary equation of motion, multiplied by the conjugate complex of the displacement and summed over all the co-ordinates considered.

III

In applying the result just enunciated to a rotating star, we first consider oscillations such that the displacement is symmetric about the axis of rotation and does not depend on the azimuthal polar angle ϕ. If R is the distance of a mass element from the axis and ω is its angular velocity around the axis, then, during its motion,

$$R^2\omega = \text{Const.} = C\,, \tag{11}$$

say. The quantity C has to be regarded as a cyclic momentum. The palpable co-ordinates are the polar co-ordinates r and θ of the mass elements. The total kinetic energy is the sum of independent parts arising from the palpable and the cyclic co-ordinates, this entailing appropriate simplifications in the general theory.

In a small oscillation of period $2\pi/\sigma$, let the polar co-ordinates r and θ of a mass element alter by r' and θ' from their values in steady rotation. The equations governing the oscillation are

$$\rho\,(\sigma^2 r' + r\sin^2\theta\omega^2) = \frac{\partial p}{\partial r} + \rho\frac{\partial U}{\partial r},$$

$$\rho\,(\sigma^2 r^2\theta' + r^2\sin\theta\cos\theta\omega^2) = \frac{\partial p}{\partial \theta} + \rho\frac{\partial U}{\partial \theta},$$

where U is the gravitational potential. Expressed in terms of C instead of ω, these become

$$\rho\left(\sigma^2 r' + \frac{C^2}{r^3\sin^2\theta}\right) = \frac{\partial p}{\partial r} + \rho\frac{\partial U}{\partial r},$$

$$\rho\left(\sigma^2 r^2\theta' + \frac{C^2\cos\theta}{r^2\sin^3\theta}\right) = \frac{\partial p}{\partial \theta} + \rho\frac{\partial U}{\partial \theta}.$$

To obtain the appropriate form of Rayleigh's principle, these equations must be multiplied by r'^* and θ'^*, respectively, added together, and integrated throughout the star's volume, τ. Here r' and θ' can be taken as real; hence

$$\sigma^2\int\rho\,(r'^2 + r^2\theta'^2)\,d\tau = \int\Big\{r'\Big[\frac{\partial p}{\partial r} + \rho\frac{\partial U}{\partial r} - \frac{\rho C^2}{r^3\sin^2\theta}\Big] + \theta'\Big[\frac{\partial p}{\partial \theta} + \rho\frac{\partial U}{\partial \theta} - \frac{\rho C^2\cos\theta}{r^2\sin^3\theta}\Big]\Big\}\,d\tau.$$

The quantities in the brackets on the right vanish in steady rotation; hence the equation can be replaced by

$$\sigma^2\int\rho\,(r'^2 + r^2\theta'^2)\,d\tau = \int\rho\Big\{r'\delta\Big[\frac{1}{\rho}\frac{\partial p}{\partial r} + \frac{\partial U}{\partial r} - \frac{C^2}{r^3\sin^2\theta}\Big] + \theta'\delta\Big[\frac{1}{\rho}\frac{\partial p}{\partial \theta} + \frac{\partial U}{\partial \theta} - \frac{C^2\cos\theta}{r^2\sin^3\theta}\Big]\Big\}\,d\tau, \tag{12}$$

where δ denotes the variation due to the oscillation.

If approximate values of r' and θ' are substituted in equation (12), the corresponding values of $\delta\rho$, δp, etc., being calculated from the continuity equation and similar kinematical equations, a good approximation to the value of σ^2 can be obtained. If the values of r' and θ' for oscillations of the corresponding nonrotating star are known, these can with advantage be used in equation (12); the resulting value of σ^2 is then correct up to terms of the second degree in the angular velocity.

IV

Now consider oscillations which, in the absence of rotation, would be wholly radial. In equation (12) write $\theta' = 0$ and take the value of r' to be that in the absence of rotation. Then

$$\sigma^2\int\rho\,r'^2 d\tau = \int\rho\,r'\,\delta\Big[\frac{1}{\rho}\frac{\partial p}{\partial r} + \frac{\partial U}{\partial r} - \frac{C^2}{r^3\sin^2\theta}\Big]\,d\tau. \tag{13}$$

In this, owing to the rotation, ρ depends on the polar angle θ, and hence so also do $\delta\rho$, δp, etc. But if powers of the angular velocity higher than the second are ignored, this complication can be removed. The different variables in equation (13) can be expanded in series of the form

$$\rho = \rho_0 + \rho_1 P_1 + \rho_2 P_2 + \cdots,$$

$$\delta p = \delta p_0 + \delta p_1 P_1 + \delta p_2 P_2 + \cdots,$$

etc., where $\rho_0, \rho_1, \ldots, \delta p_0, \delta p_1, \ldots$, are functions of r alone and $P_1, P_2, \ldots$, here are Legendre polynomials in $\cos\theta$; $\rho_1, \rho_2, \ldots, \delta p_1, \delta p_2, \ldots$, vanish in a nonrotating star, and in a rotating star they involve squares and higher powers of the angular velocity. When these expressions for ρ, δp, etc., are substituted in equation (13), terms involving squares or products of $P_1, P_2, \ldots$, can be neglected because we are neglecting powers of the angular velocity higher than the square. Also terms involving a single one of $P_1, P_2, \ldots$, vanish on integration over all values of θ. It is therefore sufficient to replace ρ, $\delta p, \ldots$, by $\rho_0, \delta p_0, \ldots$. That is, in place of the actual star, distorted from the spherical form by centrifugal force, we may consider a spherical star, expanded spherically by the average radial centrifugal force $\rho r\overline{\omega^2 \sin^2\theta}$ (the average is that over a sphere of radius r concentric with the star; we do not evaluate the average explicitly at present, since the angular velocity, ω, is not at present assumed to be uniform throughout the star).

Suppose, then, that the actual star is replaced in this way by a spherical star. In the steady state of this spherical star,

$$\frac{\partial p}{\partial r} + \rho \frac{\partial U}{\partial r} = \rho r \overline{\omega^2 \sin^2\theta}. \tag{14}$$

In its oscillations the values of $\delta\rho, \delta p, \ldots$, in equation (13) can be taken either as variations at a point or following the motion. Since the star is spherically symmetric, it is convenient to use variations following the motion. Then, from the continuity equation,

$$\frac{\delta\rho}{\rho} = -\frac{\partial(r^2 r')}{r^2 \partial r}. \tag{15}$$

If γ is the ratio of specific heats, the adiabatic equation is

$$\frac{\delta p}{p} = \gamma \frac{\delta\rho}{\rho}. \tag{16}$$

Finally, if m is the mass in a sphere of radius r concentric with the star,

$$\frac{\partial U}{\partial r} = \frac{Gm}{r^2}, \qquad \delta\left(\frac{\partial U}{\partial r}\right) = -\frac{2Gm\,r'}{r^3}. \tag{17}$$

Hence, since $\rho r^2 dr$ is constant following the motion, equation (13) takes the following form:

$$\begin{aligned}
\sigma^2 \int \rho r'^2 d\tau &= \int \rho r' \delta\left\{\frac{1}{\rho}\frac{\partial p}{\partial r} + \frac{\partial U}{\partial r} - \frac{1}{r^3}\frac{\overline{C^2}}{\sin^2\theta}\right\} d\tau \\
&= \int \rho r' \left\{\frac{\delta(r^2)}{\rho r^2}\frac{\partial p}{\partial r} + \frac{1}{\rho}\frac{\partial \delta p}{\partial r} - \frac{2Gm\,r'}{r^3} + \frac{3r'}{r^4}\frac{\overline{C^2}}{\sin^2\theta}\right\} d\tau \\
&= \int \rho r' \left\{\frac{2r'}{\rho r}\frac{\partial p}{\partial r} + \frac{1}{\rho}\frac{\partial \delta p}{\partial r} - \frac{2Gm\,r'}{r^3} + 3r'\overline{\omega^2 \sin^2\theta}\right\} d\tau.
\end{aligned} \tag{18}$$

If in equation (18) we further approximate by putting $r'/r = \text{Const.} = k$, Ledoux's result[3] is at once recovered; for in this case, by equations (15) and (16), $\delta\rho/\rho = -3k$ and $\delta p/p = -3\gamma k$; hence, substituting for $\partial p/\partial r$ from equation (14), we obtain

$$\begin{aligned}
\sigma^2 \int \rho r^2 d\tau &= \int \rho + \left\{(2-3\gamma)\left(-\frac{Gm}{r^2} + r\overline{\omega^2 \sin^2\theta}\right) - 2\frac{Gm}{r^2} + 3r\overline{\omega^2 \sin^2\theta}\right\} d\tau \\
&= \int \left\{(3\gamma - 4)\frac{Gm\rho}{r} + (5-3\gamma)\rho r^2 \overline{\omega^2 \sin^2\theta}\right\} d\tau.
\end{aligned}$$

That is,

$$I_0\sigma^2 = (3\gamma-4)\Omega + (5-3\gamma)\,2T\,, \tag{19}$$

where I_0 is the moment of inertia with respect to the center, $-\Omega$ the gravitational potential energy, and T the rotational kinetic energy. This, apart from a slight difference in interpretation, is Ledoux's result.

An alternative form of equation (18) is obtained as follows: In the term $-2Gmr'/r^3$, put

$$\frac{Gm}{r^2} = \frac{\partial U}{\partial r} = -\frac{1}{\rho}\frac{\partial p}{\partial r} + r\overline{\omega^2 \sin^2\theta}\,.$$

Then the equation becomes

$$\sigma^2 \int \rho\, r'^2 d\tau = \int r' \left\{ \frac{4\,r'}{r}\frac{\partial p}{\partial r} + \frac{\partial\, \delta p}{\partial r} + \rho\, r' \overline{\omega^2 \sin^2\theta} \right\} d\tau\,.$$

The terms involving $\partial p/\partial r$ and $\partial \delta p/\partial r$ are now integrated by parts with respect to r, remembering that $d\tau$ has $r^2 dr$ as a factor. Then, using the adiabatic equation (16) and eliminating the derivatives of r' by equation (15), we have

$$\int \rho\, r'^2 (\sigma^2 - \overline{\omega^2 \sin^2\theta})\, d\tau = \int p \left\{ \gamma \left(\frac{\delta\rho}{\rho}\right)^2 + \frac{8\,r'}{r}\frac{\delta\rho}{\rho} + 12 \left(\frac{r'}{r}\right)^2 \right\} d\tau\,. \tag{20}$$

This form of the equation is especially suitable for numerical work, since the assumption that r' has the value characteristic of the nonrotating star implies that $\delta\rho/\rho$ also has such a value.

V

We have used equation (20) to determine σ^2 numerically for the gravest oscillation of a uniformly rotating polytropic star. The cases considered were with polytropic index $n = \frac{3}{2}$ and $\gamma = \frac{5}{3}$; and with $n = 3$ and $\gamma = \frac{5}{3}$, $\frac{29}{18}$, and $\frac{1}{7}\frac{0}{0}$. Equation (20) is, for a uniformly rotating star,

$$\sigma^2 - \tfrac{2}{3}\omega^2 = \left[\int p \left\{ \gamma \left(\frac{\delta\rho}{\rho}\right)^2 + \frac{8\,r'}{r}\frac{\delta\rho}{\rho} + 12 \left(\frac{r'}{r}\right)^2 \right\} d\tau \right] \left[\int \rho\, r'^2 d\tau \right]^{-1}. \tag{20'}$$

The angular velocity appears implicitly as well as explicitly in this. Each of ρ and p can be expressed as the sum of two parts, the first being the value in a nonrotating star, the second giving the (spherically symmetric) distortion due to rotation.

In order to apply equation (20′), $\delta\rho/\rho$ and r'/r had to be determined fairly accurately for a nonrotating star. This was done, for the polytrope $n = \frac{3}{2}$, by the iteration process indicated by the equations

$$\left(\sigma_s^2 + \frac{4Gm}{r^3}\right)\rho\, r'_s = \frac{\partial\, \delta p_{s+1}}{\partial r}\,, \qquad -\frac{\delta p_{s+1}}{\gamma p} = -\frac{\delta\rho_{s+1}}{\rho} = \frac{\partial (r^2 r'_{s+1})}{r^2 \partial r}\,,$$

where σ_s^2, r'_s, $\delta\rho_s$, and δp_s here denote the sth approximations to σ^2, r', $\delta\rho$, and δp. The value of σ_s^2 was taken as that determined from r'_s and $\delta\rho_s$, using Rayleigh's principle for nonrotating stars. The iteration proved rapidly convergent, yielding the values listed in Table 2. The work of Schwarzschild[5] having been overlooked, a similar iteration was attempted for the polytrope $n = 3$, with $\gamma = \frac{5}{3}$. The method had to be modified a little because of the extremely rapid fall-off of ρ and p near the boundary of this model; even after modification, it proved a little difficult to control. The final values indicated an increase of r'/r about in the ratio 16:1 on passing from the center to the boundary, whereas Schwarzschild's solution indicates a 17:1 increase. No great accuracy could be

[5] *Ap. J.*, **94**, 124, 1941.

claimed for our values; but the value of σ^2 obtained by applying Rayleigh's principle for a nonrotating star to our solution was a shade less than that similarly derived from Schwarzschild's, indicating that our solution was at least no less accurate than his.

An attempt was later made to get a better solution in this case by combining our solution linearly with Schwarzschild's, taking that linear combination which gave the least value of σ^2 by Rayleigh's principle. This gave an appreciably smaller value of σ^2, but the corresponding solution differed impossibly far from both our solution and Schwarzschild's. It became clear, on examination, that the lower value of σ^2 was spurious, being obtained simply because of the sensitivity of the method to slight numerical errors; it appeared that an overelaborate use of Rayleigh's principle was prone to give misleading results. The attempt was accordingly abandoned.

The values of r'/r and $\delta\rho/\rho$ for the polytrope $n = 3$, with $\gamma = \frac{10}{7}$ and $\gamma = \frac{29}{18}$, were taken from Schwarzschild's tables. In each set of computations, the values of ρ and p for a rotating polytrope were taken from Chandrasekhar's[6] tables; in his notation they are

$$\rho = \rho_c\,(\theta^n + n\,v\,\theta^{n-1}\psi_0)\,,$$

$$p = K\rho^{1+1/n} = K\rho_c^{1+1/n}\,(\theta^{n+1} + [n+1]\,v\,\theta^n\psi_0)\,,$$

TABLE 1*

VALUES OF $\Sigma^2(=\sigma^2/4\pi G\rho_c)$ IN TERMS OF $v\,(=\omega^2/2\pi G\rho_c)$ FOR DIFFERENT POLYTROPIC MODELS

n	γ	Equation (20′)	Equation (19)
3	$\frac{10}{7}$	$0.021-0.075v$	$0.023+0.03v$
3	$\frac{29}{18}$	$.040-0.84\ v$	$.050-0.32v$
3	$\frac{5}{3}$	(i) $.057-1.92\ v$†	$.082-0.73v$
		(ii) $.057-1.95\ v$	.....
1.5	$\frac{5}{3}$	$0.150-0.15\ v$	$0.155-0.13v$

* Given by our formula (eq. [20′]) and that of Ledoux (eq. [19]).

† Of the two values of Σ^2 calculated from eq. (20′) for the model $n = 3$, $\gamma = \frac{5}{3}$, (i) was calculated from the values of r' and $\delta\rho$ given in Table 2; (ii) was calculated from those of Schwarzschild (*Ap. J.*, **94**, 124, 1941).

where ρ_c is the central density and $v = \omega^2/2\pi G\rho_c$. As Chandrasekhar showed, the mass of a rotating polytrope may differ slightly from that of the corresponding nonrotating model, from which r' and $\delta\rho$ are calculated; negligible errors are, however, introduced by using these values of r' and $\delta\rho$ in Rayleigh's principle.

The values of σ^2 obtained from equation (20′) for the different models are given in Table 1, with the values which we obtained from Ledoux's approximate formula (19). Actually, the quantity tabulated is $\sigma^2/4\pi G\rho_c$; it is to be remembered that σ^2 depends on ω^2 through the dependence of ρ_c on ω^2, as well as through the appearance of v in the table. The precise dependence of ρ_c on ω^2 is somewhat difficult to assess; in actual stars the central conditions are largely determined by energy generation, and it is rather difficult to work this into the polytropic pattern. Rotation can, however, be expected always to reduce ρ_c; hence Table 1 indicates that rotation always reduces σ^2 and that Ledoux's formula normally underestimates the reduction considerably. The v-term is obtained as the difference of two much larger terms; this explains why it was possible for Ledoux's formula actually to give the sign of the v-term incorrectly in one case. For the same reason the rough agreement between our results and Ledoux's in the case $n = \frac{3}{2}$, $\gamma = \frac{5}{3}$, is perhaps a little fortuitous.

[6] *M.N.*, **93**, 390, 1933.

The result given by Pekeris and Ledoux[1] in the nonrotating case for $n = 1.5$, $\gamma = \frac{5}{3}$, was slightly different from that which would be obtained from the above; in our notation it is equivalent to $\Sigma^2 = 0.151$.

VI

Equation (12) can also be used to discuss oscillations which, though not "radial," are still symmetric about the axis of revolution. However, since few numerical results exist for such oscillations, even in the absence of rotation, we shall not try to develop general formulae for these.

Instead, we now consider oscillations which are not symmetric about the axis of rotation. A unique period of oscillation cannot be said to exist unless the star rotates uniformly; when masses at different distances from the center rotate at different rates, they must vibrate up and down with slightly different periods if the upward surges at all points of a given radius are to keep pace. Attention will therefore be confined to a uniformly rotating star.

The azimuthal polar angle, ϕ, of an element of mass can be expressed as a sum $\phi_0 + \psi$, where $\phi_0 = \omega t$ and ω is the angular velocity of the star in the absence of oscillations. To include ϕ_0 in the Lagrangian scheme, we can imagine it to be the azimuthal angle for an infinitesimal mass traveling uniformly in a circle around the axis of the star and exerting no forces on the elements of the latter; then ψ is the azimuthal displacement of a general element of the star relative to this imagined mass. The angle ϕ_0 is a cyclic co-ordinate; the corresponding generalized momentum, P, is the angular momentum around the axis of rotation, and

$$P = \int \rho r^2 \sin^2 \theta \, (\omega + \dot{\psi}) \, d\tau \, . \tag{21}$$

Let r' and θ' denote, as before, the changes in the r and θ of an element of mass during an oscillation, and let ψ' be the corresponding change in ψ (ψ' and ψ differ by a quantity which is constant for any element of mass). Then the equations of a small oscillation of period $2\pi/\sigma$ are

$$\begin{aligned}
\rho \, (\sigma^2 r' + r \sin^2 \theta \, [\omega^2 + 2\omega\iota\sigma\psi'] \,) &= \frac{\partial p}{\partial r} + \rho \frac{\partial U}{\partial r} \, , \\
\rho r^2 \, (\sigma^2 \theta' + \sin \theta \cos \theta \, [\omega^2 + 2\omega\iota\sigma\psi'] \,) &= \frac{\partial p}{\partial \theta} + \rho \frac{\partial U}{\partial \theta} \, , \\
\rho r \sin\theta \, (\sigma^2 r \sin \theta\psi' - 2\omega\iota\sigma \, [\, r' \sin \theta + r \cos \theta\theta'] \,) &= \frac{\partial p}{\partial \phi} + \rho \frac{\partial U}{\partial \phi} \, .
\end{aligned} \tag{22}$$

To obtain the Rayleigh equation from these, we should, according to earlier statements, substitute for ω in terms of P in equations (22); the resulting equations should then be multiplied by r'^*, θ'^*, and ψ'^*, added and integrated throughout the star's volume. However, the introduction of P instead of ω, which in any case appears highly artificial, is here entirely unnecessary. In oscillations of the type now being considered, r', θ', and ψ' are periodic functions of ϕ, proportional to $e^{\iota\lambda\phi}$, where λ is a nonzero integer. Hence the moment of inertia, I, of the star about its axis is, to the first order of small quantities, constant during an oscillation; and equation (21) reduces to the obvious form

$$P = I\omega \, .$$

Since I is constant, it is clearly immaterial whether ω or P appears in the Rayleigh equation.

On multiplying the three equations (22) by r'^*, θ'^*, and ψ'^*, adding and integrating, the Rayleigh equation is obtained in the form

$$\sigma^2\int\rho\,(r'r'^*+r^2\theta'\theta'^*+r^2\sin^2\theta\psi'\psi'^*)\,d\tau+2\omega\iota\sigma\int\rho\,(r\sin^2\theta\,[\psi'r'^*-r'\psi'^*]+r^2\sin\theta\cos\theta\,[\psi'\theta'^*-\theta'\psi'^*])\,d\tau$$
$$=\int\Big\{r'^*\Big[\frac{\partial p}{\partial r}+\rho\frac{\partial U}{\partial r}-\rho r\sin^2\theta\omega^2\Big]+\theta'^*\Big[\frac{\partial p}{\partial\theta}+\rho\frac{\partial U}{\partial\theta}-\rho r^2\sin\theta\cos\theta\omega^2\Big]+\psi'^*\Big[\frac{\partial p}{\partial\phi}+\rho\frac{\partial U}{\partial\phi}\Big]\Big\}d\tau\,. \tag{23}$$

Since the expressions in the brackets vanish in the absence of oscillations, they can be replaced by

$$\delta\Big[\frac{\partial p}{\partial r}+\rho\frac{\partial U}{\partial r}-\rho r\sin^2\theta\omega^2\Big],$$

etc., where δ denotes an increment due to the oscillation.

VII

Equation (23) involves terms of first degree in ω; the value of σ^2 may therefore be expected also to involve terms linear in ω. If it is desired simply to determine these terms, so that ω^2 can be neglected, a great simplification can be made. Because ω^2 is neglected, p, ρ, etc., can be taken as the same in the rotating star as in the same star without rotation. Hence if r', θ', and ψ' are taken to be the same as in the corresponding oscillations of the nonrotating stars, so also are δp, $\delta\rho$, etc.; and the right-hand side of equation (23) becomes

$$\int\Big\{r'^*\delta\Big[\frac{\partial p}{\partial r}+\rho\frac{\partial U}{\partial r}\Big]+\theta'^*\delta\Big[\frac{\partial p}{\partial\theta}+\rho\frac{\partial U}{\partial\theta}\Big]+\psi'^*\delta\Big[\frac{\partial p}{\partial\phi}+\rho\frac{\partial U}{\partial\phi}\Big]\Big\}d\tau\,;$$

or, using Rayleigh's principle for the nonrotating star,

$$\sigma_0^2\int\rho\,\{r'r'^*+r^2\theta'\theta'^*+r^2\sin^2\theta\psi'\psi'^*\}\,d\tau\,,$$

where σ_0 is the value of σ for the nonrotating star. Hence equation (23) reduces to

$$\sigma^2+2\omega\sigma A=\sigma_0^2\,, \tag{24}$$

where

$$A=\frac{\iota\int\rho\,(r\sin^2\theta\,[\psi'r'^*-r'\psi'^*]+r^2\sin\theta\cos\theta\,[\psi'\theta'^*-\theta'\psi'^*])\,d\tau}{\int\rho\,\{r'r'^*+r^2\theta'\theta'^*+r^2\sin^2\theta\psi'\psi'^*\}\,d\tau}. \tag{25}$$

The solution of equation (24), which approximates to $\sigma=\sigma_0$ as $\omega\to 0$, is, of course,

$$\sigma=\sigma_0-\omega A\,. \tag{26}$$

For example, for an incompressible homogeneous liquid star,

$$r'=\frac{\partial\chi}{\partial r},\qquad r^2\theta'=\frac{\partial\chi}{\partial\theta},\qquad r^2\sin^2\theta\psi'=\frac{\partial\chi}{\partial\phi},$$

where

$$\chi=r^nP_n^m(\cos\theta)\,e^{\pm\iota m\phi}\qquad(m=0,1,2,\ldots,n)\,.$$

Using these expressions in equation (25), we find the value of A to be $-m/n$. Thus if n is kept constant and m varies, the corresponding oscillations (which all have the same frequency, σ_0, in a nonrotating star) have, in a rotating star, evenly spaced frequencies

$$\sigma = \sigma_0\,, \qquad \sigma_0 \pm \frac{\omega}{n}\,, \qquad \sigma_0 \pm \frac{2\omega}{n}\,, \ldots\,, \qquad \sigma_0 \pm \omega\,.$$

TABLE 2

VALUES OF r'/r AND $\delta\rho/\rho$ FOR THE PRINCIPAL RADIAL OSCILLATION OF THE EMDEN POLYTROPES $n=3$ AND $n=1.5$, EACH WITH $\gamma=\frac{5}{3}$

ξ*	$n=1.5$		ξ	$n=3$	
	r'/r	$-\delta\rho/\rho$		r'/r	$-\delta\rho/\rho$
0	1	3	0	1	3
0.3	1.002	3.012	0.5	1.020	3.088
0.6	1.010	3.051	1.0	1.073	3.362
0.9	1.022	3.115	1.5	1.169	3.868
1.2	1.041	3.211	2.0	1.321	4.714
1.5	1.066	3.344	2.5	1.553	6.064
1.8	1.099	3.518	3.0	1.898	8.192
2.1	1.140	3.740	3.5	2.407	11.505
2.4	1.191	4.021	4.0	3.146	16.489
2.7	1.253	4.380	4.5	4.216	24.241
3.0	1.329	4.833	5.0	5.788	36.282
3.3	1.423	5.409	5.5	8.083	54.286
3.6	1.539	6.157	6.0	11.324	80.110
			6.5	15.962	120.7

* The variable ξ is Emden's nondimensional variable proportional to the distance from the center.

There is a similar result for nonhomogeneous stars. In a general nonrotating star

$$r' = \chi_1 S_n\,, \qquad \theta' = \chi_2 \frac{\partial S_n}{\partial \theta}\,, \qquad \sin^2\theta\psi' = \chi_2 \frac{\partial S_n}{\partial \phi}\,, \tag{27}$$

where χ_1 and χ_2 are certain functions of r and S_n is a surface harmonic function of order n in θ and ϕ. For a given n, the function S_n can take $2n+1$ distinct forms,

$$S_n = P_n^m(\cos\theta)\, e^{\pm im\phi} \qquad (m = 0, 1, 2, \ldots, n)\,, \tag{28}$$

all corresponding to the same χ_1, χ_2, and σ_0^2. The oscillations of a rotating star corresponding to equations (27) and (28) have slightly different periods; and it can be shown, by substituting from equations (27) and (28) into equation (25) and integrating by parts with respect to θ, etc., that the frequencies corresponding to different values of m again have evenly spaced values, of the form $\sigma_0 \pm mk\omega$, where k is a pure number.

DYNAMICAL FRICTION

MARVIN LEE WHITE
Yerkes Observatory
Received September 13, 1948

ABSTRACT

The coefficient of dynamical friction is reconsidered, taking into account a "correction term" which arises principally from those field stars which travel with velocities greater than the velocity of the particular star. A table of this correction term is provided. The new values for the coefficient of dynamical friction are used to redetermine the half-lives for galactic clusters; a value slightly less than that obtained previously is found.

1. *Introduction.*—In an earlier paper by S. Chandrasekhar an expression for the coefficient of dynamical friction, η, was obtained directly from an analysis of stellar encounters. He gave the formulae[1]

$$\eta = \pi m^2 \frac{G^2}{v_2^3} \int_0^\infty \frac{1}{v_1} N(v_1) J(v_1;\ v_2)\, dv_1 , \tag{1}$$

where

$$J(v_1;\ v_2) = \begin{cases} 8 v_1 \log q\,(v_2^2 - v_1^2) & (v_1 < v_2) \\ 4 v_1 \log 4 q\, v_1^2 - 8 v_1 & (v_1 = v_2) \\ 8 v_1 \log \dfrac{v_1 + v_2}{v_1 - v_2} - 16 v_2 & (v_1 > v_2) \end{cases}, \tag{2}$$

v_1 is the velocity of a typical field star, v_2 is the velocity of a particular star, and

$$q = \frac{D_0}{G(m_1 + m_2)} . \tag{3}$$

In Chandrasekhar's further considerations[2] the following approximation to J was used:

$$J = \begin{cases} 8 v_1 \log q \overline{|u|^2} & (v_1 < v_2) , \\ 0 & (v_1 > v_2) , \end{cases} \tag{4}$$

where $\overline{|u|^2}$ is the mean square velocity of the stars in the system. According to equations (1), (2), and (4), we have the remarkable result that the dynamical friction experienced by a particular star is due mainly to encounters with field stars which have speeds less than itself. To illustrate this, we have plotted in Figure 1 the function $J(v_1; v_2)v_1^{-1}$ for a few typical cases.

The high degree of accuracy of approximation (4) for ordinary regions of our galaxy such as those in the neighborhood of the sun is apparent from Curve *I*. Even for clusters with fifty thousand stars, the approximation would seem sufficiently accurate (see Curve *II*). However, Curve *III* clearly shows that, for clusters with four hundred members, it would be important to consider the departures from approximation (4). It is the object of this paper to evaluate exactly this correction term to equations (4) for various values of the parameter v_2 and, using these correction terms, to redetermine the half-life of a galactic cluster.

[1] *Ap. J.*, **97**, 255 eqs. (25) and (30), 1943.

[2] *Ibid.*, eq. (31).

2. *The evaluation of the correction term.*—Combining equations (1) and (2) and assuming that the velocities v_1 are distributed according to Maxwell's law,

$$N(v_1)\,dv_1 = \frac{4j^3}{\pi^{1/2}} N e^{-j^2 v_1^2} v_1^2 dv_1, \tag{5}$$

where N denotes the number of stars per unit volume and j is a parameter which measures the dispersion of the velocities in the system, we obtain

$$\eta = 64\pi^{1/2} N m^2 G^2 [F_D + F_C]\, v_2^{-3}, \tag{6}$$

where the dominant term, F_D, is given by

$$F_D = \frac{\pi^{1/2}}{8} \log\left(\tfrac{2}{3} q \overline{|u|^2}\right) [\Phi(x_0) - x_0 \Phi'(x_0)] \tag{7}$$

and the correction term, F_C, is given by

$$\begin{aligned} F_C = \frac{\pi^{1/2}}{8} &(1 - 2\Phi[x_0]) + \tfrac{1}{2}\int_0^\infty (\log[x + x_0])\, e^{-x^2} x^2 dx \\ &+ \int_0^{x_0} (x_0 - x)(\log[x_0 - x])\, e^{-x^2}(x - x^3)\, dx \\ &+ \int_{x_0}^\infty (x - x_0)(\log[x - x_0])\, e^{-x^2}(x - x^3)\, dx. \end{aligned} \tag{8}$$

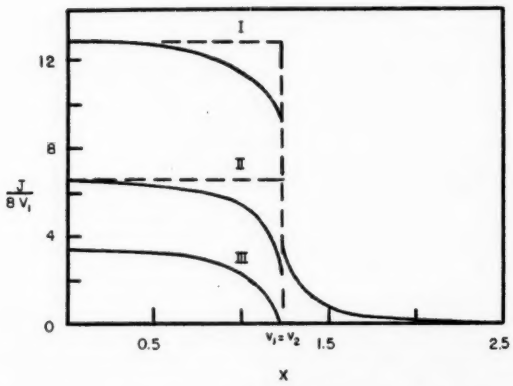

FIG. 1.—Illustration of dynamical friction: the ordinate $(J(v_1; v_2)/8v_1)$ is a measure of the influence of field stars of velocity $v_1 = jx$ in decelerating a particular star having a velocity equal to the root mean-square velocity. Curve *I* refers to the average conditions of the galaxy in the neighborhood of the sun; Curve *II* refers to a cluster of fifty thousand stars; and Curve *III*, to a cluster of four hundred stars.

In the foregoing equations

$$\Phi(x) = \frac{2}{\pi^{1/2}} \int_0^{x_0} e^{-x^2} dx \tag{9}$$

is the error integral, where

$$x_0 = j v_2 \quad \text{and} \quad x = j v_1.$$

The integrals occurring in equation (8) were evaluated by standard numerical methods and are tabulated for various values of x_0 in Table 1. Table 2 shows the variations of the following quantities for nine values of the parameter x_0: (1) the correction term, F_C; (2) the dominant term, F_D; and (3) the ratio of $F_D + F_C$ to F_D.

TABLE 1

VALUES OF THE INTEGRALS NEEDED TO FIND THE CORRECTION TERM, F_C, TO THE COEFFICIENT OF DYNAMICAL FRICTION, η

x_0	$\frac{1}{2}\int_0^\infty [\log (x+x_0) \cdot e^{-x^2} x^3 dx]$	$\int_0^{x_0} [(x_0-x) \cdot \log (x_0-x) e^{-x^2} \cdot (x-x^3) dx]$	$\int_{x_0}^\infty [(x-x_0) \cdot \log (x-x_0) e^{-x^2} \cdot (x-x^3) dx]$
0.1	+0.02720	−0.00058	−0.19831
0.2	+ .04773	− .00314	− .16774
0.4	+ .08285	− .01651	− .10232
0.6	+ .11269	− .03621	− .04237
0.8	+ .13871	− .05210	+ .00245
1.0	+ .16183	− .05374	+ .02783
1.5	+ .21051	+ .02461	+ .02893
2.0	+ .25017	+ .16163	+ .00905
3.0	+0.31268	+0.35111	+0.00012

TABLE 2

THE FUNCTIONS F_D, F_C, AND $(F_D + F_C)/F_D$

x_0	F_C	F_D	$(F_D+F_C)/F_D$
0.1	0.0000	+0.00048	
0.2	−0.00027	+ .00377	+0.92838
0.4	− .00425	+ .02808	+0.84865
0.6	− .01191	+ .08437	+0.85884
0.8	− .01822	+ .17073	+0.89328
1.0	− .01593	+ .27433	+0.94193
1.5	+ .05751	+ .50536	+1.11380
2.0	+ .20137	+ .61204	+1.32901
3.0	+0.44236	+0.64128	+1.68981

The value of the dominant term appearing in Table 2 is calculated for a cluster of four hundred stars and makes use of the approximation

$$q = \frac{D_0}{2Gm}, \tag{10}$$

where[3]

$$D_0 = \frac{Gm}{|u|^2} n^{2/3}. \tag{11}$$

In Figure 2, the term F_D is compared with the term $F_C + F_D$. It is seen that the correction to the coefficient of dynamical friction becomes increasingly significant for larger values of the velocity.

[3] Cf. S. Chandrasekhar, *Principles of Stellar Dynamics*, p. 202, eq. (5.215) (Chicago: University of Chicago Press, 1947).

3. The rate of escape of stars from clusters allowing for the correction term.—In an earlier paper,[4] the diffusion equation governing the distribution $W(\boldsymbol{u}, t)$ of $\boldsymbol{u}$ at a time t was solved with the appropriate boundary conditions.

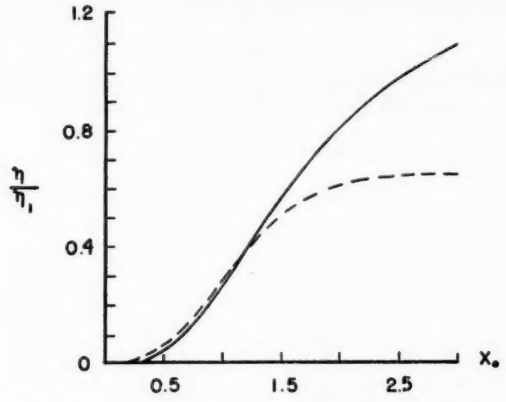

FIG. 2.—A comparison of the approximate with the exact evaluation of the coefficient of dynamical friction.

TABLE 3

THE FUNCTIONS $\nu(\rho)$ AND $-d \log \nu/d\rho$

ρ	$\nu(\rho)$	$-(d \log \nu)/d\rho$	ρ	$\nu(\rho)$	$-(d \log \nu)/d\rho$
0.00	1.0000	0.000	1.50	0.3456	0.993
0.10	0.9702	.513	1.60	.3129	0.998
0.20	0.9060	.755	1.70	.2832	0.991
0.30	0.8330	.879	1.80	.2567	0.980
0.40	0.7716	.614	1.90	.2325	0.997
0.50	0.7323	.512	2.00	.2107	1.001
0.60	0.6951	.538	2.10	.1901	1.016
0.70	0.6565	.614	2.20	.1718	1.019
0.80	0.6170	.635	2.30	.1553	1.007
0.90	0.5759	.725	2.40	.1405	0.973
1.00	0.5355	.742	2.50	.1276	0.943
1.10	0.4965	.772	2.60	.1165	0.904
1.20	0.4571	.861	2.70	.1066	0.872
1.30	0.4184	.915	2.80	0.0979	0.848
1.40	0.3811	0.949			

We now express the coefficient of dynamical friction in the form

$$\eta = \eta_0 \nu(j|\boldsymbol{u}|) = \eta_0 \nu_D(j|\boldsymbol{u}|) \frac{F_C + F_D}{F_D}, \tag{12}$$

where η_0 and ν_D are defined as (compared with "Dynamical Friction III")

$$\eta_0 = 8\pi N m^2 G^2 (\log_e [\tfrac{2}{3} q \overline{|\boldsymbol{u}|^2}]) \left(\frac{3}{2\overline{|\boldsymbol{u}|^2}}\right)^{3/2} \frac{4}{3\pi^{1/2}} \tag{13}$$

[4] Cf. Chandrasekhar, *Ap. J.*, **98**, 54, 1943. This paper is referred to as "Dynamical Friction III."

and

$$\nu_D = \frac{3\pi^{1/2}}{4} \rho^{-3} [\Phi(\rho) - \rho\Phi'(\rho)] . \tag{14}$$

The function $\nu(\rho)$ needed for the integration of equation (25) of "Dynamical Friction III" is given in Table 3. The factors $(F_c + F_D)/F_D$ needed to compute $\nu(\rho)$ were obtained by graphical interpolation of the values given in Table 2. In this manner, the value of λ for which the boundary condition $\rho = \rho_\infty$ is satisfied was found to be

$$\lambda = 0.0100 , \qquad \rho_\infty = 2.456 . \tag{15}$$

According to equation (47) of "Dynamical Friction III,"

$$\text{The half-life of the cluster} = (\lambda_1 \eta_0)^{-1}. \tag{16}$$

With η_0 and λ_1 as given by equations (13) and (15), the half-life is found to be 0.85 times the value previously obtained for the half-life of the Pleiades. However, the result that the half-lives of galactic clusters like the Pleiades are of the order of 3×10^9 years remains essentially unchanged.

The smaller half-life is explained in the following manner: When performing the above calculations, it became apparent that, for smaller values of x_0, the solution was insensitive to the correction term but became significant for the larger values of x_0. Examining Figure 2, it is seen that for larger values of x_0, the coefficient of dynamical friction is larger when the correction term is taken into consideration. Furthermore, as the coefficient of dynamical friction is proportional to the diffusion coefficient, it follows that the stars would diffuse out of the cluster more rapidly than the previous calculations would indicate.

In conclusion, I wish to express my sincere appreciation to Dr. S. Chandrasekhar for suggesting this problem and for many helpful discussions.

A NONHOMOGENEOUS COSMOLOGICAL MODEL

GUY C. OMER, JR.
California Institute of Technology
Received September 18, 1948

ABSTRACT

Various theories about the extragalactic red shift are considered. It is concluded that actual recessional motion is the most plausible explanation of the observed red shifts. To avoid the well-known difficulties of the homogeneous cosmological models, a group of relativistic, nonstatic, nonhomogeneous, cosmological models which have spherical symmetry, zero pressure, and co-moving co-ordinates are considered. As a first approximation the observer is assumed to be near the center of symmetry. Then, following the general procedures of Hubble and Tolman, we can derive the necessary relations between the theoretical model and the astronomical observations.

The average density of matter in the neighborhood of the observer at the present time is assumed to be 10^{-29} gm/cc. The cosmological constant is taken to be 8.78×10^{-19} (light-years)$^{-2}$. For the radius of curvature in the neighborhood of the observer we assign $1/R^2 = -10^{-20}$ (light-years)$^{-2}$. Then the total time elapsed in the neighborhood of the observer since the beginning of the expansion would be 3.64×10^9 years. The calculated red shifts agree with the observed red shifts given by Hubble to within 0.1 mag., except for the two Ursa Major clusters, for which the observational data are unreliable. The calculated values of log N, where N is the nebular count per square degree, depart from the observed values presented by Hubble by 0.002 or less. The expansion in this model does not begin simultaneously everywhere, but begins at progressively later epochs for those spatial regions which have larger radial co-ordinates. This suggests a possible explanation of the red excesses observed by Stebbins and Whitford for the E nebulae in the clusters.

The hypothetical nature of the model must be emphasized, since the theoretical assumptions have been oversimplified and the observational data are not too reliable. The chief value of the model possibly lies in showing that currently accepted astronomical data can be treated by accepted physical principles without the necessity of introducing new physical hypotheses.

E. Hubble[1] has shown that the observational data which he has obtained do not agree satisfactorily with the homogeneous relativistic cosmological models. Using the approximate formulae developed by Hubble and Tolman,[2] he has fitted a homogeneous model to his red shift against magnitude data to within 0.1 mag., except for the two Ursa Major clusters, for which the observational data are unreliable. He has fitted this model to his limiting magnitude against log N data, where N is the nebular count per square degree, to within 0.05 mag. or less. The residuals between the calculated and the observed values of log N are all negative and average about 0.045. This fit to the two primary bodies of observational data could be accepted, except that the homogeneous model requires the three following novelties:

a) The constants of the model require a mean density of matter of the general order of 10^{-26} gm/cc. This is about a thousand times the current estimations of the average density of matter in the universe and is roughly a hundredth of the estimated average density in the solar neighborhood.

b) The model is small and closed, with a radius of curvature of about 4.7×10^8 light-years. This would indicate that the 100-inch reflector has already surveyed a large fraction of the existing universe. This might be true, but it seems philosophically repugnant.

c) The model has a short time scale. The present age of the model must be less than 1.2×10^9 years.[3] This is about one-third the recent estimation of the age of the earth

[1] *Ap. J.*, **84**, 517, 1936; *Mt. W. Contr.*, No. 557.

[2] *Ap. J.*, **82**, 302, 1935; *Mt. W. Contr.*, No. 527.

[3] The calculation of this maximum age for the homogeneous model has recently been shown to me by R. C. Tolman.

as an independent body, made by A. Holmes.[4] This is probably the most serious difficulty of the homogeneous model.

Because of the unrealistic aspects of the homogeneous relativistic model, Hubble proposed an alternate model which would be essentially static and homogeneous and in which the red shift would be produced by some unknown but nonrecessional mechanism. Hubble assumed that the radiation from a nebula was essentially that of a black body at 6000° K. Then, after properly correcting for the dimming effect of the red shift, he found a linear relation between red shift and distance. The residuals between the calculated and the observed values of magnitudes for the observed red shifts in the clusters were less than 0.1 mag. The relation between log N and distance was found to be compatible with a uniform distribution of matter. The residuals between the calculated and the observed values of log N for the limiting magnitudes of the surveys were 0.009 or less. The average density of matter, the time scale, and the extent of physical space are not determined by the constants of this nonrecessional model. Therefore, the proposed model would seem to be consistent with the observations and their reductions. J. L. Greenstein,[5] however, has criticized Hubble's assumed effective temperature of 6000° K and has concluded that the effective temperature of the nebulae would have to be less than 5250° K. This lower temperature would invalidate both the linear red-shift law and the uniform distribution of matter in Hubble's nonrecessional model.

There have been several suggestions of possible mechanisms which would produce red shifts without having actual physical recession. F. Zwicky[6] has proposed that photons may lose energy with time, perhaps by a gravitational interaction with the matter along their trajectories. R. C. Tolman,[7] however, has shown that "gravitational drag" cannot account for the observed red shift if the relativity theory is valid. If the extragalactic red shift were produced by "gravitational drag," we should expect to measure red shifts within our own local group which would be greater than those indicated by Hubble's linear law, since the mean density of matter within the local group is greater than the average density of matter for the entire universe. If the photon's loss of energy were dependent upon time alone, we should expect to measure red shifts within our own local group which would be exactly equal to those predicted by Hubble's linear law.

E. A. Milne[8] has attempted to develop a cosmological mechanics, a posteriori, from the observations themselves rather than from an a priori extension of small-scale physics to gross-scale physics. H. P. Robertson,[9] however, has shown that Milne's kinematic relativity is equivalent to the homogeneous relativistic cosmologies. Milne[10] more recently has suggested that the universe is governed by two different time scales, which are logarithmically related. If this suggestion is recast into a single time scale, it is equivalent to the hypothesis that the values of the physical constants vary with time. Consequently, Milne's various interpretations of the red shift need not be examined individually.

P. A. M. Dirac[11] has proposed that the physical "constants" are not constant with time but may vary in a systematic manner. This proposal would account for an observed red shift without any actual physical recession. Moreover, the red shift should be independent of any gravitational grouping of the objects observed. According to Dirac's hypothesis, we should expect to measure red shifts within our own local group which would be exactly equal to those predicted from Hubble's linear red-shift law. E. Teller[12]

[4] *Endeavour*, **6**, 99, 1947.

[5] *Ap. J.*, **88**, 605, 1938.

[6] *Proc. Nat. Acad. Sci.*, **15**, 773, 1929.

[7] *Relativity, Thermodynamics, and Cosmology* (Oxford: Clarendon Press, 1934), pp. 285 ff.

[8] *Relativity, Gravitation, and World Structure* (Oxford: Clarendon Press, 1935).

[9] *Ap. J.*, **82**, 284, 1935.

[10] *Ap. J.*, **91**, 129, 1940.

[11] *Proc. R. Soc. London, A*, **165**, 199, 1938.

[12] *Phys. Rev.*, **73**, 801, 1948.

has recently criticized Dirac's proposal, since there is considerable geological and biological evidence that the surface temperature of the earth has been reasonably constant for the last 5×10^8 years. With Dirac's hypothesis and the additional assumption that the masses of the earth and of the sun have remained constant, Teller finds that the surface temperature of the earth would have been near the boiling-point of water within this time interval. With the alternate assumption that the masses of the earth and of the sun have increased as the square of the age of the universe, the surface temperature of the earth would have been brought below the freezing-point of water within this time interval.

A rather pragmatic test on the nature of the red shift is given by measuring the red shifts of the other members of our local group. If the red shift is to be explained by one of the nonrecessional hypotheses, the measured apparent recessional velocities of the other members of the local group should be equal to or greater than those predicted from Hubble's linear red-shift law. On the other hand, if the red shifts are produced by actual recession, as is assumed in relativistic cosmology, probably no systematic red shifts would be expected within the local group. Zwicky[13] has concluded that the Coma, Perseus, and Hydra clusters are "stationary assemblies of nebulae." If our smaller and less symmetrical local group is at least quasi-stable, only random motions would be expected between its members, and consequently only random Doppler shifts should be measured.

Hubble[14] has reported nine measured radial velocities within the local group. For six known members of this group he has found a random distribution of observed velocities, after correcting for the solar motion. Three of the corrected velocities are of approach, and three are of recession. The largest corrected velocity of recession was 45 km/sec, while the largest expected red shift, calculated from Hubble's linear law, was 210 km/sec. Three probable members of the local group had corrected velocities of recession ranging from 30 to 90 km/sec. The expected red shifts for these three objects, however, ranged from 265 to 370 km/sec. Hubble finds that the data "suggest that the law of red-shifts does not operate within the local group." N. U. Mayall[15] has measured the apparent radial velocities of three additional members of the local group and has concluded that "it would appear that there is little reason to correct radial velocities of local group members for red-shifts observed in the general field." Accordingly, the measured radial velocities within the local group support the view of relativistic cosmology that the red shifts are Doppler shifts produced by actual recessional motion.

Although the explanation of the red shifts as Doppler shifts is the simplest and the most natural, still the homogeneous cosmologies give an unrealistic picture of the physical universe. Perhaps this should not be too surprising, since Tolman[16] has shown that, subject to certain simplifying conditions, a homogeneous model is unstable under perturbations in density. Any local tendency to expand would be emphasized by further expansion. Likewise, any local tendency to contract would be followed by further contraction. Thus if a homogeneous model is disturbed, it becomes nonhomogeneous.

We shall develop here a nonhomogeneous cosmological model as a higher approximation to the cosmological problem than that given by the homogeneous models. Since the partial differential equations are nonlinear, we shall make the following simplifying assumptions, so that a solution will not be too difficult:

1. The mechanical behavior of the model is assumed to allow the use of "co-moving co-ordinates." These co-ordinates are widely used in cosmology, but they do restrict the possible types of motion. For example, if co-moving co-ordinates are used to describe

[13] *Pub. A.S.P.*, **54**, 185, 1942.

[14] *Science in Progress* (New Haven: Yale University Press, 1942), **3**, 22.

[15] *Ap. J.*, **104**, 290, 1946.

[16] *Proc. Nat. Acad. Sci.*, **20**, 169, 1934.

the entire history of the model, neither systematic dispersions in particle velocities nor nonrigid rotations of the model are possible.

2. A spherically symmetric distribution of matter is assumed. This is a logical first approximation to any nonhomogeneous distribution of matter that would be expected within the physical universe.

3. The pressure within the model is considered to be vanishingly small. That is, we shall neglect the effects of radiation pressure and tidal interactions between the nebulae in comparison to their gravitational forces. This would seem to be a reasonable approximation within our observational neighborhood at the present time. This is a dangerous assumption, however, if we attempt to extrapolate our model to regions of high density at other epochs.

With these assumptions the line element may be written as follows:

$$ds^2 = -\left[\frac{\left(\frac{\partial y}{\partial r}\right)^2}{1+g}\,dr^2 + y^2 d\theta^2 + y^2 \sin^2\theta\, d\phi^2\right] + dt^2\,, \tag{1}$$

where y, a function of both r and t, must be a solution of the following nonlinear partial differential equation,

$$\left(\frac{\partial y}{\partial t}\right)^2 = g + \frac{h}{y} + \tfrac{1}{3}\Lambda y^2\,. \tag{2}$$

In the line element (1) and the partial differential equation (2), g and h are arbitrary functions of r, and Λ is the cosmological constant. The proper density at any r and t is given by

$$8\pi\rho = \frac{\frac{dh}{dr}}{y^2\left(\frac{\partial y}{\partial r}\right)}. \tag{3}$$

These equations, except for changes in notation, are identical with those given by Tolman.[16]

The partial differential equation (2) has been solved completely in terms of Weierstrassian elliptic functions,[17] but here only approximate solutions will be used. The arbitrary functions g and h will be taken in the form of the two following infinite series:

$$g(r) = \frac{r^2}{R^2}(1 + b_1 r + b_2 r^2 + \ldots)\,, \tag{4}$$

$$h(r) = \tfrac{8}{3}\pi\rho_0 r^3(1 + a_1 r + a_2 r^2 + \ldots)\,, \tag{5}$$

where R is the curvature and ρ_0 is the average density at the co-ordinate origin of the model at the present time. If both series (4) and (5) are reduced to their initial terms, the model becomes homogeneous. It is the higher-power terms in these series which produce the nonhomogeneity in the model.

The dependent function, y, will be taken in the form:

$$y(r, t) = r(1 + c_1 t + c_{12} rt + c_2 t^2 + c_{13} rt^2 + c_{23} r^2 t + c_3 t^3 + \ldots)\,. \tag{6}$$

The coefficients of series (6) are determined by substituting series (4), (5), and (6) in the differential equation (2) and equating the terms. If the model reduces to a homogeneous

[17] G. C. Omer, Jr., doctoral thesis, California Institute of Technology, 1947.

one, it will be found that the cross-terms, c_{ij}, vanish. The double Taylor series used in series (6) is not the most general expansion, since higher-power terms in r alone do not appear. A more general series expansion in the co-ordinate $\bar{r}$ can always be reduced to the series form (6) by a transformation $r = f(\bar{r})$. This transformation is relevant, however, only if the line element (1) and the co-moving character of the co-ordinates are undisturbed. It is easily seen that the transformation $r = f(\bar{r})$ leaves the line element (1) unchanged in form. Moreover, if the $\bar{r}$ co-ordinate is co-moving, it is obvious that an r co-ordinate defined by $r = f(\bar{r})$ is also co-moving. Thus the co-ordinate transformation is allowable, and the specialized series expansion (6) will be used. It can, in fact, be shown[17] that the specialized series (6) is necessary if a simple relationship is to be established between the relativistic co-ordinate r and a unit of physical measure, such as the light-year.

In order to derive cosmological conclusions which will have a relationship to the observational data, it is now necessary to make some assumption as to the location of the observer. Lacking any definitive observational data as to the isotropic or nonisotropic distribution of nebular counts and red shifts, we make one more assumption:

The observer is considered to be near the center of symmetry as compared to the distances of nebulae of the twenty-first magnitude.

We may now follow the procedures of Hubble and Tolman[2] and derive the necessary formulae which will give the observational content of our cosmological model. By combining the line element (1) with the density equation (3) and integrating over the angle variables, we see that the amount of matter contained between r and $r + dr$ is

$$dM = \frac{\dfrac{dh}{dr}}{2\sqrt{1+g}}\, dr\,. \tag{7}$$

By substituting from equations (4) and (5), expanding equation (7) into a power series and integrating the resulting series term by term, we find that the total amount of matter contained within co-ordinate radius r is

$$M = \tfrac{4}{3}\pi\rho_0\left[r^3 + a_1 r^4 + \left\{ a_2 - 0.3\,\frac{1}{R^2} \right\} r^5 + \left\{ a_3 - \frac{1}{R^2}\left(\frac{a_1}{3} + \frac{b_1}{4} \right) \right\} r^6 + \ldots \right]. \tag{8}$$

Since co-moving co-ordinates have been used, the amount of matter, of course, is independent of the time.

The total number of nebulae within co-ordinate radius r will be proportional to equation (8). We can parallel the reasoning of Hubble and Tolman for the counts within a homogeneous model exactly in all details and write to the same order of approximation for the counts within our nonhomogeneous model,

$$\log N = 0.6\left(m - 4\,\frac{\delta\lambda}{\lambda} \right) + F^* + C\,, \tag{9}$$

where N is the total number of nebulae counted per unit area of the sky down to limiting magnitude, m. The $4\delta\lambda/\lambda$ term is Hubble's approximation for the more general corrections $5 \log (1 + \delta\lambda/\lambda) + K$, which correct for the energy and number effects of the red shift and convert from bolometric to photographic magnitude. The red shift to be used is that for a nebula having an absolute magnitude $\bar{M}$, taken by Hubble to be -15.15 and having an apparent magnitude equal to the limiting value, m, of the counts. The constant C depends upon the conventions adopted. Hubble reduced his counts to nebulae per square degree and found statistically that $C = -9.052$. The term F^* con-

tains the effects of both the nonhomogeneity and the curvature of the model. By making the parallel derivation of equation (9) we find that

$$F^* = \log\left[1 + a_1 r + \left\{a_2 - 0.3\frac{1}{R^2}\right\} r^2 + \left\{a_3 - \frac{1}{R^2}\left(\frac{a_1}{3} + \frac{b_1}{4}\right)\right\} r^3 + \ldots\right]. \tag{10}$$

In this derivation we have used a relation between co-ordinate distance and apparent magnitude which is yet to be derived.

The derivation of the red shift is not quite so simple. It can be shown that the radial lines of our co-ordinate system are null-geodesics. Let us consider a wave crest of light, leaving a source at the co-ordinate r_1 at the time t_1 and arriving at the origin at the time t_0, which will be taken as comparable to zero. Then, from the line element (1) we shall have formally

$$\int_0^{r_1} \frac{1}{\sqrt{1+g}} \frac{\partial y}{\partial r}\, dr = t_0 - t_1 . \tag{11}$$

By substituting equations (4) and (6) in equation (11) and expanding, we can write the integrand as an infinite series. Unfortunately, the integrand contains terms in both r and t in such a form that they cannot be separated. However, at any given time, t, the wave crest, is passing through a definite co-ordinate, r. If the relation $t = f(r)$ were known, we could substitute it in equation (11), write the integrand as a power series in r alone, and consequently be able to integrate equation (11) directly.

The desired relationship between t and r can be approached by successive approximations. If only the first term of the infinite series expansion of equation (11) is taken, the first approximation of $t = t_0 - r$ can easily be found. By substituting this back in equation (11) and now taking the first two terms of the series expansion of the integrand, the second approximation of $t = t_0 - (1 + c_1 t_0)r + \frac{1}{2}c_1 r^2$ is obtained. By successive steps it is possible to approximate to $t = f(r)$ to as high an order of accuracy as may be desired.

To obtain the red shift, consider two successive wave crests; one leaving r_1 at t_1 and arriving at the origin at the time 0, while the other leaves r_1 at the later time $t_1 + \delta t_1$ and arrives at the origin at time δt_0. By making the fourth successive approximation of $t = f(r)$ and subtracting the travel times for the two wave crests, large blocks of terms will be canceled. Furthermore, since δt_0 is very small, all powers greater than unity may be neglected. Then we find that

$$\frac{\delta t_1}{\delta t_0} = 1 - c_1 r_1 + \left\{\tfrac{1}{2}c_1^2 + c_2 - c_{12}\right\} r_1^2 - \left\{\tfrac{1}{6}c_1\left(c_1^2 - \frac{1}{R^2}\right) + \tfrac{4}{3}c_1 c_2 - c_1 c_{12} + c_3 - \tfrac{4}{3}c_{13} + c_{23}\right\} r_1^3 + \ldots . \tag{12}$$

But, since $\delta t_0/\delta t_1 = 1 + \delta\lambda/\lambda$, we can solve equation (12) for the red shift. Thus the red shift observed at the origin and the present epoch for a source which is located at r will be

$$\frac{\delta\lambda}{\lambda} = c_1 r + \left\{\tfrac{1}{2}c_1^2 - c_2 + c_{12}\right\} r^2 + \left\{\tfrac{1}{6}c_1\left(c_1^2 - \frac{1}{R^2}\right) - \tfrac{2}{3}c_1 c_2 + c_1 c_{12} + c_3 - \tfrac{4}{3}c_{13} + c_{23}\right\} r^3 + \ldots . \tag{13}$$

When the cross-terms, c_{ij}, vanish, the model becomes homogeneous. In this special case it can be seen, after a necessary transformation of the notation, that the red shift given by equation (13) is equal to that given by the formula of Hubble and Tolman.

The last relation that must be developed is one between co-ordinate distance and observed magnitude. This relation must be derived with caution, since the null-geodesics will be deformed by the nonhomogeneous distribution of matter within the model. Thus a nebula may appear to be either brighter or dimmer than would be expected from the simple inverse-square law because of a partial focusing or defocusing effect. The sign and the magnitude of this focusing effect depend upon the nature of the inhomogeneity of the matter.

Magnitude determinations are fundamentally measures of the rate of energy flow, subject to the absorption in the instrument and the atmosphere and to the spectral sensitivity of the receptor. Thus we are concerned with the amount of energy which flows through our telescope aperture in a unit time. Let us take the center of our telescope aperture exactly at the co-ordinate origin of our model and outside the earth's atmosphere. Every photon that leaves the source at co-ordinate r_1 travels along a null-geodesic line in our co-moving co-ordinate system. We are concerned with the very minute cone of null-geodesics which has its apex at the source and just fills the telescope aperture. Energy flows into the cone from the source at the rate $\Delta E_1/\Delta t_1$ but flows out of the cone into the telescope at the different rate, $\Delta E_0/\Delta t_0$. The difference in the entrance and exit rates of energy flow is caused by the relative motion of the source and the telescope. Since the model is expanding, each photon that enters our telescope has been degraded in energy by the Doppler shift. Moreover, a block of energy flowing into the cone from the source in unit time is spread out within a longer tube by the relative motion between the source and the observer and will require more than unit time to flow into the telescope. Thus we have two effects which will reduce the rate of energy flow into our telescope from the original rate of energy flow into the cone from the source. We have, in fact,

$$\frac{\Delta E_0}{\Delta t_0} = \left(\frac{\lambda}{\lambda + \delta\lambda}\right)^2 \frac{\Delta E_1}{\Delta t_1} . \tag{14}$$

The central line of the cone of null-geodesics will be a radial line of the co-ordinate system. Let us consider the small angle, ω, measured in proper units at the source between this radial line and one of the extreme rays of the cone which will just barely enter the telescope. Then the rate at which energy flows into the cone from the source will be

$$\frac{\Delta E_1}{\Delta t_1} = (\text{constant})\ I\omega^2 , \tag{15}$$

where I is the total emissive power of the source and the constant contains the various factors of proportionality. The angle ω in proper units is given from the line element (1) as

$$\tan\omega = -\left[\frac{y\sqrt{1+g}}{\dfrac{\partial y}{\partial r}}\frac{d\phi}{dr}\right]_{r=r_1} . \tag{16}$$

The value of the derivative $d\phi/dr$ to be used in equation (16) for the extreme ray must be found by integrating the geodesic equations. For the line element (1), these geodesic equations are

$$\frac{d^2r}{ds^2}+\left[\frac{y''}{y'}-\frac{\frac{dg}{dr}}{2(1+g)}\right]\left(\frac{dr}{ds}\right)^2+2\frac{\dot{y}'}{y'}\frac{dr}{ds}\frac{dt}{ds}-\frac{(1+g)y''}{y'}\left(\frac{d\theta}{ds}\right)^2 - \frac{(1+g)y}{y'}\sin^2\theta\left(\frac{d\phi}{ds}\right)^2=0\,, \tag{17}$$

$$\frac{d^2\theta}{ds^2}+2\frac{y'}{y}\frac{dr}{ds}\frac{d\theta}{ds}+2\frac{\dot{y}}{y}\frac{d\theta}{ds}\frac{dt}{ds}-\sin\theta\cos\theta\left(\frac{d\phi}{ds}\right)^2=0\,, \tag{18}$$

$$\frac{d^2\phi}{ds^2}+2\frac{y'}{y}\frac{dr}{ds}\frac{d\phi}{ds}+2\cot\theta\frac{d\theta}{ds}\frac{d\phi}{ds}+2\frac{\dot{y}}{y}\frac{d\phi}{ds}\frac{dt}{ds}=0\,, \tag{19}$$

$$\frac{d^2t}{ds^2}+\frac{y'\dot{y}'}{1+g}\left(\frac{dr}{ds}\right)^2+y\dot{y}\left(\frac{d\theta}{ds}\right)^2+y\dot{y}\sin^2\theta\left(\frac{d\phi}{ds}\right)^2=0\,. \tag{20}$$

The notation is a common one, in which the dots represent partial differentiation with respect to t, while the primes represent partial differentiation with respect to r.

If in equation (18) we take $\theta=\frac{1}{2}\pi$ and $d\theta/ds=0$ as initial conditions, then $d^2\theta/ds^2=0$. This means that, if a geodesic initially lies within this plane, it remains within the same plane throughout its trajectory. Similarly, in equation (19), if the geodesic was initially a radial line with $d\phi/ds=0$, then $d^2\phi/ds^2=0$ and the geodesic remains a radial line. This verifies the earlier statements that the radial lines are null-geodesics. But only one geodesic within the cone will be a radial line. For all the other geodesics $d\phi/ds$ will have a nonzero initial value. However, with $\theta=\frac{1}{2}\pi$, equation (19) may be integrated exactly as

$$\frac{d\phi}{ds}=\frac{K_1}{y^2}\,, \tag{21}$$

where K_1 is a constant of integration.

By using the line element (1) in a degenerate form, since $ds=0$ for a null-geodesic, and by using the initial condition $\theta=\frac{1}{2}\pi$, equation (20) may be restated in the form

$$\frac{d}{dt}\log\left(\frac{dt}{ds}\right)=-\frac{\dot{y}'}{y'}+\left[y^2\frac{\dot{y}'}{y'}-y\dot{y}\right]\left(\frac{d\phi}{dt}\right)^2. \tag{22}$$

For the homogeneous special case in which the cross-terms c_{ij} vanish, equation (22) may be integrated exactly as $dt/ds=K_2r/y$, where K_2 is another constant of integration. But in the nonhomogeneous models it is not possible to integrate equation (22) exactly; hence an approximate solution must be made. Let us assume that the nonhomogeneous model is nearly homogeneous. Accordingly, the cross-terms c_{ij} in series (6) will be vanishingly small as compared with the purely time-dependent terms. We shall take as our approximate expression for y the purely time-dependent terms plus a small nonhomogeneous correction term which will be the largest of the cross-terms, as, for example, c_{12}. For convenience in notation take $\delta=K_1/K_2$. Then to the desired order of approximation $d\phi/dt\approx\delta/ry$. From this result and the approximate expression for y in equation (22),

$$\frac{dt}{ds}\approx K_2\frac{r}{y}\frac{(1+\frac{1}{3}c_1c_{12}r^3+\ldots)}{r^{c_{12}\delta^2}}. \tag{23}$$

After substituting equations (23) and (21) in the line element (1), the differential equation which must be satisfied by the null-geodesics in the co-moving co-ordinates is found to be

$$\frac{y'^2}{y^2(1+g)}\left(\frac{dr}{d\phi}\right)^2 \approx \frac{r^2}{\delta^2}\frac{(1+\frac{1}{3}c_1c_{12}r^3+\ldots)^2}{r^{2c_{11}\delta^2}}-1\,. \tag{24}$$

The solution of this differential equation is a distorted conic section. The semi-minor axis of this distorted conic section is determined by the condition $dr/d\phi = 0$. Because of the smallness of the remaining factors on the right-hand side of equation (24), this condition is satisfied to a very high order of approximation by $r = \delta$. Thus, to obtain the initial angle of the extreme ray within the null-geodesic cone, the constant of integration δ must be taken equal to the radius of the aperture of the telescope. Then

$$\omega \approx \tan\omega \approx \frac{\delta}{r_1}\frac{(1+c_{12}\delta^2\log r_1+\ldots)}{(1+\frac{1}{3}c_1c_{12}r_1^3+\ldots)}\,. \tag{25}$$

Substituting equation (25) in equations (15) and (14), we find that

$$\frac{\Delta E_0}{\Delta t_0} \approx \frac{\text{constant}}{r_1^2}\left(\frac{\lambda}{\lambda+\delta\lambda}\right)^2\left[\frac{1+c_{12}\delta^2\log r_1+\ldots}{1+\frac{1}{3}c_1c_{12}r_1^3+\ldots}\right]^2. \tag{26}$$

This is an extension of the similar results of Hubble and Tolman in that the factor in the brackets is the correction term for the focusing effect present in nonhomogeneous models. In the numerical model which will be presented here, however, this correction term differs insignificantly from unity. For the twenty-first-magnitude survey, for which the focusing effect would be the greatest, the change in the apparent magnitude for the particular model to be discussed is only 0.012 mag. and hence may be totally disregarded. Consequently, the desired relation between the co-ordinate distance and the apparent photographic magnitude for a source of absolute photographic magnitude M located at r and having an observed red shift of $\delta\lambda/\lambda$ is

$$\log r = 0.2\left(m - 4\frac{\delta\lambda}{\lambda} - M\right)+1\,, \tag{27}$$

where Hubble's approximation of $4\delta\lambda/\lambda$ has once more been used for the remaining corrections. This is an anticlimax to an involved derivation. Nevertheless, the focusing effect does exist for nonhomogeneous distributions of matter and must be calculated for each conceptual model, since the effect might be quite appreciable for some model of interest.

Equations (9), (13), and (27) are the relations required for computations with the model. A set of relativistic units in which the velocity of light and the constant of gravitation are both 1 will be used in these calculations. This particular set of units includes the year as the unit of time, the light-year as the unit of length, and a corresponding unit for mass. Fixing the values of the cosmological constant and of the series coefficients of equations (4) and (5) determines the entire behavior of the model. We shall take the following values:

$\rho_0 = 10^{-29}$ gm/cc $\qquad \Lambda = 8.781\times10^{-19}$ (light-years)$^{-2}$

$\frac{1}{R^2} = -10^{-20}$ (light-years)$^{-2}$

$a_1 = 6.66\times10^{-10}$ (light-years)$^{-1}$ $\qquad a_2 = 1.217\times10^{-18}$ (light-years)$^{-2}$

$b_1 = -2.7\times10^{-8}$ (light-years)$^{-1}$ $\qquad b_2 = 9.165\times10^{-18}$ (light-years)$^{-2}$

For the present average density near the observer, ρ_0, the currently most widely accepted value has been chosen, and the remaining constants have been taken to give a good fit to the observational data and yet provide a reasonable time scale. Only the first three terms of series (4) and (5) have been found necessary to represent Hubble's data.

With the foregoing constants, the red-shift equation (13) will be

$$\frac{\delta\lambda}{\lambda} = 5.37\times10^{-10}r + 2.54\times10^{-19}r^2 + 0r^3 + \cdots , \tag{28}$$

which is the same numerical form as that used by Hubble.[1] Hubble's data were too scant to determine actually the third-power term of the red-shift series but served only to show that this term must be small. To have a definite value, this term has been assumed to be zero in this work, and the constant b_2 was determined accordingly. Any moderate uncertainty in the third-power series term is reflected entirely in a corresponding uncertainty in the b_2 constant but not in the values of any of the remaining constants.

The theoretical relationship between apparent magnitude and red shift can be calculated by using series (28) in conjunction with equation (27). The theoretical model may

TABLE 1

RED SHIFTS

Cluster	$(\delta\lambda/\lambda)_{obs}$	$(Mag.)_{obs}$	$(\delta\lambda/\lambda)_{calc}$	C−O	$(Mag.)_{calc}$	C−O
Virgo	0.0041	10.50	0.0042	+0.0001	10.467	+0.033
Pegasus	.0127	12.92	.0126	− .0001	12.940	− .020
Perseus	.0174	13.53	.0166	− .0008	13.634	− .104
Coma	.0245	14.30	.0235	− .0010	14.393	− .093
UMa I	.0517	16.27	.0561	+ .0044	16.075	+ .195
Leo	.0653	16.53	.0629	− .0024	16.614	− .084
Cor. Bor.	.0707	16.75	.0692	− .0015	16.800	− .050
Boötes	.1307	18.28	.1306	− .0001	18.283	− .003
UMa II	0.1403	18.15	0.1225	−0.0178	18.461	−0.311

be compared to the observational data by either of two equivalent procedures. For a given set of objects, either the measured magnitudes or the measured red shifts may be substituted in equations (27) and (28), and then the predicted values of the remaining data may be calculated for comparison with the observed values. The observational data given by Hubble[1] are listed in the first three columns of Table 1. For the nine clusters in the first column, the second column gives the average observed red shift and the third column the observed apparent magnitude of the fifth brightest nebula in the cluster, corrected for galactic obscuration. Tolman,[18] for logical consistency, prefers to assume the measured magnitudes and to calculate the red shifts. Accordingly, the calculated values of the red shift in the fourth column of Table 1 were obtained by substituting in equations (27) and (28) the observed values of the magnitudes from the third column. The differences between the calculated and the observed values of the red shift are listed in the fifth column. Except for the two Ursa Major clusters, the differences between the calculated and the observed values are less than 4 per cent. The observational data for the two Ursa Major clusters were obtained from a single spectrogram of a single nebula in each case and are not to be given much statistical weight. Contrariwise, Hubble[19] regards the measured red shifts as the better-determined data and prefers to assume the red shifts and to calculate the magnitudes. Consequently, the calculated values of the magnitudes given in the sixth column of Table 1 were obtained by substituting in equa-

[18] Private communication.

[19] Private communication.

tions (27) and (28) the observed values of the red shifts from the second column. The differences between the calculated and the observed values of the magnitudes are listed in the last column. Except for the two Ursa Major clusters, the residuals are 0.1 mag. or less.

Similarly, by using equation (9) in conjunction with equations (27) and (28), we can calculate the logarithm of the mean number of nebulae per square degree to any given limiting magnitude. These calculated values are given in the third column of Table 2 for the five nebular-count surveys listed in the first column. The observed values given in the second column were taken from Hubble.[1] The last column lists the differences between the calculated and the observed values. As can be seen, the constants of the theoretical model have been adjusted to give a very good fit to the observational data.

By a graphical integration of equation (2) the age of the model (total time elapsed since the beginning of the expansion) in the neighborhood of the observer was found to be 3.64×10^9 years. Holmes[4] has recently estimated the age of the earth as an independent body to be 3.35×10^9 years. B. J. Bok[20] has examined nine independent criteria for the duration of astronomical time and has concluded that the most probable age of the

TABLE 2

NEBULAR COUNTS

Survey to Limiting Magnitude	$(\log N)_{obs}$	$(\log N)_{calc}$	C−O
21.03	3.162	3.1625	+0.0005
20.00	2.686	2.6883	+ .0023
19.40	2.342	2.3404	− .0016
19.00	2.161	2.1604	− .0006
18.47	1.886	1.8864	+0.0004

universe must lie between 3 and 5×10^9 years. A third independent value of 4×10^9 years was given by H. Jeffreys[21] as the calculated age of the earth-moon system from their tidal interactions. Thus the calculated age given by this nonhomogeneous model is in good agreement with the presumed age derived by a number of independent methods from observational data.

The model is one that is monotonically expanding everywhere. However, since the model is nonhomogeneous, the local density and the rate of expansion vary over the model with the r co-ordinate at any given time. Nevertheless, at any given locality the local behavior is similar to that which is usually designated as M_1 in the homogeneous cosmologies. Within any given spatial neighborhood the model begins to expand from an initial singularity of extremely high density and continues to expand monotonically, approaching an empty de Sitter end-stage in an infinite time. If equation (28) is a good representation of the red shift over the model, an "optical horizon" would be found at $r \approx 1.2 \times 10^9$ light-years, where the red shift would be 1 at the present time. Not even a perfect telescope of unlimited aperture could detect objects beyond this limit. However, the particular co-ordinate given for the "optical horizon" is very tentative because of the uncertainty in the third-power term of the red-shift series (28) and because of the possible existence of higher-power terms.

The model is demonstratively nonhomogeneous. The mean density of matter in the neighborhood of the origin at present has been taken to be 10^{-29} gm/cc. The present mean local density elsewhere may then be calculated and is found to increase outward

[20] *M.N.*, **106**, 61, 1946.

[21] *The Earth* (Cambridge: At the University Press, 1924), p. 229.

with radius, becoming 1.68×10^{-29} gm/cc at $r = 4 \times 10^8$ light-years. This is approximately the estimated mean distance of the faintest nebulae recorded with the 100-inch reflector under optimal conditions. This outwardly increasing density distribution may appear strange, but it has a satisfactory dynamical explanation. The expansion in the model begins first at the co-ordinate origin and then the initiating impulse is propagated outward along the r co-ordinate with a finite velocity. Thus the more remote localities began their expansions at a later time than the origin and consequently are not so fully expanded at the present time. This would account for their presently higher mean densities.

This mechanism of decreasing "age" with increasing radius accounts for the present outward-increasing density but introduces a rather novel time scale. From photoelectric measures of the colors of E nebulae in four clusters Stebbins and Whitford[22] recently found that color index increased with distance. For the Boötes cluster, which was the most distant measured, the color excess was about 0.3 mag. over and above that which can be accounted for by the red shift of 0.13 measured for this cluster. M. Schwarzschild[23] has suggested that this red excess may be at least partially a time effect. Nebulae of the E type, being composed of stellar population II, may in the past have contained a number of giant red stars which have consumed their store of energy and have disappeared at the present time. Consequently, more-distant E nebulae now being measured would be expected to be redder than the E nebulae closer at hand. Graphical integration with the nonhomogeneous model gives an "age" of 2.58×10^9 years for an object at $r = 2 \times 10^8$ light-years distance from the observer. This distance is somewhat less than the estimated distance to the Boötes cluster. Thus the nonhomogeneous model predicts that the light now being received from the Boötes cluster is from objects only about two-thirds as old as similar objects in the immediate neighborhood of the observer. This gives an ample time scale for considerable change in stellar composition.

Although the nonhomogeneous model gives a rather good fit to the currently accepted observational data, nevertheless it must be regarded with due caution. Since the model was derived subject to several mathematically simplifying assumptions which may not be valid in the physical universe, it will be wise to examine these assumptions critically. The model begins its expansion rapidly at any given point from an initial state of extremely high density. Physically, we should expect a dispersion in the initial particle velocities, and we should expect to find fast-moving particles overtaking and passing the more slowly moving particles throughout the history of the model. However, this logical expectation violates both the assumptions of co-moving co-ordinates and zero pressure. G. Gamow[24] has quite logically suggested that a good cosmological model should be in rotation. If this rotation is to be relativistically significant, it must be a nonrigid rotation. Co-moving co-ordinates could not be used to describe the entire history of such a rotating model.

The assumption of spherical symmetry is probably the most acceptable of the four special assumptions which were made. Nevertheless, this is only a first approximation to the physical universe and should be regarded solely as a basis upon which to build higher and better approximations in the future. The assumption of zero pressure would certainly be violated at the beginning of the expansion about any given point. Radiation pressure and tidal interactions between the closely spaced nebulae would be expected to exceed the gravitational interactions by a large factor. The zero-pressure assumption is probably good within our spatial neighborhood at the present time and may remain a fair approximation as we extrapolate our model backward in time until the local average density becomes too high. By graphical integration with the model we find that the epoch at which the local average density near the origin was 10^{-26} gm/cc was 3.36×10^9 years

[22] *A.J.*, **53**, 204, 1948.

[23] Stebbins and Whitford, *op. cit.*, p. 205.

[24] *Nature*, **158**, 549, 1946.

ago. Thus the zero-pressure assumption would seem to be a fair approximation for more than nine-tenths of the estimated age of the model near the origin. Hence the computed age of the model, which is the only predicted value that would be seriously affected by the presence of pressure at the beginning of the expansion, would not be seriously revised even if pressure terms were included in the solution.

The assumption of a central observer may seem to be philosophically objectionable. However, with the present observational data there is no other logical position in which to locate him. Further observational work which would clearly show nonisotropy in nebular counts or red shifts would be welcome. Then there would be some basis for assigning a definite noncentric position to the observer and proceeding to construct a more realistic cosmological model. The varying time scale with radial co-ordinate in the model is interesting and might provide a theoretical basis for the red excesses observed by Stebbins and Whitford. On the other hand, the varying time scale can equally well be regarded as a flaw in the model.

The observational data employed in constructing the model are also uncertain. The red excesses found in the E nebulae are potentially quite significant. Similar photoelectric color measures upon late-type spirals, composed of stellar population I, in which the giants can presumably be regenerated, might help to differentiate between the two hypotheses—time effect and intergalactic obscuration—which have been advanced to explain the red excesses. If the observed red excess is due to intergalactic obscuration, the estimation of the average density of matter in the universe must be increased by a factor of at least 10, and the estimated distances of the objects observed must be scaled down drastically. If the red excess is caused by a time effect, an increase in the absolute luminosity of E nebulae with distance is implied. Since the relation of red shift to magnitude is based primarily upon the nebular clusters, which are predominantly composed of E nebulae, the derived relation of red shift to distance would have to be revised. Either explanation of the observed red excesses would require a revised cosmology.

It has been necessary to extrapolate the relation of red shift to magnitude far beyond the last measured point. Red-shift measurements to greater distances are required. An error of only a few hundredths in the extrapolated values of the red shift would influence any cosmological conclusion. Beyond the sixteenth magnitude, the scale is currently being regarded with suspicion. Yet the nebular-count surveys lie between the eighteenth and the twenty-first magnitudes. An error of only a few tenths of a magnitude here could require a completely different cosmology.

Thus both theoretical and observational cosmology would appear to be equally tentative. Possibly the chief value of the nonhomogeneous cosmological model which has been presented here is the demonstration of the very real flexibility of the general theory of relativity. It is not necessary to invent any new physical principles to rationalize the currently accepted observational data.

The author would like to thank Dr. E. Hubble for many stimulating and fruitful discussions. The author is particularly indebted to the late Dr. R. C. Tolman, who first suggested this problem and gave continued guidance and encouragement to its development.

NOTES

PHOTOELECTRIC OBSERVATIONS OF W VIRGINIS

The cepheid variable star W Virginis was placed on the photoelectric program of the Lick Observatory at the request of R. F. Sanford, who was observing it spectrographically at Mount Wilson. The purpose of the observations was to obtain new times of minimum and maximum light, since previous work had shown the period, the shape of the light-curve, or both, to be variable. Observations were made through a 1-mm thickness of Corning 3385 filter glass, with the 12-inch refractor equipped with our 1P21(*c*) multiplier phototube. The signals were sent through a direct-current amplifier to a Weston Model 271 milliammeter or to an Esterline-Angus recorder. The effective wave length with this filter for observations of W Virginis was approximately at λ 5000. Data concerning the cepheid and the comparison star are given in Table 1.

TABLE 1

CEPHEID AND COMPARISON STAR

STAR	1900 R.A.	1900 Dec.	MAG. VIS. (MEDIAN)	SPECTRAL CLASS
W Virginis	$13^h 20^m.9$	$-2° 52'$	$9^m.9$	pec.
BD−3°3460	13 18.9	−3 41	9.2	A0

TABLE 2

PHOTOELECTRIC OBSERVATIONS OF W VIRGINIS AT λ 5000

JD 2430000+	No.	Δm	P.E.	Phase		Observer*
2683.71	4	$+0^m.771$	$\pm 0^m.006$	$0^d.01$	$0^p.005$	K, M
2686.76	4	+0.050	.004	3.15	.182	K, M
2688.69	4	+0.103	.006	5.08	.294	K, M
2693.73	4	+0.431	.004	10.12	.586	K, G
2695.74	4	+0.995	.015	12.13	.703	K, G
2696.76	4	+1.249	.010	13.14	.761	K, G
2697.76	4	+1.392	.016	14.15	.819	K, M
2703.71	4	+0.061	.005	2.83	.164	K, G
2709.74	4	+0.214	.004	8.85	.513	K, G
2715.82	4	+1.157	.006	14.94	.865	S, M
2751.72	6	+0.860	.008	16.29	.943	E
2752.73	4	+0.840	.006	0.03	.016	E
2753.71	3	+0.675	.021	1.01	.058	K, G
2754.71	3	+0.251	.010	2.01	.116	K, G
2755.71	4	−0.085	.004	3.00	.174	E
2756.73	3	0.000	0.010	4.03	0.233	E

* K = Kron, M = Mattson, G = Gordon, S = Stackpole, E = Eggen.

The results listed in Table 2 are the means of the observations made during one night. The number of sets of observations is indicated in the second column. A group of four

sets extends over a 15-minute interval. The magnitude differences are in the sense variable *minus* comparison star. The heliocentric phases, given in days and fractions of a period, were computed from S. Gaposchkin's[1] ephemeris:

$$\text{Minimum light} = \text{JD } 2420472.543 + 17^{d}.271671E\,.$$

The magnitude differences are plotted in Figure 1. The magnitude of W Virginis on the International Photographic Scale was determined by O. J. Eggen as $10^{m}.13$ at phase $0^{p}.233$ when the magnitude difference was $0^{m}.00$. A comparison of the present results with those read from Gaposchkin's mean curve indicates that the minimum occurred $0^{p}.14$ early at JD 2432698.

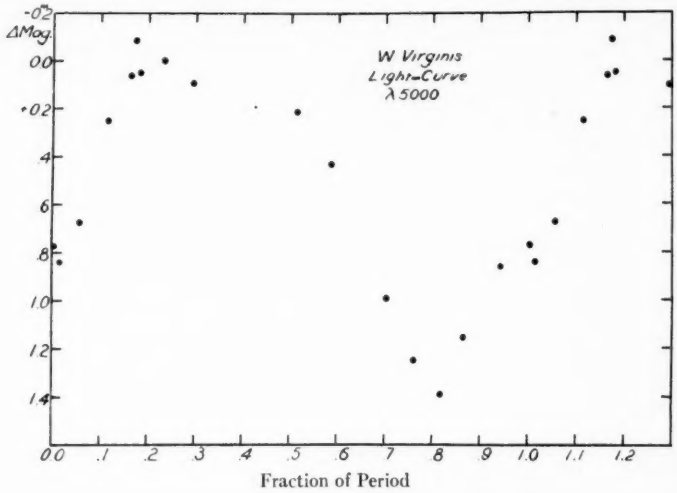

FIG. 1.—Photoelectric observations of W Virginis

Comparisons of the shape of the light-curve were also made with A. Nielsen's mean curve[2] and with a plot of K. Graff's observations.[3] The four curves appear quite dissimilar. Our results, which give deviations from a smooth curve much larger than the probable errors, indicate that the shape of the light-curve is variable, to an extent intermediate between the variability of TU Cassiopeiae and that of T Monocerotis, as determined last year.[4] The accumulated evidence now also shows that the period varies, but its determination is undoubtedly complicated by the variation in shape of the light-curve. The period would have to be shortened to $17^{d}.26713$ to make our time of minimum coincide with that of the next most recent light-curve, given by Graff's observations.

KATHERINE C. GORDON AND GERALD E. KRON

LICK OBSERVATORY
October 1, 1948

[1] *Harvard Bull.*, No. 906, 1937.

[2] *A.N.*, **262**, 422, 1937. [3] *A.N.*, **266**, 163, 1938. [4] *Ap. J.*, **106**, 318, 1947.

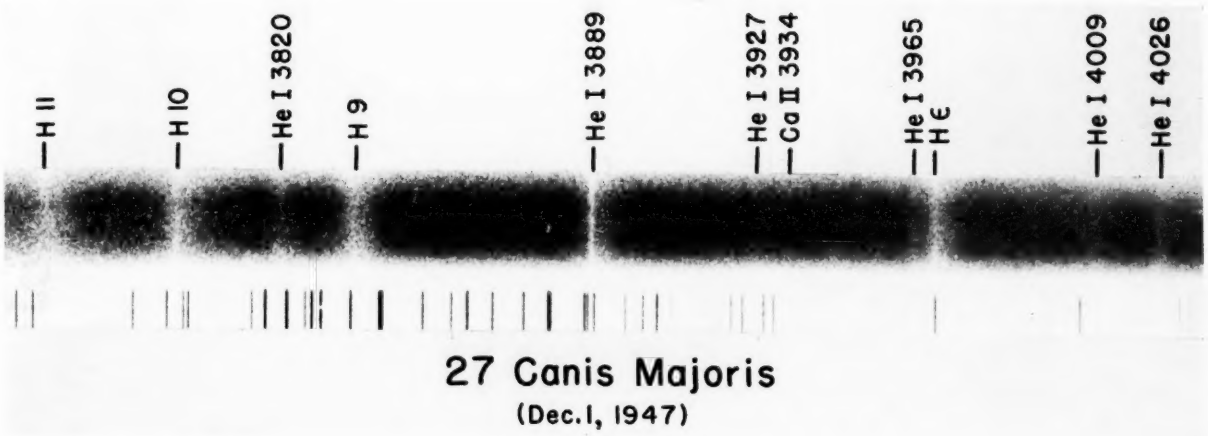
H 11
H 10
He I 3820
H 9
He I 3889
He I 3927
Ca II 3934
He I 3965
H ε
He I 4009
He I 4026
27 Canis Majoris
(Dec. 1, 1947)

FIG. 1

NOTE ON THE PAPER, "THE ABSORPTION-LINE SPECTRA OF THE CENTRAL STARS OF THE PLANETARY NEBULAE"[1]

Dr. Olin Wilson has kindly permitted me to compare tracings of his coudé plate of the nucleus of NGC 2392 with my lower-dispersion material. From this comparison, errors in the interpretation of the McDonald tracings have been found, e.g., the dip attributed to λ 3965 *He* I is part of λ 3970 (*He* II+*H* I). The corrected intensities from the McDonald plates of the NGC 2392 nucleus are given in the accompanying tabulation.

λ	*W*	λ	*W*	λ	*W*
3970	1.70	3835	0.85	3770	0.55
3889	1.02	3813	0.32	3750	0.45

The revised log N_{02} *H* is 15.08, and the resultant apparent mass is eleven times that of the sun (Berman's distance scale assumed). The coudé hydrogen-line profiles, however, resemble those of 10 Lacertae; and, if the surface gravities of the two stars are the same, the apparent mass is slightly less than that of the sun.

LAWRENCE H. ALLER

OBSERVATORY
UNIVERSITY OF MICHIGAN
January 3, 1949

EDITOR'S NOTE

The plate to accompany the note by Struve and Kao on 27 Canis Majoris (*Ap. J.*, **108**, 537, 1948) was inadvertently omitted. A copy of the illustration is inclosed with this number.

[1] *Ap. J.*, **108**, 462, 1948.

REVIEWS

Centennial Symposia, December, 1946. "Harvard Observatory Monographs," No. 7. Cambridge, Mass.: Published by the Observatory, 1948. Pp. viii+385. $5.00.

The Harvard College Observatory came into being gradually: In 1839 William Cranch Bond installed some of his own instruments in a large house near Harvard Yard; in 1843 the great comet of that year inspired the planning of a research observatory; and between 1845 and 1847 the astronomical observations were started on Summer House Hill, the present location of the Cambridge headquarters of the observatory. The centennial celebration was held in connection with the Christmas, 1946, meeting of the American Astronomical Society and was high-lighted by four symposia on modern developments in astronomy and astrophysics.

The first symposium, on "Interstellar Matter," was organized by B. J. Bok and consisted of papers by J. Stebbins ("Interstellar Absorption in Our Own and Other Galaxies"); C. Schalén ("Color Effects in Reflection Nebulae"); J. L. Greenstein ("Stars in Diffuse Nebulae"); J. G. Baker ("Surface Photometry of Line Emissions in Nebulosities"); B. J. Bok ("Dimensions and Masses of Dark Nebulae"); H. C. van de Hulst ("Evolution and Physics of Solid Particles"); L. Spitzer, Jr. ("The Formation of Cosmic Clouds"); and F. L. Whipple ("Kinetics of Cosmic Clouds"). These papers cover an enormous range: Not only do they discuss the observational results and the conclusions directly derived from them as to the size of the interstellar particles, their distribution, and their physical properties, but they stress in particular the relation between stars and dust clouds and attempt to trace the evolution of the particles, the formation and growth of the dust clouds, their condensation into "globules" and "protostars," and even the "possibilities of planetary evolution in a collapsing interstellar cloud." There is no longer any doubt that a close connection exists between the T Tauri variables and some of the largest and densest dust clouds in the galaxy. If we think of the groups of emission-line objects discovered by Joy in the Taurus cloud and at McDonald Observatory in the Scorpius-Ophiuchus cloud as "stellar associations" in the sense of Ambarzumian, we must conclude that these groups were formed in the relatively not very distant past—perhaps one hundred million years ago—because otherwise they would have been unable to resist the disrupting forces constantly at work in the galaxy. But perhaps they are not real "associations," in the sense of very wide clusters, but represent accidental groupings of stars which have drifted into the dust cloud and show similar spectroscopic features only because they happen to be subjected to the same physical influence—bombardment by interstellar grains—while they are located within the cloud. We have as yet no definite way to decide which view is the correct one, and Greenstein does not offer an opinion. But the present tendency seems to be to accept the former, rather than the latter, view.

It is, of course, tempting to search for a connection between the T Tauri stars and Bok's "globules," but we must admit that at present there is no evidence of any objects that could be considered intermediate between these two groups. Bok and Reilly have found approximately fifty "globules" along the Milky Way, but their discovery is only possible against the background of a diffuse nebula, or a star-rich field. Nevertheless, theoretical reasoning leads us to suspect that large aggregations of stars are being formed at the present time or, at least, that some have been formed in the very recent past. It is logical to assume that they are condensed from dust clouds. If so, then it is rather surprising that there are so few "globules," or, as Spitzer calls them, "protostars," in the observable regions of the Milky Way. Bok estimates that this prestellar stage may last for 10^7 or 10^8 years. However, we do not know whether the final process of star-formation may not be much more rapid. If it were, then we would not necessarily expect to observe a faintly glowing "globule" while the object contracts from its average diameter of 100,000 astronomical units to the diameter of a supergiant star of, say, 10 astronomical units.

An important difficulty with which all investigators have to struggle, sooner or later, is that of the predominantly filamentary structure of most interstellar formations. Not only do they suggest violent, irregular motions in the original dust cloud which must result in large angular momenta from glancing collisions of such cloud formations, but Bok mentions that some of the

"globules" in M8 also appear to have a filamentary structure on photographs obtained by Baade with the 100-inch reflector on Mount Wilson. Turbulent motions on a vast scale appear to be the normal condition of interstellar clouds and not the exception. Spitzer and Whipple make use of the concept of turbulent viscous friction to damp out rotation and random motions, and the former has also suggested that "a galactic magnetic field might produce eddy currents in a rotating protostar, which would then damp out the angular momentum." It is probably significant that in all theories of cosmogony we encounter the difficulty of the angular momentum.

The second symposium, on "Electronic and Computational Devices of Interest to Astronomers," was organized by J. S. Hall, then of Amherst, and consisted of papers by G. E. Kron ("The Adaptation of Photoelectric Devices to the Properties of the Electron"); A. E. Whitford ("Infrared Detectors and Their Astronomical Applications"); and W. J. Eckert ("Electronic and Electromagnetic Measuring, Computing and Recording Devices"). Kron concludes that improvements in design may give increases in sensitivity of a *CsO-Ag* photocell by a factor of 2.9 and that a further factor of 1.4 would result from "making the same photosurface the cathode of a multiplier tube."

The third symposium, on "Eclipsing Binaries," was arranged by Z. Kopal and included the first Russell Lecture of the American Astronomical Society, by Professor H. N. Russell, "The Royal Road of Eclipses." The other contributions were by O. Struve ("Spectrographic Studies of Eclipsing Binaries"); R. M. Petrie ("The Spectrophotometric Determination of Relative Luminosities of Components in Two-Spectra Binary Systems"); H. Shapley ("The Relative Frequency of Low-Luminosity Eclipsing Binaries"); and Z. Kopal ("Some Problems in the Theory of Eclipsing Variables"). The last of these papers is of special interest because it outlines several of the most pressing problems of astrophysics. For example, it lays great stress upon the question of gravity darkening which Russell and others have used for many years in their discussions of the light curves but which also offers a challenge to the spectroscopist. Is there not a reliable procedure by means of which we can observe the spectroscopic analogue of gravity darkening and separate it from the equally important spectroscopic analogue of limb darkening? Among the two thousand known eclipsing variables there must be some which would permit us to observe just before and after a total eclipse the spectrum of an equatorial region of a rapidly rotating star; and there must be others, of similar physical characteristics, in which the eclipse is partial or almost grazing, so that at mid-eclipse we would observe the spectrum of the polar region of an equally rotating star. One of Kopal's questions has already received a rather definite answer. He asks (see p. 262): "Are some of the eclipsing binaries of the W Ursae Majoris type . . . so close that the surfaces of their components are in contact—or are some of them even single rotating dumbbell figures?" The answer is "Yes"; and it has been given independently by several astronomers who have used the velocity curves of nine systems thus far investigated spectroscopically. All show double lines, in agreement with the photometric evidence that the luminosities of the components are not very different, and all show mass ratios of the order of 2 or more, showing that the less massive components must be overluminous by several magnitudes. The explanation is probably that the components[1] "have a common envelope through which an adjustment in the outer layers takes place, which renders the components spectroscopically and photometrically more nearly alike than would be consistent with the mass-luminosity relation."

The last symposium, "On the Gaseous Envelope of the Earth," was organized by D. H. Menzel and contains papers by L. Goldberg and D. H. Menzel ("The Solar Corona and Ultraviolet Radiation"); W. O. Roberts ("Solar Activity"); J. H. Dellinger ("The Ionosphere"); D. H. Menzel ("Earth-Sun Relationships"); H. T. Stetson ("The Sun and Conditions in the Upper Atmosphere"); F. L. Whipple ("Meteors and the Upper Atmosphere"); B. Haurwitz ("Solar Activity, the Ozone Layer and the Lower Atmosphere"); and H. C. Willett ("Solar Activity and the General Circulation of the Lower Atmosphere"). Goldberg and Menzel conclude that the absence of *H* emission in the corona requires $T > 700{,}000°$ and that the coronal spectrum may be explained, formally, in terms of excitation by a flux of energy from the photosphere consisting of a black-body component at $T = 6000°$ and a gray-body component at $T = 10^6$ degrees with a dilution factor of 10^{-13}. Several of the papers reflect the growth of interest in each other's problems of the astronomer and the meteorologist.

OTTO STRUVE

Yerkes Observatory

[1] *Ann. d'ap.*, 11, fasc. 2, 117, 1948.

Eleven and Fifteen-Place Tables of Bessel Functions of The First Kind, to All Significant Orders. By ENZO CAMBI. New York: Dover Publications, Inc., 1948. Pp. v+153. $3.95.

The main table gives $J_n(x)$ for x varying from 0 to 10.5 at intervals 0.01 to 11 places, and for $n = 0(1)29$. Such ranges cover the scope of most applications in physics.

A supplementary table gives $J_n(x)$ for x varying from 0 to 0.5, at interval 0.001, to 15 p'aces of decimals; n is extended up to $n = 11$, that is, through all values of $J_n(x)$, for the range of x in question, which are greater than 10^{-15}

Tables of Bessel Functions of Fractional Order, Vol. 1. Prepared by the COMPUTATION LABORATORY OF THE NATIONAL APPLIED MATHEMATICS LABORATORIES, NATIONAL BUREAU OF STANDARDS. New York: Columbia University Press, 1948. Pp. xiii+413. $7.50.

Bessel functions of fractional order occur in many problems of elasticity, heat conduction, wave propagation in stratified media, hydrodynamics, and other branches of applied mathematics. They are also important for the approximate solution of differential equations of the second order of the form $y''(x) + p(x)y(x) = 0$ in the neighborhood of a zero of $p(x)$. Functions whose order is the half of an odd integer have already been tabulated; the present work is concerned with Bessel functions of orders $\pm\frac{1}{4}$, $\pm\frac{1}{3}$, $\pm\frac{2}{3}$, $\pm\frac{3}{4}$.

Tables: $J_\nu(x)$ for $x = 0(0.001)X$ (0.01)25 to $10D$, where $X = 0.9$ for $\nu = -\frac{3}{4}, -\frac{2}{3}$; $X = 0.8$ for $\nu = -\frac{1}{3}, -\frac{1}{4}$; $X = 0.6$ for $\nu = \frac{1}{4}, \frac{1}{3}$; and $X = 0.5$ for $\nu = \frac{2}{3}, \frac{3}{4}$. The functions $A_\nu(x)$ and $B_\nu(x)$, which occur in the asymptotic development of $J_\nu(x)$ for large values of x (namely, $J_\nu(x) \sim A_\nu(x) \cos [x - \frac{1}{4}(2\nu + 1)\pi] - B_\nu(x) \sin [x - \frac{1}{4}(2\nu + 1)\pi]$), are tabulated for $x =$ 25(0.1) 50(1) 500(10) 5000(100) 10,000(200) 30,000 to $10D$ for the same values of ν. The first 30 zeros, to $10D$, of $J_\nu(x)$ for the above values of ν with approximate formulae for the computation to at least 10 decimal accuracy of the later zeros. Everett interpolation coefficients for second- and fourth-order central differences. Lagrangian interpolation coefficients $L_\nu(\mu)$ for the eight base points, $\pm\nu = \frac{1}{4}, \frac{1}{3}, \frac{2}{3}, \frac{3}{4}$ and for $\mu = 0(0.001)1$. Multiples of $\pi/2$ and various constants.

Nuclear Physics Tables. By J. MATTAUCH; and "An Introduction to Nuclear Physics," by S. FLUEGGE. Translated from the German by EUGENE P. GROSS and S. BARGMANN. (Published and distributed in the public interest with the consent of the Alien Property Custodian.) New York and London: Interscience Publishers, Inc., 1946. Pp. viii+173+8 pls. $12.

This book includes a comprehensive set of tables of nuclear physics data compiled by J. Mattauch and an "Introduction to Nuclear Physics" by S. Fluegge. The valuable part of the book is in the tables which will doubtless be of value to astrophysicists. A brief description of the tables follows.

The first table gives a list of all the measured constants of stable nuclei. This includes relative abundance, spin, magnetic moment, quadrupole moment, and mass defect. The third table gives mass differences for all the important doublets used in the mass-spectrographic determinations of isotopic weights. The fourth table gives a list of all isotopes, stable and unstable, and their isotopic weights, with probable errors of the determination. It gives the details of half-life, radiations emitted, and method of formation for all radioactive isotopes. This table is specially valuable, since it provides in separate columns for the thirteen common methods of formation of radioactive isotopes: (α, p), (α, n), (p, γ), (p, n), etc. The sixth table gives a list of energy yields (Q-values) of a large number of nuclear reactions of atomic number less than 33.

There is, finally, a chart of the well-known "wall type" in which all known nuclei are represented by black, red, or green squares, depending on whether they are stable, unstable, or isomeric, while arrows show all possible transitions.

The tables are complete with references and contain all information available in 1941. Their principal deficiency today is in the list of fission products and their properties, most of this information having been released within the last year by the various atomic-energy projects.

Cosmic Rays. By L. JÁNOSSY. Oxford: Clarendon Press, 1948. Pp. xiii+424. $10.

This volume is the first complete account of cosmic rays. It is a difficult subject to write about, not the least of the difficulties being the extremely rapid rate at which the subject continues to develop.

The book includes a historical introduction; a description of experimental techniques; a summary of the results of quantum electrodynamics and of meson theory, which are of importance for the interpretation of cosmic-ray phenomena; a discussion of the nature and properties of high-energy particles; a detailed account of Stormer's theory of the forbidden cone and related geomagnetic effects; and a discussion of theoretical and experimental results concerning air showers and meson production. The recent work at Bristol (Powell *et al.*), using photographic methods to investigate meson behavior, is briefly reported in an appendix.

The book is not so clearly written as one could have wished: the style is extremely variable, and it is needlessly repetitious. Nevertheless, the author has taken great pains to insure the comprehensive character of the book and has succeeded in large measure. It represents a source of extremely useful information.

Practical Astronomy. 4th ed. By GEORGE L. HOSMER and JAMES M. ROBBINS. New York: John Wiley & Sons, Inc.; London: Chapman & Hall, Ltd., 1948. Pp. xv+355. $4.50.

The new revision of this volume has closely adhered to the purpose stated in the Preface to the first edition, i.e., to furnish a text in practical astronomy adapted to the needs of engineering students and to observations that can be made with the engineer's transit. The text and problems will provide such a student with the fundamentals required to determine latitude, longitude and time, and azimuth in a simple, concise manner. The reviewer noted the omission of reference to the "Sky Diagrams" now published in the *American Air Almanac* which, in his experience, are more convenient than the "Rude Star Finder." A more important omission is the reference to the National Bureau of Standards' time signal transmitted continuously over WWV which is very convenient for checking a watch in the field.

Although a discussion of celestial navigation would be out of place in such a text, it is unfortunate that reference is not made to the method of determining latitude and longitude from two or more "lines of position."

DANIEL L. HARRIS III

Yerkes Observatory

Practical Astronomy. By JASON J. NASSAU. 2d ed. New York: McGraw-Hill Book Co., Inc., 1948. Pp. xii+311. $5.00.

The revised edition divides the subject matter into two parts: Part I, covering the fundamentals of astronomy needed for the determination of time and longitude, latitude and azimuth, using an engineer's transit or a sextant; and Part II, covering the precise determination of these quantities using a theodolite, astronomical transit, zenith telescope, and astrolabe.

In Part I, which is designed for engineering students, the *American Nautical Almanac* is used throughout. The presentation is therefore greatly simplified by not requiring the use of sidereal time and right ascension. On the other hand, Part II is designed for use by astronomical students who are interested in learning how to employ more precise methods of determining time and position. The section on the determination of position by equal altitudes using the astrolabe is a new and valuable addition.

The arrangement makes this a very convenient reference book for engineer and astronomer, although the volume is essentially a textbook and contains many examples and exercises for the student.

D. L. H.

Astronomy. By WILLIAM L. KENNON. Boston: Ginn & Co., 1948. Pp. vii+737. $5.50.

This new volume covers the subject of general astronomy in a very thorough manner. It is written in an attractive style, the diagrams and illustrations are good, and the reproductions of photographs are excellent. However, the reviewer noted several points that tend to detract from the value of the book. A number of typographical errors and obvious mistakes have been noted: F. Hayle for F. Hoyle, R. A. Lyttelton for R. A. Lyttleton, Mercury's inclination being quoted as the highest of all the planetary orbits, etc. Several recent observations, which one would expect to find referred to in a new book, have been omitted: the discovery of an atmosphere on Titan by G. P. Kuiper, the spectroscopic solar parallax determination of $8''.805 \pm 0''.007$ by W. S. Adams, the rotation period of Venus of 225 days confirmed by A. Danjon.

The author has included a list of references at the end of each chapter and has incorporated a few footnote references to the results of investigations mentioned in the text. An extension of this feature would be greatly appreciated by students who wish to refer to the original papers. It is unfortunate that the author did not indicate the uncertainties connected with the observed data; for example, the rotation period of Neptune is given as "15 hr 48 sec" (probably a typographical error for "15 hr 48 min") instead of 15.8 ± 1.0 hours (Moore and Menzel).

In spite of these detractions, the book merits the careful consideration of teachers who wish to select a text for their course.

D. L. H.

THE OBSERVATORY

FOUNDED 1877

* * *

A Magazine presenting current developments in Astronomy by means of Articles, Correspondence, Notes on discoveries and Reviews of important astronomical books. The papers read at the Meetings (Astronomical & Geophysical) of the Royal Astronomical Society and the discussions which follow are also fully reported.

* * *

Annual subscription for 6 issues, post free, 15/– should be sent to

The Editors, ROYAL OBSERVATORY
Greenwich, London S.E., 10

Astronomical
LANTERN SLIDES

Since 1903, the Yerkes Observatory of the University of Chicago has been reproducing in lantern slides, transparencies, and prints the original astronomical photographs made at Williams Bay.

The lantern slides are uniformly 4×3¼ inches in size. The frequent call for small sets of slides for school and lecture purposes has led to the preparation of a list of 100 representative slides, a catalogue of which may be obtained upon request to the University of Chicago Press, 5750 Ellis Avenue, Chicago.

Prints as well as slides can be furnished, and for many subjects window transparencies are also supplied.

For catalogue and further information write

The University of Chicago Press
5750 Ellis Avenue, Chicago, Ill.

POPULAR ASTRONOMY

A magazine now in its fifty-seventh year, devoted to the elementary aspects of Astronomy and allied sciences.

Published monthly, except July and September.

Yearly subscription rates: Domestic $4.00; Canadian $4.25; Foreign $4.50.

Address

POPULAR ASTRONOMY
CARLETON COLLEGE
NORTHFIELD, MINNESOTA, U.S.A.

ASTROPHYSICAL MONOGRAPHS

Sponsored by the Editors of the Astrophysical Journal

PRINCIPLES OF STELLAR DYNAMICS

By S. CHANDRASEKHAR

In this monograph the dynamical methods of interpreting the motions in the galaxy, spiral nebulae, and star clusters are developed from a coherent point of view. "This book should exert a profound influence on the future developments in the field of galactic dynamics. I can recommend its study unreservedly to newcomers in the field and to those who already have a passing acquaintance with its problems. The experts can profit from reading it."—BART J. BOK, in *Science*. 1942. *$5.00*

AN ATLAS OF STELLAR SPECTRA. By W. W. MORGAN, PHILIP C. KEENAN, and EDITH KELLMAN

This work represents approximately ten years of spectrographic observations with the 40-inch telescope at Yerkes Observatory. It consists of fifty-five photographic prints, size 6 by 10 inches, in a portfolio. In the booklet accompanying the prints a complete summary of the spectral classification is given. The atlas and text have been prepared with the needs of the stellar astronomer in mind and the whole work is technical in nature. 1943. *$10.00*

SPECTRA OF LONG-PERIOD VARIABLE STARS

By PAUL W. MERRILL

This monograph is devoted largely to the observational side of the subject, but some discussion of the physical significance of various spectral features is included. A brief introduction and a historical chapter are inserted for the benefit of the reader who is not a specialist in stellar spectra. "To one wishing an intimate view of our present knowledge of the spectra of long-period variable stars, whether he be a student, astronomer, physicist, or chemist, the present monograph is recommended."—J. H. MOORE in *Astronomical Society of the Pacific*. 1940. *Paper, $2.50*

THE MASSES OF THE STARS, WITH A GENERAL CATALOGUE OF DYNAMICAL PARALLAXES

By HENRY NORRIS RUSSELL and CHARLOTTE E. MOORE

"Astrophysicists will be grateful to the authors for so thorough an examination of available knowledge. . . . We may be permitted to congratulate the senior author on this magnificent outgrowth from an idea which germinated in his mind thirty years ago."—PROFESSOR A. S. EDDINGTON, *The Observatory* (England). 1940. *Paper, $4.50*

AN INTRODUCTION TO THE STUDY OF STELLAR STRUCTURE. By S. CHANDRASEKHAR

Treats in a deductive manner the subject of stellar interiors. The necessary physical theories and mathematical methods are fully explained. Includes accounts of the foundations of thermodynamics, the theory of radiation, the quantum theory of a perfect gas, and a discussion of the elements of nuclear physics. "The material is throughout presented with enviable crispness and clarity of expression. The work will undoubtedly become an indispensable handbook for future researchers in this field."—*Nature* (England). 1939. *$10.00*

THE DISTRIBUTION OF THE STARS IN SPACE

By BART J. BOK

". . . . an extremely important contribution to the field of galactic structure, invaluable alike to both students and research workers in the field."—*Science*. The large number and variety of researches carried out in this field during the past fifteen years are discussed critically in this study with clarity and dispatch. 1937. *Paper, $2.50*

THE UNIVERSITY OF CHICAGO PRESS